Synthesis and tunable self-assemblies of *peri*-naphtho dyes

A Thesis Submitted in Partial Fulfilment of the Requirements for the Degree

of

Doctor of Philosophy

by

Indraneel Debnath

Roll no 186122012

Department of Chemistry

Indian Institute of Technology, Guwahati

Guwahati-781039

Thesis supervisor

Dr. Kingsuk Mahata

Department of Chemistry

Indian Institute of Technology, Guwahati

Guwahati-781039

Dedicated to family and friends

"There is no doubt that creativity is the most important human resource of all. Without creativity, there would be no progress, and we would be forever repeating the same patterns." —Edward de Bono

Declaration

I do hereby declare that the research work embodied in this thesis entitled "**Synthesis and tunable self-assemblies of *peri*-naphtho dyes"** has been carried out by me under the supervision of **Dr. Kingsuk Mahata** in the Department of Chemistry, Indian Institute of Technology Guwahati, Assam-781039, India.

In keeping with the general practice of reporting scientific observations, due acknowledgements have been made wherever the work described is based on finding of other investigators.

Guwahati

13/11/2024

Indraneel Debnath

186122012

Department of Chemistry

Acknowledgement

I would like to take this opportunity to express my earnest gratitude to my thesis supervisor Dr. Kingsuk Mahata. Without his continuous optimism, enthusiasm, encouragement and support this work would hardly reach its novelty. I am grateful for the opportunity of working under his guidance. His sincerity towards critical thinking and the effort will always be my inspiration to work on what I believe.

I would also like to express my sincere gratitude to the doctoral committee: Prof. A.S. Achalkumar, Dr. Manabendra Sarma and Dr. Shyam Prosad Biswas for their insightful comments and encouragement, also for the hard questions which drove me to widen my research from various perspectives.

I thank Department of Chemistry, Central Instruments Facility, IIT Guwahati for allowing me to use the necessary instrumental service for my Ph.D work. I am thankful to the people associated with the smooth running of our laboratory and instrumental facilities. I would also like to acknowledge IIT Guwahati for the financial assistance during the course.

I am definitely thankful to all the fellow lab mates past and present namely Dharismita, Priya, Pranaam and Vaishnavi for keeping their support throughout the entirety of my PhD duration, and Poulomi as well for their noteworthy contribution towards my lab work.

Finally, I am taking this opportunity to acknowledge my family and friends. I am thankful towards my father, mother, sister and brother-in-law for their immense belief in me throughout this and my life in general. I am also in gratitude towards people close to me - Ria Deb, Tirupati Roy, Somnath Paik, Mongoli Brahma, Priyanka Adhikary and my other colleagues in IIT, for their constant companionship and approval inspite of my shortcomings. It's been almost six years since this journey began in July 2018. No matter where I go from here, the things I learned in this campus will always remain with me.

CERTIFICATE

This is to certify that **Mr. Indraneel Debnath** (Roll No. 186122012) has been working under my supervision since August, 2018 as a regular registered Ph. D student. His thesis entitled **"Synthesis and tunable self-assemblies of *peri*-naphtho dyes"** is an authentic record of the results obtained from the research work carried out under my supervision in the Department of Chemistry, Indian Institute of Technology Guwahati, Assam - 781039, India.

I am forwarding his thesis to submit for the award of degree of Doctor of Philosophy, from this institute. I hereby certify that he has fulfilled all the requirements, according to the rules of this institute regarding the investigations embodied in his thesis and this work has not been submitted elsewhere for a degree.

Guwahati
November 2024

Dr. Kingsuk Mahata
(Thesis supervisor)

Associate Professor
Department of Chemistry
Indian Institute of Technology, Guwahati
Guwahati-781039

Table of Contents

Synopsis

Index

Chapter 1 : Introduction

Peri-naphthoindigo, a novel molecule that is the naphthalene analogue of indigo, was proposed by R.A.Nathan in a patent in 1977[1] and theoretical research was done on its di-keto indigo-like structure by Zhang *et al.*[2] Both have proposed some remarkable properties that has potential in the organic electronics industry. However, the synthesis of this molecule was a challenge, and it was finally prepared by Mahata *et al.* in 2018.[3] The currently determined structure of PNI consists of a cross-conjugated donor acceptor moiety, sandwiched between the 1,8-positions of naphthalene. Unlike its benzene counterpart, indigo, PNI exists in a mono-enol form. We aim to delve into the effect caused by any substitution either in the chromophore or on the naphthalene ring and subsequent changes in their applicability. Enhancements that we were looking forward to, include- better solubility, increase in emission efficiency, shift of emission towards NIR region to take advantage of the bio-optical window, better performance in organic electronics and such.

One direction of work that we have investigated is the co-ordination of a boron difluoride moiety with the -OH group of PNI, forming a 6-membered ring with lone pair of the imine nitrogen. Boron complexes of indigo and nindigo have been reported and have displayed fascinating properties such as near infra-red emission and redox activity.[5] As PNI-BF_2 molecule exists as N,O-coordinate, this offers a relatively new angle as most complexes are N,N or O,O- cordinate.[7-8] However, compared to the nindigo–boron complexes, and also to the original PNI, solubility is reduced for PNI-BF_2 complex, as a more planar structure is enforced, hence examination of redox activity was an obstacle.

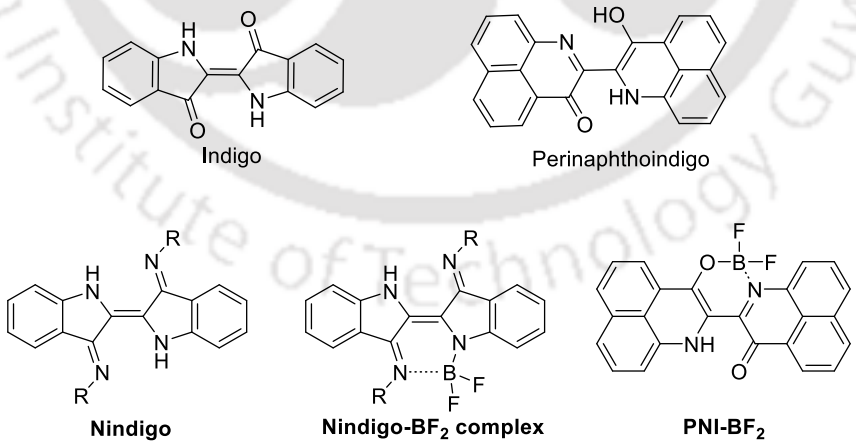

Fig 1: Indigo, *peri*-naphthoindigo, Nindigo and boron-difluoride complex of Nindigo

Self-assembly is a domain of supramolecular chemistry, which denotes the tendency of a molecule to avoid a solvent environment, through interaction with another molecule of its own structure and chemical makeup; so that the groups least favoured by the environment are in a state of protection, or

'hiding'; alkyl chains prefer non-polar solvents, hydroxyl groups prefer polar solvents and so on Self-assembly, or even co-assembly, has a very important consequence in which if a molecule is susceptible to rotation about a single bond, aggregation causes the stacking of these molecules, such that no free movement is allowed, hence no energy is lost in molecular movement, leaving emission the only outlet for the molecule to lose energy. This is aggregation induced emission, whereby a non-emissive molecule may start fluorescing in aggregates. Stacking also causes chromophores of different molecules to interact with each other, leading to several other consequences, such as relaxation or deactivation of the fluorescing entity, resulting in aggregation caused quenching. A highly interesting topic is the control on the pathway through which the molecules come together to form the aggregate, i.e. how much influence a single factor in the ambient environment may have in the shape of the aggregate formed and distinction between the kinetic and thermodynamic path. This type of energy landscapes, through which a molecule may pass to access thermodynamic equilibrium aggregate systems are prevalent in nature, however artificial systems replicating such adaptive behaviour are fascinating to work on.[9-15] A detailed photo physical study on the aggregation of PNI-BF_2 showed the possibility of such a system being replicated by our molecule, and indeed some BF_2-systems are known to show such adaptive behaviour.[16]

Another field of study we have embarked upon is the naphthalene analogue of unsubstituted isatogen, which we have termed as *peri*-naphthoisatogens. The main component is the presence of a nitrone in conjunction with a carbonyl enclosed in a cyclic structure. This isatogen moiety is present in the synthetic route of some biological molecules[17] and we are looking into the potential of naphthalene analogues for use as similar or better alternatives. A previous report in 1971 indicated the existence of C2-substituted PNTI, but the field was not explored any further.[18] Leaving the C2 position unsubstituted may open up the field for new synthetic derivatives. Presence of ambipolar groups also leads to potential of unique aggregation tendencies, which may also be a precursor to smart materials. Derivatization is also possible for these PNTIs, which will lead to newer materials for research.

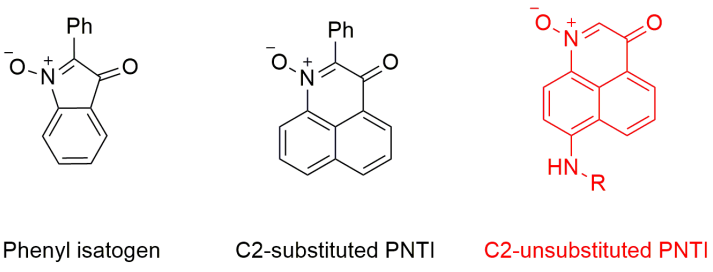

Fig 2 : Depiction of molecules related to discussion regarding PNTI

Chapter 2 : Chromophoric modification of PNI- Boron difluoride complex of *peri*-naphthoindigo and its supramolecular polymorphism

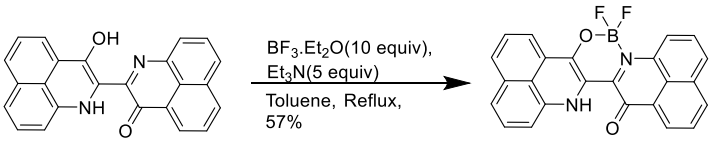

Scheme S1: Preparation method for PNI-BF_2.

Due to the presence of the N,O-coordination potential, a BF_2- complex was prepared. The geometry-optimised structure of the compound shows high planarity where the boron atom produces a six membered ring with the N,O-sites and remains coplanar with the naphthalene rings, while two F-atoms stay outside of the plane. Due to the presence of polar functional groups and a hydrophobic aromatic surface in the PNI-boron difluoride complex, it has ambipolar characteristics and thus has the tendency to aggregate in both polar and non-polar solvent environments. This behaviour of the molecule has been exploited to provide different assemblies in methylcyclohexane and THF-water mixture. It was also observed that at an intermediate ratio of water:THF, the aggregate assembly displayed flexibility which could be achieved at higher temperatures, and on slow cooling of the same, provided a slightly different spectroscopic signature, indicating a delicate change in the aggregate shape. This change is also reflected in the FESEM images. This kind of adaptive self assemblies are a well-known part of biological processes, where the molecule is subjected to a variety of conditions such as pH, temperature, moisture etc.

Measurement of the photophysical properties showed a bathochromic shift in absorption maxima compared to the parent dye, more fine structure and increased emission yield which is to be expected as a result of structural rigidity enforced by boron coordination. For the study of aggregation properties, a mixture of 1,2-DCE and methylcyclohexane in the ratio of 1:99 was chosen as the non-polar medium. An increase in extinction co-efficient, an additional shoulder and increased emission was seen, compared to the dye solution in 1,2-DCE. FESEM images exhibited the formation of linear nanoaggregates (Fig 3).

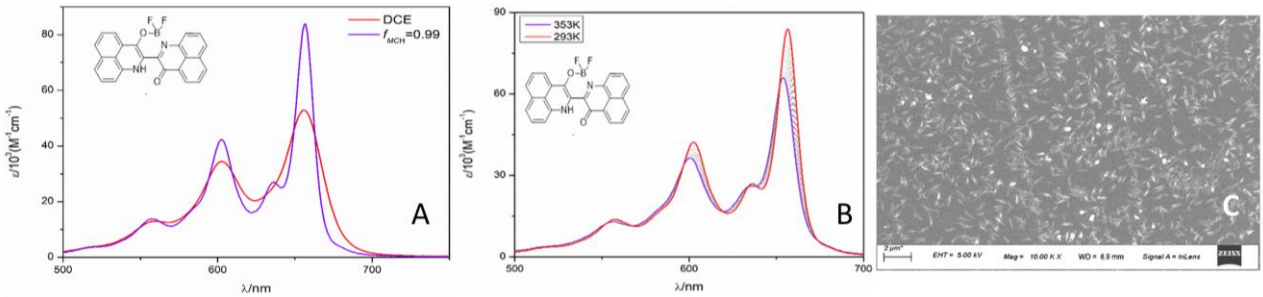

Fig 3: From left- A) Absorption spectra at pure 1,2-DCE and 1,2-DCE/MCH (v/v=1:99) ; B) absorption spectra of a 1:99 v/v mixture of 1,2-DCE/MCH dye solution at different temperatures ; C) FESEM images of linear nanoaggregates

In a mixture of water: THF, kinetically controlled aggregation nanoellipsoids **Agg2** is seen at 80:20 ratio, while at 70:30 mixture, the dye exists as monomeric in nature. Thus a 76:24 ratio is chosen to examine the flexibility of this aggregate (Fig 4). After heating this mixture upto 328 K, a monomer like absorption spectra is obtained and slow cooling of this species back to room temperature produces a different spectroscopic signature, which is indicative of **Agg3**, existing as nanospheres. However **Agg2** on standing at room temperature for 48 hours does not convert to **Agg3** (Fig 4). This formation of different aggregates can also be explained through SA/V ratios, where the unfavourable interactions between the molecular assemblies and solvent molecules is least in nanospheres due to lower SA/V ratio compared to nanoellipsoid. This causes the spherical structures to be more thermodynamically stable and exist at a global minimum on the energy landscape, while the ellipsoid structures exist at a local minimum. At a fraction of 95:5 water:THF, only **Agg2** is seen, and is unaffected by temperature.

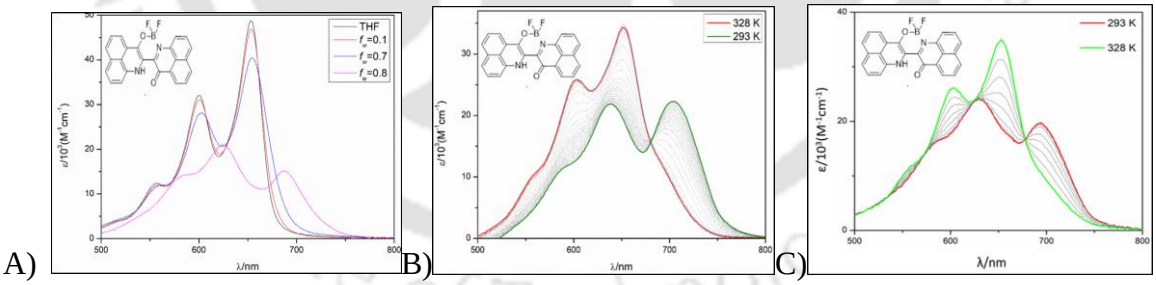

Fig 4 : A) Absorption spectra of PNI-BF_2 in THF/Water at various fractions B) Disassembly absorption spectra of **Agg2**,C) Assembly absorption spectra of **Agg3**

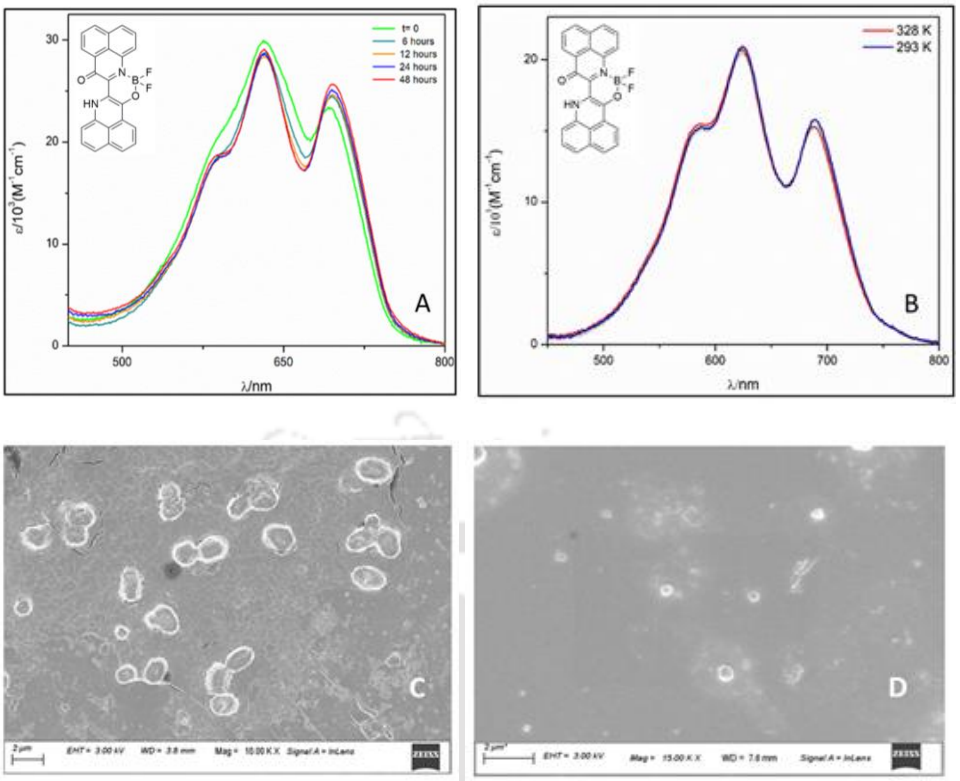

Fig 5: A) Persistence of **Agg2** at room temperature, B) Persistence of **Agg2** at higher temperatures in 95:5 water:THF C) FESEM images of **Agg2** and D) **Agg3**

Thus we have synthesized a dye derivative which has the potential to exhibit supramolecular polymorphism by the utilization of a temperature and solvent polarity pathway. This could open up a lot of avenues for the preparation of smart materials that display flexibility in their aggregation lanes and thus leads to functional supramolecular systems.

Chapter 3 : Ring substitution on *peri*-naphthoindigo and supramolecular rearrangement through incorporation of guest

Aggregation of PNI was previously studied by our team, along with its co-aggregation with another molecule NH_2-NMI.[19] Mainly its aggregation in non-polar solvent was studied, which provided cuboidal type structures. In our experiments we have prepared both the butyl and phenyl derivatives. For this study we currently deal with only the butylated derivative. The structural difference between PNI and butylPNI is the presence of a butyl group at both the tail ends of the PNI molecule. With the butyl group, approach is hindered from the tail end, providing two-dimensional growth instead of three-dimensional in PNI. FESEM provides images of fibre type aggregates in MCH and toluene,

which also coorelates with the two-dimensional growth. Simultaneously, emission too is increased as a consequence of aggregation, which is also seen in PNI.

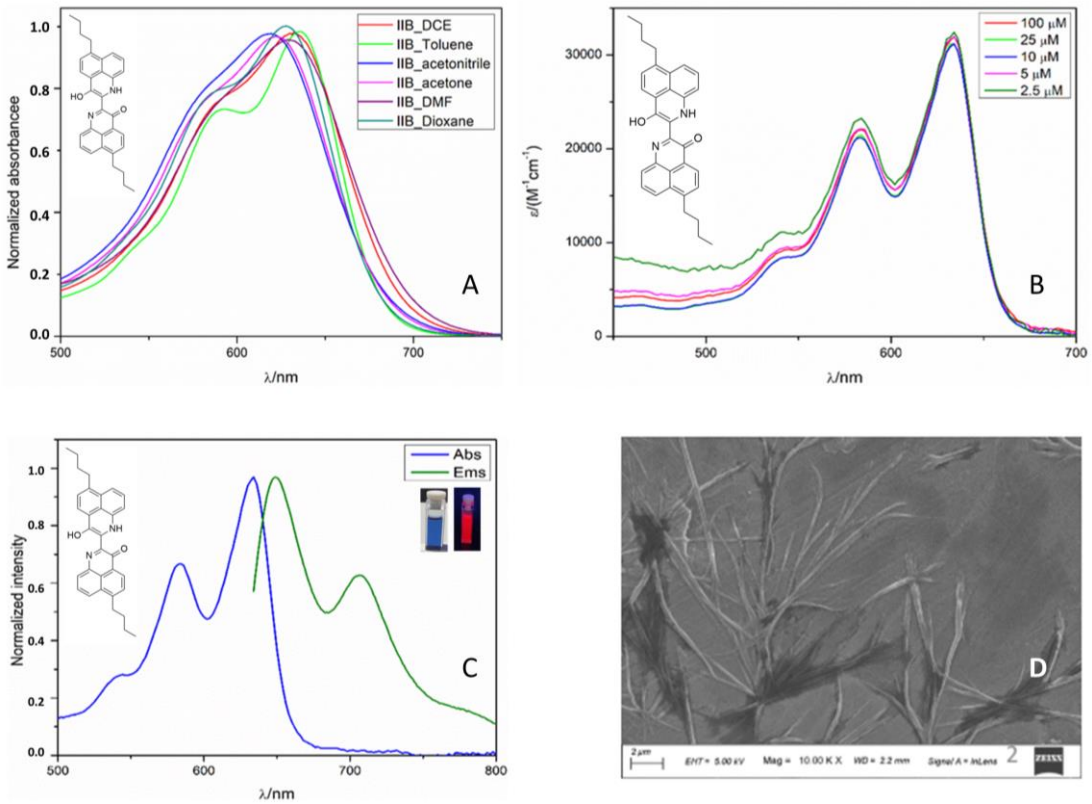

Fig 12 : A) Solvent screening of ButylPNI in different solvents indicating a slight shoulder in toluene- a non-polar solvent, B) concentration dependent absorption spectra of ButylPNI in MCH, C) absorbance and emission of ButylPNI in MCH, D) FESEM images indicate long linear fibres in MCH.

Influence of acid too provides an important change in the aggregate structure of butylPNI in MCH. The absorption maxima undergoes a bathochromic shift upon addition of trifluoroacetic acid and complete quenching of fluorescence, however rapid precipitation is also a consequence of the addition of acid. Investigation of the FESEM image of the resultant aggregates indicates extensive coiling of the aggregates, and the original aggregate can be reverted back to upon addition of triethylamine, even after a long interval of time. However this is not a case of protonation of the molecule by the acid, which entails dissociation of the acid; rather it can be considered as hydrogen bonding of acid to the lone pair on the imine nitrogen. This kind of interaction is also seen in other kinds of molecules, as previously reported.[20]

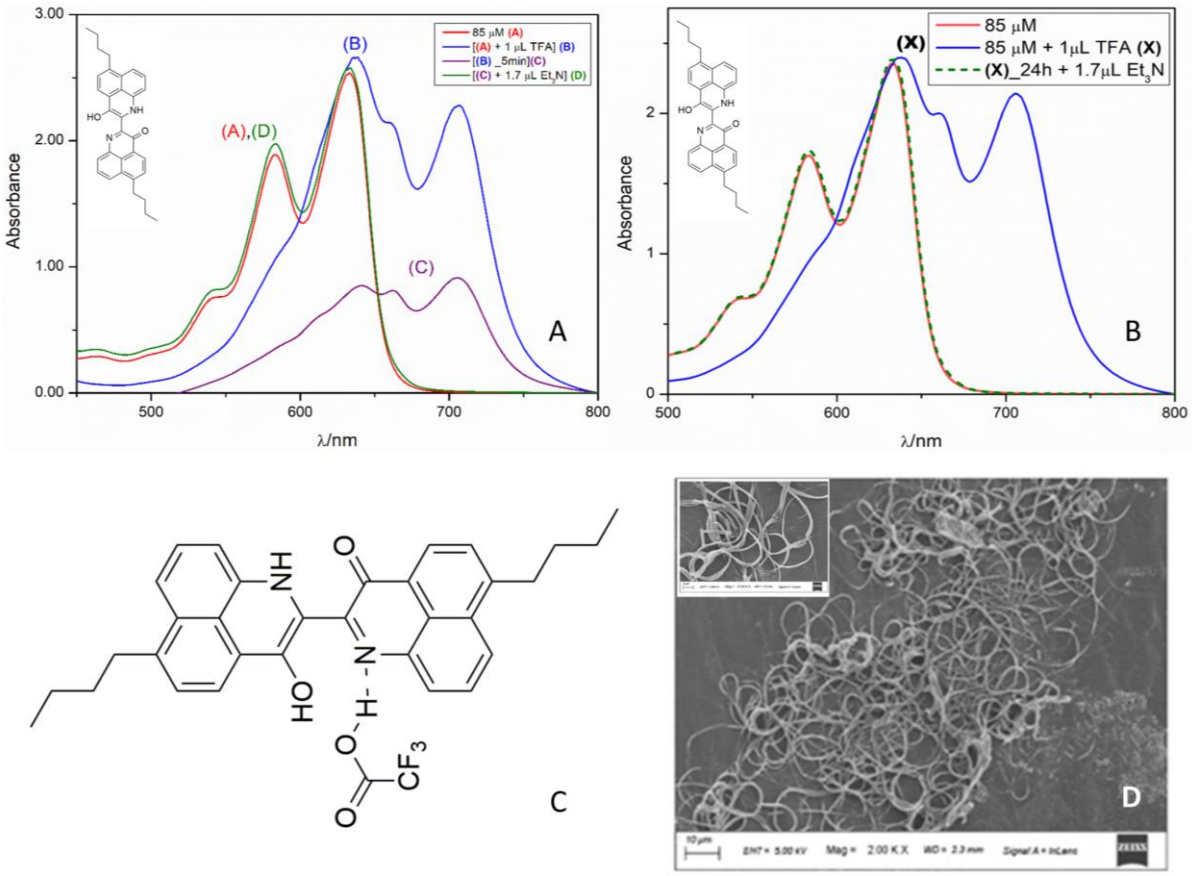

Fig 13 : A) Effect of addition of acid to a solution of butylPNI in MCH and addititon of Et_3N within short durations. B) Effect of addition of acid to a solution of butylPNI in MCH and addititon of Et_3N after 24h, C) Acid coordination to butylPNI, D) FESEM images of acidified aggregates indicating extensive coiling.

We then look into the charge transfer complex of butylPNI with fullerene C_{60}. A solution of butylPNI in toluene is taken and to it fullerene is added. Fullerene complexes with dyes are an ongoing branch of research in today's scientific world.[21] A hypsochromic shift in absorption maxima is observed along with broadening of the maxima. FESEM images show organization of previously present linear fibre like structures into a type of network. Fullerenes are known to act as both electron acceptors and electron donors depending upon the molecule they form a complex with. Since addition of acid to a non-polar solution of butylPNI can also be considered as a host guest interaction, experiments are underway to induce supramolecular rearrangement in such a system through addition of both guests but in order. For the next experiments we switched to toluene, as addition of acid causes precipitation in MCH, which is unsuitable for UV studies, and fullerene itself precipitates out in MCH.

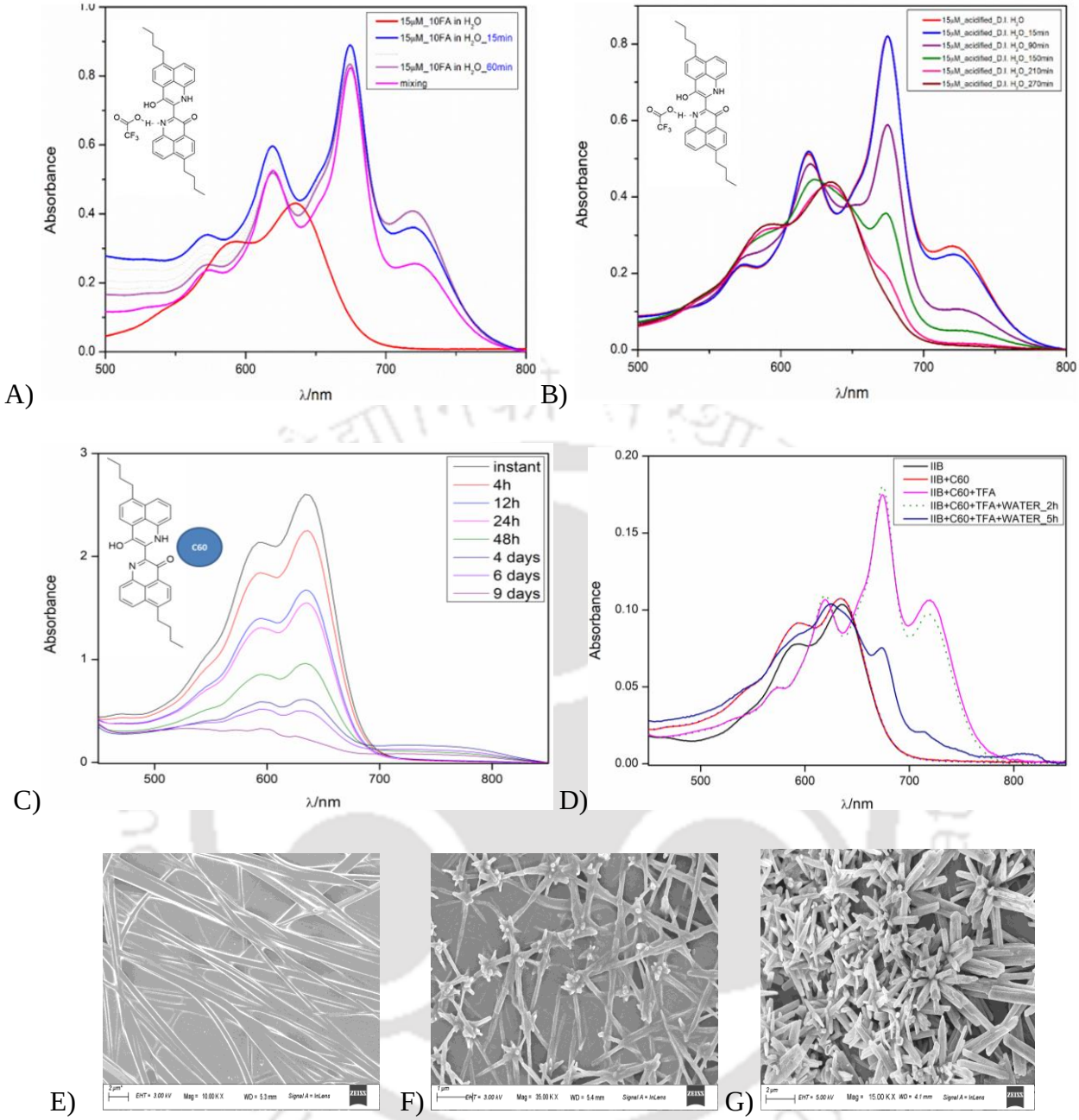

Fig 14: A) Absorption spectra of butylPNI in toluene indicating diffusion of acid from water to toluene B) Absorption spectra of butylPNI in Toluene indicating diffusion of acid from water to toluene absorption spectra of butylPNI in toluene (75 μM) on addition of 1 mg of fullerene (excess equivalence), B) Time dependent absorption spectra of butylPNI (3 μM) in toluene with C60 and TFA. FESEM images of C) butylPNI in toluene D) butylPNI /C60 in toluene E) butylPNI /C60/TFA in toluene

Chapter 4 : Synthesis of *peri*-naphthoisatogens via 'aldrone' condensation

As observed in the reaction of PNI, the reactant 8-nitroacetylnaphthalene has the nitro group acting as electrophile, while the $-CH_3$ of the acetyl group acts as the nucleophile. This is an important point in understanding the reaction capabilities of *peri*-functionalities. There are reports of both intermolecular and intramolecular reaction occuring between nitro and acetyl group in highly basic conditions, such as KOH-DMSO and NaOH-EtOH.[22] However such reactions are also accompanied by various side reactions. An attempt was made to increase the electrophilicity of the nitro group so that intramolecular reaction could be attempted between the *peri* positioned nitro and acetyl groups. There are early reports of protonation of nitro group in strong acids[23], which serves to elevate the electrophilic character of the nitro group.

A reaction was carried out with 8-nitroacetylnaphthalene in heated toluene and triflic acid. After 16h, TLC of the reaction mixture confirmed no further change and hence the major product was isolated. However analysis through NMR spectroscopy indicated that the acetyl $-CH_3$ was still intact, and two more singlets were obtained in the aliphatic region, each integrating to 3 protons. Similarly the aromatic region indicated an increase in the number of protons to an additional 8. A thereby unfortunate conclusion to this reaction was that toluene itself attacked the naphthalene ring, and there are reports of toluene undergoing such reactions in strong acids.[24] This led us to the conclusion that the intended reaction of ring closure was not fulfilled.

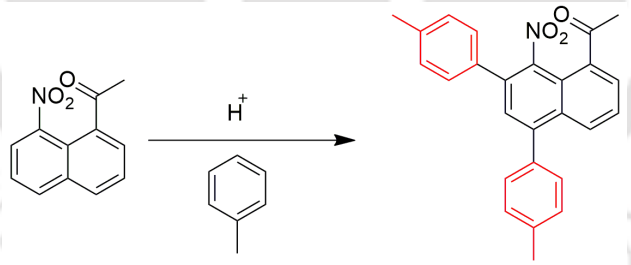

Scheme 2 : Reaction of 8-nitroacetylnaphthalene with toluene in strong acid.

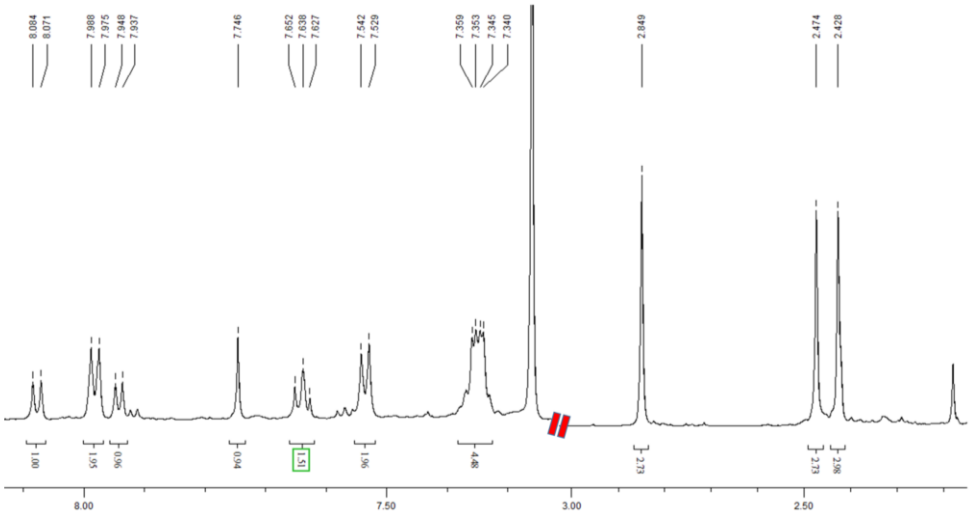

Fig 6 : NMR of the product of above mentioned reaction, toluene methyl singlets at 2.47 and 2.43 and acetyl -CH_3 at 2.85, some of the NMR spectra is omitted.

A derivative of the previous reactant was prepared with an amino-alkyl group in the para position of the nitro group. The reasoning behind this was to offset the electron deficiency of the ring, and also to hinder the approach of the toluene molecule. The prepared reactant was subjected to the earlier reaction conditions, and as imagined, a product was formed which after careful investigation using ^{1}H, ^{13}C and HRMS data, proved itself to be a cyclic nitrone, namely the naphthalene analogue of isatogen, but where the C2 position was still unsubstituted. Thus a new class of dye-perinaphthoisatogens or PNTIs was formed and this previously unreported single reaction between nitro and acetyl groups was termed as ‘aldrone’ condensation. Isolation and identification of the product further solidified our belief that the alkyl amino group plays a vital role in isolation of the C2 unsubstituted product, and also serves to increase the electrophilicity of the nitro group.

Optimization of the reaction conditions were carried out to obtain the best possible yields for the PNTI product. Five different alkyl chains were used, and trial with both simple butyl and butoxy groups in lieu of aminoalkyl groups led to disappointing results, further highlighting the importance of the amino-alkyl group in the procurement of an isolable PNTI product.

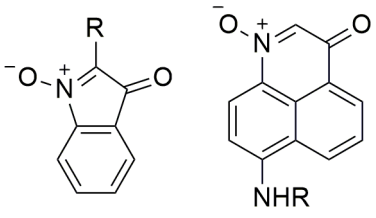

Isatogen **PNTI**

entry	substrate	acid	temp. (°C)	Time (h)	yield (%)
1	2r	TfOH[a]	80	1.5	25
2	2r	TfOH	35	2.5	trace
3	2r	H_2SO_4	35	2.5	27 (54)
4	2r	H_2SO_4	60	2.5	(39)
5	2r	HNO_3	60	12	nr
6	2r	HCl	35	12	nr
7	2r	HCl	60	2.5	trace
8	2r	AcOH	reflux	2.5	trace
9	2r	TFA	35	2.5	trace
10	3r	H_2SO_4	35	2.5	17
11	4r	H_2SO_4	35	2.5	18

[a] In toluene; nr = no reaction; yields mentioned in parentheses are NMR yield.

Further reaction of the PNTI **2p** was carried out : 1,3-dipolar cycloaddition of diene is a well-known reaction of nitrones. The diene used was ethyl acrylate, in toluene at 80^0C. The product obtained was analysed through NMR and HRMS techniques. It was determined that the intended formation of iso-oxazolidine ring, did occur but then proceeded and went further in which the ring snapped at the N-O bond and the formed product was **2p1′**. Both the structures of PNTI and **2p1′** were further established through ground state DFT studies. The energy of **2p1′** was lesser compared to **2p1**, which is the product with the isoxazolidine ring intact.

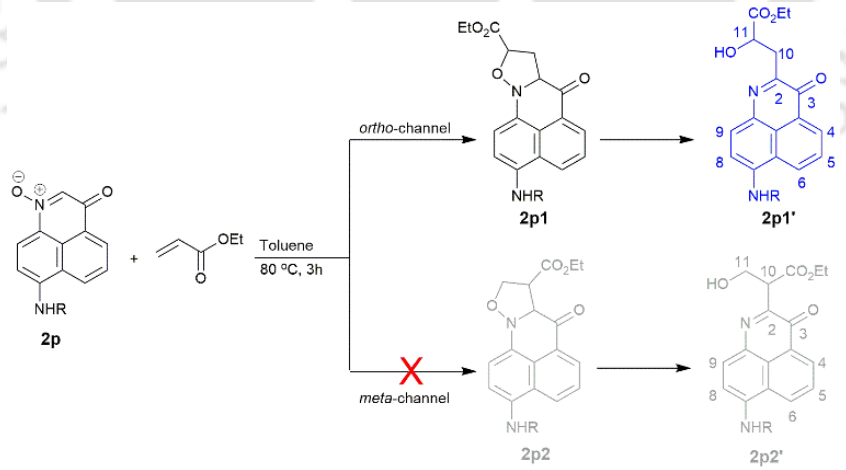

Scheme 3 : 1,3-dipolar cycloaddition of ethyl acrylate with PNTI **2p**.

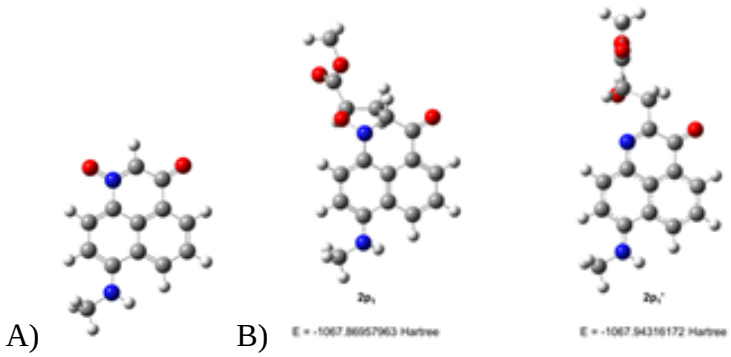

Fig 7 : DFT optimized structures of A) PNTI and B) **2p1** and **2p1',** alkyl groups are replaced with methyl to reduce complexity

UV-vis investigations of both the PNTI and 1,3-dipolar cycloaddition product in chloroform revealed the maximas at 551 nm and 563 nm respectively for absorbance and 594 nm and 635 nm for emission respectively. PNTIs **2-6p** all displayed generally the same absorption maxima, indicating the inertness of absorbance towards the length of alkyl chain and dependence only on the donation of the lone pair on nitrogen of the amino-alkyl group. Quantum yields for the PNTIs and **2p1′** were measured in $CHCl_3$, provided an average value of 12%. Shifting to polar solvents causes bathochromic shift in both absorption and emission maxima of both PNTI and **2p1′**. Solubility of PNTIs in non-polar solvents is hindered, which is to be expected from the structure determined for PNTI..

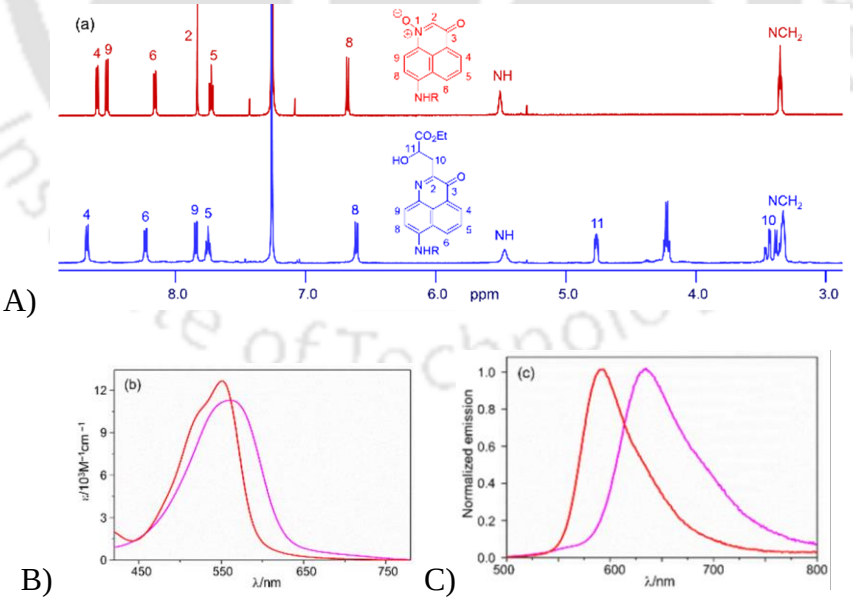

Fig 8: A) NMR comparison of PNTI and **2p1'**, B) Absorbance and C) emission comparison of PNTI (red) and **2p1'**(pink). PNTIs generally have the same characteristics regarding NMR (excluding alkyl chain) and photophysics**.**

Synthesis and identification of the PNTIs opens up a completely new field of inqury where there is opportunity of derivatization at the C-2 position, further 1,3-dipolar cycloaddition products and also potential candidates for tunable self-assemblies. One example of supramolecular organization is being studied in the next section.

Chapter 5 : Thermally assisted supramolecular rearrangement of PNTI

An ambipolar dye tends to have low affinity for both the extreme ends on the solvent polarity spectrum. Depending on the overall polarity of the solvent environment, the molecules tend to assemble in different stackings or arrangements, which may have a substantial effect on the chromophore. In the field of supramolecular chemistry, there are two important types of aggregates : H and J-aggregates. The difference between the aggregates is that H-aggregation leads to blue shifted absorption maxima and depleted emission, while J-aggregation generally provides a red shifted maxima, with enhanced extinction and increased emssion capability. Interconversion between this two aggregates is an ongoing topic of interest in supramolecular field so as to be used as smart functional materials, where temperature, pH, addition of new influencing agents or minimal change in solvent composition may play a huge role in causing a significant change.[25]

Our newly synthesized PNTI dyes **6p** and **4p** were used as model molecules for this study, and a polar environment was taken as environment for research. **6p**, with a dodecyl chain is supposed to have a greater aversion to water compared to **4p**, with a hexyl chain. This is reflected in the absorbance studies of both the molecules in different ratios of THF:water volumes. Both **4p** and **6p** have identical absorption spectra in THF with maxima at 542 nm, which is the general characteristic of PNTIs. Addition of water is the trigger for aggregation in order to protect the naphthalene rings. The molecule **4p** retains bathochromic shift upto a water fraction of 90%, with increased emission. But in case of **6p**, bathochromism is retained upto only an water fraction of 70%, and at 80%, there is a sudden shift to favour hypsochromism, and at 90%, the maxima is significantly blue shifted. Emission too follows a similar trend, increasing in intensity up until 70%, with a sudden drop at 80%, and almost quenched emission at 90% water. This discrepancy in behaviour compared to **4p** arises due to the assumed need for the dodecyl chain itself to avoid a hydrophilic environment, which is not as severe in case of a hexyl chain.

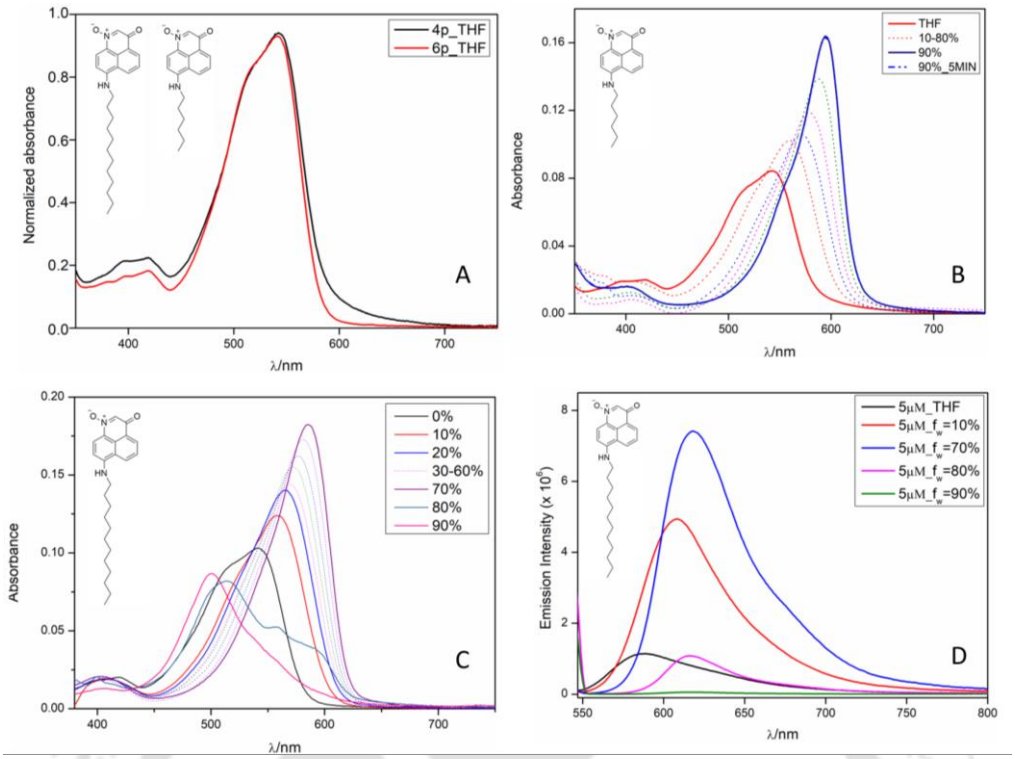

Fig 9 : A) Absorbance spectra of **4p** and **6p,** B) absorbance spectra of **4p** at 5 μM at various water fractions (percentages indicate water volume in a mixture of THF and water), C) absorbance spectra of **6p** at 5 μM at various water fractions (percentages indicate water volume in a mixture of THF and water), D) emission spectra of 6p at various water percentages.

With this interesting observation taken into consideration, we aim to devise a method through which interconversion can be achieved between these two aggregate systems. For this reason, first a suitable solvent composition for **6p** is to be selected. The H-aggregate at 90% water fraction is quite stable, and undergoes minor changes in extinction coefficient or maxima depending on changes in temperature or storing for longer times. After simple elimination through UV-vis monitoring, a solvent composition of water percentage at 83% is selected. At this environment and ambient temperatures, on first addition of the monomer, the hypsochromically shifted maxima is obtained, indicative of H-aggregate. On heating this mixture upto 55°C, conversion is achieved to the J-aggregate within a short duration, and cooling the solution back to 25°C returns the aggregate to its H-form. This form of reversible interconversion between H and J-aggregates is generally unheard of in previous scientific literature. Further experiments are being undertaken for procurement of more data in this regards, so as to have a clearer understanding of the mechanism of this fascinating aggregation and interconversion. Flexibilities in aggregate morphology and subsequent photophysics allow for utilization in real world applications, where a simple example would be observation of emission only at different temperatures.

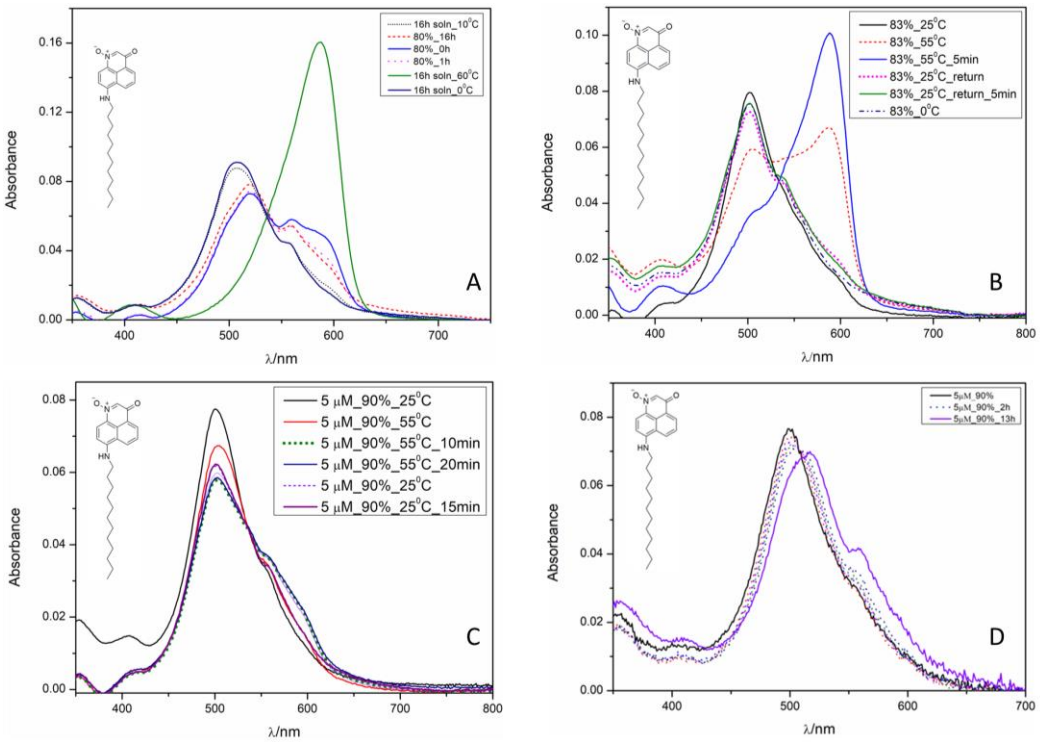

Fig 10 : A) Absorbance spectra of **6p** at 5 μM at f_w = 0.80, indicating mismatch between original spectra and spectra of recooled solution, B) Absorbance spectra of **6p** at 5 μM at f_w = 0.83, indicating almost perfect match between original spectra and spectra of recooled solution, general stability of **6p** aggregates at f_w = 0.90 with regards to C) temperature and D) only slight shift in maxima with time.

AFM images were collected by drying at 25°C and 55°C on a glass plate. The ambient temperature dried plate shows the presence of nanofibre, which can be atributed to H-aggregate. The plate dried at 55°C, on the other hand, also shows the co-existence of spherical nanoparticles. Temperature dependent fluorescence measurements indicate a manifold increase in intensity in emission upon heating to 55°C, and cooling the solution back to 25°C quenches the previous emission.

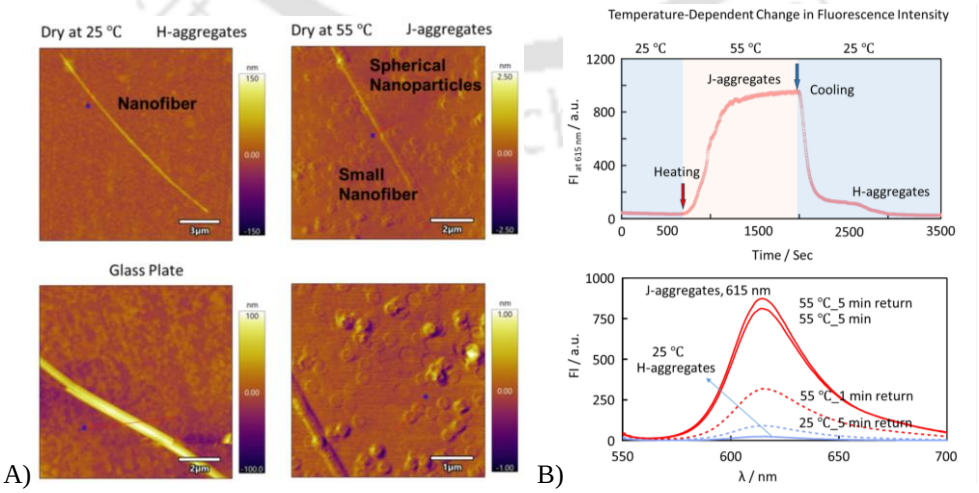

Fig 11 : A) AFM images dried at 25C (LEFT) and 55C (Right) , B) Change in fluorescence intensity with temperature

Chapter 6 : Conclusion and future prospective

6.1 : Conclusion

We have focused on two kinds of *peri*-functionalized dyes in this current thesis. One is the modification of *peri*-naphthoindigo, namely chromophoric modification by the creation of a boron difluoride complex, which displays supramolecular polymorphism in polar environments, and another is the ring modification by addition of groups on the naphthalene rings, and studying their behaviour on addition of acid and fullerenes, which is currently underway. The other type is PNTI, the naphthalene analogue of unsubstituted isatogen, which we have managed to synthesize through 'aldrone' condensation, and a derivative of PNTI was prepared using 1.3-dipolar cycloaddition with ethyl acrylate, and are currently studying tunable supramolecular self assembly of PNTI, in a mixture of THF and water.

6.2 : Future scope

PNTI is a completely new breed of molecule which may pave the way for new kinds of biological molecules by way of synthetic modification or optical materials due to their strong absorption in the visible region. Modification of PNI is still quite in its infant stage and it is hoped that this thesis is a small contribution in understanding the dye chemistry behind PNI, and the effect substitution may play on its applicability in the scientific world. Supramolecular rearrangement via addition of dual additive will help in establishing systems that can change their properties depending on time and portion control of additive. In addition to this, tunable self-assemblies of these dyes may find applications as smart materials. J-aggregates are already being looked into in research as functional materials such as artifical light harvesting systems, thus this study is our potential contribution in this regard.

References

1. Nathan, R.A.; Schwerzel, R.E.; Adelman, A.H.; Wyant, R.E., U.S. Patent 4004572. **1977.**
2. Zhang, S.; Chen, X.; Fan, J.; Ren, A.; *Organic Electronics*, **2015**, 24, 12-25.
3. Das,R.J.; Mahata, K.; *Org. Lett*., **2018,** 20, 16, 5027-5031.
4. Mellerup, S.K.; Wang, S.; *Chem. Soc. Rev.*, **2019**, 48, 3537-3549.
5. Nawn, G.; Oakley, S.R.; Majewski, M.R.; McDonald, R.; Patrick, B.O.; Hicks, R.G.; *Chem.Sci*., **2013**, 4, 612-621
6. Chen, P.-Z.; Niu, L.-Y.; Yang, Q.-Z.; *Coord. Chem. Rev*. **2017**, 350, 196-216.

7. a) Loudet, A., Burgess, K.; *Chem. Rev*. **2007**, 107, 4891-4932. b) Ulrich, G.; Ziessel, R. Harriman, A. *Angew. Chem., Int. Ed*. **2008**, 47, 1184-1201. c) Kowada, T.; Maeda, H.; Kikuchi, K.; *Chem.Soc. Rev.* **2015**, 44, 4953-4972.
8. a) Kubota, Y.; Tanaka, S.; Funabiki, K.; Matsui, M.; *Org. Lett.* **2012**, 14, 4682-4785 b) Wu, Z.; Sun, J.; Zhang, Z.; Yang, H.; Xue, P.; Lu, R.; *Chem. Eur. J.* **2017**, 23, 1901-1909 c) Yu, Z.; Wu, Y.; Xiao, L.; Chen. J; Liao, Q.; Yao, J.; Fu, H.; *J. Am. Chem. Soc.* **2017**, 139, 6376-6381 d) Tan, G.; Schrader, M.L.; Daniliuc, C.; Streith-Kalthoff, F.; Glorius, F.; *Angew. Chem., Int. Ed*. **2020,** 59, 21541-21545
9. a) Sorrenti, A.; Leira-Iglesisas, J.; Markvoort, A.J.; de Greef, T.F.A.; Hermans, T.M.; *Chem. SOC. Rev*. **2017,** 46, 476-5490 b) Matern, J.; Dorca, Y.; Sánchez, L.; Fernández, G.; *Angew Chem., Int Ed*. **2019**, 58, 16730-16740
10. de Greef, T.F.A.; Smulders, M.M.J.; Wolffs, M.; Schenning, A.P.H.J.; Sijbesma, R.P.; Meijer, E.W.; *Chem. Rev.* **2009**, 109, 5687-5754 b) Wehner, M.; Würthner, F.; *Nat. Rev.* **2019**, 4, 38-53
11. Korevaar, P.A.; George, S.J.; Markvoort, A.J.; Smulders, M.M.J.; Hilbers, P.A.J.; Schenning, A.P.H.J.; de Greef, T.F.A.; Meijer, E.W.; *Nature* **2012**, 481, 492-496.
12. Aliprandi, A.; Mauro, M.; de Cola L.; *Nat. Chem.* **2016**, 8, 10-15
13. Herkert, L.; Droste, J.; Kartha, K.K.; Korevaar, P.A.; de Greef, T.F.A.; Hansen, M.R.; Fernández, G.; *Angew. Chem. Int. Ed*. **2019**, 58, 111344-11349
14. Wehner, M.; Röhr, M.L.S. Stepanenko, V.; Würthner, F.; *Nat Commun* **2020**, 11, 5460-5469.
15. Greciano, E.E.; Calbo, J.; Orti, E.; Sanchez, L.; *Angew. Chem., Int. Ed.* **2020**, 59, 17517-17524
16. Morita, S.; Yoshimura, T.; Matsuo, J; *Green Chem.*, **2021**, 3, 23, 1160-1164
17. Reddy, V.N., Ramana, C.V., *Chem. Commun*., **2013**,49, 9767-9769
18. Leznoff, C. C., Hayward, R. J., *Can. J. Chem*. **1971**, 49, 3596–3601.
19. Das, R.J., Mahata, K., *Soft Matter*, **2019**,15, 5282-5286
20. Kartha, K.K., Allampally, N.V., Yagai, S., Albuquerque, R.Q.,Fernandez, *G, Chem. Eur. J.* **2019**, 25, 9230-9236.
21. Ooyama, Y., Koji, U., Kamimura, T., Ozako, S., Kanda, M., Koide, T., Tani, F.,,*RSC Adv*.**, 2016**,6, 16150-16158
22. a) N.V. Moskalev, M.I. Tartynova, *Russ Chem Bull* **1998**, 47, 1603–1604 ; b) H. Hattori, S. Yokoshima, T. Fukuyama, *Angew. Chem. Int. Ed.* **2017**, 56, 6980.
23. a) Ohwada, T.; Ohta, T.; Shudo, T.; *J. Am. Chem. Soc.* **1986**, 108, 3029-3032, b) Ohta, T.; Shudo, K.; Okamoto, T.; *Tetrahedron Lett.* **1984**, 325
24. Prakash, G.K.S.; Yan, P.; Török, B.; Otah, G.A.; *Catal. Lett*, **2003,** 87, 109
25. Rhodes, S., Liang, W., Wang, X., Reddy, N.R., Fang, J., *J. Phys. Chem. C* **2020**, 124, 11722−11729

.

List of Abbreviations

General terminology

NMR	Nuclear magnetic resonance
FESEM	Field emission scanning electron microscope
HRMS	High resolution mass spectrometry
IR spectroscopy	Infra -red spectroscopy
Uv-vis	Ultra violet and visible spectroscopy
XRD	X-ray diffraction
HOMO	Highest occupied molecular orbital
LUMO	Lowest unoccupied molecular orbital
AIEE	Aggregation induced enhanced emission
DSSC	Dye sensitized solar cell
NIR	Near infra-red
AFM	Atomic force microscopy
VT	Variable temperature

Mathematical Symbols

λ	Wave length
ϕ_F	Fluorescence quantum yield
ϵ	Molar extinction co-efficient
f_w	Volume fraction of water
f_{MCH}	Volume fraction of methylcyclohexane

Units

V	Volt
eV	Electron Volt
µm	Micro meter
nm	Nano meter
ppm	Parts per million
Hz	Hertz
K	Kelvin
^oC	Degree Celsius

µM	micromolar

Chemical symbols

DCM	Dichloromethane
THF	Tetrahydrofuran
DMF	N,N'-dimethyl formamide
MeCN	acetonitrile/methyl cyanide
DCE	1,2-dichloroethane
MCH	methylcyclohexane
DMSO	dimethyl sulfoxide
EtOH	ethanol
$CHCl_3$	Chloroform
^{t}BOC	tert-Butyloxycarbonyl
Bu	Butyl
PNI	*peri*-naphthoindigo
PNTI	*peri*-naphthoisatogen
TFA	Trifluoroacetic acid

Chapter 1

Introduction

❖ 1.1 Foreword

Peri-annulation of naphthalenes is an important and relevant scientific domain that is being studied since the last decades. This can give rise to a multitude of molecules- the most common of which are naphthalene monoimide, naphthalene diimide and perylene bisimide. Some relatively less studied molecules of this class include an amide group appended to the *peri*-positions of naphthalene, which includes naphthalene monoamide or naphtholactam, and naphthalene bisamides. In this similar vein, perimidiniums also fall into the category of *peri*-functionalized naphthalenes, so would naphthisatins, the isatin analogue of naphthalene, mostly, found in plant alkaloids. *Peri*-functionalized naphthalene dyes have been an integral part of the scientific field. Many organic electronics such as dye-sensitized solar cells,[1] organic semiconductors,[2] energy storage materials,[3] liquid crystalline polymers[4] and such are constituted by naphthalene dyes; as are biologically significant molecules such as drugs and antimicrobial agents. The most prevalent *peri*-annulation for scientifically important dyes are represented in Fig 1. 1. The importance of *peri*-annulated naphthalene molecules is something that cannot be exagerrated. Besides the individual properties of these molecules in their monomeric forms,depending on solvent polarity, many of these dyes stack among themselves or with other molecules of different species, and may give rise to adaptive behaviour, thus resulting in the formation of smart materials.[5] These are respectively termed as self-assembly and co-assembly. Those smart materials display the ability to exhibit different properties depending on the environment, and in some cases minute changes in this environment can bring about a huge change in the stacking of these dye monomers, thus providing a completely new arrangement. This new arrangement then leads to a unique property exhibition, quite different from its original supramolecular form. These factors that induce change may include temperature, pH, solvent polarity or addition of a new molecule. Thus these materials can essentially function as sensors, or even biological delivery or

imaging [6]systems, considering biological procedures operate at different pH, each separate process within the biological domain meticulously unique to themselves.

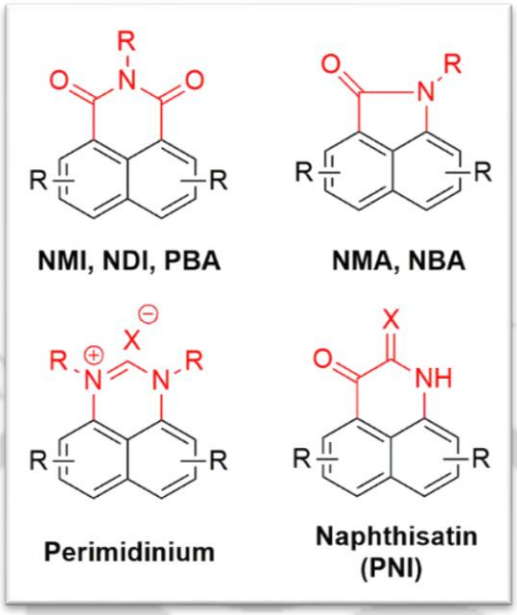

Fig 1. 1 Some important examples of *peri*-annulation in relevance to dye chemistry in scientific context.

❖ 1.2 Importance of dye

To proceed further, the term dye must be defined. A dye is any molecule that absorbs strongly in the visible region; from ~400 nm to ~700 nm and thus exhibits a strong colour to the naked eye. Dyes are an important part of the historical and scientific aspect of the world. Ranging from edible food colourants, paints, textiles to many other such applications, dyes have always fascinated the curious minds of this world.[7] Dyes range from the organic and natural kind to the synthetic kind, which are prepared by scientists and researchers upon the observance of scope for improvement. Dyes are also versatile in that they can be either organic or inorganic, such as organic dyes containing chromophores dealing with the visible region, where charge transfers occur within the same molecule or metal complexes in which various kinds of charge transfer are possible such as metal to ligand, ligand to metal, metal to

metal and such. The main reason for the observance of colour is the excitation of electrons, as a result of energy transfer from visible light. This excitation also manifests itself into utilization in the field of science and research, such as transfer of electrons in semiconductors. Absorption of light in the visible region by these dyes provides an excellent opportunity to prepare electronic materials such as dye sensitized solar cells.[8] As of recent times, most of the *peri*-annulated naphthalene do come under the broad definition of naphthalene dyes. Many of the common and well known dyes of different chemical species include indigo, acid black, reactive red, direct yellow 11, the common species associated with organic dyes and self assembly include coumarins, indigoids, pthalocyanins, naphthalene imide species etc. For the current thesis, a discussion of the different dye strcutures prevailing only in organic dyes are important, as metal based dyes are a completely different topic irrevelant to the core discussion of this work. Below are presented some organic dyes classified according to their core chromophores from which they are derived, however it is important to remember that these are just the prominent ones, and a multitude of other structures too are present in known literature and scientific domain.[9]

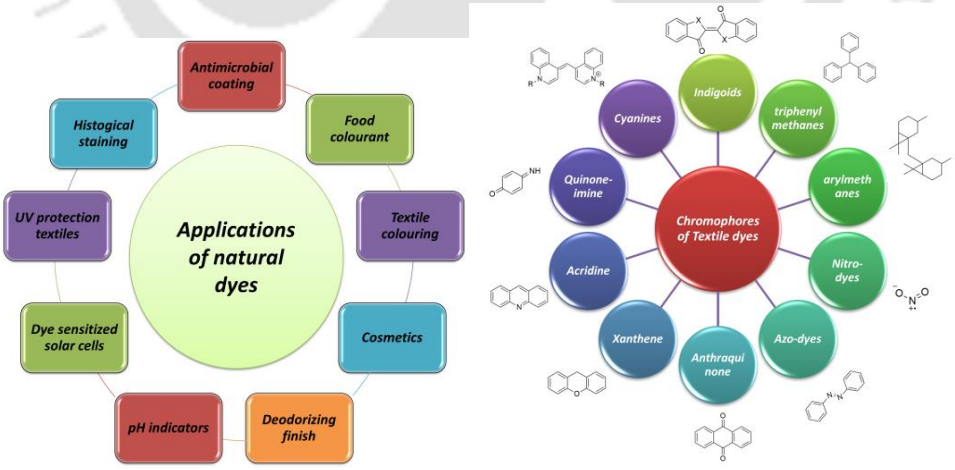

Fig 1. 2 Some important applications of dyes **(left)** and classification of dyes based on the structure of their chromophoric core. **(right).**

❖ 1.3 Indigo

Indigo is quite an important molecule when a discussion about dyes in the scientific field is being held. It consists of two benzene rings with a cross-conjugated cromophore sandwiched in between, consisting of a donor and acceptor. This versatility of this dye upon functionalization lends to its utilization in various areas, starting from household applications such as food colouring and clothing dye to organic electronics such as semiconductors and solar cells.[10]

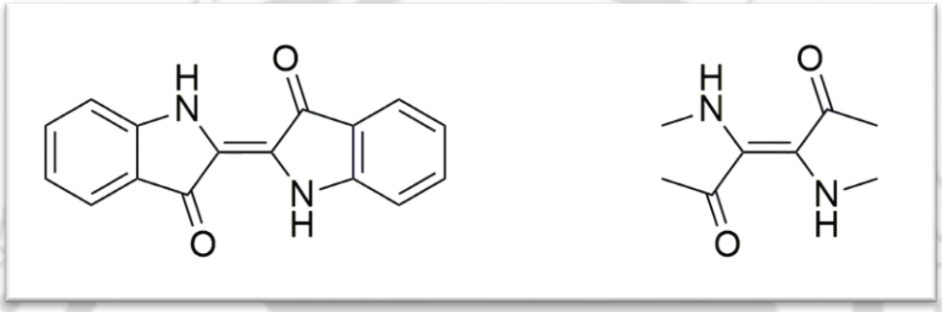

Fig 1. 3 Representation of indigo **(left)** and the H-Chromophore **(right).**

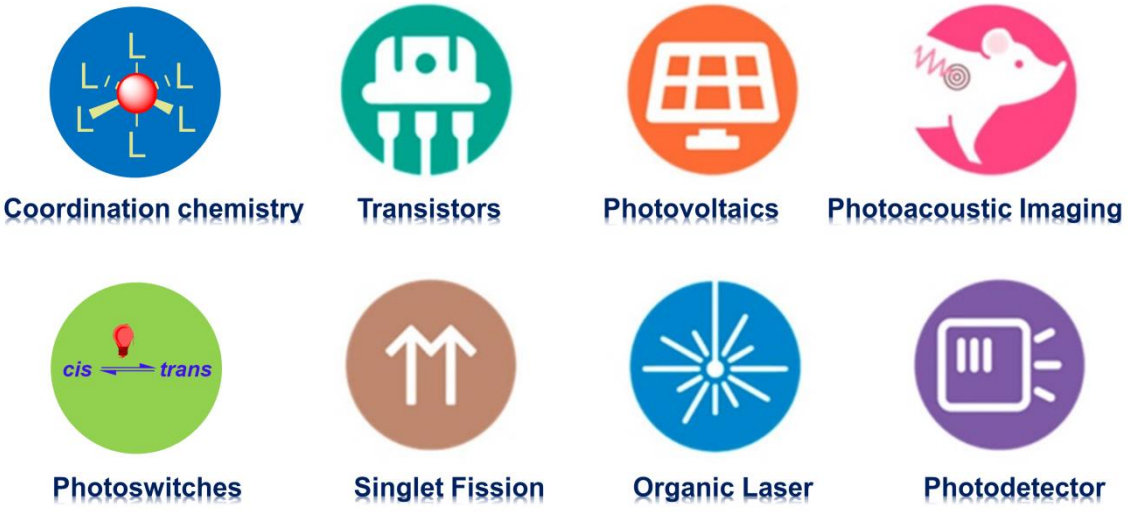

Fig 1. 4 Some known uses of indigo in today's scientific world.

❖ 1.3.1 Chromophore modification of indigo

Derivatives of indigo include changes at the chromophore, including bay-annulation and even replacement of the chromophoric carbonyl group with amine groups, producing Nindigo. As evidenced from previous literature, substitution at the chromophore can cause disruption in the planar structure, such as replacement of the NH protons with bulky groups, or further reinforcement of the planar structure through complexation or bay-annulation. Each of these substitutions have their unique consequences for the dye with distinct differences in their optical and electronic properties. N,N'-disubstitution is a convenient way to achieve cis-trans photoconversion which was not possible in case of indigo due to NH-CO hydrogen bonding, causing restriction in bond rotation. N,N-dimethylindigo was first reported in 1912 by Friedlander,[11] and a bathochromic shift was observed in its absorption maxima due to twisting around the C=C bond. N,N'-dimethylindigo was shown by Weinstein and Wyman, to possess considerably larger single bond character compared to indigo. The absorption maxima of this derivative in a variety of solvents were recorded, such as isoooctane, CCl_4, $CHCl_3$, Me_2CO, C_6H_6; absolute,95% and 30% EtOH, and also concentrated HCl. The wave length of the visible absorption band of N,N-dimethylindigo is strongly dependent on the nature of the solvent; hydrophillic solvents, in particular, cause a strong bathochromic shift.[12]

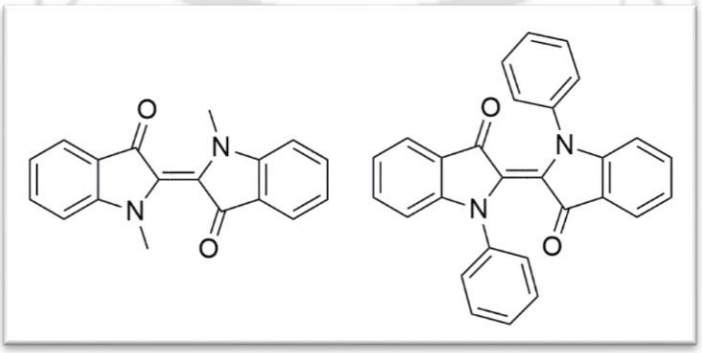

Fig 1. 5 first instances of N,N-substituted indigo

N,N'-diphenylindigo too was first reported by Friedlander in 1922, and basic absorption properties were measured.[13]

N,N-diacyl and N-acyl indigoes were prepared by several groups by different methods which are relatively simple, an act of boiling indigo in the corresponding acyl chloride, or the anhydride in pyridine.[14] A work in 1965 obtained N,N-oxalylindigo by treatment of indigo with oxalyl chloride, which adopts a cis-form and is bridged by two carbonyl groups. Meticulous observation by Wyman and Zenhausern showed that this formation proceeds though a trans-form of N,N'-dioxalylindigo.[15] Studies showed that diacylation with bulky groups, produced large bathochromic shifts due to perturbation in electronic structure.

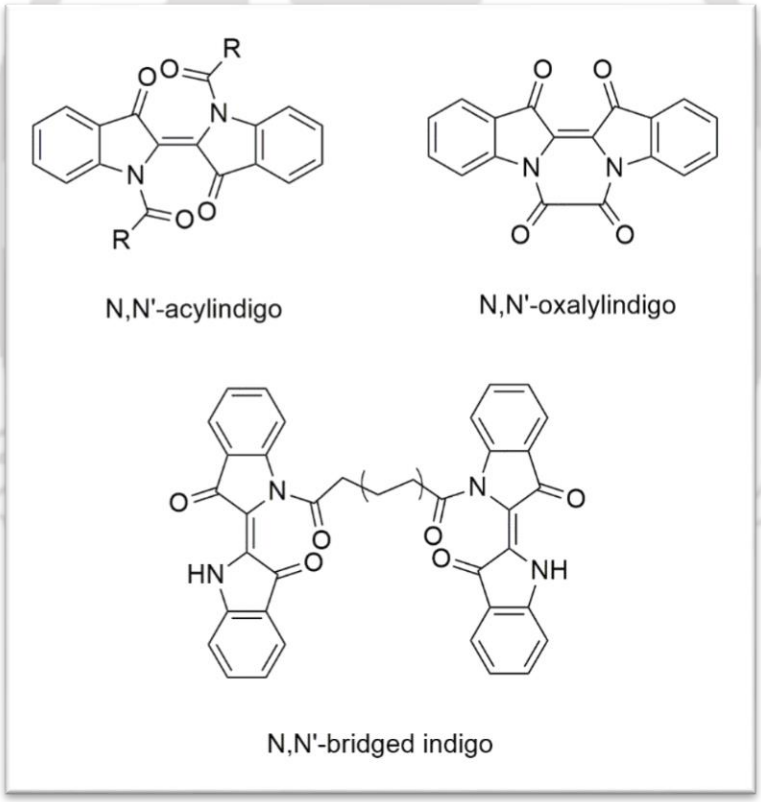

Fig 1. 6 Examples of N,N'-substituted indigo prepared via treatment with acyl groups.

One of the first intramolecuar bridging through the use of a long alkyl chain was also reported in 1984, where azelaoyl and sebacoyl dichloride were used. In the same report,

intermolecular bridging was also achieved.[16] Another work in the same year also involved a long chain acylation, with myristoyl chloride, with a 13-C alkyl chain. This derivative was studied for its photochemical conversion rates in hydrocarbon solvents. Preparation of N-aryl and N,N-diaryl indigos were carried out in 2003 by refluxing the corresponding aryl iodide or bromide in o-dichlorobenzene, and photophysical studes were carried out on them by Hitoshi *et al*. t-boc indigo was first reported in 2013 by Sariciftci *et al* as a facile protection-deprotection agent in order to obtain semiconductor thin films.[17] This particular derivative turned out to be quite a popular choice for introducing indigo into a molecular structure and producing an electroactive polymer, which can be cleaved later according to requirement through application of heat. Li *et al* prepared indigo based donor-acceptor conjugated polymers with N,N'-disubstitution being 2-hexyldecanoyl and 2-octyldodecanoyl acyl groups.[18] In 2016, an N,N'-disubstituted dibromoindigo was found as a good photoinitiator among a variety of dyes studied for the radical polymerization of acrylate and/or epoxide monomers. Thus in conclusion, substitution at the chromophore has the ability to bring about distinct changes in the photophysics of the original dye, and this kind of substitution is utilized for various purposes. N,N'-disubstitution brings forth the potential of indigoids to function as red-light photoswitches.[19]

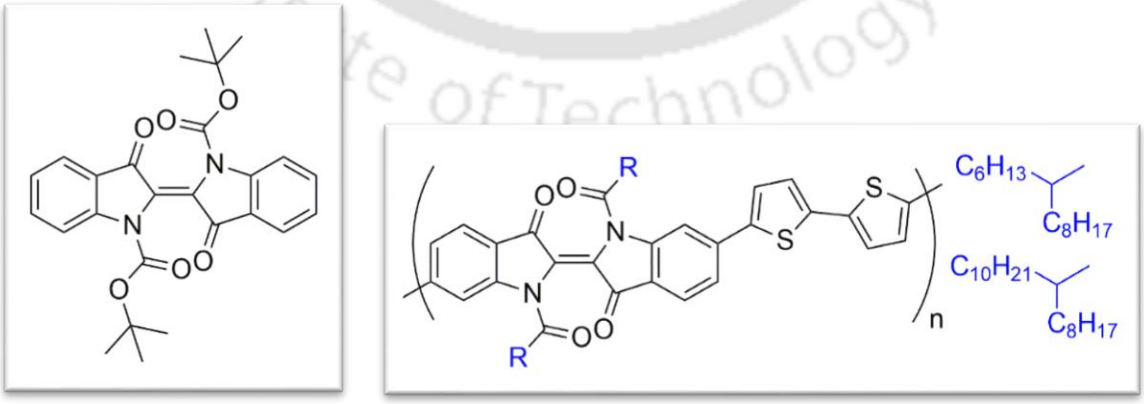

Fig 1. 7 t-boc indigo **(left)** and example of N,N'- disubstituted indigo employed in electronic polymers **(right)**

❖ 1.3.2 Ring substitution in indigo

Ring substitution of indigo is also a significant contributor to the versatility of indigo, and in conjunction with chromophore substitution, plays a pivotal role in fabrication of organic electronics. Substitution on the benzene rings affects the original dye through various ways, ranging from simple benefits such as solubility to significant impacts on the photophysical properties and redox behaviour, with effects even on the stacking of molecules. A perfect example of indigoes finding good use on being made water soluble by ring substitution is the molecule indigo carmine (Fig 1. 8). This dye, available as a sodium salt, finds use as food colourant, pH indicator and also a biological staining and diagnostic dye. Ring halogenated indigoes are potential candidates for semiconductor synthesis due to low toxicity and stability in ambient conditions. These indigoes allow for coupling through the halogens to form semiconducting polymers and in some cases donor-acceptor units for semiconductors. Liquid crystalline motifs have also been known to be prepared utilizing ring substituted indigo. Troshin et al examined the performance of ring functionalized indigoes- ranging from halogens to thiophene coupled indigoes (Fig 1. 9), in organic electronics.

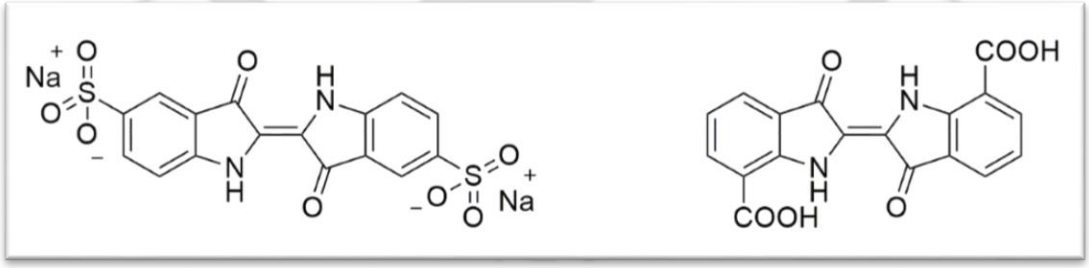

Fig 1. 8 examples of water soluble indigoes – indigo carmine (**left**) and indigo-n,n'-carboxylic acid. (**right**)

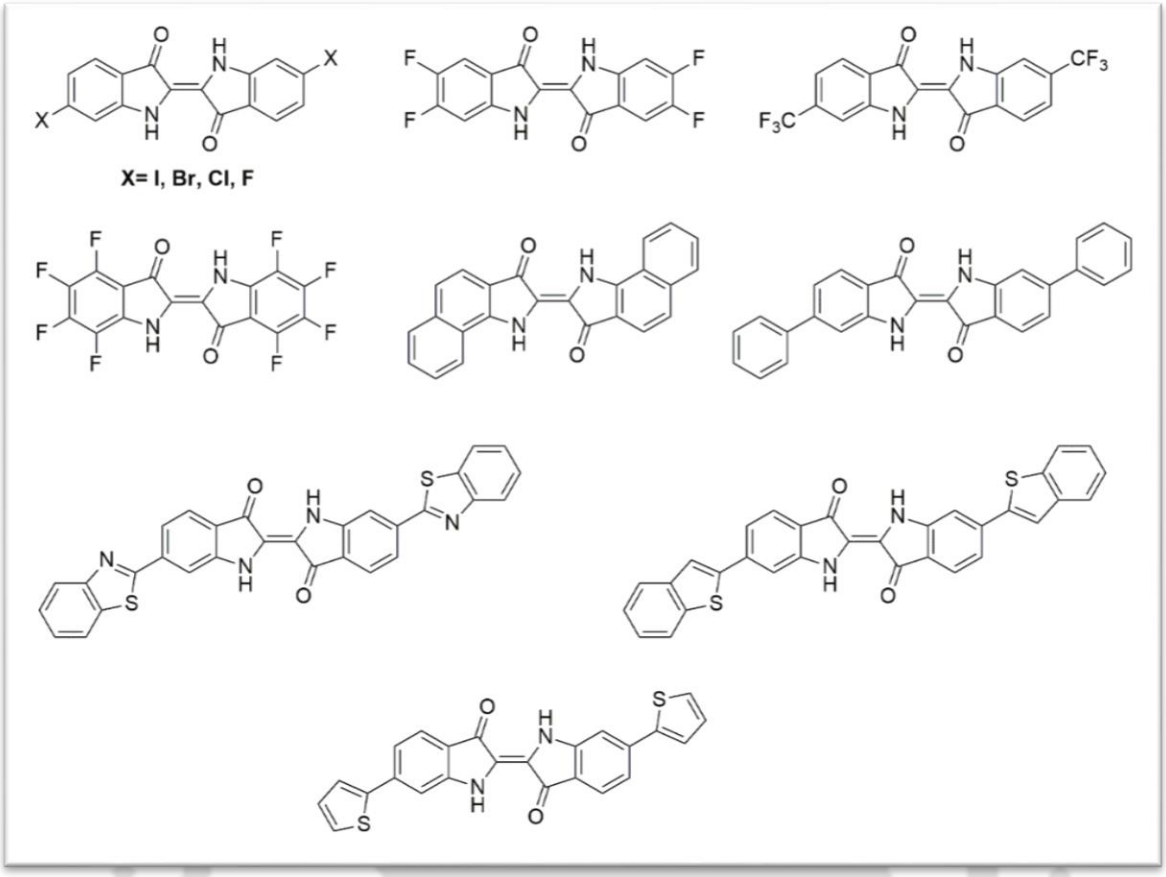

Fig 1. 9 examples of ring substituted indigoes studied for their performance in electronics.

❖ 1.3.3 Indigoids as ligands

Considering the structure of the chromophore of indigoids; indigo and nindigo-where the carbonyl groups have been replaced by amine groups, are also known to function as ligands, and form complexes with various metals.[20] The metals include Pd, Ru, Au, Zn, Cu, Ni and such. The binding occurs through bidentate and monodentate schemes via –NH and carbonyl dentacity, or even 1:2 complexes of metal:ligand, and also as cis indigo via N,N or O,O bonding. Below is the representation of some binding mechanisms for indigoids depending on the metal or the oxidation state of the metal.

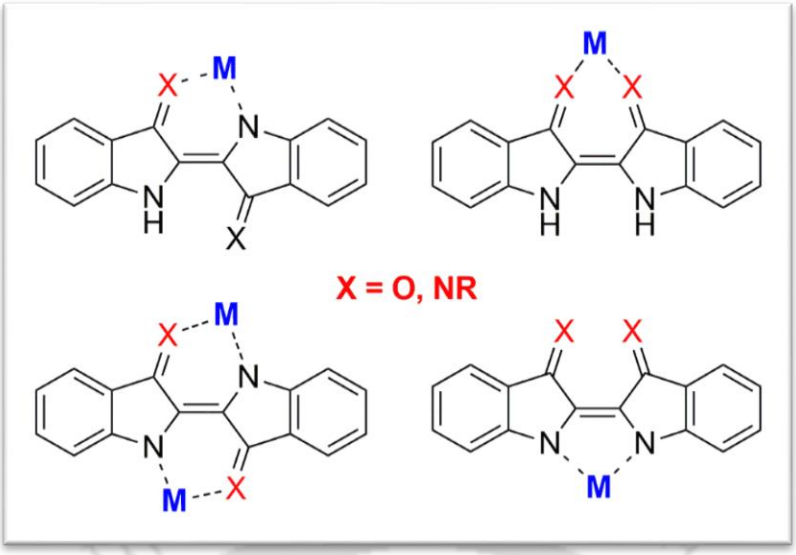

Fig 1. 10 Binding of metals to indigo and nindigo

❖ 1.4 *peri*-naphthoindigo

Peri-naphthoindigo, a novel molecule that is the naphthalene analogue of indigo, was proposed by R.A.Nathan in a patent in 1977[21] and theoretical research was done on its di-keto indigo-like structure by Zhang *et al*.[22] Both have proposed some remarkable properties that has potential in the organic electronics industry. However, the synthesis of this molecule was a challenge, and it was finally prepared by Mahata *et al.* in 2018.[23] The currently determined structure of PNI consists of a cross-conjugated donor acceptor moiety, sandwiched between the 1,8-positions of naphthalene. Unlike its benzene counterpart, indigo, PNI exists in a mono-enol form (Fig 1. 11). PNI exhibits better solubility in organic solvents, along with a bathochromic shift in absorption and emission maxima and also increased emission intensity. PNI also displays halochromism in response to a decrease in pH. PNI engages in supramolecular stacking on either ends of the solvent polarity spectrum. PNI can engage in both self-assembly, and also co-assembly on interaction with different molecular species, in non-polar solvents such as hexane, as examined by Mahata *et al*. According to previous

report, PNI has the ability to exhibit ehanced emission upon aggregation, and also install the same on another molecule that is incapable of such a phenomenon by itself.[24] We aim to delve into the effect caused by any substitution either in the chromophore or on the naphthalene ring and subsequent changes in their applicability. Changes that we looked forward to, include, better solubility, increase in emission efficiency, shift of emission towards NIR region to take advantage of the bio-optical window, better performance in organic electronics and such.

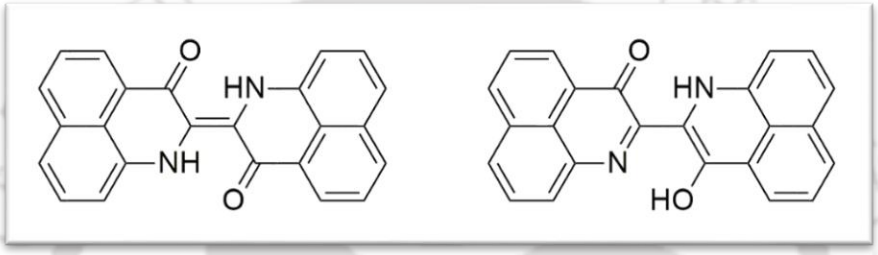

Fig 1. 11 proposed diketo form of PNI **(left)** and mono-enol form of PNI that was obtained **(right).**

❖ 1.5 Effect of boron complexation to dye

One example of chromophoric modification is boron difluoride complexation. Attachment of a boron moiety ususally occurs via an anion which can be generated from either a hydroxyl group or an amine group; and the boron also accepts a lone pair of electron via a coordinate bond due to its Lewis acidity. This essentially generates a closed system or a ring thus hindering rotation in any freely (single bond containing) or semi freely rotating systems (completely free rotation is hindered through steric or repulsive action). Boron difluoride complexes of dyes have gained quite a popularity among researchers due to their complexation properties, which endows upon a molecule various other features such as increased photoluminescence and change in chromophoric attributes.[25] Many prominent studies draw out a host of important relations between the supramolecular assembly of such

complexes and their resultant photophysical properties.[26] A study by Tang et al in 2009 discovered a complex relation between intramolecular rotation and emission yield in BODIPYs, and supramolecular aggregation causing the dyes to emit efficiently. BODIPYs are one of the most common types of boron complexes that have been studied in exhaustive detail. A significant number of different kinds of boron complexes are known to exhibit aggregation induced emission or crystallization induced emission. Boron β-ketoiminate complexes, first prepared in 2013, too exhibit AIE, in contrast to boron β-diketonate complexes, which exhibit ACQ. There are also numerous reports where the fluorine atoms are substituted by other groups, and these changes have a substantial impact on the photophysics of the dye.

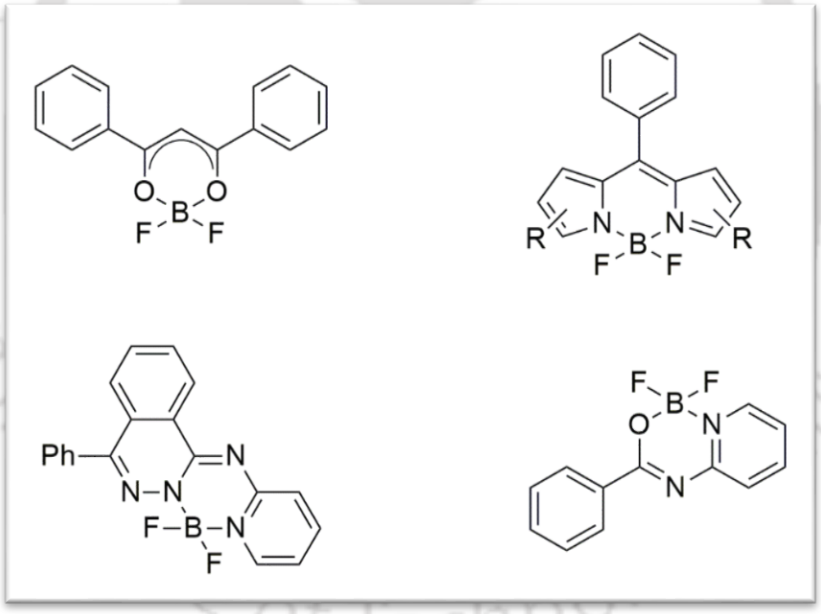

Fig 1. 12 Some important examples of boron difluoride coordination complexes with organic molecules.

This manifests itself as adaptive luminescence or luminescence under different environmental conditions and also smart and adaptive supramolecular stacking. Adaptive and pathway dependent supramolecular aggregation and stacking in solid state is a well-known feature of such complexes.[27] This can manifest itself as either polymorphs where the molecule is packed

in different stackings in solid state, or supramolecular polymorphs, where monomers can change between aggregate morphologies at similar polarity conditions via treatment with any physiological factor. A respective example would be an azomethine-boron complex which settles into two forms dependent on crystallization from different solvents;[28] and a BODIPY dye that aggregates into two different forms depending on H-bonding. [29] Such polymorphs of boron complexes are already reported. PNI being a novel molecule, and the ligand capacity to allow for boron complexation; is a perfect candidate for such studies, due to an added benefit of being an ambipolar molecule. Boron complexes of nindigo and indigo have been already prepared in previous literature.[30] However, their self assembly properties have not been studied in detail. Redox behaviour have been studied for boron difluoride complexes of indigo, however such a study for indigo is restricted by restriction in solubility of these complexes.

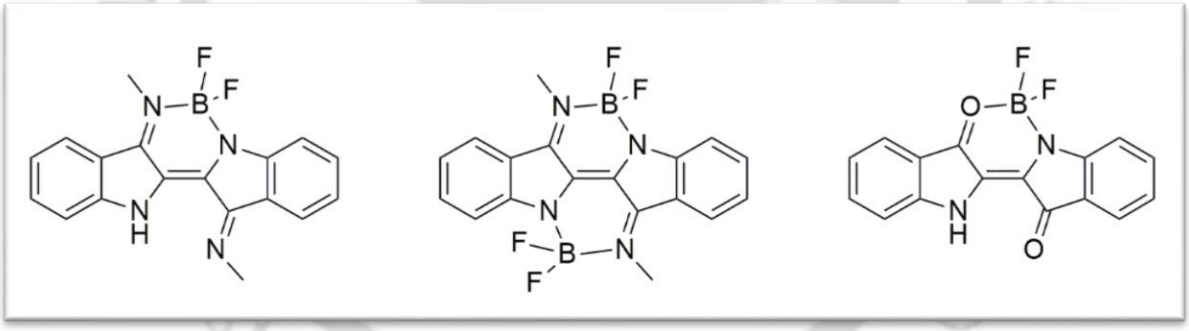

Fig 1. 13 boron complexes of indigoids reprted in previous literature

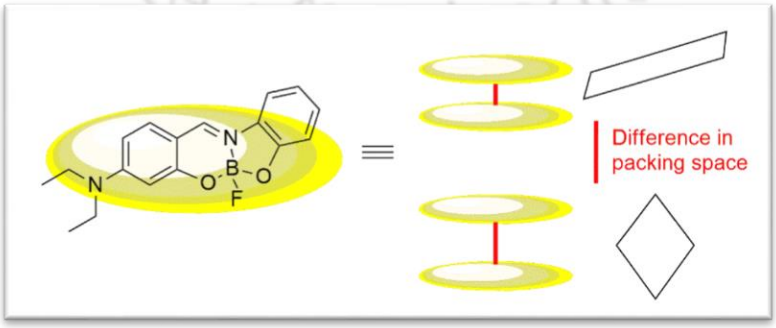

Fig 1. 14 Example of a boron complex exhibiting polymorphism in crystal.

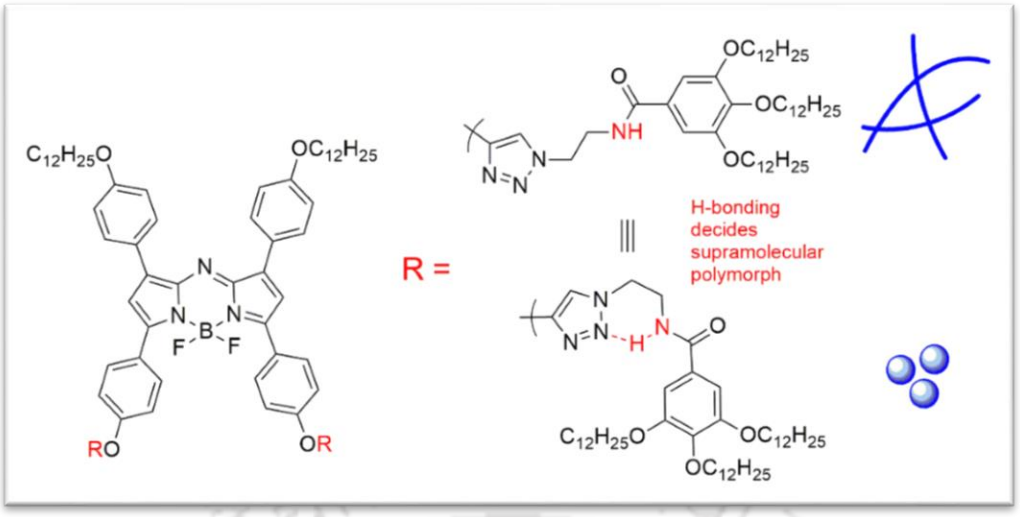

Fig 1. 15 Example of a BODIPY complex exhibiting supramolecular polymorphism.

❖ 1.6 What is self-assembly ?

Since the term self-assembly has already been brought up multiple times, and will be repeatedly mentioned in the upcoming sections, it is very important to delve into slight detail about the world of supramolecular chemistry. Self-assembly, in supramolecular chemistry, denotes the process that a system of disorganized molecules undergoes, to avoid a solvent environment via interaction with another molecule of its own structure and chemical makeup, ensuring optimum non-interaction of solvophobic groups; long alkyl chains are averse to polar solvents, hydroxyl groups are repulsed by non-polar solvents and so on.[31] Self-assembly, or even co-assembly, has a very important consequence in which if a molecule is susceptible to rotation about a single bond, aggregation causes the stacking of these molecules, in such a constricted manner that no free movement is allowed, hence no energy is lost in molecular movement through bond rotation, leaving emission the only outlet for the molecule to lose energy upon excitation. This is Aggregation induced Emission, whereby a non-emissive molecule may start fluorescing in aggregates.[32] Below a very simplistic representation of restriction in bond rotation via the action of self assembly is provided (Fig 1. 16).

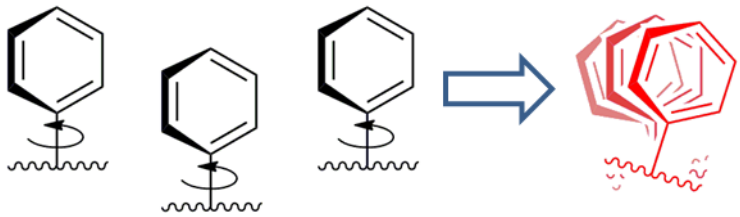

Fig 1. 16 Simplistic reprentation of restriction in bond rotation via aggregation, curvy bonds indicate molecular fragments.

Stacking also causes chromophores of different molecules of similar species to interact with each other, leading to several other consequences, such as relaxation or deactivation of the fluorescing entity, resulting in aggregation caused quenching. An simple example of such would be an emissive molecule dependent upon a donor-acceptor charge transfer interaction for emission. If such a molecule is forced into a situation such that the donor lone pair or the acceptor group is involved in extensive hydrogen bonding, resulting in the disruption of the relation. A highly interesting topic is the control on the pathway through which the molecules come together to form the aggregate, i.e. the amount of influence a single factor in the ambient environment may have in the shape of the aggregate formed and distinction between the kinetic and thermodynamic path. This type of energy landscapes, through which a molecule may pass to access thermodynamic equilibrium aggregate systems are prevalent in nature, however artificial systems replicating such adaptive behaviour are fascinating to work on.[33] Morphology control on the molecular self-assembly through intelligent substituent design provides the opportunity for preparation of materials which respond extraordinarily to external stimulus or stimuli, thus allowing for use as molcular machines, rotors, self-healing gels, adaptive luminogens and such. Numerous examples of such responsive materials can already be found in previous literature uptil recently,[34] and thus as is seen, the demand for newer materials with better scope for utilization is never ending and the research into such materials is being regularly pursued with vigour. Primary interactions that dictate self-

assembly are hydrogen bonding (both intra and intermolecular), π-π stacking of aromatic rings and shielding of groups disfavoured by the solvent of choice, however some other mechanisms exist too such as induced dipoles among molecules or electrostatic interactions.

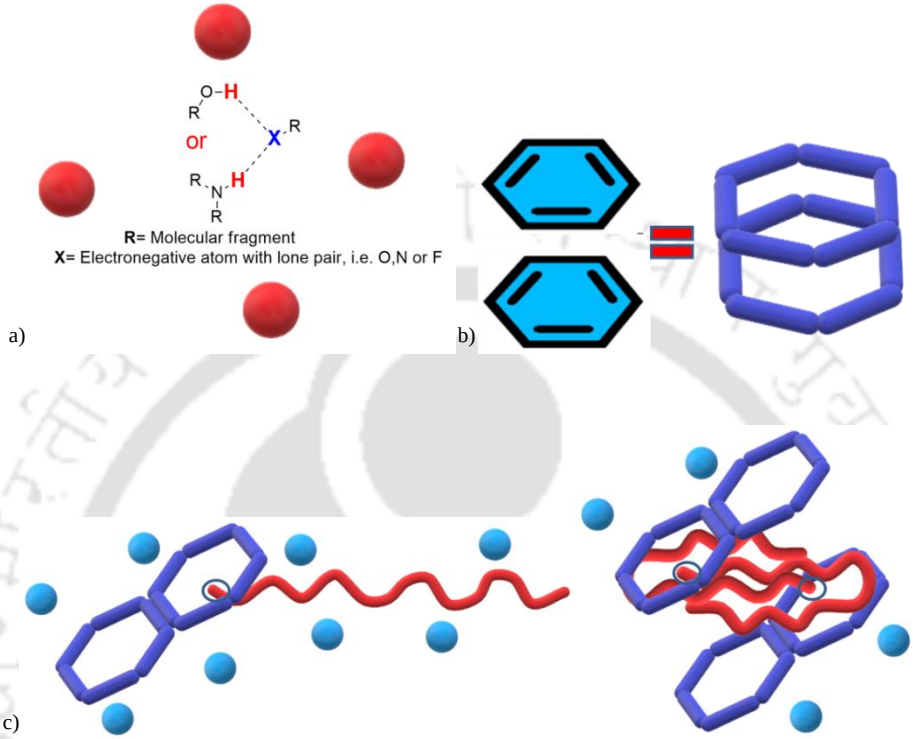

Fig 1. 17 Some primary non-covalent intractions dictating self-assembly a) hydrogen bonding b) π-π stacking c) shielding

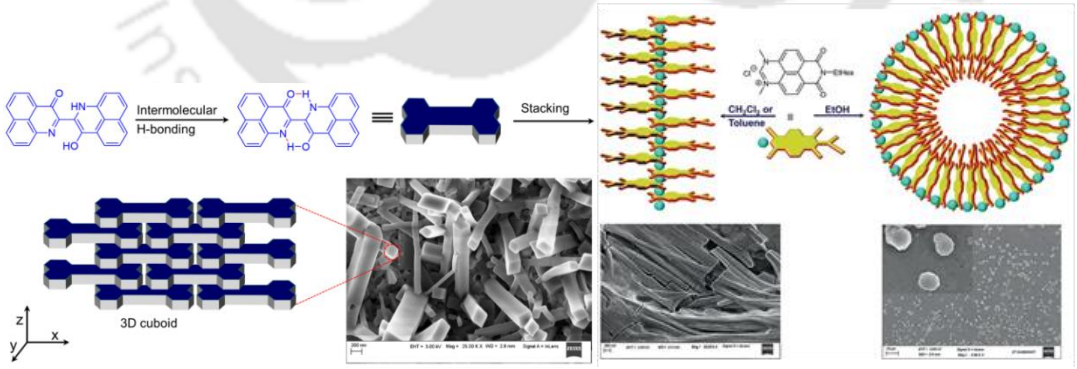

Fig 1. 18 Representation of how self-assembly gives rise to various morphologies depending in interactions.

❖ 1.7 Isatogens – importance and synthetic relevance

Another field of study we have embarked upon is the naphthalene analogue of unsubstituted isatogen, which we have termed as *peri*-naphthoisatogens (PNTI). The main component is the presence of a nitrone in conjugation with a carbonyl enclosed in a cyclic structure. The inspiration for PNTIs are isatogen, which consists of a benzene ring, and a cyclic nitrone sandwiched between the ortho positions of the ring (Fig 1. 19), The presence of a dipolar N-oxide group and the carbonyl group instills activity into the substituted carbon sandwiched between these two groups, thus making the molecule susceptible to chemical attack.

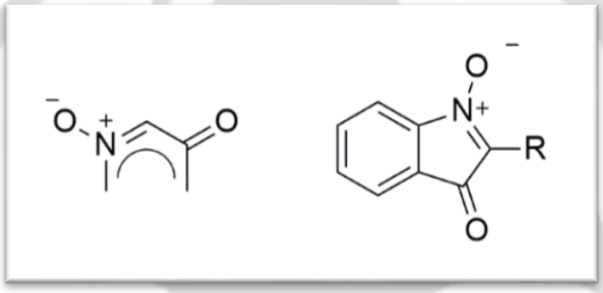

Fig 1. 19 Representation of nitrone **(left)** and 2-substituted isatogen **(right)**.

Isatogens, also known as indolone-N-oxides often function as important intermediates for the synthesis of natural alkaloids and bioactive molecules (Fig 1. 23).[35] Isatogens were first prepared by Baeyer, and are traditionally prepared via acid or base treatment of 2-nitrophenylacetylenes (Fig 1. 20). More recent methods make the use of transition metals as catalysts for the preparation of isatogens.[36]

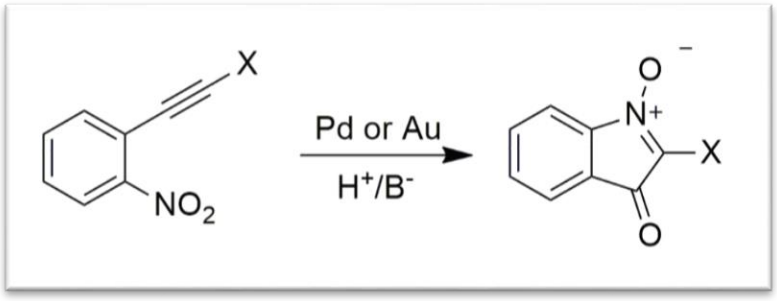

Fig 1. 20 General procedure for synthesis of isatogens.

We are looking into the potential of naphthalene analogues for use as similar or better alternatives. PNTIs consist of the cyclic nitrone attached to the peri-positions of the naphthalene ring. PNTIs are neither well known nor well studied, inspite of the obvious beneficial applications of isatogens. A previous report in 1971 indicated the presence of C2-substituted PNTI (Fig 1. 21), but the field was not explored any further.[37] Presence of a naphthalene ring opens up a chance for better derivatization scope via multiple ring substitution.

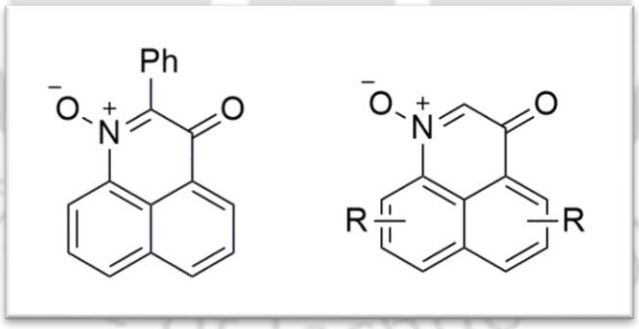

Fig 1. 21 Only known example of PNTI (with substituted C2 position) **(left)** and the target of the present research work **(right)**.

The primary focus was the procurement of the C2-unsubstituted isatogen analogue of naphthalene, as leaving the position unsubstituted is both a challenge, and leaves us with the oppurtunity for late stage derivatization. Thus, leaving the C2 position unsubstituted should

open up the field for new and potentially significant synthetic derivatives, which may find use in pharmacological or biological molecular chemistry, as well as isatogens themselves are pharmacologically active molecules.[38] The naphthalene ring and the C2 position are both open for different varieties of chemical attack, be it nucleophilic, electrophilic or ring substitution aided by the presence of the nitrone, thus allowing for a decent range of functionalization capacity. Following the example of isatogens, some of which are described below[39] in Fig 1. 22, PNTIs too can be subjected to like reactions and thus have the potential to go hand in hand with isatogen research.

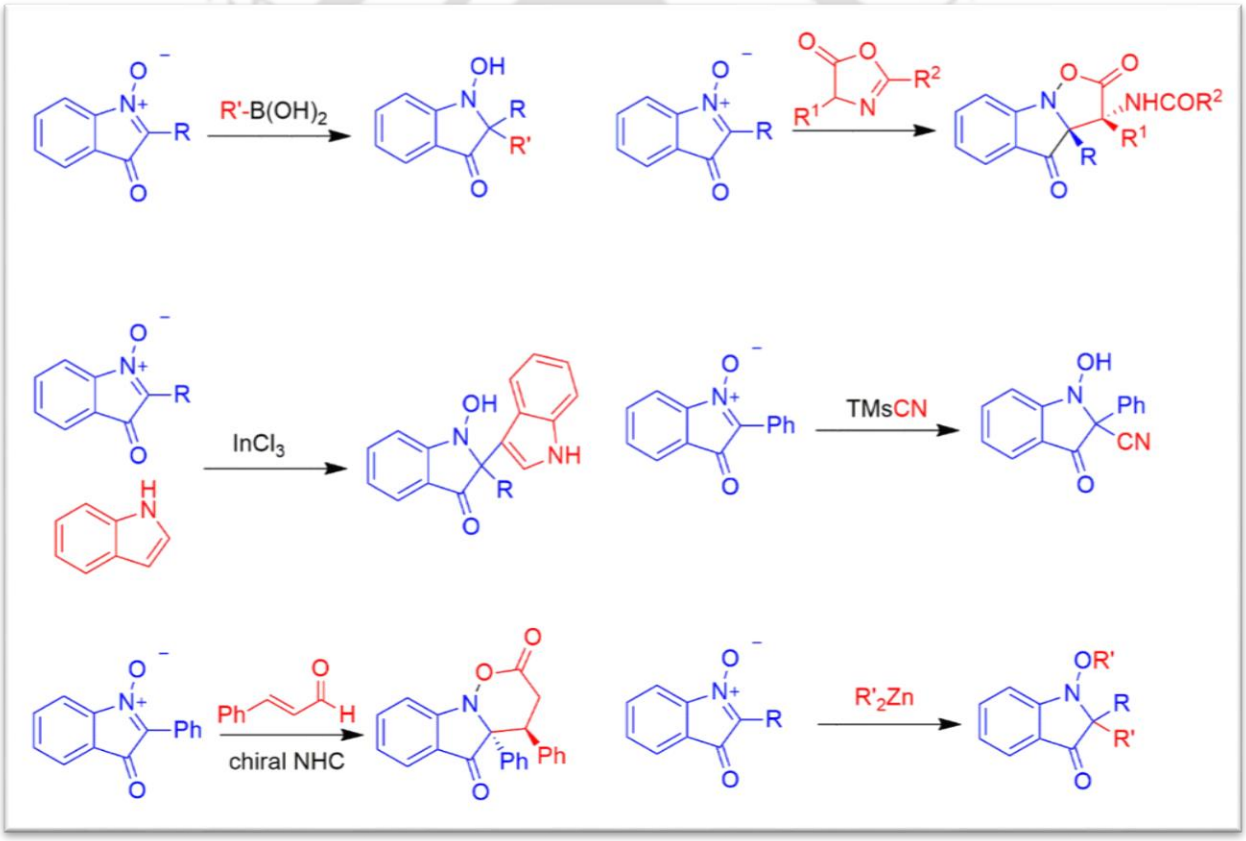

Fig 1. 22 Some important reactions of isatogens involving the C2 position reported in previous literature.

Even 1,3-dipolar and similar cycloaddition is a quite viable strategy for producing derivatives of such molecules, due to the presence of a dipole in the nitrone.[40] Detection of the formation of an isatogen, or in some cases even a nitrone, is achieved via reaction through dipolar

addition due to the ease of such a reaction. Thus, as is known, nitrones and isatogens are quite receptive towards derivatization via dipolar addition[41] and important derivatives are born from such reactions, a result which is hoped to be replicated in the case of PNTIs; observing the obvious similarity of structure between the two molecules.

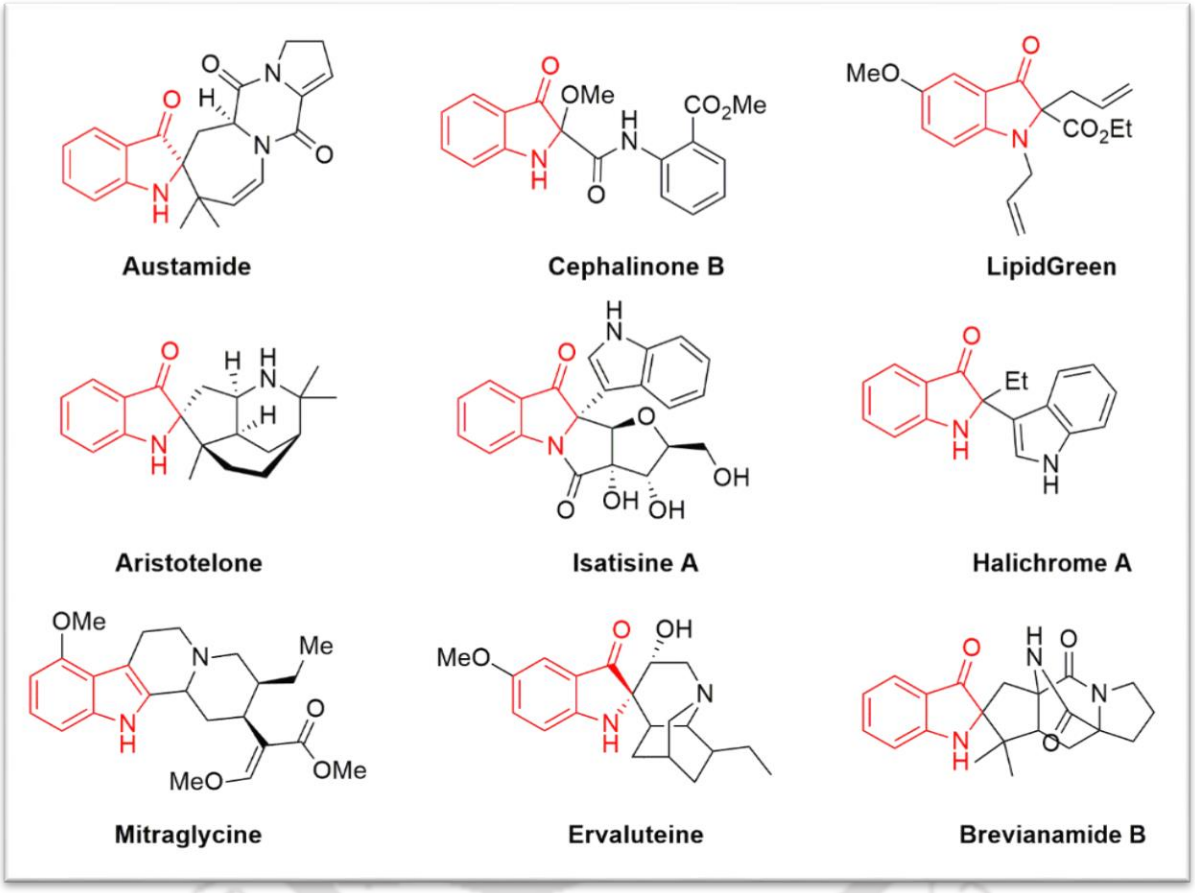

Fig 1. 23 Some examples of biologically significant molecules which proceed through a synthesis route involving isatogens.

As observed in most of the reactions of isatogens, the C2 carbon in PNTI is also assumed to be quite susceptible to several kinds of reagents. On the other hand, in view of the obvious presence of both polar groups such as the cyclic nitrone; and the non-polar groups represented by the aromatic benzene ring, the isatogen molecule can be considered as an ambipolar molecule. As such, the isatogen molecule has the potential to display supramolecular interactions depending on the environment the molecule is subjected to.

However, this approach was never explored in previous literature. This missed oppurtunity is aimed to be rectified upon accomplishment of the synthesis of PNTIs.

❖ 1.8 Objective

The objectives of this thesis can be outlined in three simple parts-

1. Investigate the effect of substitution on the novel dye peri-naphthoindigo and its optical properties.
2. Investigate any novel and fascinating self-assembly properties of substituted PNIs and the role of the substituents in the self-assembly.
3. Attempt for the synthesis and study of a new kind of peri-annulation inspired by isatogen, an important feedstock in the synthesis of bioactive molecules, thus granting a whole new field to work with.

❖ 1.9 References

[1] (a) Sahiner, F.; Ali, A.K.; Denizalti, S.; Kandemir, Z. and Erten-Ela, S.; *New J. Chem.*, **2020**,44, 15526-15537. (b) Bobe S.R.; Gupta A.; Rananaware A.; Bilic A.; Xiang W.; Li J.; Bhosale S.V. and Bhosale S.V., Evans R.A. *Dyes Pigments*, **2016**, 134, 83-90. (c) Jameel, M.A.; Yang, T.C.-J.; Wilson, G.J.; Evans, R.A.; Gupta, A. and Langford, S.J.; *J. Mater. Chem. A*, **2021**,9, 27170-27192, (D) You, X.; Shen, H.; Wu, Q.; Li, Y.; Wu, D. and Xia, J.; *Chem. Asian. J.* **2023**, 18, e202201186

[2] (a) Shukla, D.; Nelson, S. F.; Freeman, D. C.; Rajeswaran, M.; Ahearn, W. G.; Meyer, D. M. and Carey, J. T.; *Chem. Mater.*, **2008**, *20* (24), 7486– 7491. (b) Birajdar, S.S.; Brixi, S.; Rao, P.S.; Bhosale, R.S.; Kobaisi, M.A.; Gupta, A.; Lessard, B.H.; Bhosale, S.V. and Bhosale, S.V.; *ChemistryOpen*, **2021**, 10 , 414 —420. (c) Behera, P. K.; Yadav, K.; Rao, D. S. S.; Pandey, U. K. and Sudhakar, A. A.; *Chem. Asian. J.* **2023**, 18, e202300086.

[3] (a) Song, Z.; Zhan, H. and Zhou, Y.; *Angew. Chem. Int. Ed.*, **2010**, 49, 8444 –8448. (b) Biradar, M.R.; Bhosale, S.V.; Morajakar, P.P. and Bhosale, S.V.; Fuel, **2022**, 310, 122487.

[4] Vishwakarma, V. K.; Roy, M.; Singh, R.; Rao, D. S. S.; Paily, R. and Sudhakar, A. A.; *ACS Appl. Electron. Mater.* **2023**, 5, 2351– 2364.

[5] (a) Kobaisi, M.A.; Bhosale, S.V.; Latham, K.; Raynor, A.M. and Bhosale, S.V.; *Chem. Rev.* **2016**, 116, 19, 11685–11796 ; (b) Roy, T.; Debnath, I. and Mahata, K.; *Synlett* **2024**, 34, 125–129

[6] (a) Choudhury, M.; Das, K. and Das, P.K.; *Langmuir* 2017, 33, 18, 4500–4510. (b)

[7] (a) Chengaiah, B.; Rao, K.M.; Kumar, K.M.; Alagusundaram,M. and Chetty, C.M.; *Int. J. Pharmtech Res.***, 2010**, 2, 144-145. (b) , **2017**, 4, 57-60.

[8] Sharma, K., Sharma, V. and Sharma, S.S.; *Nanoscale Res Lett* , **2018**, 13, 381.

[9] (a) Ferreira, E.S.B.; Hulme, A.N.; McNab, H. and Quye, A.; *Chem. Soc. Rev.***, 2004**,33, 329-336 (b) Yadav, S.; Tiwari, K.S.; Gupta, C.; Tiwari, M.K.; Khan, A. and Sonkar, S.P.; *Results Chem.* **2023**, *5*, 100733.

[10] (a) Qi-yue, Y.; Ting, Z.; Ya-nan, H. *et al. Chin Med*, **2020**, 15, 127. (b) Irimia-Vladu, M.; Głowacki, E.D.; Troshin, P.A.; Schwabegger, G.; Leonat, L.; Susarova, D.K.; Krystal, O.; Ullah, M.; Kanbur, Y.; Bodea, M.A.; Razumov, V.F.; Sitter, H.; Bauer, S. and Sariciftci, N.S.; *Adv. Mater*., **2012**, 24, 375-380. (c) Bouzidi, A.; Yahia, I.S. and El-Sadek, M.S.A.; *Dyes Pigments*, **2017**, 146, p. 66. (d) Pitayatanakul, O.; Higashino, T.; Kadoya, T.; Tanaka, M.; Kojima, H.; Ashizawa, M.; Kawamoto, T.; Matsumoto, H.; Ishikawa, K. and Mori, T.; *J. Mater. Chem. C* **2014**, *2*, 9311– 9317.

[11] Ettinger, I. and Friedlaender, P.; *Ber*., **1912**, 45, 2074

[12] Weinstein, J. and Wyman,G.M.; *J. Am. Chem. Soc.* **1956**, 78, 16, 4007–4010.

[13] Friedländer, P. and Kunz, K.; Ber. dtsch. Chem. Ges. 1922, 55, 1597-1607.

[14] (a) Liebermann, C. and Dickhuth, F.; *Ber. Dtsch. Chem. Ges.* **1891**, 24, 4130–4136. (b) Posner, T.; *Ber. Dtsch. Chem. Ges.* **1926**, 59, 1799–1827. (c) Blanc, J. and Ross, D.L.; *J. Phys. Chem.* **1968**, 72, 2817–2824

[**15**] Wyman, G.M. and Zenhäusern, A.F.; *J. Org. Chem*. **1965**, 30, 2348–2352

[16] Omote, Y.; Tomotake, A.; Aoyama, H.; Nishio, T. and Kashima, C.; *Bull. Chem. Soc. Jpn.* **1984**, 57, 470–472.

[17] Głowacki, E. D.; Voss, G.; Demirak, K.; Havlicek, M.; Sünger, N.; Okur, A.C.; Monkowius, U.; Gąsiorowski, J.; Leonat, L. and Sariciftci, N.S.; *Chem. Commun*. **2013**, 49, 6063–6065

[18] Guo, C.;Sun, B.; Quinn, J., Yan, Z. and Li, Y.; *J. Mater. Chem. C*, **2014**,2, 4289-4296.

[**19**] Huang, C.-Y.; Bonasera, A.; Hristov, L.; Garmshausen, Y.; Schmidt, B. M.; Jacquemin, D. and Hecht, S.; *J. Am. Chem. Soc.* **2017**, *139* (42), 15205– 15211 and references cited within.

[20] Beck, W. and Sünkel, K. ; *Z. Anorg. Allg. Chem.* **2020**, *646*, 248– 255.

[21] Nathan, R.A.; Schwerzel, R.E.; Adelman, A.H.; Wyant,, R.E.; U.S. Patent, 4004572, **1977**.

[22] Zhang, S.-F.; Chen, X.-K. ; Fan, J.-X. and Ren, A.-M. ; *Org. Electron.* **2015**, *24*, 12-25.

[23] Das, R. J. and Mahata, K.; *Org. Lett*. **2018**, 20, 5027–5031.

[24] Das, R. J. and Mahata, K.; *Soft Matter*. **2019**, 15, 5282–5286.

[25] (a) Loudet, A. and Burgess, K.; *Chem. Rev.* **2007**, 107, 11, 4891–4932. (b) Murali, A.C.; Nayak, P. and Venkatasubbaiah, K.; *Dalton Trans.*, **2022**, 51, 5751-5771. (c) Gon, M.;Tanaka, K. and Chujo, Y.; *Bull. Chem. Soc. Jpn.* 2019, 92, 7–18. (d) Chinta, R. V. R. N.; Aradhyula, B. P. R.; Murali, A. C.; Venkatasubbaiah, K.; *J. Organomet. Chem.* **2019**, *891*, 20– 27

[26] (a) Jin, C.; Yang, X.; Zhao, W.; Zhao, Y.; Wang, Z. and Tan, J.; *Coord. Chem. Rev.* **2024,** 215892. (b) Tanaka, K.; Gon, M.; Ito, S.; Ochi, J. and Chujo, Y.; *Coord. Chem. Rev.* **2022,** 214779

[27] (a) Liu, Z.; Jiang, Z.; Yan, M. and Wang, X.; *Front. Chem.***2019,** 7, 712, (b) Tanaka, K.; Gon, M.; Ito, S.; Ochi, J. and Chujo, Y.; *Coord. Chem. Rev.* **2022,** 214779. (b) Bäumer, N.; Ogi, S.; Borsdorf, L.; Yamaguchi, S. and Fernández, G.; *Chem. Commun.* **2023**, 59, 8937–8940.(c) Shah, S.; Marandi, P. and Neelakandan, P. P.. *Front. Chem.* **2021**, *9*, 708854. (d) Chen, Z. and Chen, Z.; *Org. Chem. Front*., **2023**,10, 2581-2602. (e) Pan, H.; Huang, H.; Liu, Y.; Su, J.; Ren, X.-K. and Chen, Z.; *Chem. Mater.* **2024**, 36, 8, 3745–3753

[28] (a) Ohtani, S.; Gon, M.; Tanaka, K. and Chujo, Y.; *Chem.─Eur. J.* **2017**, *23*, 11827– 11833. (b)

[29] (a) Wang, H.; Zhang, Y.; Chen, Y.; Pan, H.; Ren, X. And Chen, Z..; *Angew. Chem. Int. Ed.* **2020**, *59*, 5185. Zou, J.; Fang, Y.; Shen, Y.; Xia, Y.; Wang, K.; Zhang, C. and Zhang, y.; *Angew. Chem. Int. Ed.* **2022**, *61*, e202207426; *Angew. Chem.* **2022**, *134*, e202207426.

[30] (a) Nawn, G.; Oakley, S. R.; Majewski, M. B.; McDonald, R.; Patrick, B. O. and Hicks, R. G. ; *Chem Sci.* **2013**, 4, 612. (b) Wang, S.; Zhao, Y.-L.; Zhao, C.-X.; Liu, L. and Yu, S.; *J. Fluor. Chem.*, **2013**, 156, 236–239

[31] (a) Bialas, D.; Kirchner, E.; Röhr, M.I.S. and Würthner, F.; *J. Am. Chem. Soc.*, **2021**, 143, 12, 4500–4518. (b) Ji, C., Lai, L.; Li P.; Wu, Z.; Cheng, W. and Yin, M.; *Aggregate*, **2021**; 2:e39. (c) Xu, F.; Testoff, T.T.; Wang, L. and Zhou, X.; *Molecules* **2020**, *25*, 4478 (d) Yuzhakov, V.I.; *Russian Chemical Reviews*, **1992**, 61, 613–628.

[32] (a) G. R, S.; Pandey, M. and Chakravarthy, J.; *Mater. Chem. Front.* **2021**, *5*, 1541– 1584. (b) Xia, Q.; Zhang, Y.; Li, Y.; Li, Y.; Li, Y.; Feng, Z.; Fan, X.; Qian, J. and Lin, H.; *Aggregate* **2022**, 3, e152. (c) Wu, W. and Liu , B.; *Natl. Sci. Rev.*, **2021**, 8 , nwaa222. (d) Jimenez, E.R. and Rodríguez, H.; *J Mater Sci* ,**2020**, 55, 1366–1387. (e) He, Z.; Ke, C. and Tang, B.Z.; *ACS Omega* **2018**, 3, 3, 3267–3277. (f) Balachandran, Y.L. and J. X.; *CCS Chem.***2022**, 4, 420–436. (g) Zuo, Y.; Kwok, R.T.K.; Sun, J.; Lam, J.W.Y. and Tang, B.Z.; *Chem. Phys. Rev.*, **2024**, 5, 011309.

[33] a) Sorrenti, A.; Leira-Iglesisas, J.; Markvoort, A.J.; de Greef, T.F.A. and Hermans, T.M.; *Chem. Soc. Rev*. **2017,** 46, 476-5490 . (b) Matern, J.; Dorca, Y.; Sánchez, L. and Fernández, G.; *Angew*

Chem., Int Ed. **2019**, 58, 16730-16740. (C)de Greef, T.F.A.; Smulders, M.M.J.; Wolffs, M.; Schenning, A.P.H.J.; Sijbesma, R.P. and Meijer, E.W.; *Chem. Rev.* **2009**, 109, 5687-5754 b) Wehner, M. and Würthner, F.; *Nat. Rev.* **2019**, 4, 38-53. (d) Korevaar, P.A.; George, S.J.; Markvoort, A.J.; Smulders, M.M.J.; Hilbers, P.A.J.; Schenning, A.P.H.J.; de Greef, T.F.A. and Meijer, E.W.; *Nature* **2012**, 481, 492-496.(e) Aliprandi, A.; Mauro, M. and de Cola, L.; *Nat. Chem***. 2016**, 8, 10-15. (f) Herkert, L.; Droste, J.; Kartha, K.K.; Korevaar, P.A.; de Greef, T.F.A.; Hansen, M.R. and Fernández, G.; *Angew. Chem. Int. Ed*. **2019**, 58, 111344-11349. (g) Wehner, M.; Röhr, M.L.S.; Stepanenko, V. and Würthner, F.; *Nat Commun* **2020**, 11, 5460-5469. Greciano, E.E.; Calbo, J.; Orti, E. and Sanchez, L.; *Angew. Chem., Int. Ed.* **2020**, 59, 17517-17524.

[34] Lin, Q.; Wang, Z.-H.; Huang, T.-T.; Wei, T.-B.; Yao, H. and Zhang, Y.-M.; *J. Mater. Chem. C*, **2021**, 9, 3863– 3870. (b) Zhang, Y. M.; Zhu, W.; Huang, X. J.; Qu, W. J.; He, J. X.; Fang, H.; Lin, Q.; Yao, H. and Wei, T.-B.; *ACS Sustainable Chem. Eng.* **2018**, *6*, 16597– 16606 (c) Zhao, N.; Lam, J. W. Y.; Sung, H. H. Y.; Su, H. M. and Williams, I. D.; Wong, K. S. and Tang, B. Z.; *Chem. - Eur. J.* **2014**, *20*, 133– 138 (d) Zhang, X.; Wang, B.; Xia, Y.; Zhao, S.; Tian, Z.; Ning, P. and Wang, Z; *ACS Appl. Mater. Interfaces* 2018, 10, 25146–25153 (e) Mei, J.; Huang, Y. and Tian, H.;*ACS Appl. Mater. Interfaces* **2018**, 10, 12217–12261.

[35] (a) Marien, N.; Brigou, B.; Pinter, B.; Proft, F.D. and Verniest, V.; *Org. Lett.* **2015**, 17, 2, 270–273. (b) Ji, Y.; He, X.; Peng, C. and Huang, W., *Org. Biomol. Chem*., **2019**, 17, 2850-2864.

[36] Liu, R.-R. ; Ye, S.-C. ; Lu, C.-J. ; Zhuang, G.-L. ; Gao, J.-R. and Jia, Y.-X. ; *Angew. Chem., Int. Ed*., **2015**, 54, 11205 and references cited within for synthesis of isatogens.

[37] Leznoff, C. C. and Hayward, R. J.; *Can. J. Chem.* **1971**, *49*, 3596–3601.

[38] Ibrahim, H.; Pantaleo, A.; Turrini, F.; Arese, P.; Nallet, J.-P. and Nepveu, F.; *Med. Chem. Commun.* **2011** , 2, 860 and references cited within.

[39] (a) Xie, L.; Li, Y.; Dong, S.; Feng, X and Liu, X.; *Chem. Commun.* **2021**,57, 239-242. (b) Liu, R.-R.; Ye, S.-C.; Lu, C.-J.; Zhuang, G.-L.; Gao, J.-R. and Jia, Y.-X.; *Angew. Chem., Int. Ed.* **2015**, 54 ,11205. (c) Xu, J.Y.; Hu,S.H.; Lu, Y.Y.; Dong, Y.; Tang, W.F.; Lu, T. And Du, D. *Adv. Synth. Catal.*, **2015**, 357 , 923. (d) Edeson, S.J.; Maduli, E.J.M.; Swanson, S.; Procopiou, P.A. and Harrity, J.P.A.; *Eur. J. Org. Chem.*, **2016**, 1, 83-86. (e) Xu, H.; Ye, M.; Yang*, K. and Song, Q.; *Org. Lett.* **2021**, 23, 20, 7776–7780. (f) Sakai, R.; Ishihara, N.; Harada, S. and Arai, S.; *Tetrahedron Lett.* **2024**, 137, 154909. (g) Dhote, P.S. and Ramana, C.V.; *Org. Lett.*, **2019**, 21, 16, 6221–6224

[40] (a) Ishihara, N.; Harada, S.; Nakajima, M. and Arai, S; *Org. Lett.* **2024**, 26, 15, 2908–2912. (b) Shimizu, H.; Yoshinaga, K. and Yokoshima, S.; *Org. Lett.* **2021**, 23, 7, 2704–2709.

[41] Murahashi, S.-I. and Imada, Y.; *Chem. Rev.* **2019**, 119, 7, 4684–4716.

Chapter 2

Supramolecular polymorphism of boron difluoride complex of peri-naphthoindigo

❖ 2.1 Introduction

Polymorphism in dye chemistry is an important phenomenon and gives rise to diverse range of colours, emissions and materials properties due to their different arrangements in the solid state.[1] For example, industrially significant dye copper phthalocyanine is known to exhibit 10 different types of polymorphs, each of which show their own hues and unique applications in electronics.[2] An emergence of new properties is seen from a similar material building block but in different environments due to difference in the organization of these blocks, and the resulting difference in intermolecular electronic coupling between such.[3] Polymorphism is ubiquitous in dye pigments and has been observed in many other dyes. However, the phenomenon is relatively uncommon in supramolecular chemistry. Arranging the same building block in different ways in the solution state is indeed challenging. Considering the significance of polymorphism and the emergence of new and diverse range of properties that include colours and emission intensity, introduction of the same into the supramolecular chemistry is an important objective in the area. To observe supramolecular polymorphism, several groups has investigated the topic in recent years. One of the most important works in this field was reported on the pathway-dependent stacking of chiral oligo(p-phenylenevinylene), leading to multiple modes of aggregation[4]. Further enrichment of this field was done by Würthner[5] working on PBIs, Sugiyasu on porphyrins[6] and on other such building blocks.[7-8] Wurthner working on PBIs with a slight distortion in their structure via introduction of long acyloxy chains, obtained two different kinds of assemblies just by tuning the rate of cooling of the heated monomeric state to room temperature, whereby either heterochiral or homochiral assemblies were obtained. These gave rise to columnar and lamellar liquid crystals respectively. Another study takes advantage of chiralities in the imide chains to generate helicity in aggregates. Use of temperature as a kinetic and thermodynamic control, and ultrasonication as method for conversion, allows for the accomplishment of 3

different aggregate structures. Two of the aggregate structures consist of a 1:1 conglomerate of both helicities, and are distinguished by their absorption and aggregate morphology, but lack any inherent chirality. The third aggregate was formed by ultrasonication at a higher temperature, and possessed chirality, with a hypsochromic shift in absorption (Fig 2. 1). In 2017, Wurthner *et al* managed to convert an H-aggregate assembly of a bay-substituted PBI into J-aggregate, a process which was accelerated via seeding (Fig 2. 2).

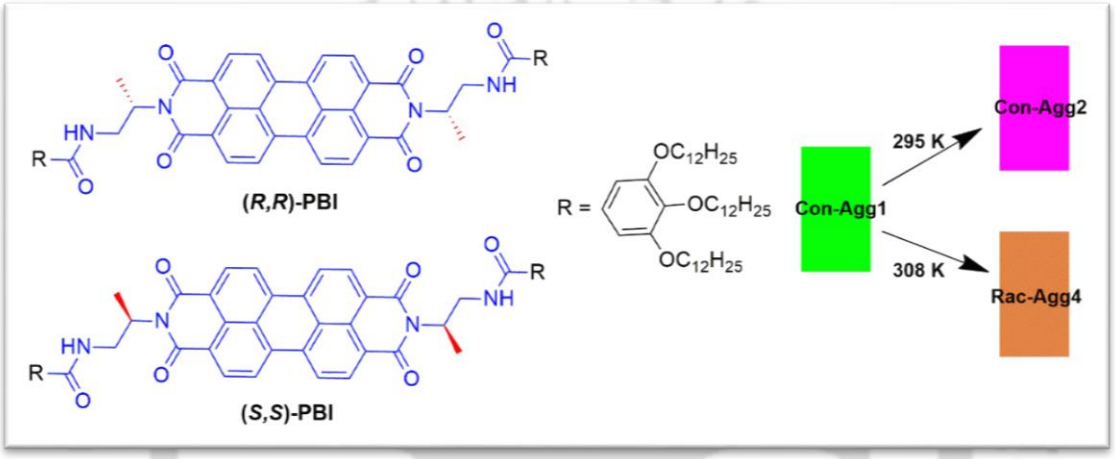

Fig 2. 1 Supramolecular polymorphism displayed via pathway complexity in chiral PBI prepared by Wurthner *et al.*

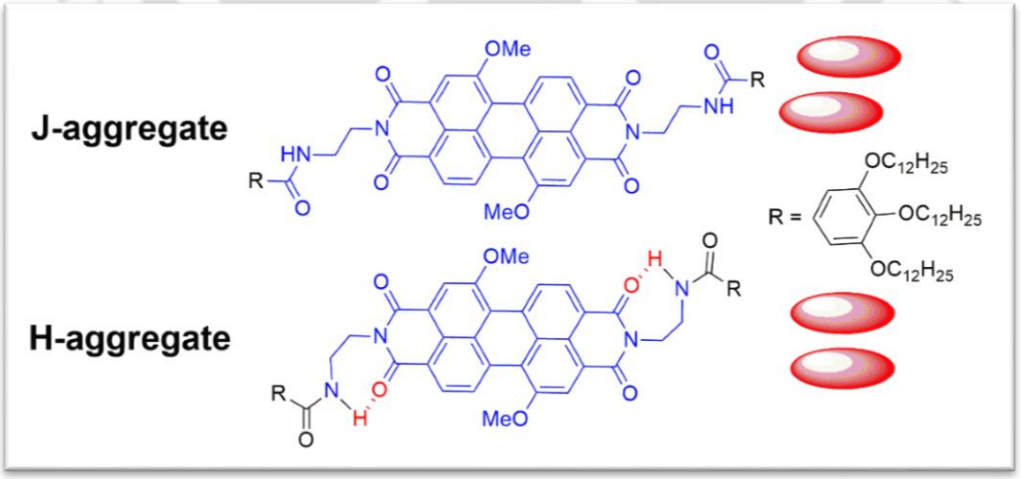

Fig 2. 2 Supramolecular polymorphism displayed via pathway complexity in PBI prepared by Wurthner *et al.*

Similar developments in aggregate ploymorphs were carried out by Sugiyasu on porphyrins[9] , an example is where a metastable assembly of porphyrin was reported to differentiate into either nanosheets or nanofibres depending on pathway control (Fig 2. 3). Depending upon the conditions, formations of multiple different supramolecular assemblies were observed in all cases. In spite of such important progress, the examples of polymorphisms in supramolecular chemistry are limited to very few examples. Therefore, supramolecular polymorphism must be explored further, especially with different and new building blocks.

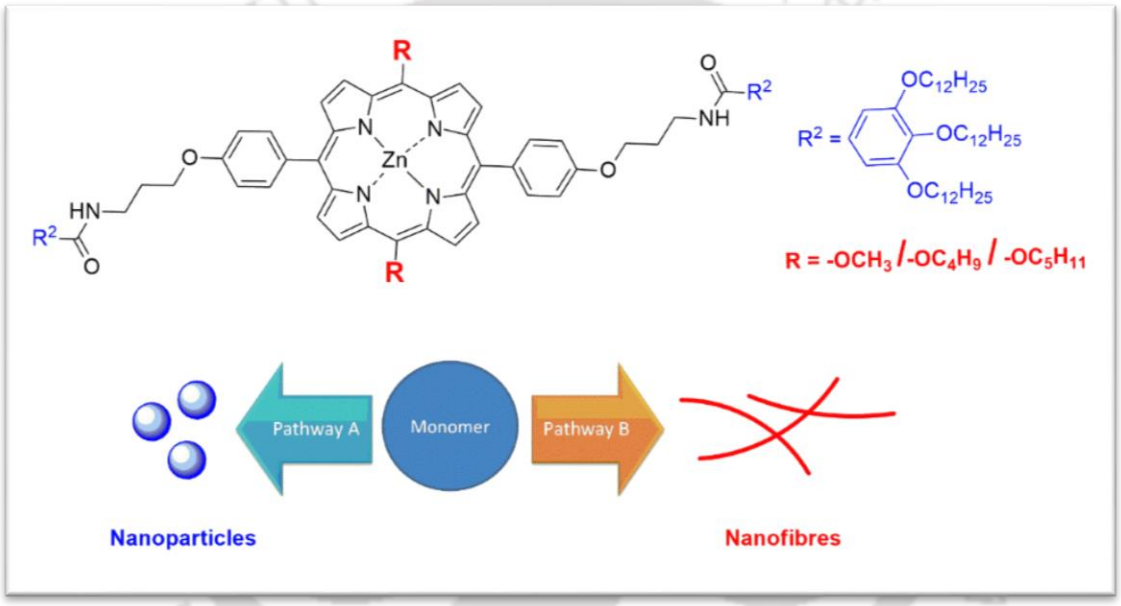

Fig 2. 3 Supramolecular polymorphism displayed via pathway complexity in porphyrin complex prepared by Sugiyasu *et al*

.

peri-Naphthoindigo (PNI) is a fascinating dye comprising of four different functional groups, sandwiched between two naphthalene rings (Fig 2.4). The 1,8 *peri*-connection and presence of four different functional groups makes the PNI dye very unique. Unlike the analogous historic dye indigo, PNI exists in mono-enol form. Despite of having larger hydrophobic surface, the dye is soluble in common organic solvents. Compared to indigo, PNI showed wider and stronger absorption in the visible region. The dye itself showed supramolecular

polymerization with aggregation-induced enhanced emission (AIEE) phenomenon.[10] PNI also installed AIEE on a dye that cannot show AIEE alone. Considering the diversity of the

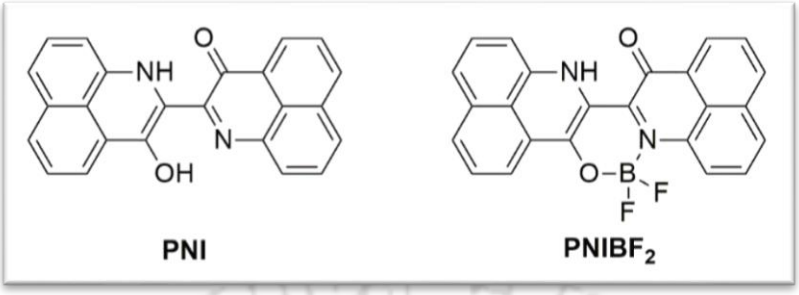

Fig 2. 4 Structure of *peri*-naphthoindigo(PNI) (**left**) and boron difluoride complex of PNI (**right**).

dye, PNI is an important building block to investigate supramolecular polymorphism. PNI itself exhibited formation of different aggregates, but in a different solvent system. Therefore, some structural modification on PNI is necessary to observe supramolecular polymorphism. The presence of two different types of bidentate ligand gives room for easy structural modification via coordination with metal ion, boron-difluoride (BF_2) coordination *etc.* BF_2-coordination to organic molecules is a simple and well known tactic to modify the self-assembly properties of the dyes.[11] The incorporation of BF_2-moiety changes the rigidity of a dye by restricting intra-molecular motion, which in turn changes the self-assembly properties. Enhancement of fluorescence intensity is often associated with BF_2-coordination. Unsurprisingly, a large number of BF_2-coordinated organic dyes with luminescent properties, fascinating optical characteristics and diverse self-assemblies have been prepared over the last years.[12] Based on the nature of the donating atoms, these dyes are classified into three types: N,N-bidentate[13], O,O-bidentate[14] and N,O-bidentate[15]. While the first two types have been thoroughly investigated with numerous examples, numbers are limited for the last case. As PNI has two sets of N,O-bidentate ligands, the dye is poised to be an ideal candidate for the study of the described areas mentioned above. Some BF_2-complexes is indeed known to

exhibit supramolecular polymorphism,[16] which gave us encouragement to modify PNI with BF_2-coordination and investigate supramolecular polymorphism.

❖ 2.2 Result and Discussion

To install BF_2-moiety into PNI, we treated the dye with BF_3•Et_2O in presence of Et_3N under refluxing condition. The synthesized compound PNI-BF_2 (Fig 2. 4) was isolated and analyzed through a combination of various analytical techniques. The HRMS data of the compound indicated the incorporation of one BF_2-moiety into PNI. The ^1H NMR spectrum of the compound showed 13 different signals. The presence of a sharp singlet for the NH-proton and disappearance of the OH proton resonance indicates the coordination of BF_2-moiety only through the anionic oxygen and lone pair of the imine nitrogen, further emphasizing the incorporation of single BF_2. Change of chemical shifts were also observed as a result of BF_2 coordination. For example, the secondary amine proton underwent a shift of 0.27 ppm towards the downfield region on moving from PNI to PNI-BF_2. The proposed structure was further established from the ^{11}B and ^{19}F NMR. Boron resonance of the dye displayed a single peak at 3.17 ppm. Fluorine resonance also showed a lone peak at -130.7 ppm. All these analytical data unambiguously established the proposed structure of PNI-BF_2. The other isomer in which coordination occurs through the amine anion and carbonyl oxygen was not observed under the present reaction conditions. Formation of single BF_2-complex was also observed in the case of analogous dye indigo.[17] A better understanding of the structure would be served by the study of solid state structures. However, all attempts to isolate suitable diffractable crystal were found to be fruitless. Theoretical calculations were performed using density functional theory (DFT) implemented in Gaussian 16. Optimized structure of the dye was obtained in chloroform using DFT/B3LYP method and 6-31+G(d,p) basis set. In the ground state, PNI-BF_2 was shown to be a highly planar structure (Fig 2.5). The boron atom

lied in the same plane with the naphthalene rings, while the fluorine atoms are placed above and below the plane. The boron atom forms a six membered ring through N,O-coordination with PNI.

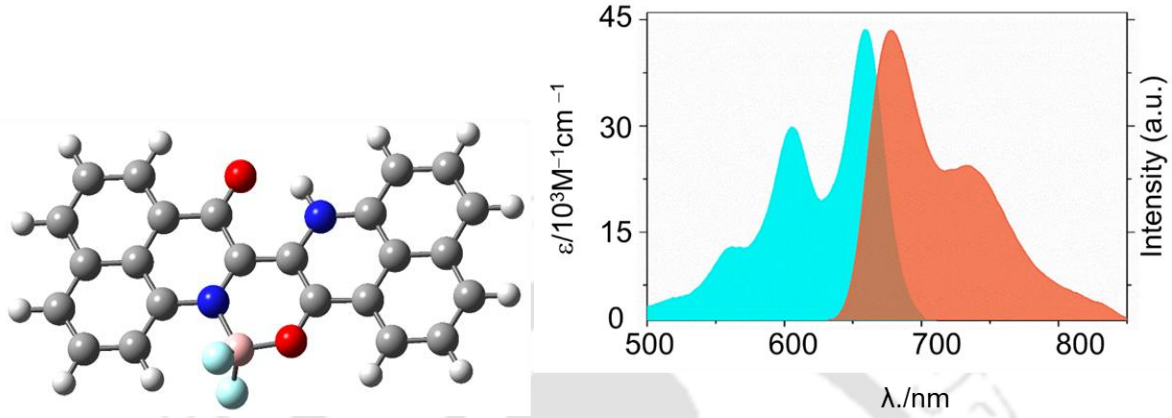

Fig 2. 5 Optimized structure of $PNIBF_2$ (**left**) and absorption and emission of the dye representing mirror image relationship (**right**).

Detailed photophysical investigations were done after unambiguous establishment of the structure. UV-visible property of the dye was investigated using wide variety of solvents, starting from non-polar solvents (toluene) to moderately polar solvents (THF, chloroform). The results are summarized in Figure 2. 6. At a concentration of ~ 2.5 µM in $CHCl_3$, PNI-BF_2 displayed an absorption maximum at 659 nm (43255 cm^{-1}) along with the first vibronic progression at 606 nm (29530 cm^{-1}). The newly prepared dye undergoes a red shift of 27 nm compared to the original PNI, accompanied by an increase in extinction and vibronic fine structure of spectra. The spectral features remained similar in all other solvents barring toluene, where additional shoulder was detected. This could be due to the aggregation.

As expected PNI-BF_2 was found to be emissive and displayed fluorescence maximum at 677 nm in chloroform. Due to structural rigidification, substantial decrease in the Stokes shift was observed when compared with the parent dye. The Stokes shift value decreased from 2235 cm^{-1} in PNI to 403 cm^{-1} in PNI-BF_2. The emission quantum yield was calculated to be 8.97%,

a thirty-fold increase from its parent dye (0.3%). The enhancement is attributed to the restriction in intramolecular motion around the chromophore. A combination of the steady-state absorption and emission data also proved the rigidification of structure by BF_2 coordination.

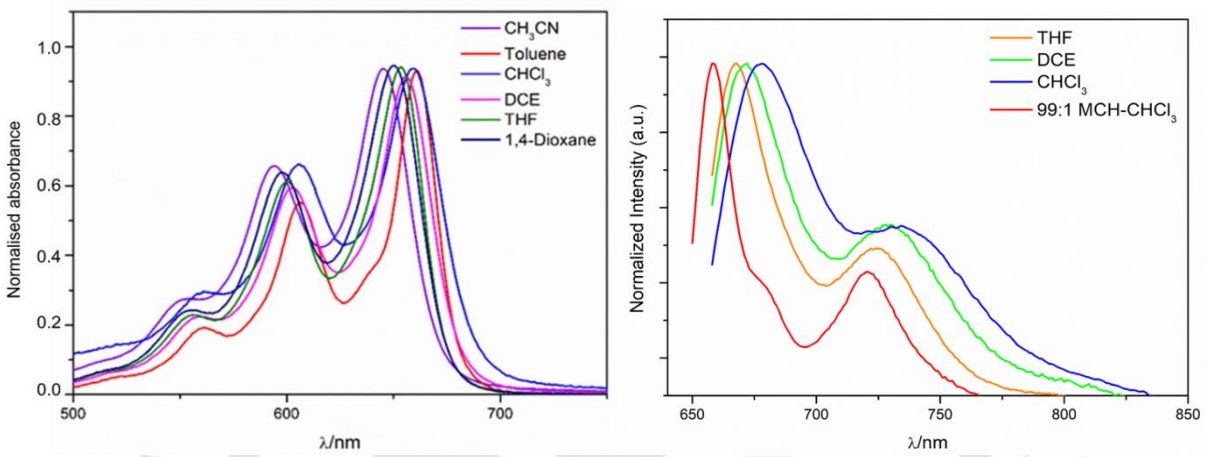

Fig 2. 6 UV-Vis (**left**) and emission screening (**right**) of PNIBF2 in different solvents.

❖ 2.2.1 Self-assembly of PNI-BF_2

The next step is to focus on the self-assembly properties of PNI-BF_2. Due to the presence of a rigidified planar structure and the presence of ambipolar groups, the dye is reasonably prone to aggregation. The presence of both polar (chromophore) and non-polar and hydrophobic (aromatic rings) groups lends it the ability to self assemble both in highly non-polar and highly polar solvents. PNI-BF_2 has the tendency to aggregate in typical non-polar solvents such as methylcyclohexane, hexane and toluene, while remaining a monomer in other solvents with a higher dielectric constant such as $CHCl_3$, 1,2-DCE or THF, observed from absorbance and emission measurements. Limited solubility of the dye in MCH or toluene brings forth the neccessity to conduct the required analysis in the next best choice, a mixture of solvents, such as $CHCl_3$/MCH or DCE/MCH. Screening in various percentage (v/v) of MCH and chloroform showed that an increase in the volume fraction of MCH caused an

increase in the absorption co-effcient and narrowing of the 0,0 vibronic band. The absorption coefficient reached a value of around 80480 cm^{-1} at the highest volume percentage of MCH possible, i.e. at 99:1 (MCH/$CHCl_3$) summarized in Fig 2. 7. A new shoulder was also observed at 635 nm in the specified solvent system. The full width at half maxima (FWHM) was also reduced greatly due to narrowing of spectra, from 835 cm^{-1} in pure chloroform to 349 cm^{-1} in 99% MCH in $CHCl_3$. The aforementioned optical changes of PNI-BF_2 in 99% MCH indicated the self-assembly of the dye in non-polar solvent. The aggregated dye, described as **Agg1**, exhibited a hypsochromic shift of 2 nm, when compared with the molecularly dissolved state of the dye in $CHCl_3$. This change could be attributed to a combined effect of solvatochromism and aggregation. The self-assembly process also brings forth an increase in photoluminescence quantum yield.

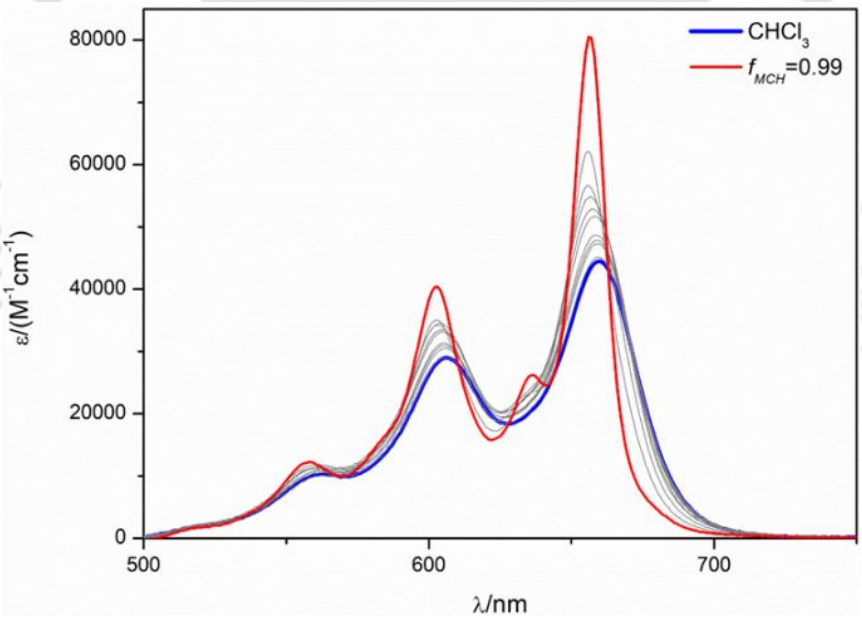

Fig 2. 7 Absorption spectra of $PNIBF_2$ in $CHCl_3$ and $CHCl_3$/MCH (v/v = 1/99).

The emission quantum yield of the self-assembled species **Agg1** was calculated be ~11.2%, which is an enhancement of 37 times than that of PNI and 1.25 times than the monomeric solution of PNI-BF_2. The emission maxima of **Agg1** has been recorded to be at 659 nm.

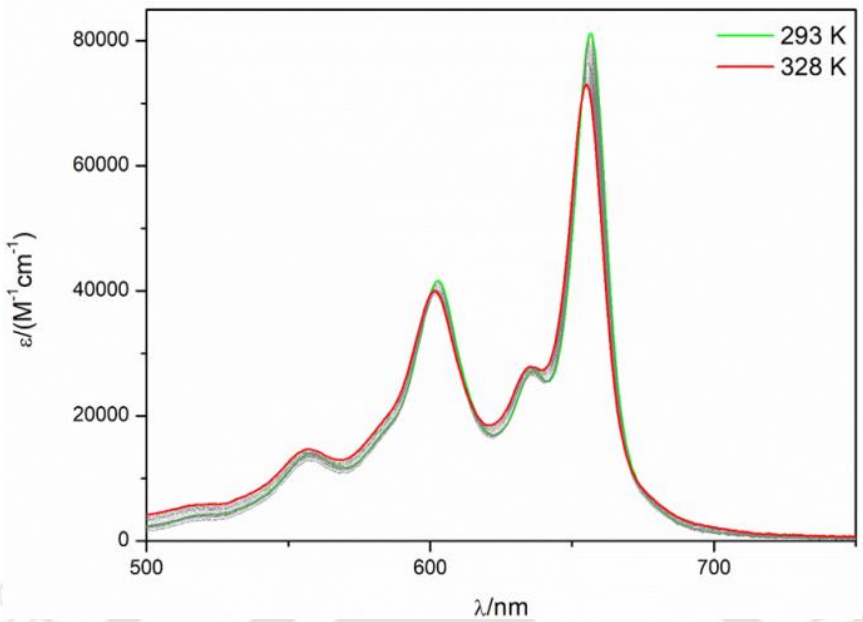

Fig 2. 8 Variable temperature absorption spectra of $PNIBF_2$ in f_{MCH} = 0.99.

In order to obtain the mechanistic details of the aggregation of the dye in non-polar solvent, absorption spectra were recorded at different temperatures. With increase in temperature, the extinction coefficient decreased and reached to the value of 73100 cm^{-1} at 328 K. Even though, there was decrease in molar extinction coefficient, the shoulder at 635 nm was still persistent at the maximum temperature, indicating the presence of a considerable amount of the aggregate (Fig 2. 8). The observation signified the presence of a monomer-aggregate equilibrium even at the elevated temperature. Due to the limitations of temperature range in the presence of a low boiling solvent like chloroform, the present solvent system was modified. Considering the high boiling point of DCE, the same was combined with MCH for further investigations. Thus, **Agg1** was instead prepared in MCH/DCE (v/v = 99/1) and variable temperature absorption measurements were carried out using this current mixture. DCE can be considered as a replacement for chloroform because the absorption spectra are very similar for both of these solvents, even in a 99/1 v/v mixture with MCH, where MCH

constitutes the major fraction. Heating a solution of **Agg1** in the specified solvent mixture caused profound changes in the extinction coefficient and the value dropped from 83880 cm^{-1} at 293 K to 66050 cm^{-1} at 353 K. The changes are much more prominent than what was observed in MCH/$CHCl_3$. There was also a shift of 4 nm upon heating upto higher temperatures – upto 353 K(Fig 2. 9). Although the magnitude of the shift in absorption maxima is less, other spectroscopic changes are still adequate to provide a clear idea about the mechanistic pathways for the aggregation, as these kinds of small shifts, although not uncommon,[18] are hardly significant enough to justify any decision procured from these data.

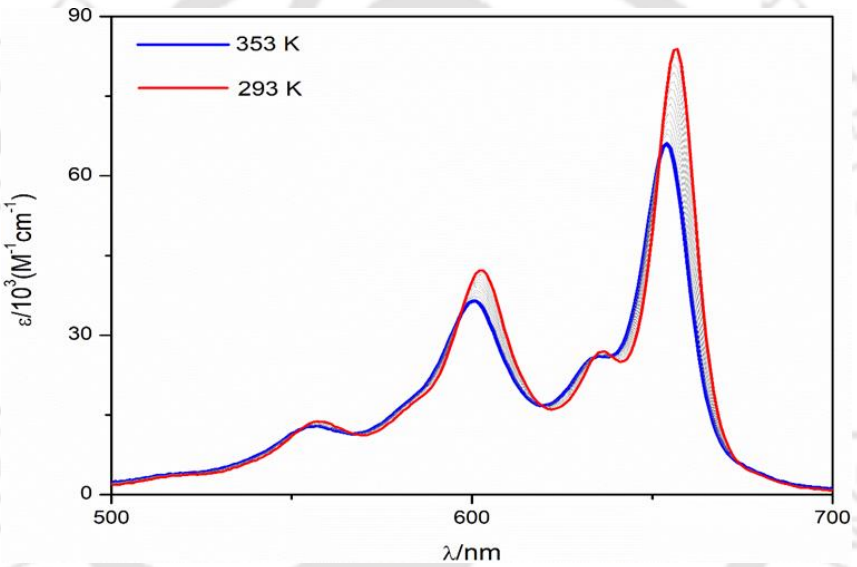

Fig 2. 9 Variable temperature absorption spectra of $PNIBF_2$ in f_{MCH} = 0.99 (f_{DCE} = 0.01)

Thermodynamic parameters for **Agg1** were determined by using denaturation model. Accordingly UV-vis absorbance spectra were recorded at various fractions of MCH and $CHCl_3$. Progressive disassembly of aggregate **Agg1** was achieved by adding a monomeric solution of the dye in chloroform into a MCH/$CHCl_3$ solution having the same concentration. A clear indication of the disassembly process was the disappearance of **Agg1** and reappearance of the monomeric spectra at 60/40 v/v fraction of MCH/$CHCl_3$. The changes at 658 nm ware tracked *vs* the volume fraction of $CHCl_3$ used, and the thermodynamic

parameters for **Agg1** were obtained curve by fitting the data. Use of the denaturation model for **Agg1** provided the Gibbs energy change (ΔG_{293}) as -31.2 kJ mol^{-1}. Isodesmic self-assembly pathway for **Agg1** was determined from the cooperativity parameter σ whose value was determined to be 1.

The proton NMR of PNI-BF_2 was recorded in 1:1 volume mixture of $CDCl_3$ and MCH, and was compared with the spectrum of the dye in pure $CDCl_3$ in order to gain a better idea about the stacking of the dye in **Agg1,** represented in Fig 2. 10(a). In such a lower polarity solvent mixture, the NH proton signal was broadened, along with that of six aromatic protons. Different chemical shifts for these protons also indicates a change in their magnetic environments. On the other hand, the shift and sharp splitting of the remaining protons were relatively unaltered. This was a reasonable proof that the molcules stack against themselves

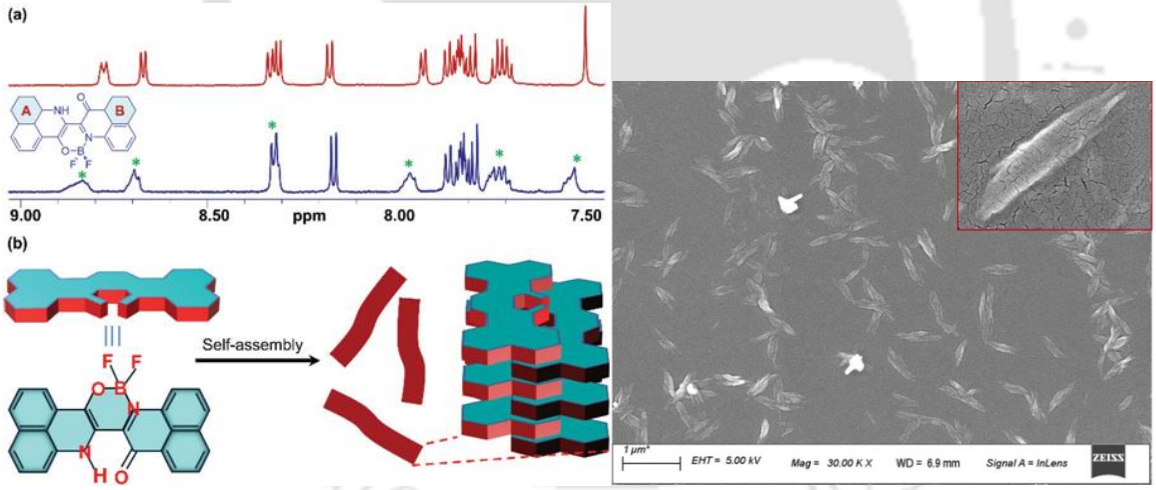

Fig 2. 10 Comparison of NMR spectra between PNIBF_2 in $CHCl_3$ (**red**) and $CHCl_3$/MCH (**blue**) (v/v = 1/1) with a diagrammetic representation of aggregation mechanism; FESEM images of **Agg1**.

via a ladder fashion. ^{1}H-^{1}H COSY NMR is used to establish that the protons experiencing changes are limited to a single side. i.e. the aromatic protons of the ring that underwent change are placed on the benzene ring containing the amine and carbonyl groups. This indicates that stacking took place along these above mentioned rings. The other rings on the

side of the BF_2 moiety remained unchanged, and hence barely affected by the aggregation (Fig 2. 10(b)). Morphological nature of the aggregates **Agg1** was also examined through field emission scanning microscopy (FESEM). On aluminium foil coated glass plates, a drop-casted solution of the dye in MCH/DCE (v/v = 99/1) was studied under the electron microscope and the resultant images were investigated. Formation of linear fibres upto a length of 1 micron was observed (Fig 2. 10). This type of linear aggregates can also be explained by the ladder-type stacking mentioned earlier, where solvophobic interactions with the non-polar solvent cause the rings containing the amine and carbonyl group to shield each other due to their polar nature. This caused the dye monomer to stack with another monomer side to side.

❖ 2.2.2 Supramolecular assembly in THF-water

After getting information about self-assembly of the dye in non-polar solvent, the arrangement of the compound in polar solvents was studied. The aggregation of **Agg1** was originated from the solvophobicity of the polar functional groups towards a non-polar environment. Therefore, it is important to study the behaviour of the dye in a solvent of opposite polarity, for example THF/water system. Accordingly, a stock solution of the dye in THF was prepared and the required volume was dispersed into various fractions of THF and water so as to achieve a final concentration of 5 μM, and gradually increasing ratio of water to THF. The effect of change in solvent polarity in the polar environment was monitored using UV-visible spectroscopy and the results are summarized in Fig 2. 11. With an increase in water percentage the molar extinction coefficient decreased and the trends continued up to a 7/3 (v/v) mixture of water/THF, while the other spectral features including absorption maxima did not change significantly. However there was a change in the absorption spectra when the volume percentage of water reached to 80%. Along with a change in the absorption

maxima, the spectra also broadened significantly. With diminished molar extinction coefficient, the vibronic structure also became less pronounced. The spectral changes were noticed for both the 0-0 and 0-1 transitions. But, the magnitude of lessening of molar extinction coefficient was more for the 0-0-transition. Thus the intensity of the transition at shorter wavelength becomes greater than that at longer wavelength. For an insight into the supramolecular assembly and its nature, an aggregate assembly was prepared at a concentration of 5 μM, and in a mixture of 76/24 (v/v) of water and THF. The absorption spectrum of the dye in the specified solvent exhibited the 0-0 and 0-1 transitions at 629 nm and 694 nm respectively. The aggregate showed no changes in its optical features over multiple days, before finally precipitation occurs from the dye solution (Fig 2. 12).

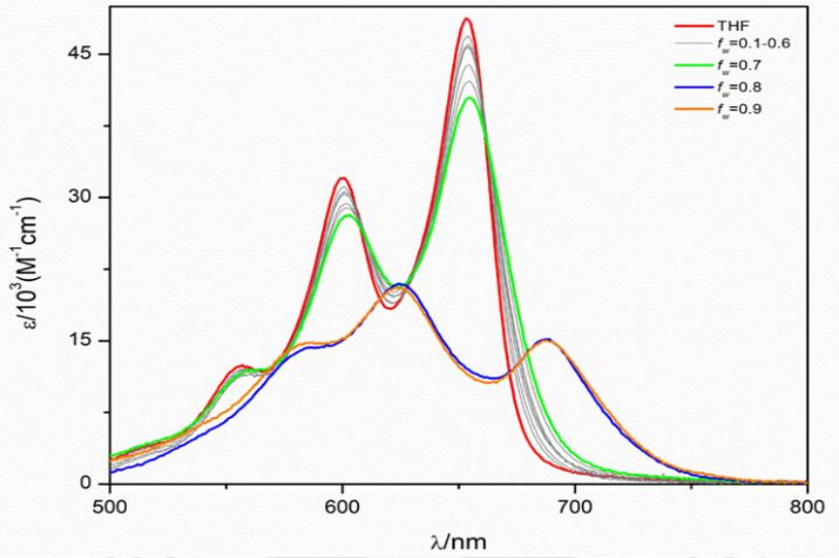

Fig 2. 11 Absorption screening of $PNIBF_2$ in various fractions of THF and water.

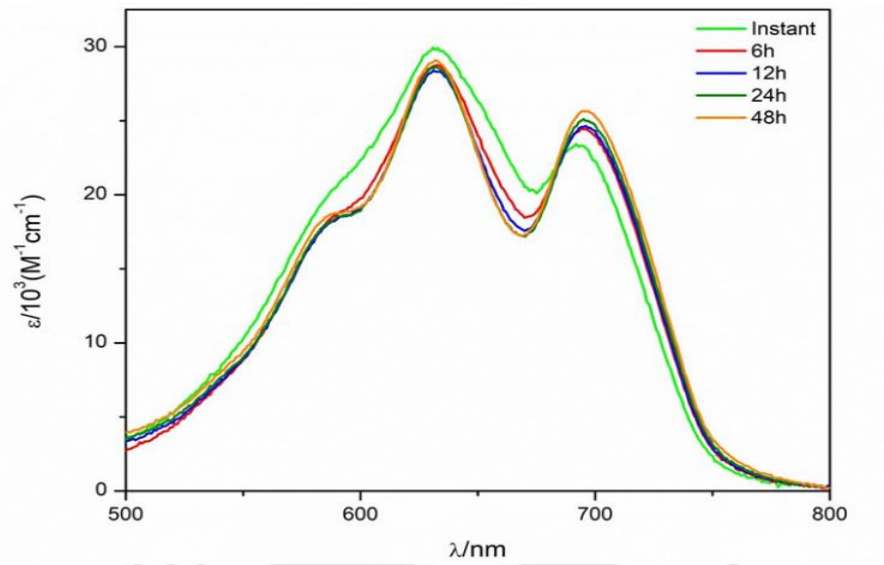

Fig 2. 12 Time dependent absorption spectroscopy of **Agg2** in f_w = 0.76 .

However, the variable temperature absorption spectra of this aggregate mixture **Agg2** displayed disassembly at higher temperatures. Upon heating from an ambient temperature of 293 K to 333 K, **Agg2** showed gradual breakdown of the self-assembled structure, and at 333 K, there was a new maximum at 652 nm while the intensity at 694 nm is almost completely diminished (Fig 2. 14). Monitoring the absorption at 652 nm *vs* the specific temperature at different concentrations, and using data for curve fitting, provided proof of an isodesmic self aggregation mechanism. Although full dis-assembly of aggregates was not achieved even at higher temperatures, the absence of a specific critical temperature allows to eliminate any cooperative mechanism. By using the equal-*K* model,[19] the average Gibbs free energy (ΔG_{298}) for formation of aggregate was estimated to be -38.7 kJ mol^{-1}. The morphology of **Agg2** was investigated using FESEM. A sample from a 76/24 (v/v) water-THF solution of the dye was drop-casted on to a glass plate coated with aluminium and FESEM images were recorded. The FESEM exhibited the formation of nano ellipsoids (Fig 2. 20). The formation of **Agg2** could be explained by considering the hydrophobicity of the naphthalene rings of the dye. In a polar environment, the rings tend to strongly avoid surroundings of polar solvent

molecules. On the other hand, the polar amine and carbonyl groups of the chromophore tend to be surrounded by the water molecules. Hence, stacking was favoured in which the naphthalene rings of adjacent monomers interact through π-π stacking, thereby shielding each other from the polar solvent. This linear arrangement was then condensed into circular patterns, providing bilayers where the polar functional groups interacted with the solvent molecules and the non-polar groups protected them from the polar water molecules. These circular patterns assembled into ellipsoidal structures. **Agg2** was of non-emissive nature, due to the excited energy transfer via vibrational pathway.

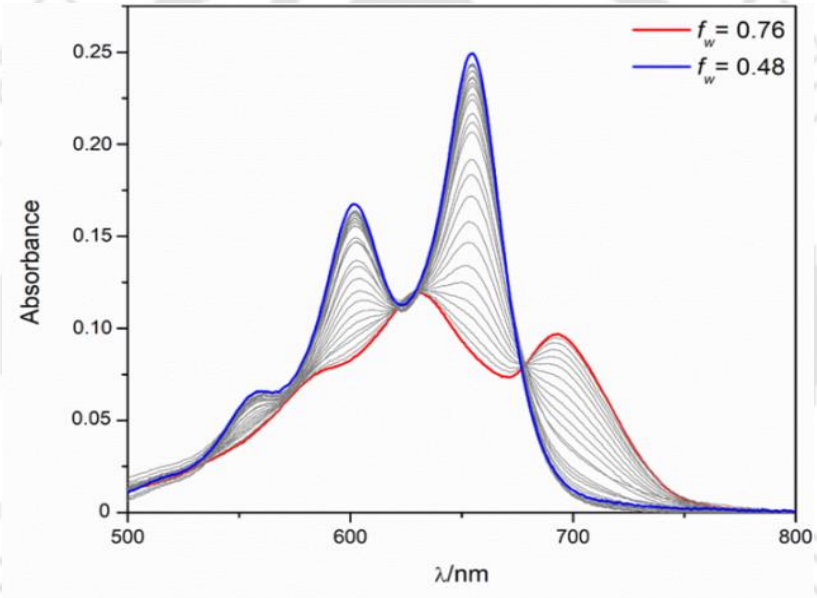

Fig 2. 13 Absorption spectra of PNIBF2 in various fractions of water and THF indicating gradual dissociation of **Agg2.**

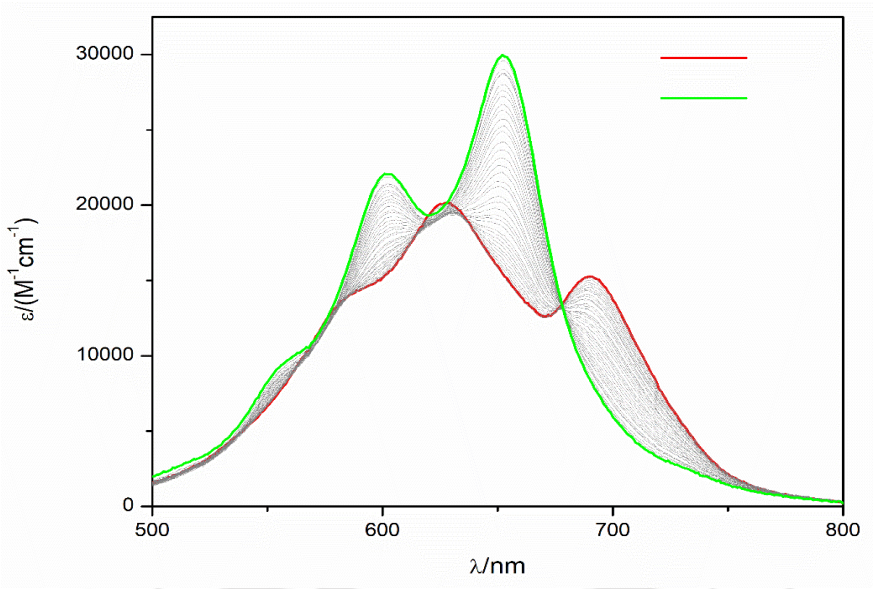

Fig 2. 14 Variable temperature absorption spectra of PNIBF2 in f_w = 0.76, indicating gradual dissociation of **Agg2. (red = 293 K, green = 328 K)**

❖ 2.2.3 Supramolecular polymorphism

After looking into the mechanism of self-assembly and dis-assembly of **Agg2**, the possibility of pathway complexity was explored. In order to achieve the goal, the molecularly dissolved state of the dye was generated by heating **Agg2** at 328 K in a 76/24 (v/v) mixture of water-THF. The mixture was then cooled down gradually, and the progress of the re-organization of PNI-BF_2 was monitored using UV-vis spectroscopy. The changes were recorded for each degree lowering of temperature, and continued till the final temperature reached to 298 K. Iinterestingly, the dye did not go back to the original assembly **Agg2**, but organized into a new supramolecular assembly, named as **Agg3**. The 0-0 and 0-1 transitions for the aggregate are characterized by absorption maxima at 703 nm and 639 nm respectively (Fig 2. 15). Both of the transitions were red shifted in comparisons to the transitions observed in case of **Agg2**. Additional changes were observed in the relative intensities of the transitions too. The value of the ratio of absorbance ($A_{0\text{-}0}/A_{0\text{-}1}$) at two transitions were found to be higher in the case of

Agg3. By recording the spectral the change at 652 nm *vs* temperature, the thermodynamic parameters for **Agg3** was obtained. A plot of the degree of aggregation with respect to temperature and subsequent curve fitting confirmed a co-operative process of self-assembly. From the curve-fitting of the data, the average Gibbs free energy was calculated to be -41.5 kJ mol^{-1}. Denaturation experiments were also supported about the greater stability of **Agg3** in comparison to **Agg2**. FESEM images provided the morphological nature of **Agg3**. From the microscopic image, the morphologies of **Agg3** were found to be spherical (Fig 2. 20). Likewise **Agg2**, **Agg3** too was found to be non-emissive. It is noteworthy to mention that the rate of cooling is an important factor for the generation of **Agg3**. If the cooling is rapid from the molecularly dissolved state, **Agg2** could be regenerated (Fig 2. 18). On the other hand cooling in a slow and gradual fashion provides the aggregate **Agg3**. It is necessary to mention that keeping the aggregate **Agg2** at 318 K over a period of 3 h did not produce any changes to the spectra barring the initial changes within the first hour. Cooling this solution down regenerated the spectroscopic feature of **Agg2**, thus failing to cause any permanent and drastic changes (Fig 2. 19). Storage of the **Agg3** for 36 h only resulted in gradual precipitation, without any discernable change in spectra (Fig 2. 17). The investigations therefore suggested that the aggregates **Agg3** and **Agg2** were produced by competitive pathways, and conversion from the latter to the former is feasible only through the monomer.

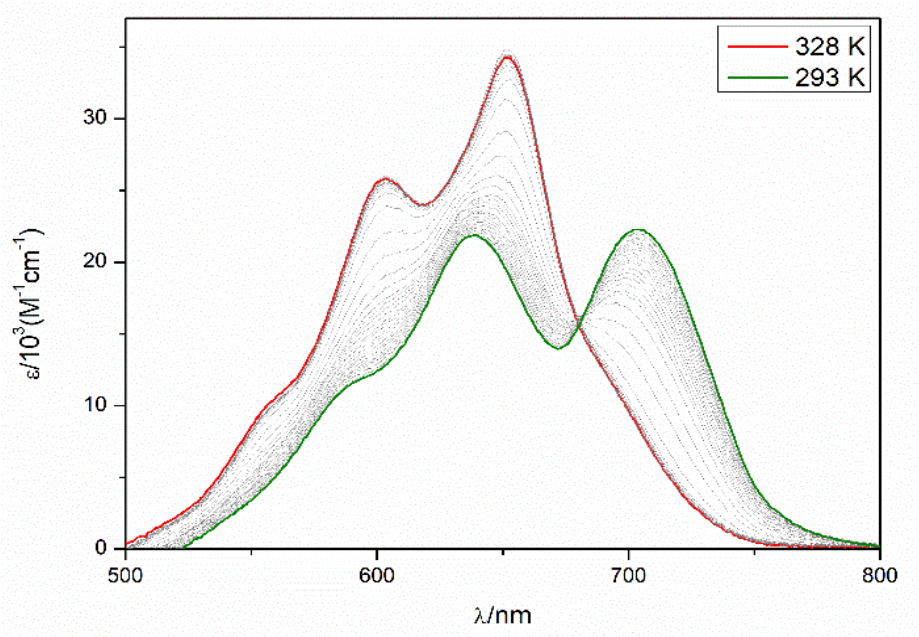

Fig 2. 15 Variable temperature absorption spectra of PNIBF2 in f_w = 0.76 , indicating gradual reassociation into **Agg3.**

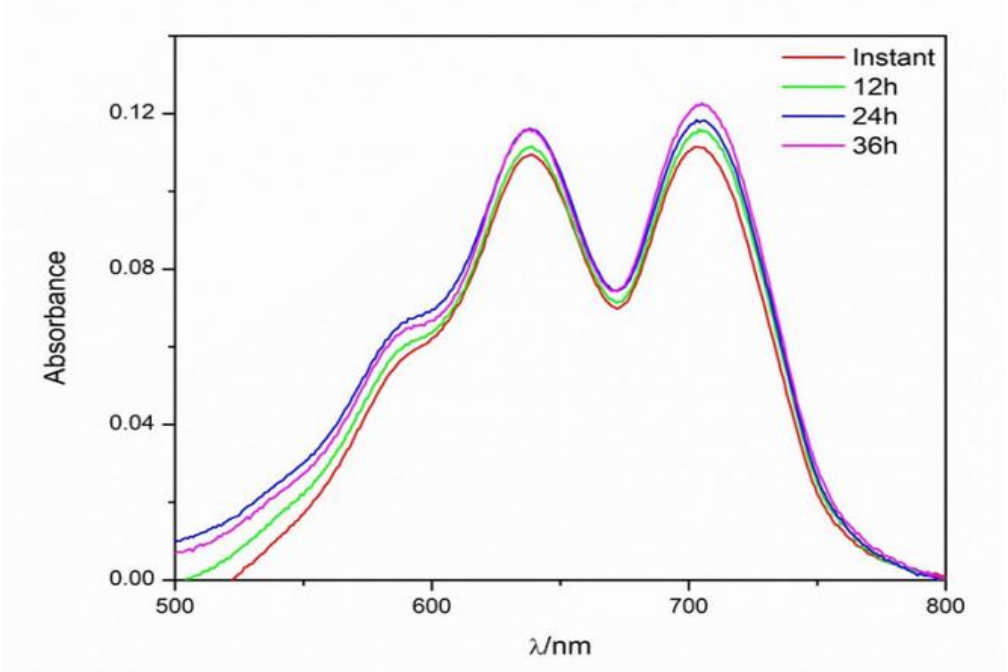

Fig 2. 16 Time dependent absorption spectroscopy of **Agg3** in f_w = 0.76 .

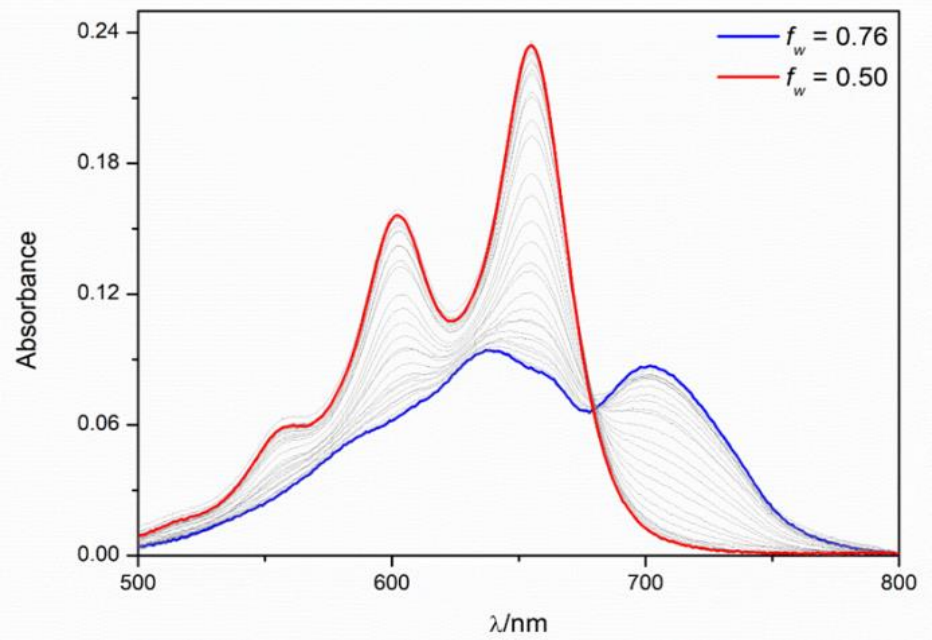

Fig 2. 17 Absorption spectra of PNIBF2 in various fractions of water and THF indicating gradual dissociation of **Agg3.**

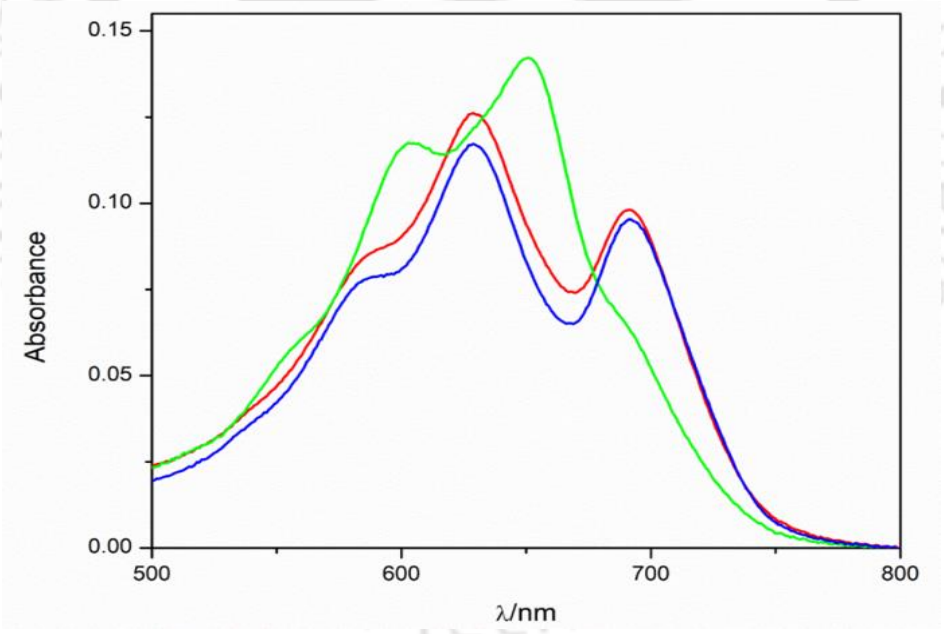

Fig 2. 18 Absorption spectra of freshly prepared **Agg2** (red), monomer (green), and regenerated **Agg2** (blue). via fast cooling. After self-assembly of **PNIBF2** into **Agg2** via dispersion method (red spectrum), the solution was heated to 328 K (green spectrum). The warm solution was then cooled down quickly by placing the container inside ice-cold water (278 K) for 10 min. The spectrum was recorded again at 293 K (blue spectrum). The spectra of freshly prepared Agg2 and regenerated **Agg2** were found to be similar.

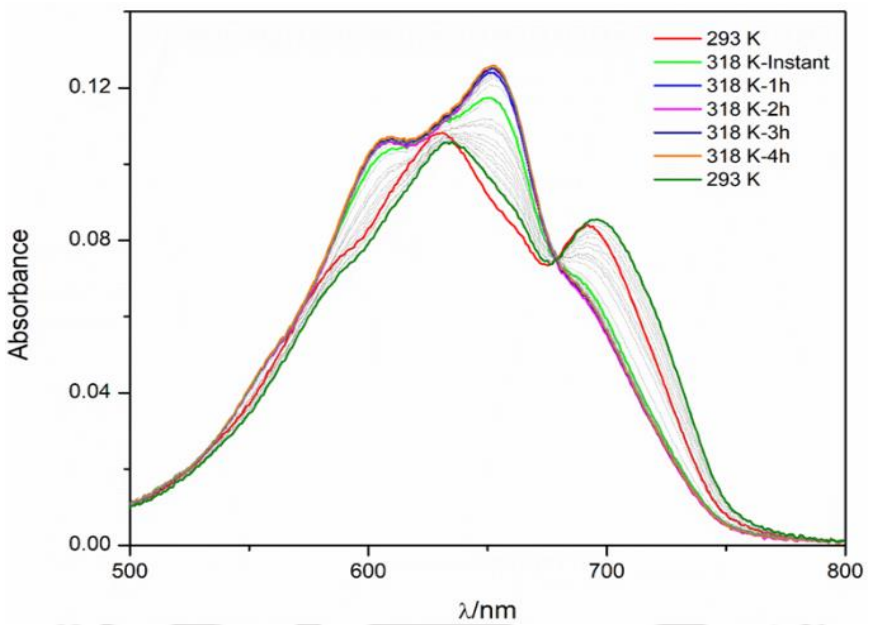

Fig 2. 19 Temperature dependent absorption spectra (c ~5.0 μM) of **Agg2** in a 76/24 (v/v) mixture of water-THF at various temperatures. After preparation, the aggregate was kept at 318 K for 4 h, and subsequently cooled down to 293 K. After partial dis-assembly (within 1 h), the spectra remained invariant.

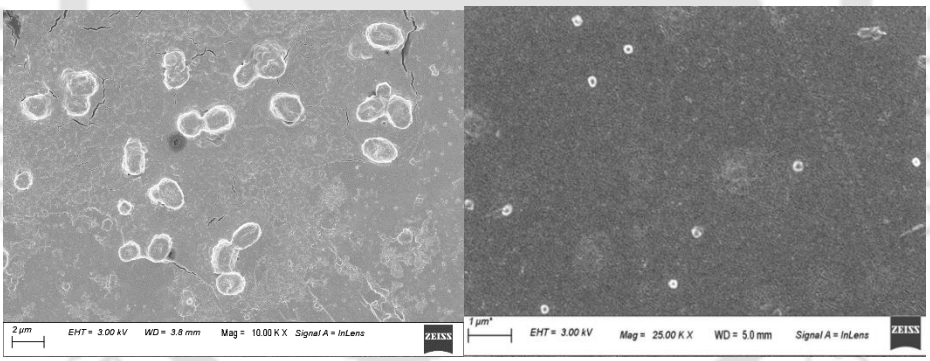

Fig 2. 20 FESEM images of **Agg2** (left) and **Agg3** (right) at f_w = 0.76.

The formation of two different aggregates in a same solvent system, albeit with different procedures, can be explained by considering the importance of surface area to volume (SA/V) ratios for cyclic structures. The primary influence responsible for the formation of both **Agg2** and **Agg3**, are hydrophobic interactions between the solvent and the non-polar aromatic rings, and hydrophilic relation with the polar amine and carbonyl groups. In each of these cases, the dye aggregated into bilayers, and further condensed to form globular aggregates. With respect

to the curvature generated, either ellipsoidal (**Agg2**) or spherical (**Agg3**) structures are preferred. The SA/V ratios determine the stability of either of these structures, where the lesser the ratio, the greater is the stability. This ratio is the least for a spherical shape, considering similar volume.[20] Therefore, with lesser surface area, the degree of hydrophobic interactions is considered to be the least for the sphere **Agg3** when compared to **Agg2**. Hence, it is a given that the aggregate **Agg3** is the more prefered stable structure thermodynamically, and thus, in relation to the energy landscape, **Agg3** corresponds to the global minimum. The **Agg2**, on the other hand, correspond to a local minimum. Faster thermal equilibration at high temperature, as in the case of **Agg3**, allowed the dye to assemble at a global minimum. On the other hand, relatively slower kinetics at room temperature led to trapping at local minima.

In order to provide a proof for this hypothesis, a solution of the dye was prepared in 95/5 (v/v) water-THF by rapidly injecting a monomeric THF solution of the dye into water, keeping the concentration of the dye ~ 5 μM. The spectral signature in the specified solvent system was observed to be quite similar to that of **Agg2**, albeit with slight shifts in absorption maxima (Fig 2. 21). Such minor changes could be ignored considering the fact that the solvent system is now different. This supramolecular aggregate, however, responded quite differently to temperature changes. Even at elevated temperatures, no dis-assembly of the aggregate was observed. The spectral features remained unaltered over the whole temperature range from 293 K to 328 K. Combination of greater hydrophobic action and very slow kinetics prompts the dye to be in a locked state of forced local minimum, preventing dis-assembly even when exposed to heat. The morphology of the shapes were found to be non-spherical, as evidenced from FESEM (Fig 2. 21).

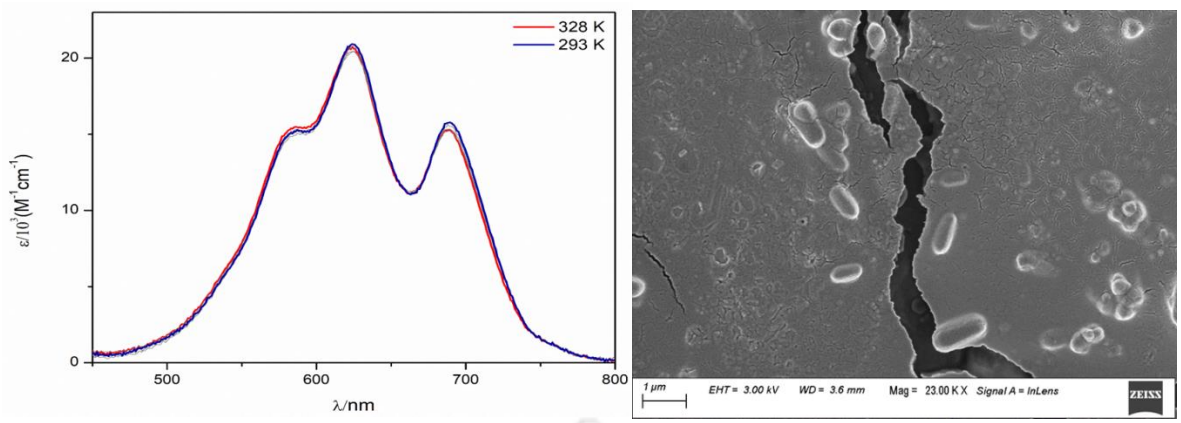

Fig 2. 21 Variable temperature absorption spectra of PNIBF2 in f_w = 95 %.indicating non-dissociation of **Agg2.** FESEM images of **Agg2** in f_w = 0.95

❖ 2.3 Curve fitting

Agg2 via heating

Method 1: Individual fits + averaging

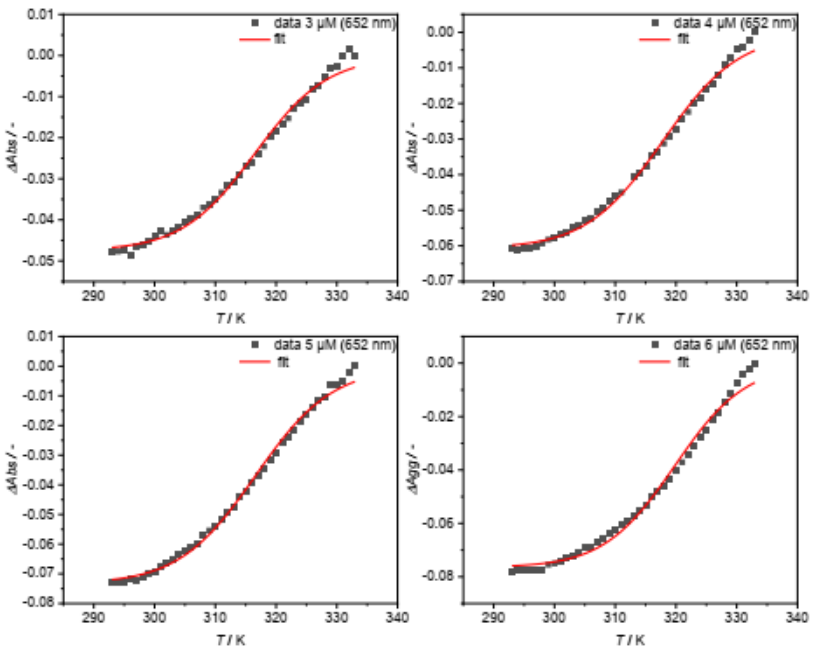

Fig 2. 22 Fit curves for the temperature-induced disassembly of **Agg2** extracted from the absorptiondata for different concentrations and corresponding individual fit curves

.

Table 2. 1 Thermodynamic parameters derived from individual fitting via heating **Agg2**.

Dataset	ΔH / kJmol^{-1}	ΔS / Jmol^{-1}	ΔH$_{nucl}$ / kJmol^{-1}	Tm/ K	ΔG/kJmol^{-1}	σ	χ^2
3µM; 652nm, absorbance	-153.81 ± 6.63	- 384.5 ± 20.7	0	316.0	-39.16	1	4.11 E-02
4µM; 652nm, absorbance	-147.53 ± 5.27	-365.1 ± 16.4	0	317.1	-38.67	1	2.64 E-02
5µM; 652nm, absorbance	-146.07 ± 4.22	-364.1 ± 13.1	0	316.0	-37.50	1	1.85 E-02
6µM; 652nm, absorbance	-161.10 ± 7.29	- 408.1 ± 22.6	0	318.8	-39.42	1	4.58 E-02
∅	**-151.63 ± 5,85**	**-380,45 ± 18.1**	**0**		**-38.69**	**1**	

Method 2: Global fitting

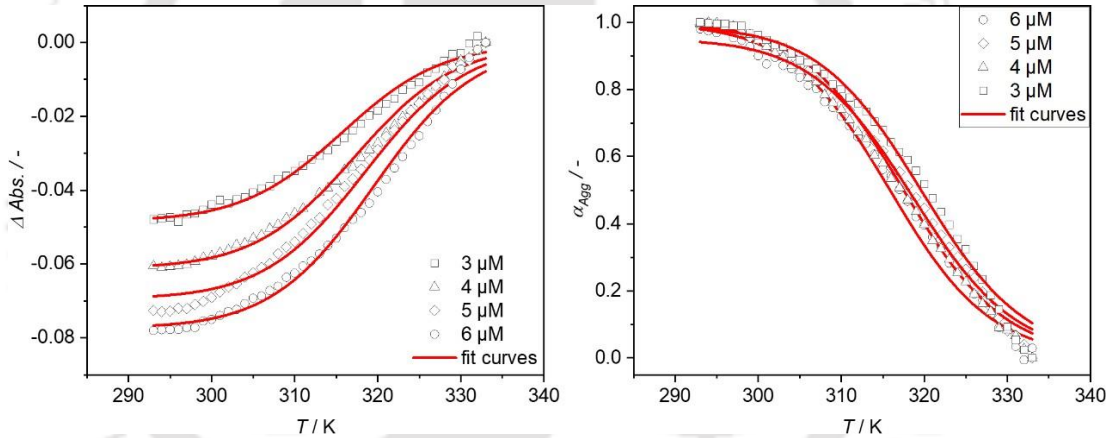

Fig 2. 23 Fit curves for the temperature-induced disassembly of **Agg2** extracted from the absorptiondata for different concentrations and corresponding individual fit curve

Table 2.2 Thermodynamic parameters derived from global fitting (heating **Agg 2**).

Dataset	T_m / K	ΔG/ kJmol^{-1}	σ	χ^2
3 µM; α_{Agg}	315.9	-38.7	1	2.02e-01
4 µM; α_{Agg}	317.5	-38.7	1	2.02e-01
5 µM; α_{Agg}	318.1	-38.7	1	2.02e-01
6 µM; α_{Agg}	319.6	-38.7	1	2.02e-01

The given data implies an isodesmic self-assembly mechanism for the formation/disassembly of **Agg2**. Both approaches, either by individual fitting of the single concentrations and

subsequent averaging or by fitting all concentrations simultaneously give a Gibbs free energy of ΔG = -38.7 kJ/mol.

Agg3 via cooling

Method : Individual fits + averaging

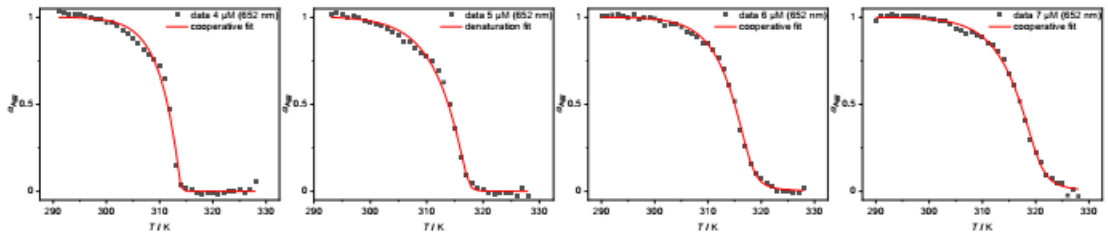

Fig 2. 24 plot of the degree of aggregation (αAgg) against the temperature for different concentrations and corresponding individual fit curves obtained from the nucleation-elongation model for **Agg3**

Table 2.3 Thermodynamic parameters derived from individual fitting to the nucleation-elongation model for **Agg3**.

dataset	ΔH^{298} / kJmol^{-1}	ΔS^{298} / Jmol^{-1}	ΔH_{nucl}^{298} / kJmol^{-1}	T_e / K	ΔG^{298} / kJmol^{-1}	K_{el}	K_{nucl}	σ	χ^2
4μM; 652nm, ALPHA	-223.7 ± 19.6	-609.1 ± 63.0	-27.8 ± 17.9	314.0	-42.1	250021.2	5.9	2.37e-05	3.65e-02
5μM; 652nm, ALPHA	-167.0 ± 10.6	-425.1 ± 33.8	-19.6 ± 4.3	317.1	-40.2	200019.3	119.0	5.95e-04	1.67e-02
6μM; 652nm, ALPHA	-202.6 ± 10.3	-538.5 ± 32.9	-10.4 ± 1.0	317.2	-42.0	166685.9	3252.2	1.95e-02	8.95e-03
7μM; 652nm, ALPHA	-182.3 ± 10.6	-471.7 ± 33.8	-9.7 ± 1.0	319.6	- 41.7	142857.5	3716.3	2.60e-02	1.20e-02
∅	**-193.9 ± 12.8**	**-511.1 ± 40.9**	**-16.9** ± **6.1**		**-41.5**				

The given data implies a cooperative self-assembly mechanism for the formation of **Agg3**. The averaged Gibbs free energy of -41.5 kJ/mol agrees well with **Agg3** being the most stable species.

❖ 2.4 Conclusions

In a summary, the chromophoric part of PNI dye was modified, and PNI-BF_2 was synthesized in good yield. The BF_2-coordinated dye was characterized well with a combination of various analytical techniques. Structural aspect of the dye was analysed from the DFT-optimized structure. Both the theoretical study and the UV-vis investigations confirmed structural rigidification after BF_2-coordination. The new dye PNI-BF_2 showed improved emission quantum yield than that of the parent PNI. The dye showed different self-assembly processes in solvents of varied polarity. Importantly, PNI-BF_2 exhibited different aggregations even in same solvent system if there is variation in preparation method. In non-polar solvents, PNI-BF_2 produced emissive linear nanoaggregates **Agg1**. Similar results were obtained either with a MCH/DCE (v/v 99/1) or with a MCH/$CHCl_3$ mixtures with same volume percentage of MCH. But, the scenarios were quite different in the case of polar solvent mixture. In a 76:24 v/v mixture of water and THF, two kinds of aggregation were seen, **Agg2** and **Agg3**. The kinetic aggregate **Agg2** was formed upon mixing a monomeric solution of THF with water at room temperature. Heating the **Agg2** and subsequently cooling it back slowly converted the aggregate to **Agg3** which would be considered as a thermodynamic aggregate. **Agg2** could also be locked kinetically by the imposition of greater hydrophobicity. In a 95/5 (v/v) water/mixture the **Agg2** did not show any change even after thermal input. The rare incidents of supramolecular polymorphism have been demonstrated using PNI-BF_2 by formation of two aggregates in the same solvent systems. Investigations on the self-assembly of PNI-BF_2 thus enriched the relatively underdeveloped field of supramolecular polymorphism.

2.5 References

[1] a) Bernstein, J.; Polymorphism in Molecular Crystals, Oxford University Press, Oxford, **2010**. b) Shen, C.-A.; Bialas, D.; Hecht, M.; Stepanenko, V.; Sugiyasu, K. and Würthner, F.; *Angew. Chem., Int. Ed*. **2021**, 60, 11949–11958.

[2] a) Erk, P.; Hengelsberg, H.; Haddow, M.F. and van Gelder, R.; *CrystEngComm* **2004**, 6, 474–483. b) Gsänger, M.; Bialas, D.; Huang, L.; Stolte, M. and Würthner, F.; *Adv. Mater*. **2016**, 28, 3615–3645.

[3] (a) Würthner, F.; Kaiser, T.E. and Saha-Möller, C.R.; *Angew. Chem., Int. Ed.* **2011**, 50, 3376–3410; b) Hestand, N.J. and Spano, F.C.; *Chem. Rev*. **2018**, 118, 7069–7163; c) Herbst, W. and Hunger, K.; Industrial Organic Pigments: Production, Properties, Applications, Wiley-VCH, Weinheim, 3rd Completely Revised edn, **2004.**

[4] (a) de Greef, T.F.A.; Smulders, M.M.J.; Wolffs, M.; Schenning, A.P.H.J.; Sijbesma, R.P. and Meijer, E.W.; *Chem. Rev*. **2009**, 109, 5687–5754; b) Korevaar, P.A.; George, S.J.; Markvoort, A.J.; Smulders, M.M.J.; Hilbers, P.A.J.; Schenning, A.P.H.J.; de Greef, T.F.A. and Meijer, E.W.; *Nature* **2012**, 481, 492– 496.

[5] (a) Fennel, F.; Wolter, S.; Xie, Z.; Plötz, P.-A.; Kühn, O.; Würthner, F. and Lochbrunner, S.; *J. Am. Chem. Soc*. **2013**, 135, 18722–18725; (b) Wehner, M.; Röhr, M.I.S.; Bühler, M.; Stepanenko, V.; Wagner, W. and Würthner,F.; *J. Am. Chem. Soc.* **2019**, 141, 6092–6107; (c) Hecht, M.; Leowanawat, P.; Gerlach, T.; Stepanenko, V.; Stolte, M.; Lehmann, M. and Würthner, F.; *Angew. Chem., Int. Ed*. **2020**, 59, 17084– 17090; (d) Wehner, M.; Röhr, M.I.S.; Stepanenko, V. and Würthner, F.; *Nat. Commun*. **2020**, 11, 5460–5469; (e) Wagner, W.; Wehner, M.; Stepanenko, V. Ogi, S. and Würthner, F.; *Angew. Chem., Int. Ed.* **2017**, 56, 16008–16012.

[6] (a) Ogi, S.; Sugiyasu, K.; Manna, S.; Samitsu, S. and Takeuchi, M.; *Nat. Chem.* **2014**, 6, 188–195; (b) Fukui, T.; Kawai, S.; Fujinuma, S.; Matsushita, Y.; Yasuda, T.; Sakurai, T.; Seki, S.; Takeuchi, M. and Sugiyasu, K.; *Nat. Chem.* **2017**, 9, 493–499.

[7] (a) Herkert, L.; Droste, J.; Kartha, K.K.; Korevaar, P.A.; de Greef, T.F.A.; Hansen, M.R. and Fernández, G.; *Angew. Chem., Int. Ed.* **2019**, 58, 11344–11349; (b) Matern, J.; Bäumer, N. and Fernández, G.; *J. Am. Chem. Soc.* **2021**, 143, 7164–7175; (c) Greciano, E.E.; Calbo, J.; Ortí, E. and Sánchez, L.; *Angew. Chem., Int. Ed.* **2020,** 59, 17517–17524; (d) Valera, J.S.; Gómez, R. and Sánchez, L.; *Angew. Chem., Int. Ed*. **2019**, 58, 510–514; (e) Sarkar, S.; Sarkar, A. and George, S.J.; *Angew. Chem., Int. Ed*. **2020**, 59, 19841–19845; (f) Chakraborty, A.; Ghosh, G.; Pal, D.S.; Varghese, S. and Ghosh, S.; *Chem. Sci*. **2019**, 10, 7345–7351; (g) Deng, J. and Walther, A.; *J. Am. Chem. Soc.* **2020**, 142, 685–689; (h) Vantomme, G.; ter Huurne, G.M.; Kulkarni, C.; ten Eikelder, H.M.M.; Markvoort, A.J.; Palmans, A.R.A. and Meijer, E.W.; *J. Am. Chem. Soc*. **2019**, 141, 18278–18285.

[8] (a) Aliprandi, A.; Mauro, M. and de Cola, L.; *Nat. Chem*. **2016**, 8, 10–15; (b) Endo, M.; Fukui, T.; Jung, S.H.; Yagai, S.; Takeuchi, M. and Sugiyasu, K.; *J. Am. Chem. Soc*. **2016**, 138, 14347–14353; (c) Langenstroer, A.; Kartha, K.K.; Dorca, Y.; Droste, J.; Stepanenko, V.; Albuquerque, R.Q.; Hansen, M.R.; Sánchez, L. and Fernández, G.; *J. Am. Chem. Soc*. **2019**, 141, 5192–5200; (d) Matern,

J.; Kartha, K.K.; Sánchez, L. and Fernández, G.; *Chem. Sci*. **2020**, 11, 6780–6788; (e) Tidhar, Y.; Weissman, H.; Wolf, S.G.; Gulino, A. and Rybtchinski, B.; *Chem. – Eur. J*. **2011**, 17, 6068–6075.

[9] (a) S. Ogi, K. Sugiyasu, S. Manna, S. Samitsu and M. Takeuchi, *Nat. Chem.* **2014**, 6, 188–195; (b) T. Fukui, S. Kawai, S. Fujinuma, Y. Matsushita, T. Yasuda, T. Sakurai, S. Seki, M. Takeuchi and K. Sugiyasu, *Nat. Chem.* **2017**, 9, 493–499.

[10] Das, R. J. and Mahata, K.; *Soft Matter*. **2019**, 15, 5282–5286.

[11] (a) Li, D.; Zhang, H. and Wang, Y.; *Chem. Soc. Rev*. **2013**, 42, 8416–8433; (b) Frath, D.; Massue, J.; Ulrich, G. and Ziessel, R.; *Angew. Chem., Int. Ed*. **2014**, 53, 2290–2310; (c) Lu, H.; Mack, J.; Yang, Y. and Shen, Z.; *Chem. Soc. Rev*. **2014**, 43, 4778–4823.
[12] Mellerup, S.K. and Wang, S.; *Chem. Soc. Rev.*, **2019**, 48, 3537–3549.

[13] (a) Loudet, A. and Burgess, K.; *Chem. Rev.* **2007**, 107, 4891–4932; (b) Ulrich, G.; Ziessel, R. and Harriman, A.; *Angew. Chem., Int. Ed*. **2008**, 47, 1184–1201; (c) Kowada, T.; Maeda, H. and Kikuchi, K.; *Chem. Soc. Rev*. **2015**, 44, 4953–4972; (d) Cherumukkil, S.; Vedhanarayanan, B.; Das, G.; Praveen, V.K. and Ajayaghosh, A.; *Bull. Chem. Soc. Jpn*. **2018**, 91, 100–120.
[14] Chen, P.-Z.; Niu, L.-Y.; Chen, Y.-Z. and Yang, Q.-Z.; *Coord. Chem. Rev.* **2017**, 350, 196–216.

[15] (a) Kubota, Y.; Tanaka, S.; Funabiki, K. and Matsui, M.; *Org. Lett*. **2012**, 14, 4682–4685; (b) Wu, Z.; Sun, J.; Zhang, Z,; Yang, H.; Xue, P. and Lu, R.; *Chem. – Eur. J*. **2017**, 23, 1901– 1909; (c) Yu, Z.; Wu, Y.; Xiao, L.; Chen, J.; Liao, Q.; Yao, J. and Fu, H.; *J. Am. Chem. Soc.* **2017**, 139, 6376–6381; (d) Shimogawa, H.; Murata, Y. and Wakamiya, A.; *Org. Lett*. **2018**, 20, 5135–5138; (e) Zhao, N.; Ma, C.; Yang, W.; Yin, W.; Wei, J. and Li, N.; *Chem. Commun.* **2019**, 55, 8494–8497; (f) Wong, J.M.; Zhang, R.; Xie, P.; Yang, L.; Zhang, M.; Zhou, R.; Wang, R.; Shen, Y,; Yang, B.; Wang, H.-B. and Ding, Z.; *Angew. Chem., Int. Ed*. **2020**, 59, 17461–17466; (g) Ohtani, S.; Nakamura, M.; Gon, M.; Tanaka, K. and Chujo, Y.; *Chem. Commun*. **2020**, 56, 6575– 6578; (h) Wang, Z.; Pan, J.; Li, Q.; Zhou, Y.; Yang, S.; Xu, J.-J. and Hua, D.; *Adv. Funct. Mater*. **2020**, 30, 2000220. (i) Tan, G.; Schrader, M.L.; Daniliuc, C.; Strieth-Kalthoff, F. and Glorius, F.; *Angew. Chem., Int. Ed*. **2020**, 59, 21541–21545.

[16] (a) Tian, D.; Qi, F.; Ma, H.; Wang, X.; Pan, Y.; Chen, R.; Shen, Z.; Liu, Z.; Huang, L. and Huang, W.; *Nat. Commun*. **2018**, 9, 2688; (b) Wang, H.; Zhang, Y.; Chen, Y.; Pan, H.; Ren, X. and Chen, Z.; *Angew. Chem., Int. Ed*. **2020**, 59, 5185–5192. (c) Helmers, I.; Ghosh, G.; Albuquerque, R.Q. and Fernández, G.; *Angew. Chem., Int. Ed.* **2021**, 60, 4368–4376.

[17] Wang, S.; Zhao, Y.-L.; Zhao, C.-X.; Liu, L. and Yu, S.; *J. Fluor. Chem*. **2013**, 156, 236–239.

[**18**] Mabesoone, M. F. J.; Markvoort, A. J.; Banno, M.; Yamaguchi, T.; Helmich, F.; Naito, Y.; Yashima, E.; Palmans A. R. A. and Meijer, E. W.; *J. Am. Chem. Soc*. **2018**, 140, 7810–7819.

[19] Smulders, M. M. J.; Nieuwenhuizen, M. M. L.; de Greef, T. F. A.; van der Schoot, P.; Schenning, A. P. H. J. and Meijer, E.W.; *Chem. – Eur. J*. **2010**, 16, 362–367.

[20] Harris, L.K. and Theriot, J.A.; *Trends Microbiol*. **2018**, 26, 815–832.

Chapter 3

Ring substituted peri-naphthoindigo and its supramolecular rearrangement through incorporation of guest

❖ 3.1 Introduction

Molecular self-assembly plays a pivotal role in obtaining complex structures and functions of many biomolecules, such as protein, nucleic acids, phospholipid membrane etc. Taking inspiration from a variety of natural supramolecular assemblies, chemists have realized a large number of nano- & supra-structures including vesicles, micelles, fibres, wires, and ribbons. In such assemblies, the repeating units are held together via different types of non-covalent interactions like hydrogen bonding, aromatic interactions, metal-ligand interactions, electrostatic interactions, host-guest interactions, hydrophilic/hydrophobic interactions etc. Unlike the traditional covalent polymers, supramolecular polymers display additional unique characteristics like stimuli-responsiveness, self-healing, and coordination capacity, due to the dynamic and reversible nature of the specified non-covalent interactions. Unsurprisingly, many of them found applications as materials for bioimaging, sensors, drug-delivery, switching etc. While initial focus of the supramolecular chemists was to increase the structural diversity of such assemblies, the current emphasis is biased towards functional aspects of them. Accordingly, various tunable assemblies have been reported in recent times. Such switching from one aggregate to another or supramolecular rearrangements have been accomplished with the help of various external inputs.[1] There have been multiple reports of supramolecular cages or macrocycles being tuned by the addition of anions, metals and other guests.[2] The dyes with coordinating site behave in different ways in presence and absence of metal ion. Therefore, addition-removal of the metal ion can lead to a change in the supramolecular aggregates. In absence of metal ion, the aggregation is guided by solvophobic interactions, but in presence the metal play significant role in final outcome of such aggregations.[3] Horne *et al*. reported the change of supramolecular coiled structures of

peptides to cyclic structures of nets and frameworks upon induction of Cu^{2+}.[4] The role of metal ions in supramolecular chemistry is established and documented in literature.[5]

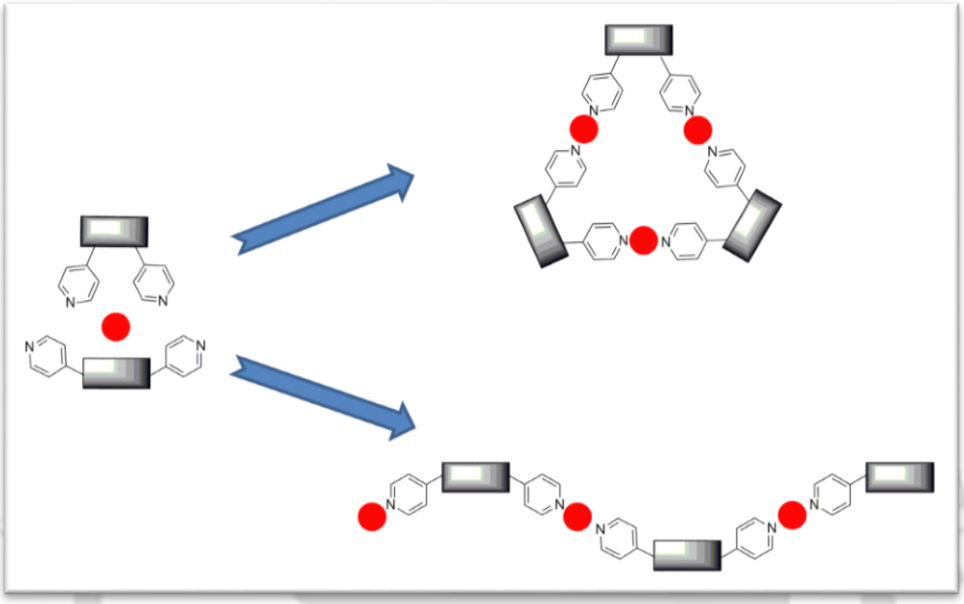

Fig 3. 1 Simplistic example of metal induced supramolecular rearrangement into supramolecular triangles or fibres.

Such flexibility or tuning of supramolecular aggregates is a key characteristic for their potential use in smart materials.[6] Supramolecular rearrangement can be achieved if a monomer possess multiple sites for non-covalent interactions. Changing the magnitude of individual non-covalent interactions can lead to the formation of different aggregates. Therefore, the external inputs or stimuli must be capable of suppressing or increasing the non-covalent interactions to cause a change in the supramolecular arrangements.[7] In such a case, one interaction should act as primary interaction, while the other settle for spectator or become secondary. The addition sequence of these agents would have to be in order of weaker to stronger influence, i.e. the continuous change in self-assembly can only be brought about by the addition of the agent which exerts a weaker action on the supramolecular

interaction of the studied motif compared to the one it precedes. This idea of morphology rearrangement has taken the interest of quite a few researchers in recent times, due to the pre-existing reports of supramolecular rearrangement by the introduction of additives into a solution of the aggregated dye.[8] This kind of supramolecular rearrangement may eventually find usage in various fields where a supramolecular response to an unique stimulus is useful to establish some kind of secondary action visible or at least measurable on a macro scale. As reported, these kinds of interactions have already been studied in the context of molecular switches, rotors, and sensors in some of the recent examples.

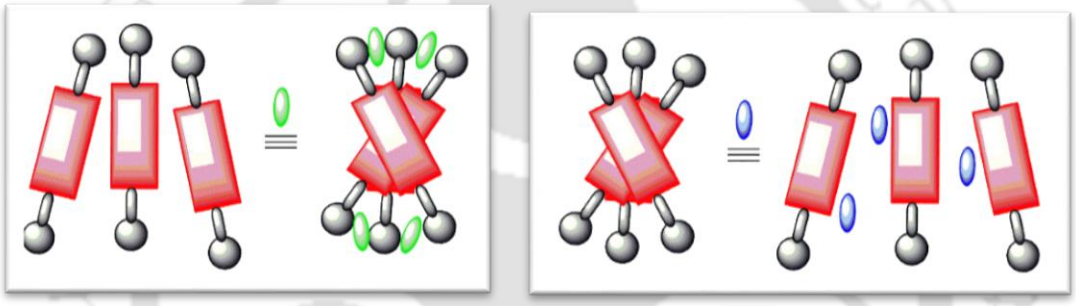

Fig 3. 2 Analyte induced aggregation (anion-cation based) and analyte induced disassembly (charge transfer), each of which may functions as sensors for the respective analyte.

In the present chapter, a derivative of a fascinating dye peri-naphthoindigo (PNI) was synthesized by installing butyl group at the *peri*-positions. Supramolecular rearrangement of the new dye was investigated in non-polar solvents, under the influence of acid (trifluoroacetic acid or TFA) and fullerene C_{60} as guests. The choice of the guests was originated from their utilization for similar purpose in recent time. For example, altering the pH of the solution of an organic molecule has been known to induce acidochromic behaviour, as demonstrated by Shinkai *et al.*,[9] among many others, which was a result of supramolecular interactions being modified as an action of the incorporated acid.[10] Fullerenes are a relatively new introduction into the field of supramolecular chemistry. Ajayaghosh *et al.* utilized

fullerenes to control gelation of their motif. A report by Hasobe *et al.* demonstrated the formation of zinc porphyrin nanorods, the control on the structure was achieved via the encapsulated fullerenes. Fullerenes were also used an effective material for disaggregation of amyloid fibres, which finds subsequent use in the medical context.

❖ 3.2 Design strategy

Peri-naphthoindigo (PNI) is a unique dye in which two donor-acceptor pairs are sandwiched between naphthalene rings through *peri*-positions. Because of its unmatched structural features, PNI showed interesting self-assembly properties. The BF_2-coordinated PNI showed supramolecular polymorphism in water-THF mixture. Depending upon the cooling rate of the molecularly dissolved state at elevated temperature, formation of two different aggregates was observed. The parent PNI also showed aggregation when a THF solution of the dye was added to hexane to make the final solvent composition hexane/THF (v/v) = 9/1.[11] As a result of aggregation, the photoluminescent intensity was enhanced. In other words, PNI exhibited aggregation induced enhanced emission (AIEE) phenomenon. However, the most intriguing feature of the dye was to install AIEE in a dye that cannot show the same alone. The dye produced co-aggregate with 4-amino naphthalene monoimide derivative NH_2-NMI. Emission intensities were increased for both the dyes, PNI and NH_2-NMI, in the co-aggregate.[12] The morphology of the co-aggregate was found to be 2D nano-wire. On the other hand, PNI alone produced 3D cubical morphology (Fig 3. 3). Such cube is very rigid and generated as a consequence of unhindered growth on all sides. Undoubtedly, different types of aggregates from the PNI core are very promising. But, the rigid 3D rigid morphology of the parent dye aggregate is a limiting factor for supramolecular rearrangements. Therefore, modification in the PNI dye is necessary, so that a more flexible aggregate could be generated. The rigidity can be attenuated by hindering the 3-D growth. Therefore, introduction of substituents could

provide a viable solution. Modification on the PNI can be done either at core chromophore or at the naphthalene rings. Alteration at the chromophore might bring a lot of changes including planarity. On the other hand, derivatization at the ring would keep the basic PNI core intact. The only difference that might result is in self-assembly behaviour. Bearing all the points in mind, ring-substituted PNI is the appropriate choice to generate switching aggregates.

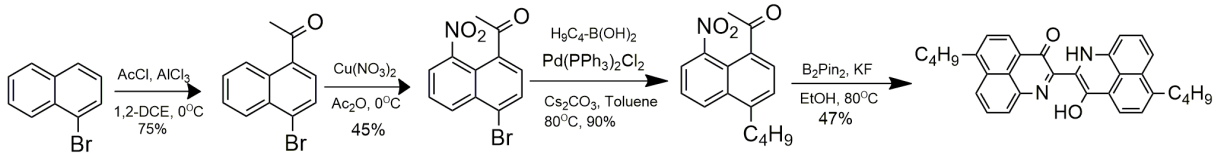

Considering the mechanism of 3D cube formation, installation of a group at the other *peri* position of the naphthalene ring would accomplish the desired goal. Accordingly, butylPNI was designed by incorporating butyl group at the *peri*-position of naphthalene. Synthesis of the dye was accomplished following the standard method of PNI synthesis. Appropriate precursor was prepared before the final dimerization of the naphthalene fragments. The overall process is summarized above. Similar to PNI, the dye molecule butylPNI exists in its mono-enol form and is an ambipolar molecule, consisting of both hydrophilic chromophore, and hydrophobic aromatic rings with butyl groups. The presence of butyl group made subtle difference in the self-assembly behaviour. Unlike 3D cube of PNI, butylPNI produced 2D nano-wire in non-polar solvent. Such 2D aggregates were converted into another form of aggregate by adding various guests like acid, C_{60} fullerene etc. Detailed investigations are described below.

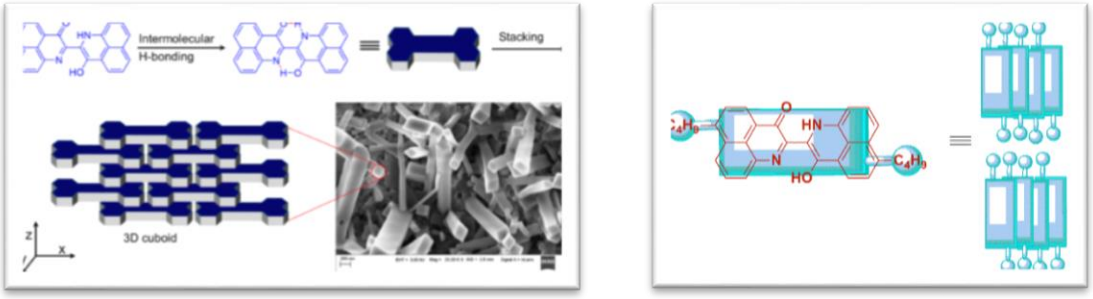

Fig 3. 3 Difference in the aggregation mechanism of PNI and butylPNI

❖ 3.3 Photophysical properties

To get idea about aggregation tendency, UV-vis absorption property of butylPNI was investigated in common organic solvents. As expected, the butyl group did not exert significant change in the absorption properties. The spectra appeared to be very similar with that of the parent PNI. [11] However there was a small bathochromic shift in the absorption maxima, indicative of the effect of alkyl auxochrome on the chromophore (Fig 3.4).

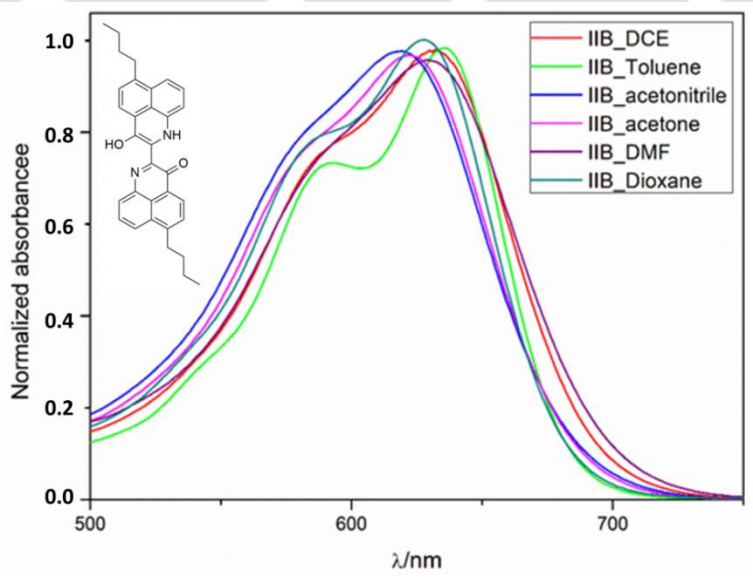

Fig 3.4 Solvent screening of ButylPNI in different solvents indicating a slight shoulder in toluene- a non-polar solvent.

As PNI produced aggregate in non-polar environment (1: 9 (v/v) THF/hexane), emphasis was given to the behaviour of ButylPNI in non-polar solvents. While the solubility of PNI was poor in non-polar solvent and required mixture of solvents for aggregation, the butyl group eased the problem out in the present scenario. It was indeed possible to record the spectra in MCH and toluene. In MCH, the dye displayed very sharp and vibronically resolved spectrum with a maximum at 634 nm (Fig 3.5). The spectral features were found to be akin with that of parent PNI in THF/hexane (1:9 v/v) mixture, suggesting aggregation of butylPNI in MCH. However, when the morphology was taken into consideration, differences in arrangement were evidenced. In case of PNI, a brick wall type arrangement took place between the polar chromophore and the non-polar solvents. Extension of the arrangements in all three directions led to the formation of cuboid aggregates (Fig 3. 3). The aggregation was

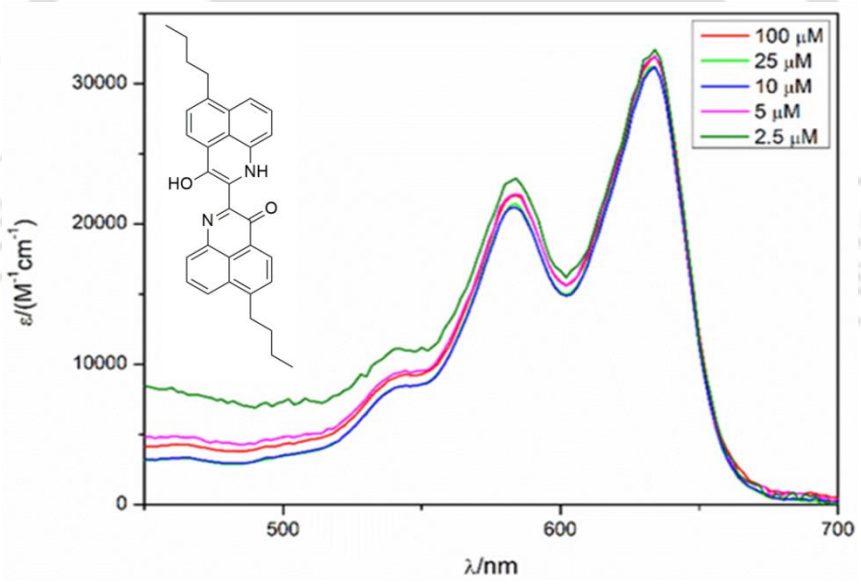

Fig 3.5 Concentration dependent absorption spectra of ButylPNI in MCH.

driven by the inherent repulsion of the polar functional groups for the non-polar solvent. Due to the presence of similar hydrophobic and hydrophilic groups, both the dyes behaved in a parallel manner. Accordingly, butylPNI molecules arranged themselves in a way to minimize

interactions between the polar chromophore and the non-polar solvents. The dye first enhanced its rigidity by forming intramolecular hydrogen bonding. The rigid monomers then arranged themselves into aggregate. However, the presence of butyl groups inhibited the growth from the side where the substituent were attached. FESEM image showed the formation fibre type aggregate in MCH (Fig 3.6). Similar self-assembly process was noticed when the investigations were carried out in another non-polar solvent toluene.

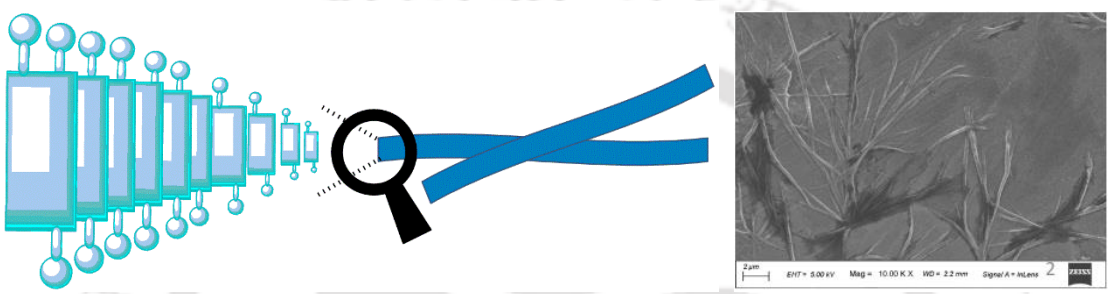

Fig 3.6 Aggregation of butylPNI into fibres evidenced by FESEM.

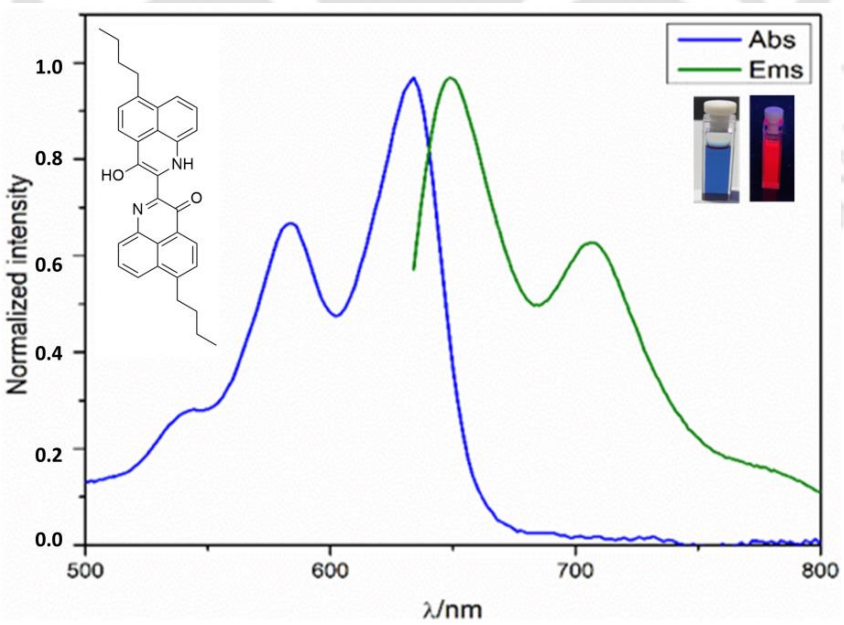

Fig 3.7 Absorbance and emission of ButylPNI in MCH.

The effect of aggregation on emission behaviour of the dye was also investigated. As demonstrated in Fig 3.6, the dye first increased its rigidity by forming intramolecular H-bonding, followed by arrangement of the rigid monomer leading to the final supramolecular assembly. In the aggregate, the rotation around the central the single bond was restricted. The non-accessibility of the chromophore to the solvent molecules also blocked the emission quenching by vibration energy transfer. Therefore, butylPNI was expected to show AIEE phenomenon, likewise to the parent dye. Unsurprisingly, the photoluminescent intensity of butylPNI was greatly enhanced in MCH. The absorbance and emission spectra of the dye in MCH exhibited a mirror image relationship (Fig 3.7).

❖ 3.3.1 Influence of acid

In next set of experiments, the effect of acids on the aggregation of butylPNI was investigated. The self-assembly process of the dye in non-polar solvents was driven by solvophobic effects, where the interaction between the polar chromophore and the nonpolar solvents were minimized. With multiple donor atoms, the chromophoric part was expected to interact with acid, which in turn could change the overall supramolecular arrangements. To test and verify the same, UV-vis property of butylPNI was measured in presence of various acid in non-polar solvents was recorded. When trifluoroacetic acid was added to a solution of the dye in MCH, the absorption maxima shifted bathochromically. The fluorescence emission of the dye quenched totally. Besides the specified optical changes, the physical state of the solution also changed, marked by precipitation of the aggregate from the solution. Microscopic investigation provided important evidence of the change in the aggregate. FESEM image of the resultant aggregates indicated extensive coiling of the aggregates (Fig 3. 10). The resultant aggregates could be reverted back to the original state simply by addition of triethylamine (Fig 3.8). To explain the change in supramolecular states, the behaviour of TFA

in the solution must be understood. It is necessary to mention that in non-polar MCH, TFA does not dissociate to generate proton. The acid molecules tried to avoid the non-polar environment of the solvents, and diffused into the intermolecular space of the aggregate. Electrostatic interaction between the functional groups of the dye and TFA stabilized the system and avoided repulsive interaction (Fig 3. 10) with solvent molecules. As a result of trapping of TFA in the intermolecular space, the morphology of the aggregate changed. Such type of interaction of acid with the functional group of dye is well known and reported recently.[13]

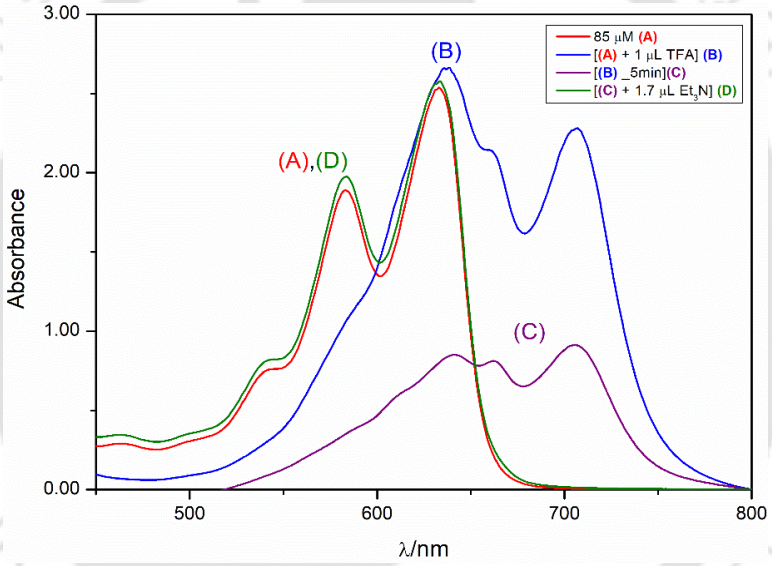

Fig 3.8 Effect of addition of acid to a solution of butylPNI in MCH and addition of Et_3N within short durations.

Attractive interactions between the functional groups of the dye and the acid also helped in the growth of the aggregate. Once complexation of the acid happened with the functional groups, the part must be kept away from the solvents. In other words, with the formation of more such complexes, the length of the aggregate increased further. Longer aggregates were found in the FESEM image with TFA than that of without the acid. The length of the aggregates in acid become so long that they were visible in naked eye. The guest induced

supramolecular rearrangement process was found to be completeley reversible. The original specrum of the aggregate without acid could be regenerated even after treating a 24 h old sample of aggregate in presence of acid. Both the spectra, the orginal and the recovered, were found to be superimposable (Fig 3 9). The study also emphasized the high stability of the aggregates.

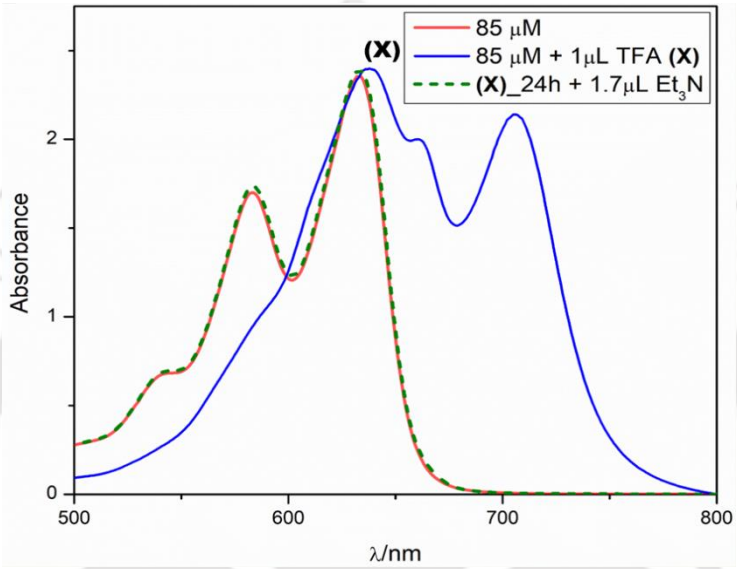

Fig 3 9 Effect of addition of acid to a solution of butylPNI in MCH and addition of Et_3N after 24 h

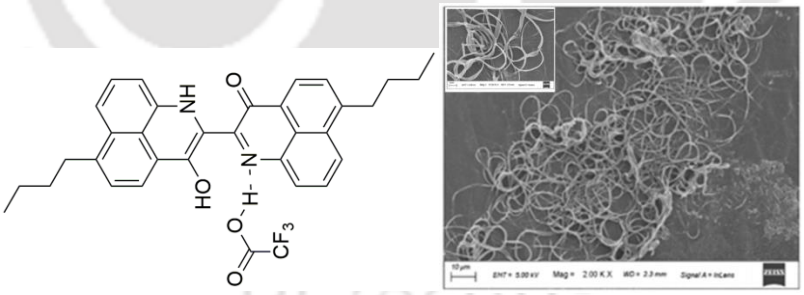

Fig 3. 10 Acid coordination to butylPNI and FESEM images of aggregates in MCH indicating extensive coiling upon addition of TFA.

❖ 3.3.2 Supramolecular rearrangement using C_{60} fullerene as guest

In the previous section, interaction between the functional groups and TFA was utilized to change the arrangement of the dye. Since four different functional groups are present in the

core, any guest that is capable to interact with the donor-acceptor pairs would cause change in the supramolecular arrangement of the dye. In the next study, C_{60} fullerene was used as guest for alteration of the self-assembly process. Fullerenes are well known for the generation of charge transfer complexes with dyes, and have been utilised in contemporary research.[14] Fullerenes have also been used to influence morphology of supramolecular aggregates, including disassembly of previously established aggregates.[15] To observe a similar rearrangement process, C_{60} fullerene was added to a solution of the dye in toluene. It is necessary to mention that in toluene butylPNI produced similar aggregate that observed in MCH. UV-vis spectrum of the dye in presence of C_{60} in toluene exhibited a hypsochromic shift of absorption maximum was observed along with broadening of the spectrum. FESEM images of the sample showed reorganization of the linear fibre like structures in absence of fullerene into a type of network. The supramolecular rearrangement can be explained by considering the formation of charge-transfer complex with C_{60}. As a result, the original supramolecular arrangement changed into a new one. Fullerenes are well known for their capabilities to form charge-transfer complex by acting either as electron acceptors or as donors depending upon the molecules they form a complex with. Since both the guests, TFA and C_{60}, are capable of bringing change in the original aggregate of the dye, experiments were designed in a way to incorporate both of them in a sequential manner. For the same purpose, MCH was avoided due to the insolubility C_{60} in MCH. In the presence of acid, butylPNI also produced precipitation. Considering the disadvantages of MCH, toluene was used as alternative solvent with similar polarity.

❖ 3.3.3 Influence of acid on butylPNI in toluene

Besides some minor differences, the UV-vis absorption spectrum of butylPNI was found to be similar in both the non-polar solvents, toluene and MCH. The absorption maxima were

detected at the same energy (634 nm). However, in toluene the spectrum becomes broadened with the loss of vibronic fine structure (Fig 3. 11). The positions of the second maximum were also found to be different. In MCH the second maximum was appeared at 584 nm, while the same was shifted 593 nm in toluene. The spectral features suggested the formation of smaller aggregates in toluene. But, the differences were thinner when the spectra in the presence of acid were considered. The UV-vis spectra of the dye in toluene at 25 °C in presence of acid was found to be very similar with that of the same in MCH at 90 °C. Therefore, it is quite reasonable to assume similar aggregation of the dye in the two specified solvent. The observations also justified the reason to replace MCH by toluene.

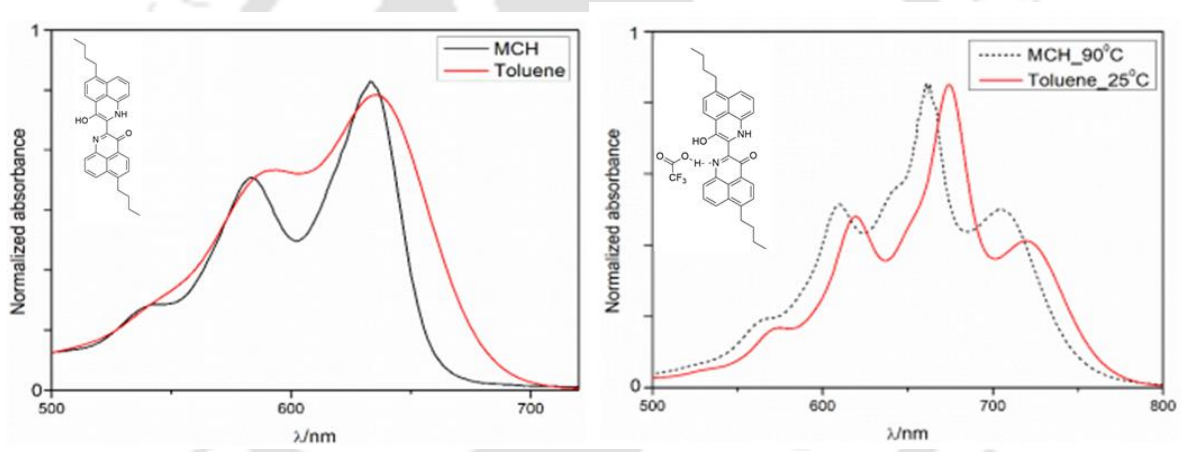

Fig 3. 11 Similarity of absorption spectra of butylPNI in MCH and toluene

In the next set of experiments, supramolecular rearrangement was controlled from remote position by adding acid indirectly via diffusion method. For the same purpose, the dye in toluene was placed over aqueous layer. Trifluoroacetic acid was used as acid source due to its good solubility both the phase. Acidity of the aqueous layer was varied to exert change in the organic layer. The experiments were carried out directly inside a UV cell, which allowed easy monitoring of the process. Diffusion of the acid vapour from the aqueous layer to the organic layer caused the supramolecular rearrangement. Replacement of the acidic water by neutral

one regenerated the original aggregate of the dye without guest. Placing the acid-trapped aggregated toluene solution over fresh de-ionised water brought the acid molecules back to the aqueous phase, releasing the trapped acid molecules from the toluene layer. In the current set-up, reversible supramolecular rearrangement was installed by controlling from remote position without the help of additional guest like triethylamine. The spectral changes due to acidification and de-acidification are depicted below in Fig 3.12 and Fig 3.13. The measurements were carried out using a 15 µM solution of butylPNI in toluene and by placing it over 10% TFA in water.

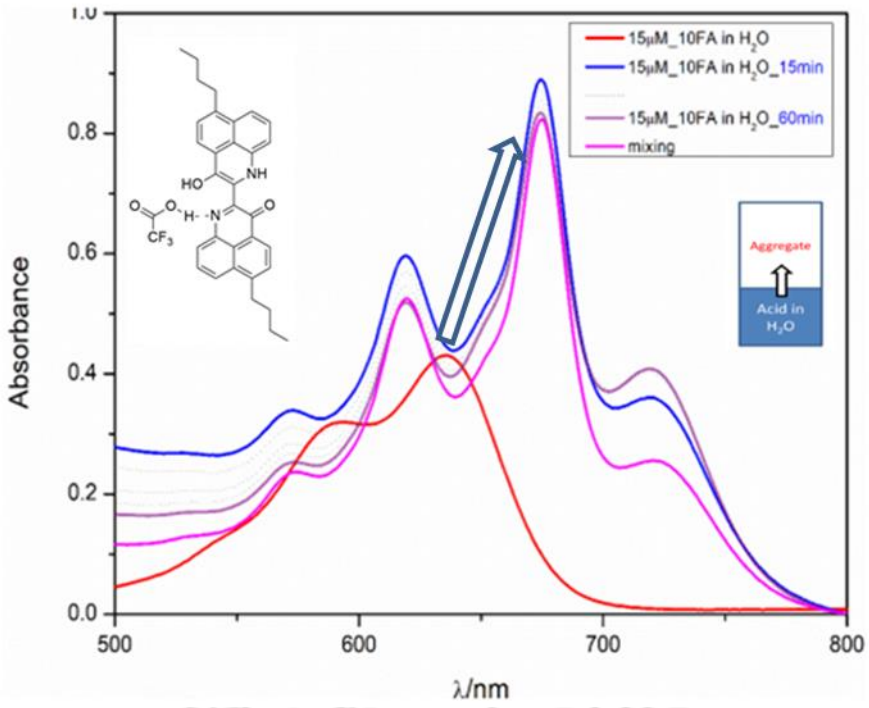

Fig 3.12 Absorption spectra of buylPNI in toluene indicating diffusion of acid from water to toluene.

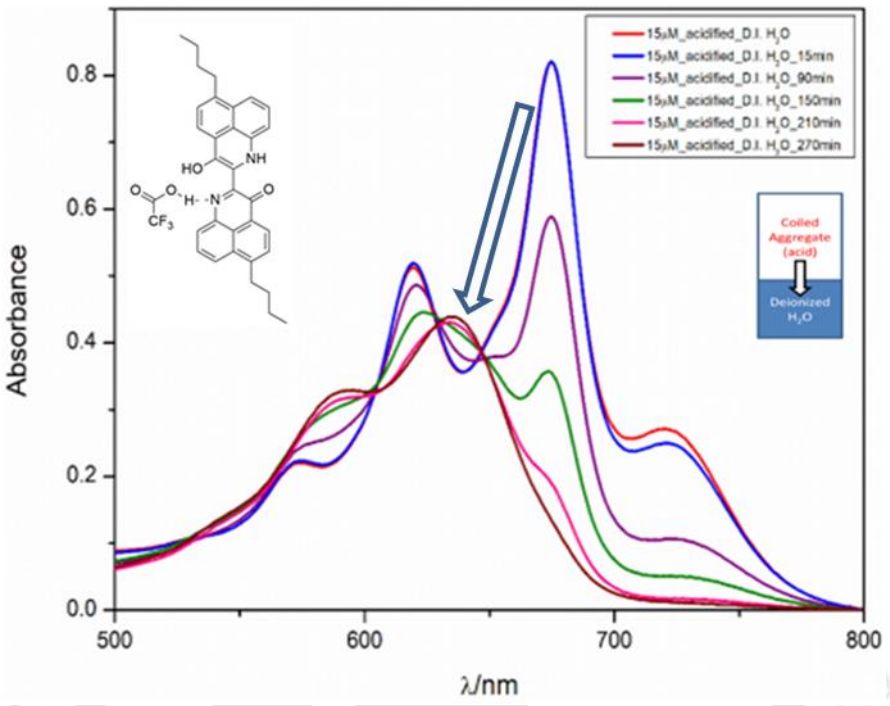

Fig 3.13 Absorption spectra of butylPNI in toluene indicating diffusion of acid from toluene to water.

❖ 3.3.4 Charge transfer complex with fullerene

Before going into the complex supramolecular rearrangement with two guests (C_{60} fullerene and acid), emphasis was given to the kinetics of charge-transfer complexation with fullerene. For the same, solid C_{60} (1 mg) was added into a solution of butylPNI (75 μM) in toluene, and the changes were recorded. Time dependent absorption spectra showed gradual change in the relative ratio of the absorption maximum (at 634 nm) and the shoulder (at 593 nm). Molar extinction co-efficient (Fig 3. 14) was also diminished with time. All the observations suggested the formation of charge-transfer complex with fullerene. The origin of the colour of PNI/butylPNI is attributed to the charge transfer from the donors to the acceptors. Once the functional groups produced charge-transfer complex with fullerene, the original charge transfer band of PNI/butylPNI decreased significantly.

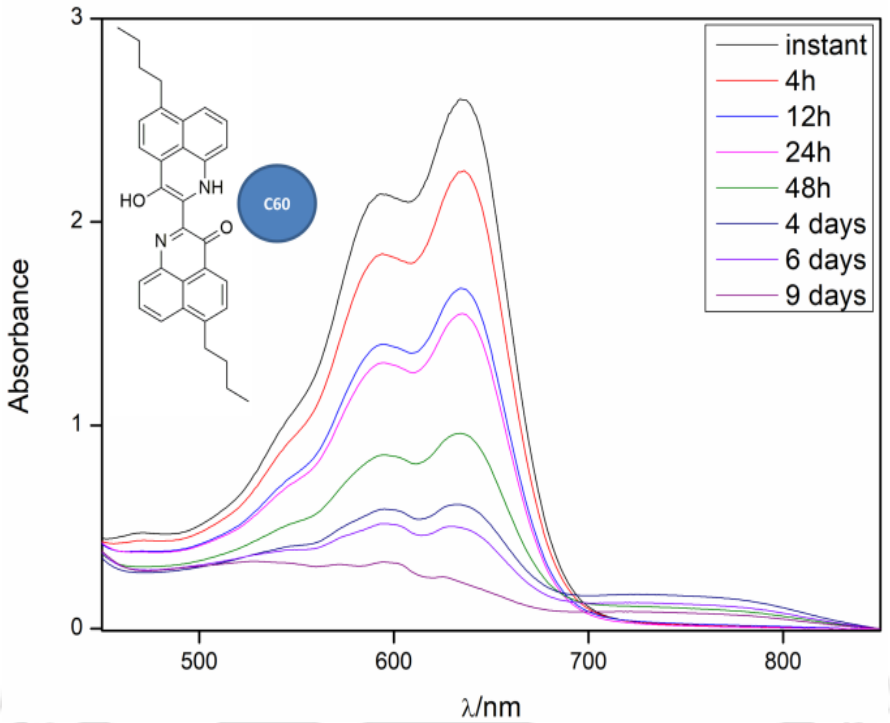

Fig 3. 14 absorption spectra of **butylPNI** in toluene (75 µM) on addition of 1 mg of fullerene (excess equivalence).

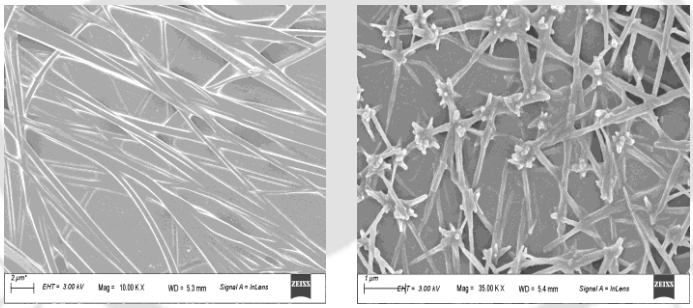

Fig 3. 15 FESEM images of butylPNI in toluene (left) and butylPNI/C_{60} in toluene(right)

❖ 3.3.5 Interaction of fullerene and acid with butylPNI

Since both the guests interacted with the dye via complexation/coordination with the functional groups, simultaneous introduction of the guests would bring a competition. In such a scenario the stronger effect would prevailed. If the charge-transfer complex is stronger over electrostatic interaction between the dye and acid molecules, then the acid-trapped aggregated

would be broken by addition of fullerene. On the other hand, if the former interaction is weaker than the later, then the charge-transfer complex with fullerene would be easily cleaved by addition of acid. To figure out the relative strength of the competing interactions, first a charge-transfer complex of the dye (3 µM) with fullerene (5 equivalents) was prepared in toluene. After confirming the same spectroscopically, 1 µL of TFA was injected to the solution. The spectroscopic signature of the C_{60}-butylPNI complex depleted with the advancement of spectral features that was resembled with the acid-trapped aggregate of the dye. Therefore, the interaction of acid with the dye was found to be stronger than the C_{60}-butylPNI charge transfer complex. However, tuning of the acid-strength remotely by diffusion method would allow us to manipulate the strength of the acid-dye interactions. Thus, fine tuning of the opposing force would allow the system to toggle between two guests. Accordingly, the acid was removed via diffusion method by placing the mixture in toluene over 1 mL of deionised water. With time, movement of acid was observed from toluene to water, as the spectra of acid coordinated dye was replaced gradually by the the spectra of the fullerene coordinated dye (Fig 3. 17). The entire sequence of the experiment is represented diagrammetically in Fig 3. 16.

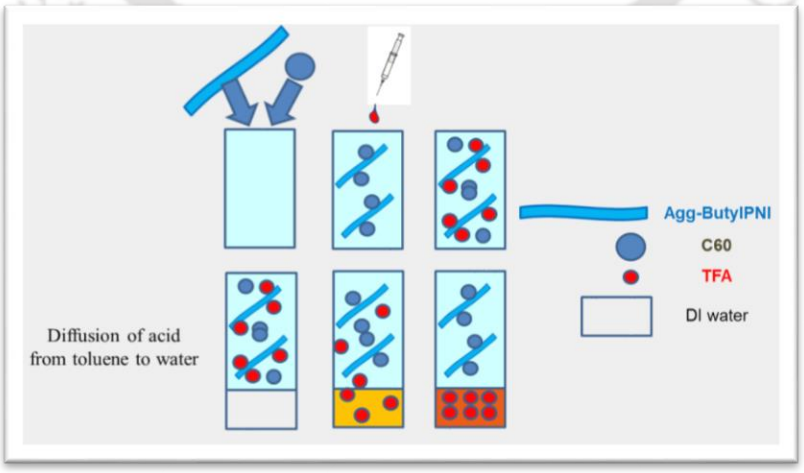

Fig 3. 16 representation of the combined experiment described above

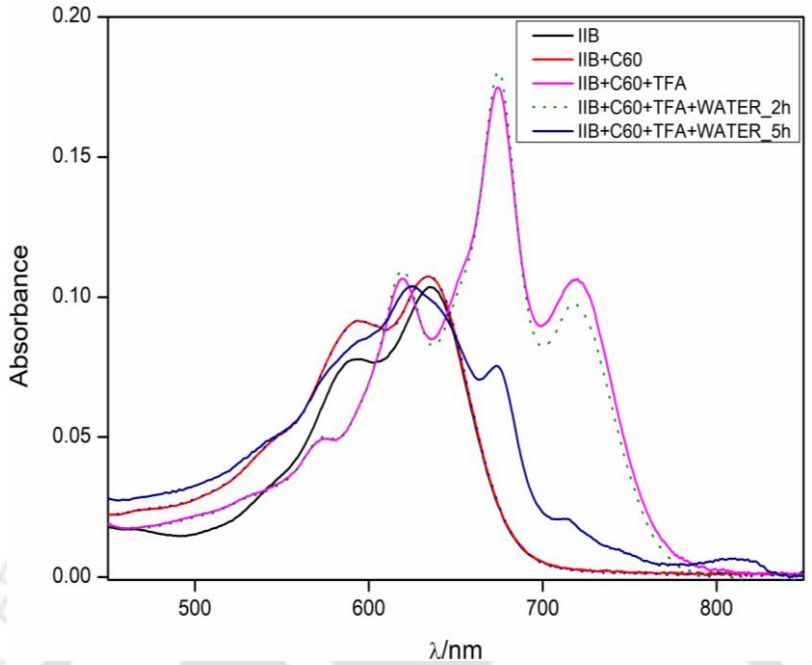

Fig 3. 17 Time dependent absorption spectra of butylPNI (3 μM) in toluene with C_{60} and TFA.

❖ 3.6 Conclusion

PNI is a recently prepared dye molecule with interesting self-assembly and co-assembly properties, but the supramolecular aggregates of PNI itself possess self imposed rigidity and limited solubility in non-polar solvents. To counter this, a derivative was prepared with butyl groups attached to the one of the *peri*-ends of the naphthalene rings. Feeble donor activity of the alkyl chain influenced slight bathochromic shifts in the absorption spectra of the dye compared to that of the original PNI. However spectral features were mostly unaffected, as the chromophore persists in the mono-enol form just like PNI. Fibre like structures were obtained in non-polar solvents as observed by FESEM and UV-vis spectroscopy. Vibronically resolved spectrum in MCH confirmed its aggregation. The aggregate in MCH was re-organised when acid was added to the solution. To avoid unfavourable interaction with solvent molecules, the acid molecules squeezed into the intermolecular space of the

aggregate. Stabilisation via electrostatic interaction with the chromophore also added to the cause. The dye was also capable of forming charge transfer complexes with fullerene, as evidenced by UV-vis spectroscopy. Sequential supramolecular rearrangements of these aggregates in non polar solvent toluene was achieved on addition of fullerene to a solution of the dye in toluene, and subsequent addition of acid, followed by removal of said acid. Each step of incorporation of additive before removal of the acid had its distinct spectral signature indicating difference in chromophore interactions in the self assemblies. The method used for acidification and subsequent removal of the acid to and from the toluene solution of the dye was relatively simple- diffusion of acid through water- toluene bilayer. The diffusion method employed here allowed gradual acidification. Similarly, the reverse process could be affected in controlled manner simply by replacing the acid-water with de-ionised water. Such remote controlled switching of the guests, hence supramolecular rearrangement, would provide a way to devise functional materials incorporating the novel dye PNI.

❖ 3.7 References

[1] (a) Shi, Q.; Javorskis, T.; Bergquist, K.-E.; Ulčinas, A.; Niaura, G.; Matulaitienė, I.; Orentas, E. and Wärnmark, K.; *Nat Commun*, **2017**, 8, 14943; (b) Herrmann-Westendorf, F.; Sachse, T.; Schulz, M.; Kaufmann, M.; Sivakov, V.; Beckert, R.; Martinez, T.; Dietzek, B. and Presselt, M.; *J. Phys. Chem. A* **2018**, 122, 9821-9832; (c) Matern, J.; Dorca, Y.; Sánchez, L. and Fernández, G.; *Angew. Chem. Int. Ed*. **2019**, 58, 16730 – 16740. (d) Fenske, T.; Korth, H.-G.; Mohr, A. and Schmuck, C.; *Chem. Eur. J*., **2012**, 18, 738-755.

[2] (a) Gimeno, N. and Vilar, R. ; *Coord. Chem. Rev.* **2006**, *250*, 3161– 3189. (b) Segarra-Maset, M. D.; Nebot, V. J.; Miravet, J. F. and Escuder, B.; *Chem. Soc. Rev.* **2013**, 42, 7086– 7098

[3] Lewis, J.E.M. and Crowley, J.D.; *ChemPlusChem* **2020**, *85*, 815.

[4] Tavenor, N.A.; Murnin, M.J. and Horne, W.S.; *J. Am. Chem. Soc.* **2017**, 139, 6, 2212–2215.

[5] Lanigan, N. and Wang, X.; *Chem. Commun.* **2013**,49, 8133-8144.

[6] (a) Chau, A. K.-H.; Leung, F. K.-C.; *Adv. Colloid Interface Sci.* **2023**, *315*, 102892. (b) Nijhuis, C. A.; Ravoo, B. J.; Huskens, J.; Reinhoudt, D. A.; *Coord. Chem. Rev.* **2007**, *251*, 1761– 1780. (c) Soto, M.A. and MacLachlan, M.J.; *Chem. Sci.*, **2024**,15, 431-441. (d) Yao, X.; Li, T.; Wang, J.; Ma, X.; Tian, H.; *Adv. Opt. Mater.* **2016**, *4*, 1322– 1349. (e) Kakuta, T.; Yamagishi, T. and Ogoshi, T.; *Acc. Chem. Res.* **2018**, *51*, 1656– 1666. (f) Chen, R.; Hammoud, A. and Aoun, P. *et al.; Nat Commun*, **2024**, 15, 4116.

[7] (a) Li, Z.; Kong, X.; Liu, X.; Qiu, H.; Zhan, L. and Yin, S.; *Chin. Chem. Lett*. **2024**, 35, 6, 109378. (b) McDowell, C.; Abdelsamie, M.; Toney, M.F. and Bazan, G.C.; *Adv. Mater.* **2018**, 30, 1707114. (c) Yamauchi, M.; Masuo, S.; *Chem.─Eur. J.* **2019**, *25*, 167– 172

[8] Shan, T.; Wang, Y.; Chen, Q., Xue, Z.; Guo, X; Li, W. and Zhong, H., *Chem. Eng. J*. **2023**, 475, 146038.

[**9**] Sugiyasu, K., Fujita, N., Takeuchi, M., Yamada, S., and Shinkai, S.; *Org. Biomol. Chem*. **2003**, 1, 895– 899

[10] (a) Wu, Z.; Sun, J.; Zhang, Z.; Gong, P.; Xue, P.; Lu, R.; *RSC Adv.* **2016**, 6, 97293– 97301. (b) Debsharma, K.; Dey, S.;Prasad, E. and Sinha, C.; *J. Indian Chem. Soc.* **2022**, 99 , 100671. (c) Xue, P. C.; Ding, J. P.; Shen, Y. B.; Gao, H. Q.; Zhao, J. Y.; Sun, J. B.; Lu, R.; *J. Mater. Chem. C* **2017**, *5*, 11532– 11541. (d) Patra, S.K.; Mahato, M.K. and Prasad, E.;*Org. Biomol. Chem.* **2024**,22, 2596-2607.

[11] Das, R. J. and Mahata, K.; *Org. Lett*. **2018**, 20, 5027–5031.

[12] Das, R. J. and Mahata, K.; *Soft Matter*. **2019**, 15, 5282–5286.

[13] (a) Kartha, K.K.; Allampally, N.V.; Yagai, S.; Albuquerque, R.Q.; Fernandez, G. *Chem. Eur. J.* **2019**, 25, 9230-9236. (b) Rest, C.; Philips, D. S.; Dünnebacke, T.; Sutar, P.; Sampedro, A.; Droste, J.; Stepanenko, V.; Hansen, M. R.; Albuquerque, R. Q.; Fernández, G.; *Chem. Eur. J.* **2020**, *26*, 10005–10013. (d) Albert, S. K.; Thelu, H. V. P.; Golla, M.; Krishnan, N. and Varghese, R.; *Chem. Eur. J*,. **2017**, 23, 8348–8352. (e) Li, Y.; Wong, K. M.-C.; Tam, A. Y.-Y.; Wu, L.; Yam, V. W.-W.; *Chem. Eur. J.* **2010**, 16, 8690–8698.

[14] Ooyama, Y.; Koji, U.; Kamimura, T.; Ozako, S.; Kanda, M.; Koide, T.; Tani, F.; *RSC Adv.* **2016**,6, 16150-16158.

[**15**] (a) Nair, V.S.; Mukhopadhyay, R.D.; Saeki, A.; Seki, S. and Ajayaghosh, A.; *Sci. Adv.* **2016**, 2,e1600142. (b) Sandanayaka, A.S.D.; Murakami, T. And Hasobe, T.; *J. Phys. Chem. C* **2009**, 113, 18369–18378. (c) Siposova, K.; Petrenko, V. I.; Ivankov, O. I.; Musatov, A.; Bulavin, L. A.; Avdeev, M. V.; Kyzyma, O. A.; *ACS Appl. Mater. Interfaces* **2020**, *12*, 32410– 32419

Chapter 4

Synthesis of peri-naphthoisatogens via aldrone condensation

❖ 4.1 Introduction

Peri-annulation of naphthalene is an important strategy to unlock the potential of naphthalene-containing organic compounds for various applications and interesting properties. Several *peri*-functionalities exist and each of them has demonstrated interesting properties to be used in various fields. Naphthalimide derivatives, both monoimide and diimide, have found applications in organic electronics and supramolecular chemistry.[1] Similar is the case for naphthalene bisamides as evidenced from semiconducting polymers and co-polymers with bisamide as core constituent.[2] Naphthalene monoamide or naphtholactams,[3] and *peri*-fused derivatives of 1,8-diaminonaphthalene also called as perimidines, are important components in medicinal chemistry. Perimidines also exhibit interesting supramolecular behaviour.[4] A new kind of *peri*-functionalized naphthalene derivative would not only increase the diversity of the field, but would generate compounds for different kind of applications

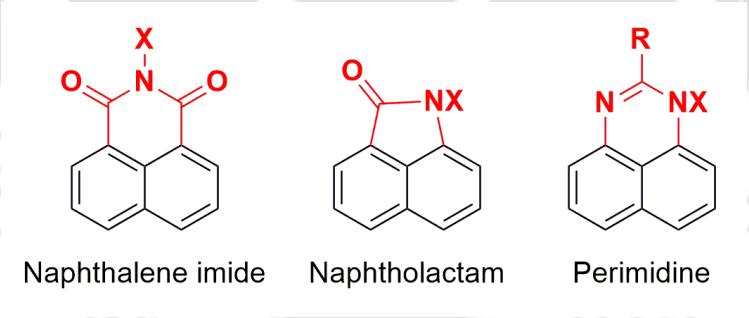

Fig 4. 1 Predominant *peri*-annulation of naphthalene in chemistry

Indolone-N-oxides or isatogens, in which a alpha-ketonitrone is attached to the ortho positions of benzene, are an interesting class of dipolar compounds, and have been used as raw material or synthetic component in preparation of many complex and pharmacologically active compounds like (±)-trigonoliimine C, (-)-isatisine A *etc*. The molecules by themselves

too exhibit modest biological influence such as antiplasmodial, antifungal, antibacterial and antileishmanial propeties.[5,6,7] Due to these reasons, isatogens have been widely investigated

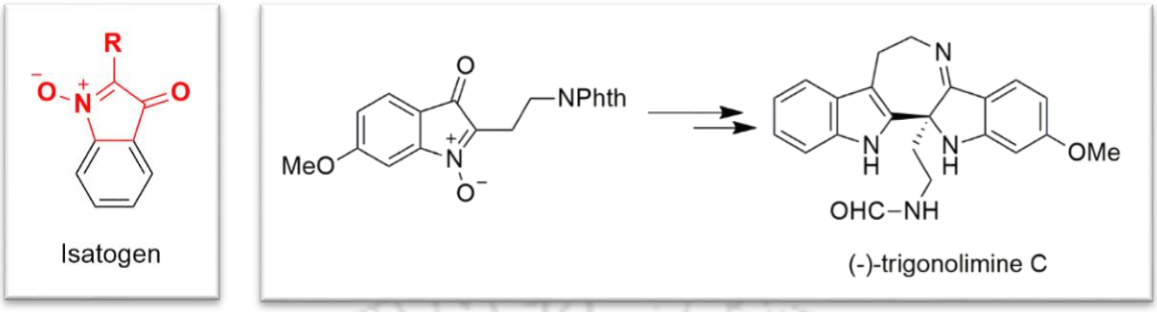

Fig 4. 2 Reprsentation of isatogen and example of its role in synthetic pathways

in the past decades in various fields of research. In addition, presence of dipolar moiety also might present interesting challenges in supramolecular field, but are yet to be studied in detail. However, in spite of the obvious oppurtunities, and already exhaustively deep studies into isatogens, research into *peri*-annulated naphthoisatogens (PNTIs), where the alpha-ketonitrone moiety is appended to the *peri*-positions of naphthalene, is suprisingly rare. The only example of PNTI was reported several decades ago in 1971[8] (Fig 4.3). Unsurprisingly, the chemistry of the compound remained unexplored. Another major restriction in the isatogen chemistry is that the compound must have a substituent at the C2-position. Without a substituent at the specific position, isatogens are unstable. Therefore, all the reported examples are ketonitrones[9]. A compound without any C2-substituent, i.e. an α-keto aldonitrone remains elusive be it in isatogen family or in PNTI family.[10]

In this chapter, we report the synthesis and characterization of C2-unsubstituted PNTIs which can be regarded as the first examples of α-ketoaldonitrones. The new molecule also undergoes 1,3-dipolar cycloaddition with the diene ethyl acrylate, providing an aza-phenalenone[11] proceeding through the formation of an iso-oxazolidine[12] ring and subsequent

fragmentation of the cyclic system. All of the PNTIs show strong absorption in the visible part of the spectrum, and are also moderately emissive. In comparison to an analogous dye, 4-amino naphthalimide derivatives, the absorbance maxima of the PNTIs are bathochromically shifted by 100 nm.

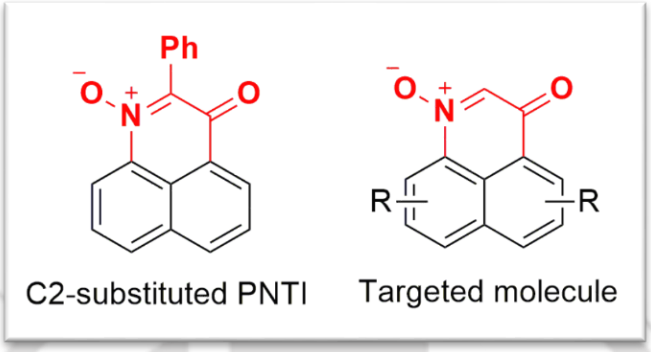

Fig 4. 3 Pre-existing PNTI **(left)** and current objective **(right)**

❖ 4.2 Design strategy

Synthesis of isatogens with C2-substitution is generally achieved by two pathways, which include either i) a cyclization reaction achieved intramolecularly in ortho-nitrostyrene or orthonitrophenylacetylene or ii) via the oxidation of a derivative of 2-substituted indole. These procedures require expensive metal complexes such as those involving Au or Pd. Failure of the conventional methods in producing an α-keto aldonitrone, a new and alternative route is to be considered. In the synthesis of *peri*-naphthoindigo (PNI), obstacles were encountered on the route of aldol reaction that involves 8-nitro-1-naphthaldehyde.[13] Change in hybridization of the carbonyl carbon to sp^3 from sp^2 was hindered by steric crowding at the *peri*-positions of naphthalene. Thus, the carbon of the carbonyl group was unable to function as a suitable electrophile in this regard. However, in 8-nitroacetylnaphthalene (**1r**, Figure 4.4), the -CH_3CO group rather acted as a nucleophile and reacted with the nitroso group that was generated insitu, producing PNI as a consequence.

Hence, a similar route might be followed for the current objective. Reaction between a carbon nucleophile and nitrogen atom of a nitro group is relatively unknown, but is not completely absent in literature,[14] and are generally performed via the use of strongly basic conditions.[15] Such reactions were typically accompanied by aditional reactions such as methanolysis[16], substitution-tautomerization[17], β-elimination of phenylsulfinate[18] *etc*. On the other hand, these problems were not encountered on using strong acidic conditions.[19] Enhancement of electrophilicity of the nitro group is also known to be achieved via acdification.[20,21]

❖ 4.3 Results and Discussion

To achieve the goal, **1r** was treated with toluene and triflic acid. However, the reaction at room temperature provided complicated mixture, hence was modified. The outcome was much better when the reaction was carried out at 80°C, producing a yellow coloured compound. After careful ^{1}H-NMR characterization, the product was found to be a undesired one (**1p**). Ncleophillic substitution (S_NArH) of the *ortho* and *para* aromatic protons took place instead of the assumed nucleophilic attack to the N-atom of the nitro group. The nucleophilic substituent was found to be the solvent toluene molecule, as evidenced from the ^{1}H NMR spectrum of the product. Proton magnetic resonance of the compound showed the intact signals of the acetyl group. Two new signals for methyl groups confirmed the introduction of two tolyl moieties at the *ortho*- and *para*-positions of the nitro group. Mass data (HRMS) could not be obtained for **1p** due to the lack of ionizable group. Additionally, stability of the compound was also a limiting factor as **1p** was turned into a blue-green solution upon standing. As the undesired S_NArH reaction was more favourable than the required reaction in **1r**, electronic nature of the naphthalene ring was modified. The main purpose was not only to diminish the probability of S_NArH reaction, but also to enhance the probability of nucleophilic attack to the N-atom of the nitro group.

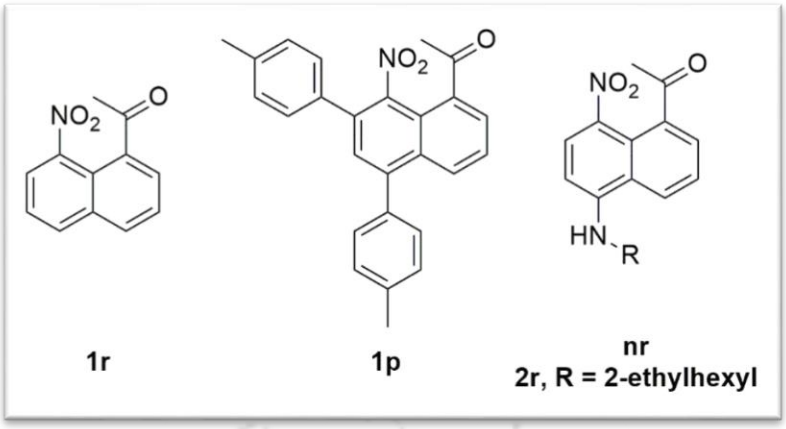

Fig 4. 4 representation of molecules **1r, 1p** and **2r**

To overcome the above mentioned problem, an alkylamino group was introduce at the 5-position of naphthalene and compound **2r** was produced. The synthesis was accomplished in three steps starting from 5-nitro-1-acetyl naphthalene. The role of the alkylamino group at the specified position was not only to block the position for nucleophilic attack, but to reduce the electron deficiency of the ring and subsequent S_NArH reaction. Treatment of **2r** with triflic acid in toluene at high temperature produced a pink compound, which was examined via common analytical techniques including ^1H and ^{13}C NMR spectroscopy, HRMS and IR spectroscopy. HRMS spectra was quite an important tool in determining the structure of the obtained product. An intense peak was obtained at 325.1893, a value less than that of the reactant by 18 Da. The observation suggested a possible dehydration reaction involving the reactant **2r**. Proton resonance of the product showed that the number of protons of the naphthalene ring remained unchanged, which was not the case for **1p**. Therefore, the possibility of a S_NArH reaction was ruled out from the ^1H NMR spectroscopy. The proton signal of the acetyl group was absent, but marked with the appearance of a new singlet at a chemical shift of 7.83 ppm. The spectral change could be attributed to the reaction involving the acetyl group **2r**. In more details, nucleophilic attack of the acetyl group to the N-atom of nitro group, followed by dehydration produced the product **2p**. An insight into the ^{13}C NMR

spectrum of the compound further strengthened our conclusion. The number of aliphatic carbon signals decreased by one, whereas an increase in signal by same number was observed in the aromatic part of the spectrum. It is noteworthy to mention that the carbonyl-carbon signal remained intact. IR spectroscopic measurements supported the above mentioned conclusions. As in the case of other analogous compound, the product showed a peak at 1704 cm^{-1} corresponding to the intact carbonyl group of α-ketonitrones. Stretching vibration at 1630 cm^{-1}, arising from C=N→O moiety, also validated the presence of the nitrone.[22] Thus all of the analytical data collectively validated the proposed structure for **2p**.

After unambiguous establishment of the structure, optimization of the reaction condition was carried out for best yield. Experiments were performed by changing solvent, acid, temperature and the duration of the reaction. The best possible yield was obtained when the reaction was carried out in neat H_2SO_4 at a temperature of 35°C. However, the yield was lowered when the temperature was elevated to 60°C. No meaningful results were obtained when the reaction was performed either in HCl or in HNO_3. Therefore, protonation and subsequent alteration in the electrophilic character of the nitrogen atom is an important step in the reaction sequence. After taking all the observations into consideration, sulphuric acid was found to be the best acid for the current purpose in terms of solubilizing the reactant, increasing electrophilicity via protonation of N-atom of nitro group and and final dehydration step. The effect of temperature could be explained by bringing the competing reaction as well into the scenario. The competing S_NArH reaction become prominent at elevated temperature, leading to the lessening of the desired PNTI formation. But, at 35°C the yield of **2p** improved due to the diminished effect of the side reaction.

In next set of experiments, the effect of the chain length was investigated and 5 different alkyl groups were used at the amino group. With an increase in chain length, the yields were increased. The observation could be can be explained by considering the probability of

protonation of amine group and subsequent deactivation of the desired reaction. With greater hydrophobicity, the deactivation via protonation decreased with increase in chain length. Longer chains also led to the better electron donation thereby causing better suppression of the competing S_NArH pathway. Better solubility of the product containing long alkyl chain in

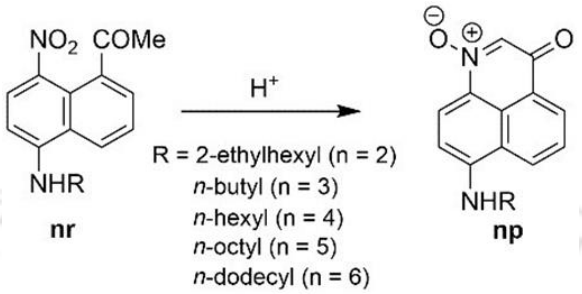

Table 4.1 Optimization of PNTI formation.

Entry	Substrate	Acid	T	t[h]	Yield [%]
1	**2r**	TfOH[a]	80 °C	1.5	25
2	**2r**	TfOH	35 °C	2.5	trace
3	**2r**	H_2SO_4	35 °C	2.5	27 (54)
4	**2r**	H_2SO_4	60 °C	2.5	(39)
5	**2r**	HNO_3	60 °C	12	Nr
6	**2r**	HCl	35 °C	12	Nr
7	**2r**	HCl	60 °C	2.5	trace
8	**2r**	AcOH	reflux	2.5	trace
9	**2r**	TFA	35 °C	2.5	trace
10	**3r**	H_2SO_4	35 °C	2.5	17
11	**4r**	H_2SO_4	35 °C	2.5	18
12	**5r**	H_2SO_4	35 °C	2.5	26
13	**6r**	H_2SO_4	35 °C	2.5	26

[a] In toluene; nr = no reaction; yields mentioned in parentheses are NMR yield.

organic solvent also contributed for the improved yield. Enhanced solubility in organic solvents facilitated the extraction of the product during aqueous work-up process. Next, the substrate scope of the reaction, along with the importance of the alkyl amino group, was studied. In place of the alkylamino group, a butoxy group was installed at the 5-position of

naphthalene and the reaction was tested with the newly prepared substrate (**7r**). However, the results were found to be unsatisfactory, as evidenced by multiple inseparable spots on TLC. Considering the proclivity of aromatic nitro group to participitate in multiple reaction pathways, the outcome was disappointing but not entirely unexpected, as treatment with acid often provides different results for similar substrates.

The outcome was found to be indifferent when the reaction was carried out with another substrate containing butyl group at the 5-position. It was clearly evident that the presence of an alkyl amino group is quite vital for the smooth proceeding of the desired reaction. The alkyl amino group not only controlled the electrophilicity of the nitro group, but also stabilized the product α-keto aldonitrone by decreasing its reactivity. This indeed allowed easy isolation of the desired PNTIs in stable condition.

As the main objective of the investigations was to isolate unsubstituted PNTIs, the unsuccessful substrates were not paid further attention. Investigations were continued with the positive results. The synthesis of the PNTIs were tested in basic condition too, and received by treating with alkali hydroxide in ethanol or DMSO, albeit with longer reaction times and lesser yields. In-situ generation of PNTI during synthesis of precursors **2-6r** also took place, but in diminished yields due to the presence of extra reagents.

❖ 4.3.1 Mechanism of reaction

It is imperative to understand the mechanism of the formation of PNTI for further development. A carbon nucleophile is known to react with a nitro group under basic conditions, for which an aldol-type or Knoevenagel kind of mechanism has been proposed. An alternative mechanism was also put forward in recent literature, where the carbon nucleophile attacks the oxygen atom of nitro group.[23] However considering the reaction proceeded through a 7-membered intermediate, it would not be feasible in a narrow space

such as the *peri*-positions of naphthalene. Hence, this scenario was eliminated for the current reaction. The mechanistic pathway was also a failure when it was concerned with an acetyl group. An aldol type mechanism is the most appropriate for the present reaction in discussion. The most crucial part of the mechanistic pathway was protonation of the nitro group. Protonation of alkylamino group was eliminated from the discussion due to the fact that the precursor was synthesized via *para* nitration in acidic medium. If the protonation had happened at the amino group, it would not have directed to *para*-position. Rather, the protonated alkyl amino group would have direct for *meta*-nitration. Increase in chain length provided greater hydrophobicity and better hindrance to protonation at the amino group. The hypothesis was very much reflected in the yields of the PNTIs of varying chain lengths. Thus protonation of the nitro group was a key step of this reaction. The protonation at the nitro group was also supported by the alkylamino group through stabilization via electron donation. This strong donation from the amino group also depleted the electrophilicity of the ring, and subsequently preventing S_NArH pathway. The next step in the reaction sequence was the nucleophilic attack of the enol moiety to the N-atom of nitro group leading to the formation of the intermediate **2ri**, which was subsequently dehydrated to produce the desired product aldonitrone **2p.** The overall process was summarised in Scheme 3.1.

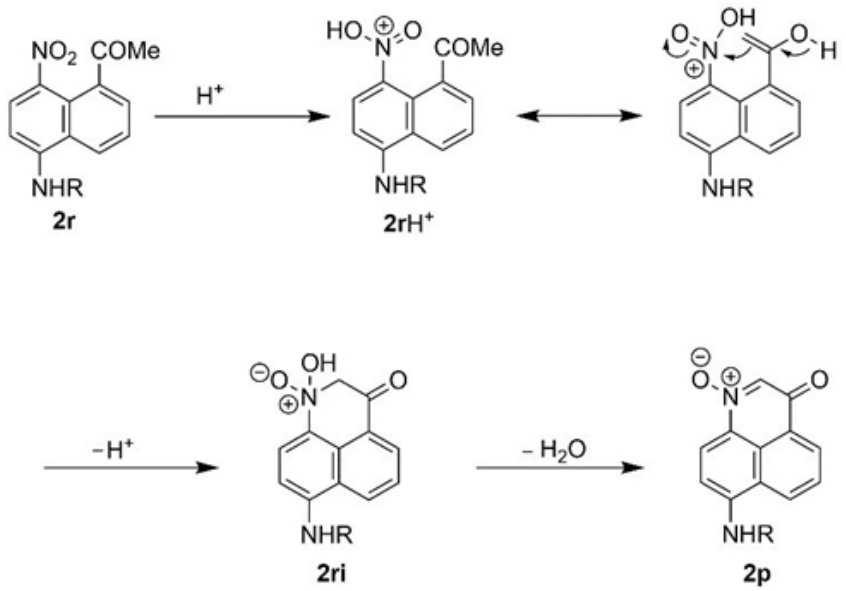

Scheme 3.1 Plausible mechanism of the prposed reaction.

In literature, such reactions were described as aldol-type condensations[24] or as aldol-Knoevanagel[25] type reactions as they possess addition-elimination step. There are numerous other reactions, however, which proceed via addition-elimination pathway. It is quite reasonable to mention that such definitions are quite ambigous. Due to similarities with aldol condensation, the newly invented addition-elimination reaction was defined as 'aldrone condensation'. The terminology should be exclusive limited to the aldonitrone formation, and formation of ketonitrone via any alternative route must be excluded from this category.[26]

❖ 4.3.2 1,3-dipolar cycloaddition reaction

As the PNTIs contain nitrone moiety, possibility of derivatization was further explored. It is necessary to point out that nitrones are known to undergo different kinds of organic reactions,[27] 1,3-dipolar cycloaddition reaction is being one such reaction of nitrones.[28] Accordingly, the cycloaddition reaction was tested for PNTI **2p** by treating with a dipolarophile - ethyl acrylate in toluene at 80°C. Formation of a new product concomitant with consumption of the reactant indeed suggested a successful outcome. An intense peak,

corresponding to the cycloaddition product of **2p** and ethyl acrylate, was observed at m/z = 425.2436 in HRMS data. However, the iso-oxazolidine ring, generated after cycloaddition reaction, was found to be unstable and underwent subsequent ring cleavage to provide an aza-phenalenone derivative **2p1'**. The structure was established from ^{1}H NMR, ^{1}H-^{1}H COSY and DFT calculations of the stipulated structure. Single set of signals in the ^{1}H NMR spectrum demonstrated the formation of only one regio-isomer, even though there was possibility of other products[29]. Careful analysis of the proton NMR revealed the disappearance of the signal at 7.83 ppm, corresponding to the C2-proton. Instead, 3 multiplets were observed between 3.00 and 5.00 ppm, representing C10 and C11 protons. No resonance for C2 was found accodring to ^{1}H-^{1}H COSY NMR analysis, indicating that an iso-oxazolidine ring was not a probable member of this new structure. Looking into the 3 multiplets mentioned earlier, the proton resonance at 4.76 ppm is constituted of two vicinal coupling constant of 4.0 Hz and 7.0 Hz, whereas the remaining two resonances are seen at 3.45 and 3.37 ppm, each containing one geminal and one vicinal coupling constants. Taking into careful consideration of both the deshielding effect of the oxygen atom and the value of the coupling constants, the first resonance at 4.76 ppm could be assigned to C10-H, while the remaining upfield signals could be attributed to the diastereostopic protons attached to C11. A quick evaluation of this complete data analysis reveals the 1,3-dipolar cycloaddition product to be **2p1′**. The aforementioned conclusion was strengthened further by theoretical calculations on the optimized structure of the 1,3-dipolar cycloaddition product. The iso-oxazolidine containing structure is non-planar, and is strained due to the presence of this ring. Instead by severing the N-O bond and rupturing the ring structure, this strain is relieved and the molecule is able to achieve planarity. This cycloaddition reaction further strengthened our proposal of the structure of **2p**, and the presence of nitrone moiety. The overall cycloaddition reaction of **2p** is summarized in **Fig 4.5**. The PNTIs **2-6p** are the first examples of aldonitrones in the

isatogen family. In other words, they are the first example of isatogens where the C2 position is unsubstituted.

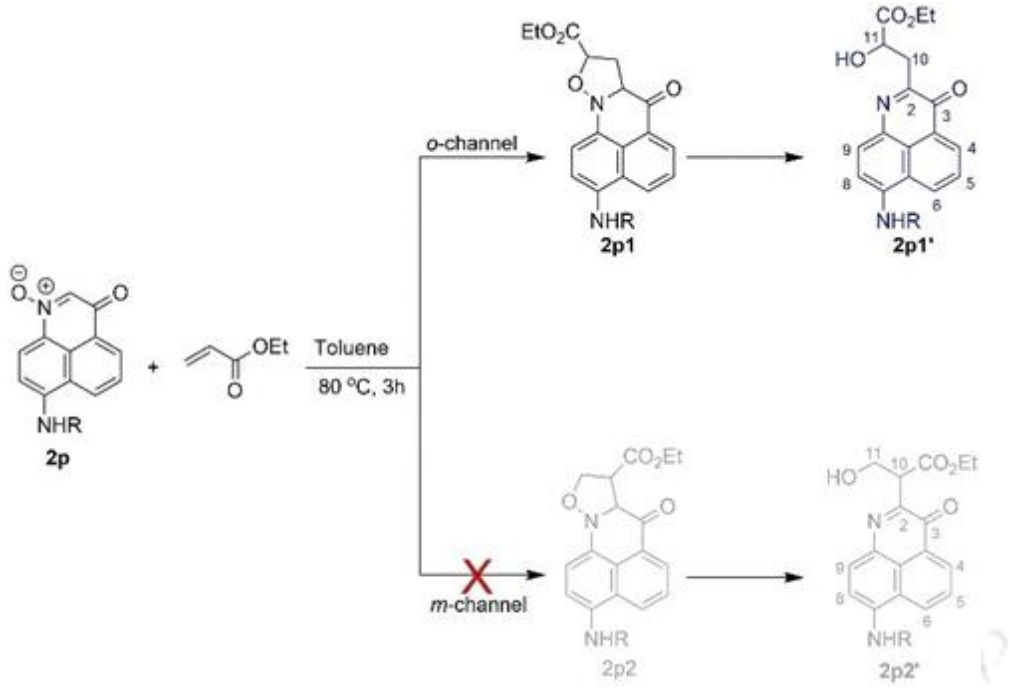

Fig 4. 5 Mechanism of 1,3-dipolar cycloaddition between PNTI **2p** and ethyl acrylate.

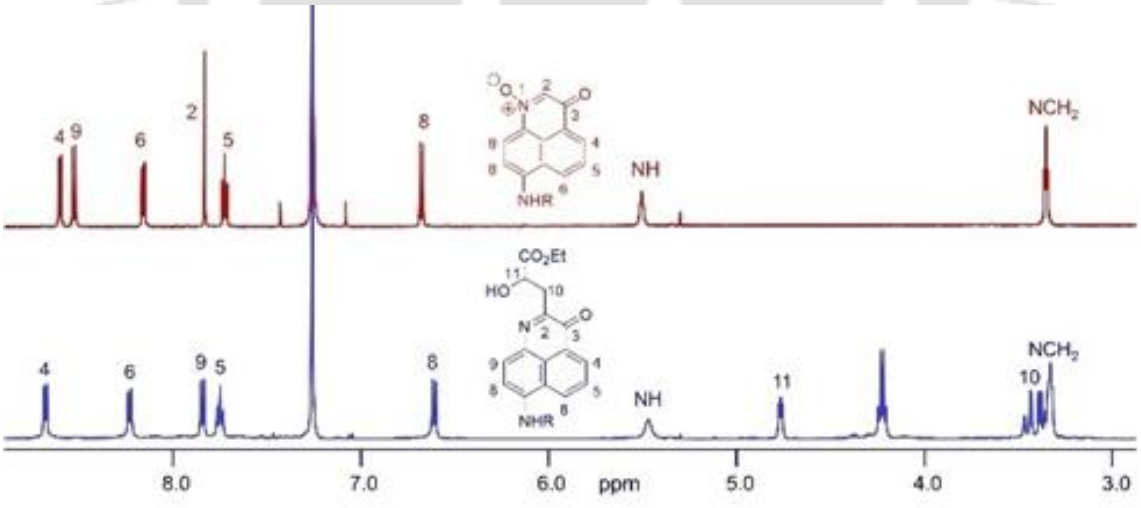

Fig 4. 6 Comparison of proton NMR of **2p** and **2p1′.**

❖ 4.3.3 Theoretical studies

In order to get geometry of the structure of both the aldonitrone and the subsequent cycloaddition product, density functional theory (DFT) calculations were performed, using Gaussian 16[30] software with the incorporation of B3LYP functional and 6-31+G(d,p) basis set in chloroform[31]. The long alkyl chain in the amino-alkyl group was replaced with methyl group to avoid any complexity. DFT calculation supported the formation of a cyclic nitrone annulated to the *peri*-positions of naphthalene. Bond distance between the C2-carbon and carbonyl carbon was estimated to be 1.44 Å in the PNTI, suggesting of conjugation. HOMO and LUMO energies were calculated via DFT/B3LYP method, and found to be -5.97 eV and -3.08 eV. FMO of the PNTI showed the presence of HOMO and LUMO extending from amino-alkyl group to the carbonyl of the nitrone, indicating a strong donor-acceptor relation in conjugation. Planar structure with ruptured iso-oxazolidine ring was established for **2p1′** as mentioned earlier from geometry optimization.

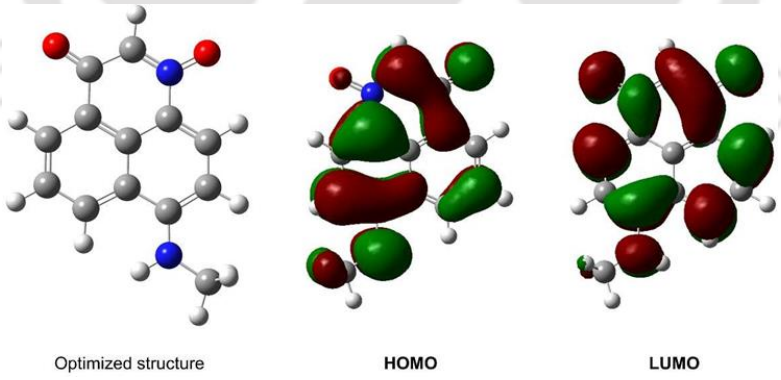

Fig 4. 7 Optimized structure of α-keto-aldonitrone derivatives along with FMO for HOMO andLUMO.

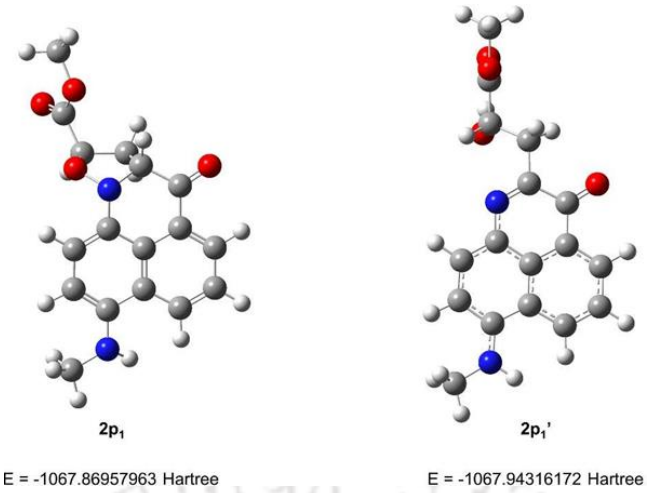

Fig 4. 8 Optimized structure of **2p1** and **2p1′.** The planar structure is more stable than the strained compound **2p1** by – 46.2 kcal/mol.

❖ 4.4 Photophysical studies

Inspired by the strong colour of all the PNTIs and **2p1′**, optical properties of all the dyes were investigated in details. The results are summarized in Table 4.2. The UV-vis properties of the PNTIs were marked by strong absorbance in the visible region. In chloroform, all the PNTIs exhibited absorption maximum at ~ 550 nm. Such low energy absorption in a relatively small molecules was probably originated from charge transfer from the alkyl amino group to the carbonyl. Change in the length of the alkyl amino did not affect the absorbance maxima of the PNTIs in chloroform in any impactful manner. Compared to the only known examples of PNTI (substituted), the maxima of the present PNTI dye molecules display bathochromic shift of ~62 nm, and in comparison to popular analogous dyes 4-amino naphthalimides, a bathochromic shift of more than 100 nm was displayed.[32] An increase in the conjugation possibly contributed to the red shift of absorption maxima. The absorption spectra of **2-6p** were devoid of vibronic fine structure, and the spectral features were similar to a previously reported *peri*-functionalised dye PNI. In order to understand the nature of the ground state of PNTI **2p**, the UV-vis properties were studied in different solvents of varying polarity. A

bathochromic shift of 22 nm was exhibited by **2p** with increase in polarity, suggesting the dye to be moderately polar at ground state. Such positive solvatochromism was also observed for the emission of PNTIs. Switching the solvent from chloroform to DMSO provided a red shift of emission maximum by 34 nm. The value of solvatochromism being higher for emission in comparison to absorption is a proof that the dye is less polar in the ground state compared to excited state. The effect of solvent was further studied by using the Lippert-Mataga equation (Eqn 1-3).[33]

Table 4.2 Optical properties of PNTIs and **2p1′**

Substrate	Solvent	λ_{abs} [nm]	λ_{em} [nm][a]	$\Delta\nu$ [cm^{-1}]	$\Delta\nu$ [nm]
2p	CHCl3	551	594	1314	43
2p	THF	545	598	1627	53
2p	acetone	547	601	1643	54
2p	MeCN	552	610	1723	58
2p	DMSO	567	628	1713	61
3p	CHCl3	549	591	1295	42
4p	CHCl3	549	590	1266	41
5p	CHCl3	550	592	1290	42
6p	CHCl3	551	591	1228	40
2p1′	toluene	552	631	2268	79
2p1′	CHCl3	563	635	2014	72
2p1′	THF	572	637	1784	65
2p1′	acetone	576	637	1662	61
2p1′	MeCN	579	642	1695	63
2p1′	DMSO	586	654	1774	68

[a] excited at absorption maximum

$$\Delta\bar{\nu} = \bar{\nu}_a - \bar{\nu}_f = \frac{2(\Delta\mu)^2}{hc\alpha^3}\Delta f + b \qquad (1)$$

$$\Delta\mu = \mu_e - \mu_g \qquad (2)$$

$$\Delta f = \frac{\varepsilon - 1}{2\varepsilon + 1} - \frac{n^2 - 1}{2n^2 + 1} \qquad (3)$$

where $\Delta\bar{\nu}$ is the Stokes shift calculated by the experimentally observed difference of peak wavenumbers between the absorption and emission, $\Delta\mu$ is the difference in dipole moments between the ground (μ_g) and excited (μ_e) states (eqn (2)), h is the Planck constant, c is the speed of light in vacuum, α is the radius of cavity of the fluorophore and Δf is the orientation polarizability of the solvents expressed by the dielectric constant (ε) and refractive index (n) of the solvents (eqn (3)).[34] The α value for **2p** was estimated from the optimised structure by taking the half of the distance between the amino nitrogen and the carbonyl oxygen atoms.[35] A linear relationship was observed from the Lippert-Mataga plot for **2p**. From the slope of the plot, the change in dipole moment was calculated to be 3.41 D. The PNTIs are emissive and exhibited relative fluorescence quantum yield of ~12 % in chloroform. Lifetime measurements provided an insight into the excited state of the dyes. Decay lifetimes of fluorescence of **2p** were measured to be 1.40 and 4.65 ns respectively in $CHCl_3$ and DMSO. Increase in lifetime in more polar solvent could be attributed to the increase in polarity of the excited, which was more stable in polar solvents. The optical properties of the cycloaddition derivative was also investigated in details. The dye showed red shifted absorption maximum when compared with the parent PNTI. Similar to the parent PNTI, the derivative showed red shift in emission maximum with increase in solvent polarity. However, the magnitude of the change was lesser than that of the absorbance maximm. Thus, a decrease in Stokes shift with increase in polarity of the solvent was observed. Accordingly, the slope of Lippert-Mataga plot was found to be negative in the case of **2p1′**.

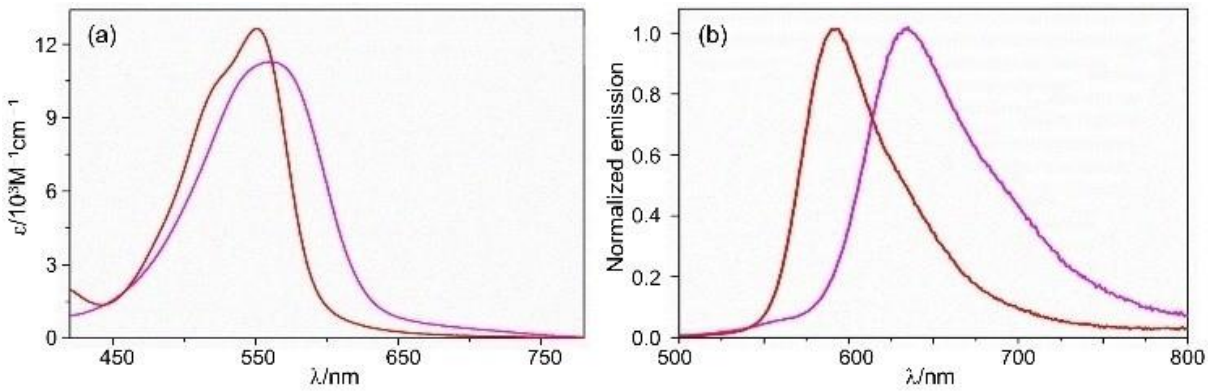

Fig 4. 9 Absorption (**left**) and emission (**right**) spectrum of 2p (red) and 2p1′ (pink).

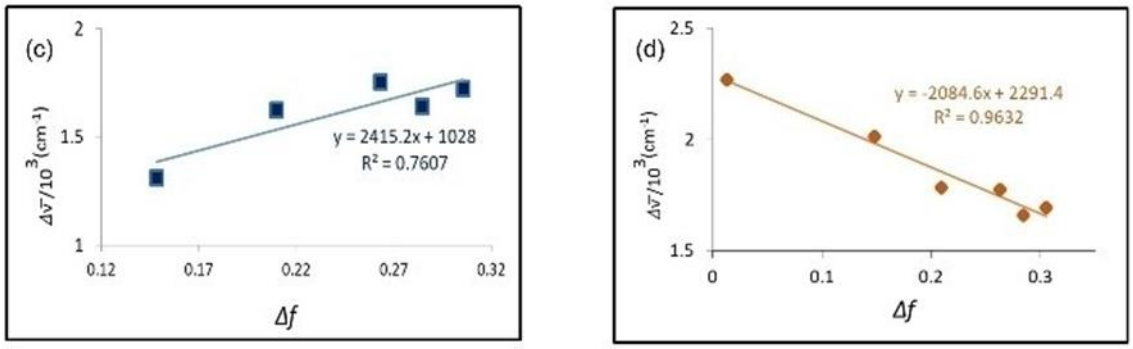

Fig 4. 10 Lippert-Mataga plots for **2p** (left) and **2p1′** (right).

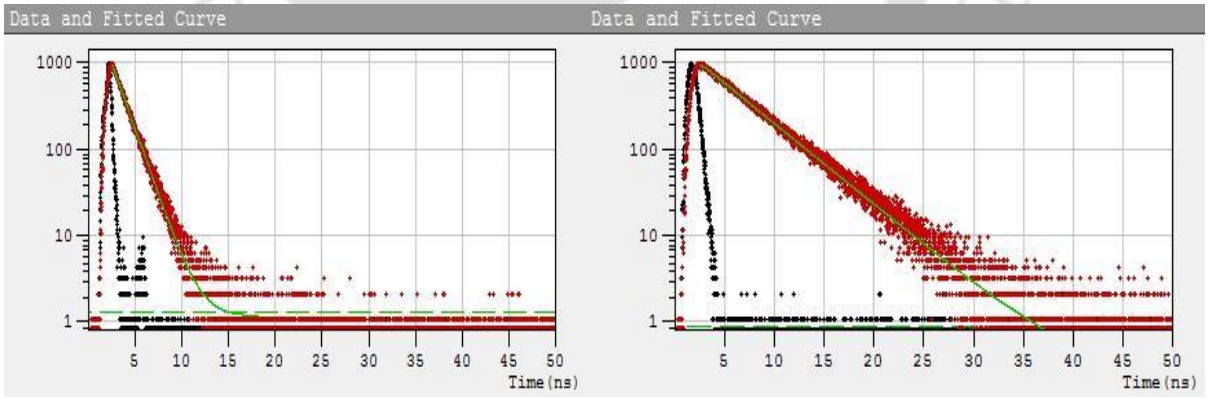

Fig 4. 11 Fluorescence decay spectra of **2p** in $CHCl_3$.and DMSO.

❖ 4.5 Conclusion

In summary, a new class of *peri*-functionalized dyes were synthesized by installing α-keto aldonitrone moiety. PNTIs are the only examples in the istogen family which are stable without a substituent in the C2 position. The synthesis was accomplished by utilizing an unusual reaction of aromatic nitro group, which is nucleophilic attack of a C-nucleophile to the N-atom of nitro group, followed by dehydration. Such reactions are very rare. Even if such reaction takes place, they are accompanied with additional reaction steps. Isolation of stable product after the addition-elimination reaction involving a C-nucleophile and N-atom of a nitro group was accomplished successfully in the present study. The new reaction was described as aldrone condensation due to the similarities with aldol condensation. The methodology is very unique to make new class of aldrones. The utility of such compounds was further demonstrated by performing 1,3-dipolar cycloaddition reaction, producing aza-phenalenone **2p1′**. All the PNTIs and the cycloaddition derivative strongly absorb in the visible region and are moderately emissive.

❖ 4.6 References

[1] a) Banerjee, S.; Veale, E.B.; Phelan, C.P.; Murphy, S.A.; Tocci, G.M.; Gillespie, L.J.; Frimannsson, D.O.; Kelly, J.M. and Gunnlaugsson, T.; *Chem. Soc. Rev.* **2013**, *42*, 1601–1618; b) Gopikrishna, P.; Meher, N. and Iyer, P.K.; *ACS Appl. Mater. Interfaces* **2018**, *10*, 12081–12111; c) Dong, H.-Q.; Wei, T.-B.; Ma, X.-Q. ; Yang, Q.-Y.; Zhang, Y.-F.; Sun, Y.-J.; Shi, B.-B.; Yao, H.; Zhang, Y.-M. and Lin, Q.; *J. Mater. Chem. C* **2020**, *8*, 13501–13529; d) Yu, H.; Guo, Y.; Zhu, W.; Havener, K. and Zheng, X.; *Coord. Chem. Rev.* **2021**, *444*, 214019. e) Bhosale, S. V.; Bhosale, S.V. and Bhargava, S.K.; *Org. Biomol. Chem.* **2012**, 10, 6455–6468; f) Suraru, S.-L. and Würthner, F.; *Angew. Chem. Int. Ed*. **2014**, 53, 7428–7448; g) Kobaisi, M. Al; Bhosale, S. V.; Latham, K.; Raynor, A. M. and Bhosale, S. V.; *Chem. Rev.* **2016**, 116, 11685–11796; h) Maniam, s.; Higginbotham, H. F. ; Bell, T. D. M. and Langford, S.J.; *Chem. Eur. J.* **2019**, 25, 7044– 7057; i) Shukla, J.; Mukhopadhyay, P.; *Eur. J. Org. Chem.* **2019**, 7770– 7786; j) Bhosale, S. V.; Kobaisi, M. Al; Jadhav, R. W.; Morajkar, P. P.; Jones, L. A. and George, S. ; *Chem. Soc. Rev.* **2021**, 50, 9845–9998.

[2] a) Eckstein, B.J.; Melkonyan, F.S.; Manley, E.F.; Fabiano, S.; Mouat, A.R.; Chen, L.X.; Facchetti, A. and Marks, T.J.; *J. Am. Chem. Soc.* **2017**, *139*, 14356– 14359; b) Eckstein, B.J.; Melkonyan, F.S.; Wang, G.; Wang, B.; Manley, E.F.; Fabiano, S.; Harbuzaru, A.; Ortiz, R.P.; Chen, L.X.; Facchetti, A. and Marks, T.J.; *Adv. Funct. Mater.* **2021**, *31*, 2009359.

[3] a) Xue, X.; Zhang, Y.; Liu, Z.; Song, M.; Xing, Y.; Xiang, Q.; Wang, Z.; Tu, Z.; Zhou, Y.; Ding, K. and Xu, Y.; *J. Med. Chem.* **2016**, *59*, 1565–1579; b) Feng, Y.; Xiao, S.; Chen, Y.; Jiang, H.; Liu, N.; Luo, C.; Chen, S. and Chen, H.; *Eur. J. Med. Chem.* **2018**, *152*, 264–273; c) Li, Y.; Chen, L.; Si, L.; Yang, Y.; Zhou, C.; Yu, F.; Xia, G. and Wang, H.; *J. Mater. Chem. B* **2023**, *11*, 2431–2439; d) Zhou, C.; Wang, M.; Guo, W.; Ye, G.; Wang, Y.; Yang, Y.; Xia, G. and Wang, H.; *Dyes Pigm.* **2023**, *213*, 111198

[4] a) Sahiba, N. and Agarwal, S.; *Top. Curr. Chem.* **2020**, *378*, 44; b) Strausser, S.L. and Jenkins, D.M.; *Organometallics* **2021**, *40*, 1706–1712.

[5] a) Baeyer, A.; *Chem. Ges.* **1881**, *14*, 1741–1746; b) Hiremath, S.P. and Hooper, M.; *Adv. Heterocycl. Chem.* **1978**, *22*, 123–181; c) Adams, D.M.; Hooper, M.; Swain, C.J.; Raper, E.S. and Stoddart, B.; *J. Chem. Soc. Perkin Trans. 1* **1986**, 1005–1010.

[6] a) Ibrahim, N.; Ibrahim, H.; Kim, S.; Nallet, J.-P. and Nepveu, F.; *Biomacromolecules* **2010**, *11*, 3341–3351; b) Ramana, C.V.; Patel, P.; Vanka, K.; Miao, B. and Degterev, A.; *Eur. J. Org. Chem.* **2010**, 5955–5966; c) Ibrahim, H.; Furiga, A.; Najahi, E.; Hénocq, C.P.; Nallet, J.-P. ; Roques, C.; Aubouy, A.; Sauvain, M.; Constant, P.; Daffé, M. and Nepveu, F.; *J. Antibiot.* **2012**, *65*, 499–504; d) Edeson, S.J.; Maduli, E. J. M.; Swanson, S.; Procopiou, P.A. and Harrity, J. P. A.; *Eur. J. Org. Chem.* **2016**, 83–86; e) Guo, L.; Tang, B.; Nie, R.; Liu, Y.; Lv, S.; Wang, H.; Guo, L.; Hai, L. and Wu, Y.; *Chem. Commun.* **2019**, 55, 10623–10626; f) Zhou, S.; Liu, Q.; Bao, M.; Huang, J.; Wang, J.; Hu, W. and Xu, X.; *Org. Chem. Front.* **2021**, 8, 1808–1816.

[7] a) Reddy, B.N. and Ramana, C.V.; *Chem. Commun.* **2013**, *49*, 9767–9769; b) Liu, R.-R.; Ye, S.-C.; Lu, C.-J.; Zhuang, G.-L.; Gao, J.-R. and Jia, Y.-X.; *Angew Chem. Int. Ed.* ***2015***, 54, 11205–11208; c) Xie, L.; Li, .; Dong, S.; Feng, X. and Liu, X.; *Chem. Commun.* **2021**, 57, 239–242.

[8] Leznoff, C.C. and Hayward, R.J.; *Can. J. Chem.* **1971**, *49*, 3596–3601.

[9] a) Shi, W.-M.; Ma, X.-P.; Su, G.-F. and Mo, D.-L.; *Org. Chem. Front.* **2016**, *3*, 116– 130; b) Lynch-Colameta, T.; Greta, S.and Snyder, S.A.; *Chem. Sci.* **2021**, *12*, 6181–6187.

[10] a) Brar, A.; Unruh, D.K.; Ling, N. and Krempner, C.;*Org. Lett.* **2019**, *21*, 6305– 6309; b) Akulov, A.A.; Varaksin, M.V.; Mampuys, P.; Charushin, V.N.; Chupakhin, O.N. and Maes, B. U. W.; *Org. Biomol. Chem.* **2021**, *19*, 297–312.

[11] a) Digby, E.M.; Sadovski, O. and Beharry, A.A.; *Chem. Eur. J.* **2020**, *26*, 2713– 2718; b) Bonfils, P.D.; Verron, E.; Sandoval-Altamirano, C.; Jaque, P.; Moreau, X.; Gunther, G.; Nun, P. and Coeffard, V.; *J. Org. Chem.* **2020**, *85*, 10603– 10616; c) Kaye, E.G.; Kailass, K.; Sadovski, O.; Beharry, *ACS Med. Chem. Lett.* **2021**, *12*, 1295–1301; d) C.-W. Kuo, N. S. Rao, P. B. Patil, T.-T. Chiang, A.A.; Kavala, V. and Yao, C.-F.; *Adv. Synth. Catal.* **2021**, *363*, 1935–1943.

[12] a) Berthet, M.; Cheviet, T.; Dujardin, D.; Parrot, I. and Martinez, J.; *Chem. Rev.* **2016**, *116*, 15235–15283; b) Martzel, T.; Annibaletto, J.; Millet, P.; Pair, E.; Sanselme, M.; Oudeyer, S.; Levacher, V. and Brière, J.F.; *Chem. Eur. J.* **2020**, *26*, 8541–8545; c) Gentile, D.; Floresta, G.; Patamia,V.; Nicosia, A.; Mineo, P.G. and Rescifina, A.; *Org. Biomol. Chem.* **2020**, *18*, 1194–1203; d) Wu, Y.; Liu, Q.; Huang, S.; Zhang, C.; Wei, W. and Li, X.; *Org. Biomol. Chem.* **2023**, *21*, 3669–3674

[13] Das, R.J. and Mahata, K.; *Org. Lett.* **2018**, *20*, 5027–5031.

[14] Mąkosza, M.; *Chem. Eur. J.* **2014**, *20*, 5536–5545.

[15] Preston, P.N. and Tennant, G.; *Chem. Rev.* **1972**, *72*, 627–677.

[16] a) McNab, H. and Smith, D.M.; *J. Chem. Soc. Perkin Trans. 1* **1973**, 1310–1314; b) Machin, J.; Mackie, R.K.; Mcnab, H.; Reed, G.A.; Sagar, A.G.J. and Smith, D.M.; *J. Chem. Soc. Perkin Trans. 1* **1976**, 394–399.

[17] Cafiero, P. A. C.; French, C.S.; McFarlane, M.D.; Mackie, R.K. and Smith, D.M.; *J. Chem. Soc. Perkin Trans. 1* **1997**, 1375–1384.

[18] Mąkosza, M. and Tyrała, A.; *Acta Chem. Scand.* **1992**, *46*, 689–691.

[19] Wahlstrom, N.; Slatt, J.; Stensland, B.; Ertan, A.; Bergman, J.; Janosik, T.; *J. Org. Chem.* **2007**, *72*, 5886–5889.

[20] Ohwada, T.; Ohta, T. and Shudo, T.; *J. Am. Chem. Soc.* **1986**, *108*, 3029–3032.
[21] Barker, S.D.; Wilson, K and Norris, R.K.; *Aust. J. Chem.* **1995**, *48*, 1969–1979.

[22] Voinov, M.A.; Shevelev, T.G.; Rybalova, T.V.; Gatilov, Y.V.; Pervukhina, N.V.; Burdukov, A.B. and Grigor'ev, I.A.; *Organometallics* **2007**, *26*, 1607–1615.

[23] Shimizu, H.; Yoshinaga, K. and Yokoshima, S.; *Org. Lett.* **2021**, *23*, 2704–2709.

[24] Moskalev, V. and Tartynova, M.I.; *Russ. Chem. Bull.* **1998**, *47*, 1603–1604.

[25] a) Hanusek, J. and Macháĉek, V.; *Collect. Czech. Chem. Commun.* **2009**, *74*, 811–833, and references cited therein; b) Livingstone, D.B. and Tennant, G.; *J. Chem. Soc. Chem. Commun.* **1973**, 96–97; c) Dudová, K.; Částek, F.; Macháĉek, V. and Šimůnek, P.; *Molecules* **2002**, *7*, 7–17.

[26] Hattori, H.; Yokoshima, S. and Fukuyama, T.; *Angew. Chem. Int. Ed.* **2017**, *56*, 6980–6983.

[27] a) Murahashi, S.-I. and Imada, Y.; *Chem. Rev.* **2019**, *119*, 4684–4716; b) Sukhorukov, A.Y.; *Adv. Synth. Catal.* **2020**, *362*, 724–754; c) Bilodeau, D.A.; Margison, K.M.; Serhan, M. and Pezacki, J.M.; *Chem. Rev.* **2021**, *121*, 6699–6717.

[28] a) Zhang, M.; Kumagai, N. and Shibasaki, M.; *Chem. Eur. J.* **2017**, *23*, 12450– 12455; b) Thakur, S.; Das, A. and Das, T.; *New J. Chem.* **2021**, 45, 11420–11456.

[29] Adjieufack, A.I.; Ndassa, I.M.; Patouossa, I.; Mbadcam, J.K.; Safont, V.S.; Oliva, M. and Andrés, J.; *Phys. Chem. Chem. Phys.* **2017**, 19, 18288–18302.

[30] Frisch, M.J.; Trucks, G.W.; Schlegel, H.B.; Scuseria, G.E.; Robb, M.A.; Cheeseman, J.R.; Scalmani, G.; Barone, V.; Petersson, G.A.; Nakatsuji, H.; Li, X.; Caricato, M.; Marenich, A.V.; Bloino, J.; Janesko, B.G.; Gomperts, R.; Mennucci, B.; Hratchian, H.P.; Ortiz, J.V.; Izmaylov, A.F.; Sonnenberg, J.L.; Williams-Young, D.; Ding, F.; Lipparini, F.; Egidi, F.; Goings, J.; Peng, B.; Petrone, A.; Henderson, T.; Ranasinghe, D.; Zakrzewski, V.G.; Gao, J.;Rega, N.; Zheng, G.; Liang, W.; Hada, M.; Ehara, M.; Toyota, K.; Fukuda, R.; Hasegawa, J.; Ishida, M.; Nakajima, T.; Honda, Y.; Kitao, O.; Nakai, H.; Vreven, T.; Throssell, K.; Jr. Montgomery, J.A,; Peralta, J.E.; Ogliaro, F.; Bearpark, M.; Heyd, J.J.; Brothers, E.N.; Kudin, K.N.; Staroverov, V.N.; Kobayashi, R.; Normand, J.; Raghavachari, K.; Rendell, A.; Burant, J.C.; Iyengar, S.S.; Tomasi, J.; Cossi, M.; Millam, J.M.; Klene, M.; Adamo, C.; Cammi, R.; Ochterski, J.W.; Martin, R.L.; Morokuma, K.; Farkas, O.; Foresman J.B. and Fox, D. J. *Gaussian 16*, revision C.01; Gaussian, Inc.: Wallingford,, CT, 2016.

[31] (a) Miehlich, B.; Savin, A.; Stoll, H. and Preuss, H. *Chem. Phys. Lett*. **1989**, 157, 200-206; (b) P. C. Hariharan, J. A. Pople, *Theor. Chim. Acta* **1973**, 28, 213-222.

[32] a) Leslie, K.G.; Jacquemin, D.; New, E.J. and Jolliffe, K.A.; *Chem. Eur. J.* **2018**, *24*, 5569–5573; b) Y. Zhao, K. Chen, E. A. Yildiz, S. Li, Y. Hou, X. Zhang, Z. Wang, J. Zhao, A. Barbon, H. G. Yaglioglu, H. Wu, *Chem. Eur. J.* **2020**, *26*, 3591–3599.

[33]Lee, C.-W.; Takagi, C.; Truong, T.; Chen, Y.-C. and Ostafin, A.; *J. Phys. Chem. C* **2010**, 114, 12459–12468

[34] Reichardt, C. and Welton, T.; Solvents and solvent effects in organic chemistry, Wiley-VCH, Weinheim, Germany, 2011 (4th, updated and e edn.).

[35] Wang, L.; Fujii, M.; Yamaji, M. and Okamoto, H.; *Photochem. Photobiol. Sci.* **2018**, 17, 1319–1328.

Chapter 5

Temperature induced supramolecular rearrangement of PNTI

❖ 5.1 Introduction

Self-assembly of dye molecules into ordered aggregates is a burgeoning field and has been investigated over the last few decades. Aggregation leads to the emergence of new properties, which are not detectable in the individual monomer. Such alterations are again highly dependent on the nature of the intermolecular arrangement among the dye molecules. Generally, in solution two types of aggregates are possible: H and J-aggregates.[1] Face-to-face arrangements of the dye are known as H-aggregates,[2] and marked by hypsochromic shift of absorption maxima. Quenching of the emission is also accompanied with the H-aggregation. On the other hand, J-aggregation is marked by bathochromic shift of absorption maxima,

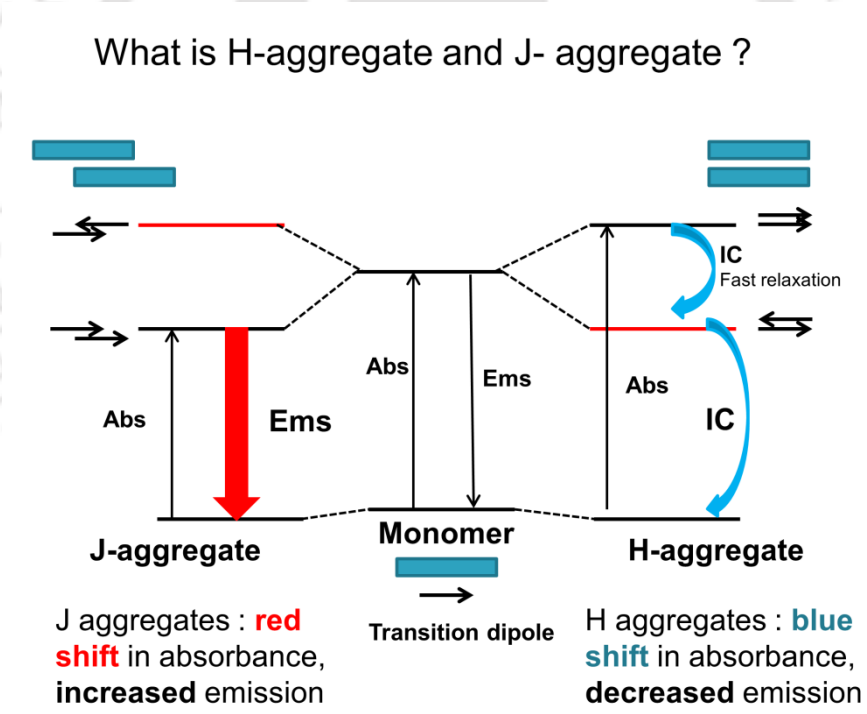

Fig 5.1 Diagrammetic representation of H-aggregate and J-aggregate.

and enhancement of molar extinction coefficient and photoluminescent quantum yield.[3] In such aggregates, the dyes are arranged in slipped stack manner. In case of J-aggregates the angle between the molecular axis and the direction of packing is small. On the other hand, a

large angle value is typical for the H-type aggregates. The boundary between the two types of aggregates is known as magic angle, the value being calculated theoretically as 54.7°. Therefore, an aggregate is defined as H-type when the angle between the molecular axis and the direction of packing is in the range of 54.7-90°. An angle with value lower than that of 54.7° is known as J-type aggregate. A brief summary of J-and H-aggregates in terms of relative orientations of transition dipoles and fate of optical properties is highlighted in Fig 5.1. For simplification the diagram is depicted with dimer only. The spectral changes remained same when the aggregates are produced with more number of dye units. As mentioned, the electronic and optical properties of such aggregates are highly reliant on the relative orientations of the dyes, which in turn are governed by the solute-solute attractions as well as the solute-solvent repulsions. The precise balance between the two contrasting forces is important to the nature of the aggregates and the functional properties of such assemblies. The role of solvents is thus very crucial when the solute-solvent repulsion has a major say on the aggregation. The unfavorable repulsive interaction between solvents and dye molecules forces them to arrange in way to minimize such interaction. The stacking difference occurs as a result of the preference of the molecule to be optimally protected from the solvent around it. The functional group(s) in the dye unit and their non-covalent interaction also play major role in the outcome of the nature of aggregates. Therefore, proper understanding of various non-covalent interactions involving the dyes and solute-solvent interactions is necessary to guide the morphologies of such aggregates. Nevertheless, both the aggregates have their benefits and disadvantages as emphasized by various studies. To emphasize the importance of H- and J-aggregates, a handful of studies are highlighted here. For example, Liu *et al*. investigated the different aggregates in fluorene based polymers to pave a way for devices dependent on a polyfluorene base.[4] He *et al.* investigated the effect of morphology on organic solar cells (OSC) and discovered the effect of additives on the aggregate structure type preffered. Their

research also discovered the effect of the type of aggregate structure on the efficiency of power conversion; each type had a different benefit on the fill factor (FF). This ultimately proved that accurate control of aggregate morphology is key for high performing OSC systems.[5] Janssen and Mas-Montoya studied the role of H- and J-aggregation in the photovoltaic performance of a thiophene-pyridine-diketopyrrolopyrole (TP molecule in bulk heterojunction solar cells; tuning of aggregation was carried out via change in the position of the side chains. It was demonstrated that J-aggregates exhibited a better performance, manifold compared to any of the H-aggregates.[6] Kwon *et al.* investigated the benefits and disadvantages of aggregation for molecules composed of thiophene linkers and cyclohexyl end groups (symmetrically or asymmetrically substituted respectively being DCX4T or ECX4T). After rigorous experiments it has been found that the molecules with asymmetric substitution preferred H-aggregation, and those with symmetric substitution ended up preferring J-type aggregates. The field–effect moblilities of the materials with H-type aggregates were found to be significantly enhanced compared to the others. The value was often approximately 100 times greater in magnitude. Utilizing this observation, they found H-aggregation in thin films to be the cause for thin film transistors prepared from these molecules to perform quite well.[7] Yang *et al*. investigated the effect of J-aggregation in solid films of squarine via tuning of solvents, and discovered that in a heterojunction PVC composed of a bilayer of squarine/fullerene, J-aggregation of the dye contributed significantly to the photocurrent, and produced a greater OPC voltage compared to devices based on H-aggregates. A study in 2012 found the opposite, where a squarine and a derivatized fullerene blend was used, and OPC voltage was greater for the blends exhibiting H-aggregates, while J-aggregation showed a huge increase in short circuit current.[8] J-aggregates of cyanine dyes in solution phase have been used by Fang *et al.* for the sensing of dopamine.[9] Thus it is clear that both H- and J-aggregation have their respective importance in

the field of supramolecular chemistry. Accordingly, both types of aggregates have been realized. In most of the cases, such aggregates were produced at the global minima and were thermodynamically stable. The major focus of such studies was circled around the nature of morphologies and related properties. Very few attempts have been dedicated to the transformation of one aggregate into another. Such switching is indeed very common in biological self-assemblies, and is crucial for their functions. In order to reduce the gap with the biological counterpart, artificial self-assembly must possess similar switching behaviour. Towards achieving such feats, in recent years, scientists have given emphasis on interconvertible aggregates. Such characteristics of the aggregates enhance their potential applications as smart materials. Interconversion between two or more aggregates is done with the help of various stimuli including temperature, pH, and addition of new influencing agents.[10] Often the switching is triggered with minimal change in solvent composition. Attempts at such changes have been made successful by consideration of either simple morphology changes through slight change in stacking, or via complex interactions between multiple aggregate structures. Some of the pioneer works in the field have been demonstrated using limited few dyes like perylene bisimides (PBIs) and porphyrins. For example, Würthner *et al.* reported about interconversion between H- and J-aggregates using PBIs. They also showed supramolecular polymorphism cases via pathway control synthesis. Temperature induced changes in intramolecular and intermolecular H-bonding led to the different aggregation.[11] Using porphyrins Sugiyasu *et al.* emphasized the formation of H and J-aggregates as a function of time.[12] Thus, it is quite evident that access to both H and J-aggregates from the same dye is crucial, specially switching from one to another is highly sought after. However, considering the importance, the examples are limited and have been reported with very few chromophores like PBIs and porphyrins. Therefore, more switching of aggregates need to be realized, especially with new chromophores.

Recently, our group has reported the synthesis of a new class of dye, *peri*-naphthoisatogens (PNTIs), for the first time using aldrone condensation. The newly invented *peri*-functionalized dyes are the only examples in the isatogen family which are stable without a substitution at C2-position. In other words, PNTI are only examples of α-keto aldonitrones. The dyes are comprised of a polar aldonitrone moiety as well as nonpolar naphthalene core along with long alkyl chain at the amine group. The amphiphilic character of the dyes makes them attractive candidates for self-assembly processes. In spite of their potential for aggregation, neither they were used for self-assembly process nor synthesized before. Inspired by the potential of the dyes, newly synthesized PNTI dyes **6p** and **4p** (Fig 5.2) were used to generate switching aggregates. In THF both the dyes exist in the molecularly dissolved state and exhibited the same optical features with an absorption maximum at 542 nm. But in a mixture of THF-water, both of them produced aggregates. The compound with hexyl chain **4p** produced only J-aggregates after increasing the percentage of water. On the other hand, compound **6p** produced both J-and H-aggregates at different fractions of water. But, the most spectacular aggregation behaviour was noticed in 83% water in THF. At room temperature, PNTI **6p** produced H-aggregates, but converted into J-aggregates upon heating at 55 °C. The process was reversible and cooling of the solution led to the generation of original H-aggregates. The details of the self-assembly process are described below.

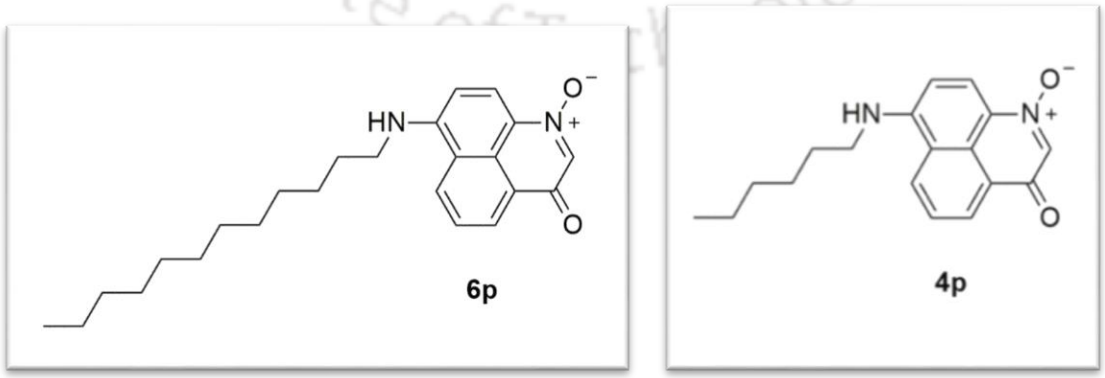

Fig 5. 2 Model molecules **6p** and **4p**, used for the upcoming sections.

❖ 5.2 Results and discussions

Even though the long alkyl chains of PNTIs do not contribute to the optical properties, they possess different degree of hydrophobicity, which in turn could lead to differences in self-assembly process. Accordingly, one compound was chosen with short hexyl chain (**4p**) and the other with long dodecyl chain (**6p**). The synthetic procedure is described in the previous chapter. As the dyes have different extent of hydrophobicity, water was used to tune self-assembly properties. However, the compounds were found to be insoluble in pure water. Hence, the investigations were carried out in a mixture of solvents. Tetrahydrofuran is considered a well-established solvent in the field of supramolecular chemistry generally suitable for obtaining a monomeric form of the dye or molecule of interest.[13] Unsurprisingly, both the PNTI dyes **4p** and **6p** exist as monomer in THF and displayed identical absorption spectra with maxima at 542 nm (Fig 5.3). Therefore, the self-assembly process was studied using a mixture of THF and water and the aggregation process was monitored using UV-vis spectroscopy. For convenient and better comparison, all the photophysical experiments were carried out using a concentration of 5 µM. Different volume percentage of water was added to the monomer in THF to trigger aggregations. The hydrophobic interaction between water and the nonpolar part of the PNTIs inaugurated aggregation. Accordingly, a preliminary UV-vis property investigations were done with 0-90 volume percentage of water in THF at room temperature for both **6p** and **4p**.

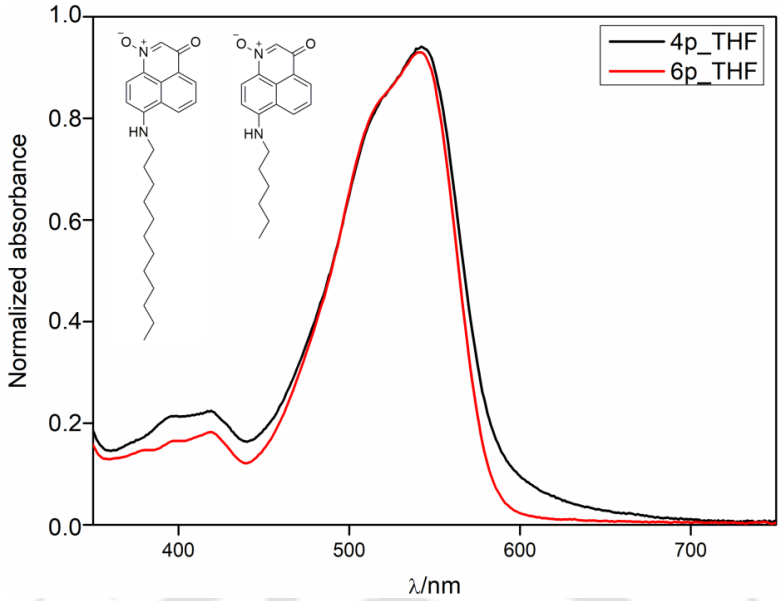

Fig 5.3 Absorption of **4p** and **6p** recorded in THF, showing similarity of feature and maxima.

With increase in volume percentage of water, PNTI **4p** displayed gradual bathochromic shift of the absorption maximum and reached to 594 nm in 90% water. Shifting of absorption maximum was noticeable even with 10% of water in THF. All the measurements in different volume percentage of water is summarized in Fig 5. 4. Besides bathochromic shift of absorption maximum, the spectral changes were marked with increase in molar extinction coefficient. Narrowing of the spectral bandwidth also accompanied with the increment of water percentage. All these spectral changes indicated the formation of J-aggregates. Further proof was obtained from photoluminescence property investigations, which showed enhancement of emission intensity. The J-aggregates in 90% water are stable and the spectral features remained same after keeping the solution at room temperature for 5 minutes (Fig 5.4).

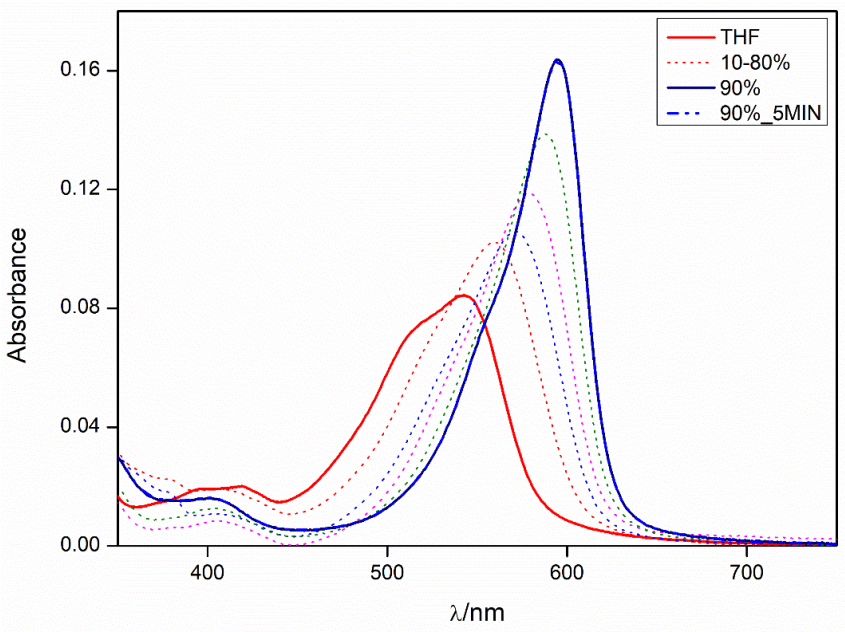

Fig 5.4 Absorption of **4p** recorded at various fractions of water and THF.

In next set of spectroscopic measurements, similar solvent systems were employed for the PNTI with **6p**. The spectral changes were found to be akin with that of observed in the case of **4p** until the volume percentage of water reached to 70%. At the specified solvent system PNTI **6p** displayed absorption maximum at 585 nm. Increase in molar extinction coefficient and narrowing of the spectral window were also accompanied with. However, unlike the hexyl counterpart, PNTI **6p** exhibited different behaviour when the water percentage was increased further. At 80% water, there occurred a sudden drop of the molar extinction coefficient along with hypsochromic shift of the absorption maximum. The spectrum becomes broader with the appearance of shoulder. With more polar solvent system (90% water in THF), the absorption maximum was completely hypsochromically shifted and appeared at 500 nm (Fig 5.5).

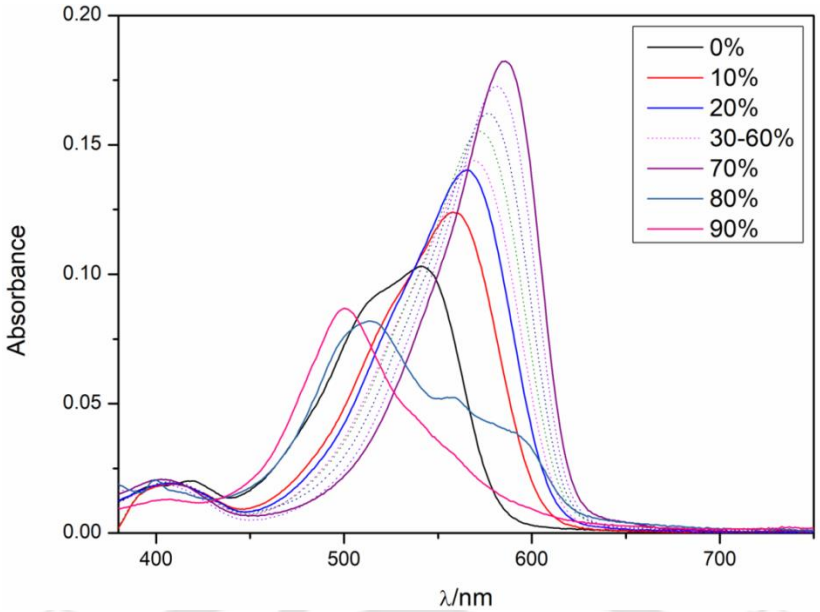

Fig 5.5 Absorption of **6p** recorded at various fractions of water and THF.

The molar extinction coefficient was found to be lesser than that of the monomer. Aggregation behaviour of the dye was also monitored using fluorescence spectroscopy. At 10% water in THF, PNTI **6p** displayed an emission maximum at 608 nm. Compared to the monomer, the emission maximum was bathochromically shifted by 20 nm. The emission intensity was also improved by approximately eight-fold. Betterment in emission intensity continued and at 70% of water the dye displayed a maximum at 617 nm. However, the emission intensity dropped significantly at 80% of water, and almost quenched at 90 volume percentage of water. (Fig 5.6).

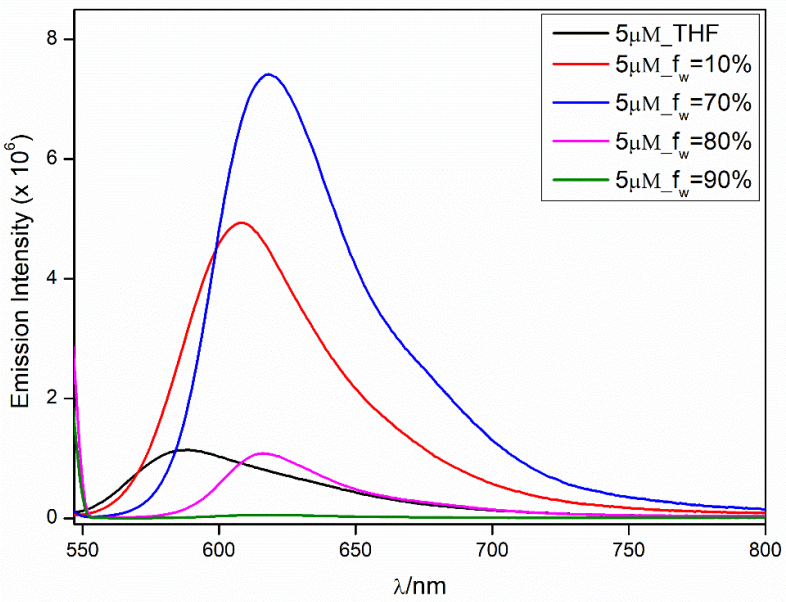

Fig 5.6 Emission of **6p** recorded at various fractions of water and THF.

When the Stokes shift of **6p** were taken into count, the values were decreased up to 70% of water, but subsequently increased with the surge in aqueous quantity. Stokes shift values were found to be 44 nm, 32 nm and 115 nm in 0%, 70%, and 90% of water respectively. Spectroscopic signatures, both from UV-vis spectroscopy and fluorescence spectroscopy, collectively proved that PNTI **6p** produced J-aggregates up to solvent system comprising of 70% water in THF. But, the dye self-assembled as H-aggregates in 90% of water. The differences in aggregation behaviour between **6p** and **4p** arises due to the additional hydrophobicity of the long dodecyl chain. Both the dyes arranged in a similar way and produced J-aggregates up to 70% of water in THF. But, at more aqueous content, with severe hydrophobic interactions, the long dodecyl chain first folded to minimize the unfavourable interaction. The aggregation happened with the folded dodecyl chain. As a result, the nature of aggregates in case of **6p** changed from J-type to H-type. In 80% of water in THF, existence of both types of aggregates has been noticed. On the other hand, with a shorter

alkyl chain in **4p**, the hydrophobic interaction was not that severe as for **6p** and the dye maintained J-aggregates even with 90% of water in THF.

❖ 5.2.2 Supramolecular rearrangement between AggH and AggJ

Taking the change of aggregation from J- to H-type as a function of solvent polarity (water percentage in THF) into account, efforts have been given to find a condition where interconversion between two types of aggregates of **6p** could be achieved in same solvent system. To achieve the feat, both aggregates, **AggH** and **AggJ**, have to be flexible enough to undergo switching in the specified solvent system. The H-aggregate formed at 90% of water in THF was quite stable, and did not show significant changes upon heating the solution. The molar extinction coefficient was dropped in small extent only (Fig 5.7). Keeping the solution

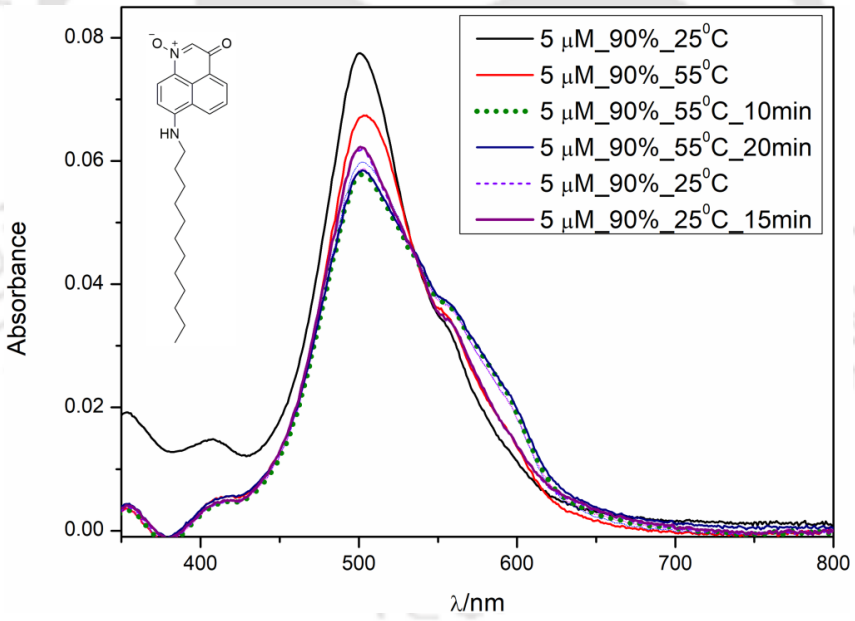

Fig 5.7 Variable temperature absorption spectra of **6p** at 90% of water in THF.

at room temperature over a period of 20 minutes at 55 °C, did show negligible changes and without deviating the properties of H-aggregates. Storing the solution at room temperature overnight displayed minor shifting of maximum with lessening of molar extinction

coefficient (Fig 5. 8). However, the characteristics of H-aggregates were maintained and the minor spectral changes are attributed to the internal adjustment of the H-aggregates.

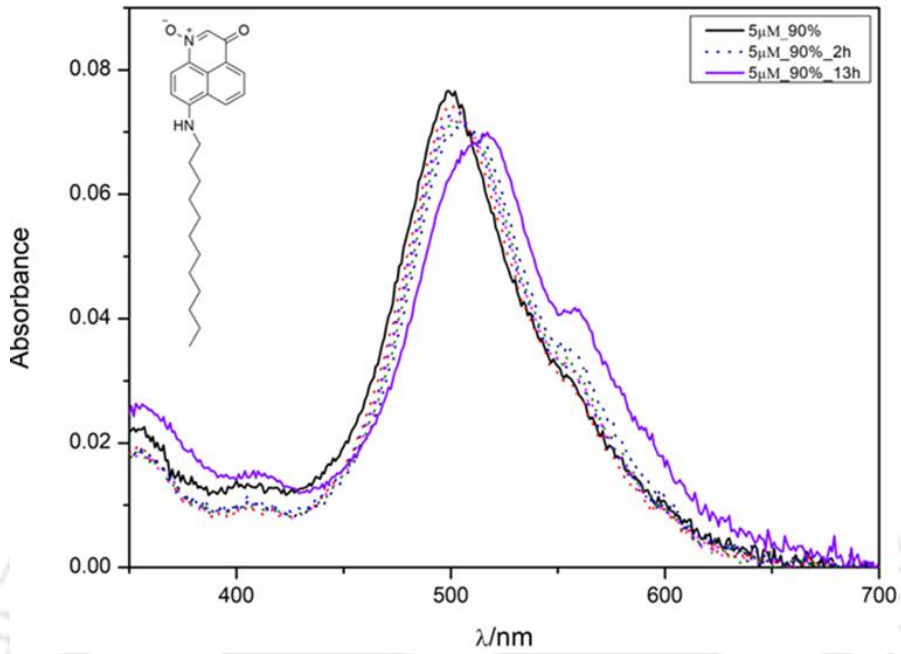

Fig 5.8 Time dependent absorption spectra of **6p** in 90% of water in THF at room temperature

Similarly the aggregates formed at 70% of water in THF did not exhibit any change in absorption maxima or any of its spectral traits, except for a decrease in the molar extinction coefficient (Fig 5.9). Drop in absorbance was probably due to the precipitation of the aggregates. Therefore, neither the H-aggregate in 90% of water in THF was converted into J-type by heating nor the J-aggregate in 70% of water was transformed into H-type upon standing. In absence of a suitable condition for interconversion between J- and H-aggregates, the search for optimum condition continued.

It was quite evident that to attain the objective of interconversion between the two types supramolecular structures, the hydrophobicity effect must be mitigated, and the volume percentage of water should be lie in between 70 to 90.

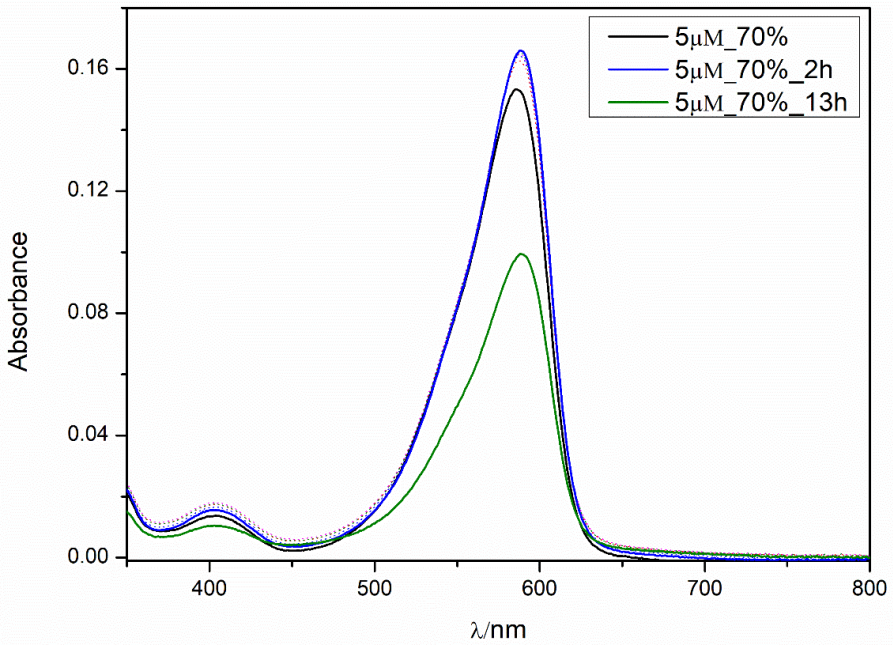

Fig 5.9 Time dependent absorption spectra of **6p** in 70% of water in THF.

In 80% of water in THF, PNTI **6p** showed the formation of both types of aggregates (Fig 5.10), **AggJ** and **AggH**. Keeping the solution at room temperature for 16 h and monitoring the same using UV-vis spectroscopy did show negligible change in the relative ratio of the two aggregates. However, storage of the solution of the dye, either at 0 °C or at 10 °C, for 16 h led to the conversation of the mixture into H-aggregates. On the other hand, keeping a mixture of the aggregates at 60 °C led to the generation of J-aggregates exclusively. In the specified solvent system, both the aggregates could be generated simply by changing the temperature. The interconversion process was found to be reversible. However, the switching process was very slow and time consuming. Additionally, at room temperature both the aggregates, **AggJ** and **AggH,** co-existed. Therefore, additional refinement of solvent system might lead to better switching process.

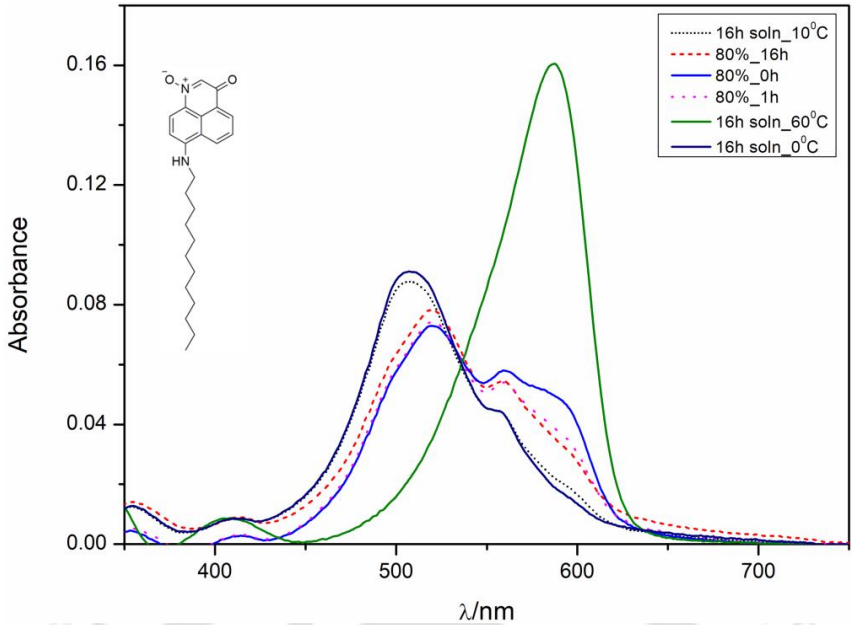

Fig 5.10 Variable temperature absorption spectra of **6p** in 80% of water in THF.

After further rational screening, the best solvent system was found to be the 83/17 v/v mixture of water/THF. When a monomeric solution of **6p** in THF was added to a mixture of THF-water to make the final solvent composition as 83% water in THF, formation of H-aggregate **AggH** was marked by appearance of an absorbance maximum at 502 nm (Fig 5.11). Upon heating the solution at 55 ℃, depletion of the H-aggregate was marked by diminishment of intensity at 502 nm. The absorption spectrum comprised of an additional maximum at 588 nm corresponding to the J-aggregate **AggJ**. Therefore, heating the solution of H-aggregates instantly produced a mixture of J- and H-aggregates. But, the scenario changed drastically when the solution was kept at 55℃ for 5 minutes. The mixture of the aggregates was converted in to J-aggregate exclusively. The spectral features were marked by narrowing of bandwidth, enhancement of molar extinction coefficient at 588 nm, and disappearance of signal corresponding to H-aggregate. The newly generated J-aggregate,

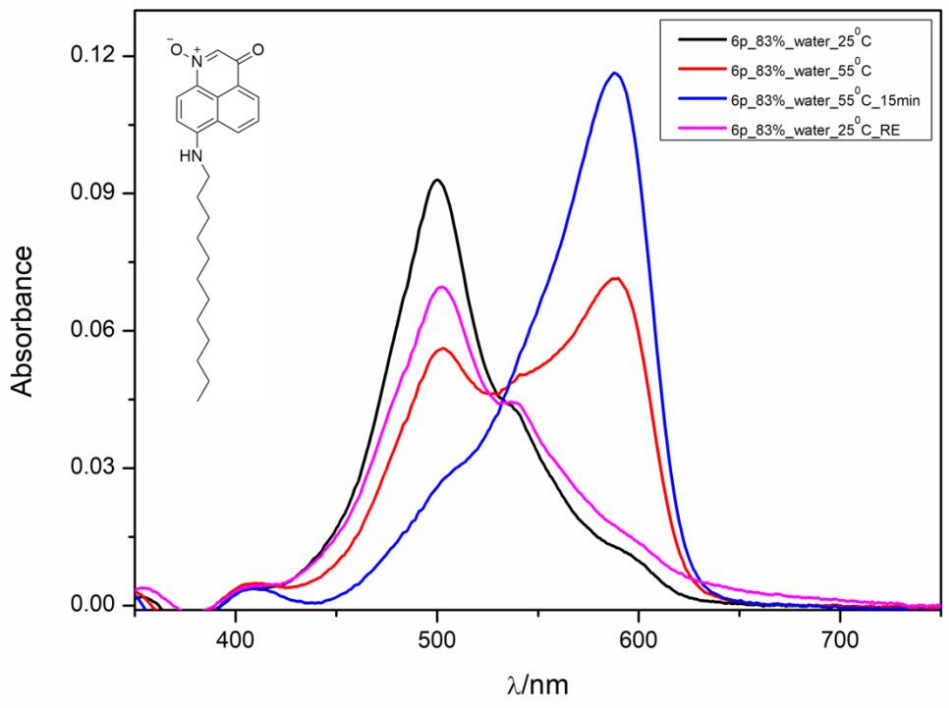

Fig 5.11 Variable temperature absorption spectra of **6p** in a solvent system containing 83% of water in THF.

however, displayed different absorption maximum than that of observed in 70% of water in THF. Considering the differences in solvent composition, minor variation in absorption maximum is acceptable. Cooling down the hot solution (83/17 v/v water/THF) of J-aggregate from 55 ℃ to 25 ℃ regenerated the H-aggregate completely, proving the reversibility of the switching process.

Efforts have been given to initiate the switching at lower temperature. Accordingly, the H-aggregate at the specified solvent system was kept at 35 ℃ for several hours. Unfortunately, the investigations were found to be unsuccessful. Beyond some insignificant changes in the absorption spectra, no other changes were noticed even after keeping the solution for 4 h. (Fig 5.12). Treating the H-aggregate of the dye at 40℃ also failed to improve the process. On the other hand, keeping the solution at 45 ℃ (Fig 5.12) and 50 ℃ caused a drastic change within first 15 minute. But, the switching process did not improve further. Conversion of H- to J-aggregate remained incomplete even after 4 h. The spectroscopic traces of H-aggregate

remained present. Preserving the solution at the same temperature for prolonged time did now show spectral changes. Indeed, the dye precipitated out from the solution.

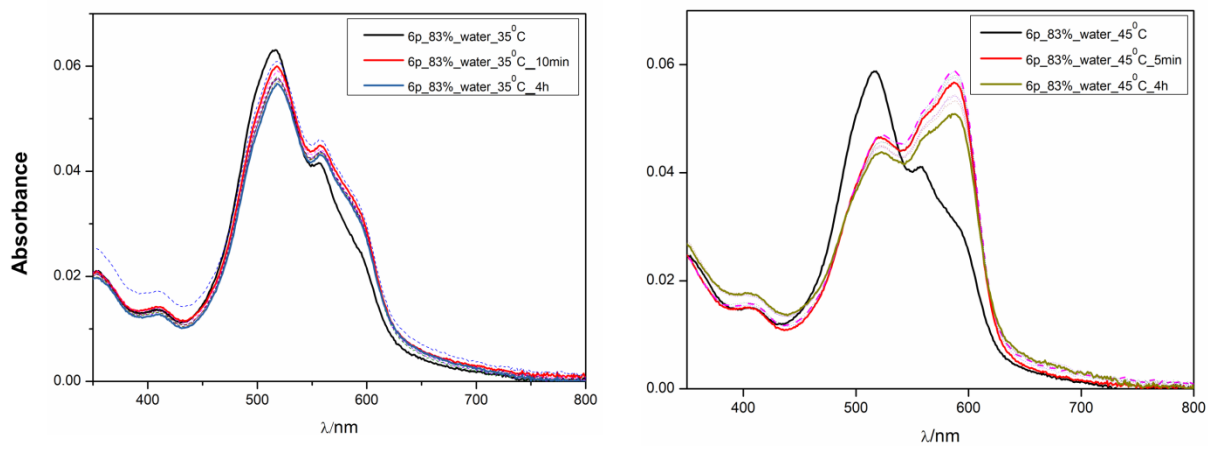

Fig 5.12 Constant temperature absorption spectra of 6p at f_w = 0.83 and temperatures of 35 ℃ and 45 ℃

Further insight into the mechanism of formation of J- and H-aggregates was obtained by doing denaturation experiments. For the same purpose, monomeric solution of **6p** in THF was added gradually to the H-aggregate in a 90/10 (v/v) mixture of water/THF. The changes were recorded spectroscopically. With the decrease in the percentage of water, the initial H-aggregate gradually converted into J-aggregate. The observations clearly demonstrated an on pathway mechanism where the **AggH** was produced via **AggJ**.

Even though some examples were reported on switching from J- to H-aggregate, and from H- to J-aggregate, the conversion was found to be unidirectional only. Reversible switching between J- and H-aggregates in solution have rarely been reported. The J-and H-aggregations of **6p** and their interconversion is the only example that happened reversibly. Inspired by the reversible switching between two different types of aggregates, photoluminescence properties were investigated to examine the potential of the dye as fluorescence thermometer. Since H-aggregates are non-emissive and J-aggregates are fluorescent, switching via heating and cooling would show variable photoluminescent properties as a function of temperature. In

other words, change in temperature could be detected by fluorescence. Accordingly, temperature dependent fluorescence measurements were done for **6p** using 83% of water in THF. At 25 ℃ the dye was found to be almost non-emissive as the aggregate was H-type. Upon heating the solution to 55 ℃, fluorescence intensity at 615 nm was enhanced by more than 1000 times **(**Fig 5.13**).** The improvement of photoluminescent property was attributed to the switching of **AggH** to **AggJ**. Similar to the UV-vis investigations, fluorescence measurements required approximately 5 minutes to complete the interconversion.

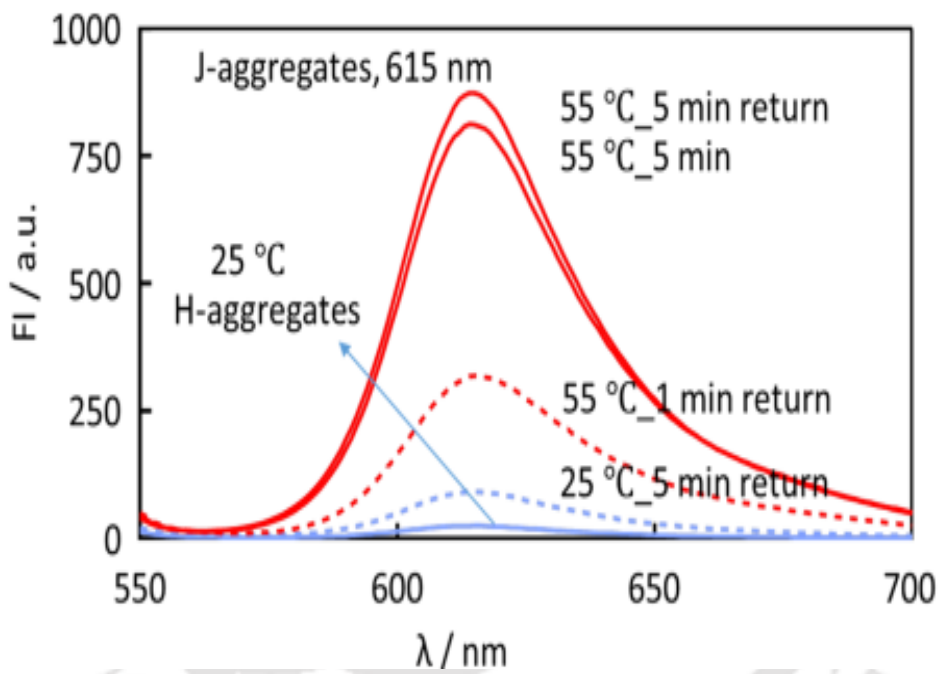

Fig 5.13 Variable temperature emission spectra of **6p** in 83% of water in THF.

After reaching the plateau, emission intensity remained constant. Cooling the solution back to 25 ℃ quenched the previously obtained emission at elevated temperature, indicating the reverse switching process i.e. conversion of **AggJ** to **AggH**. Both the aggregates were found to be stable at the respective temperatures. Keeping the solution for longer period of time at 55 ℃, did not induce change in the fluorescence intensity. Closer look at the heating and cooling process revealed that the enhancement of fluorescence was faster than the lessening

of photoluminescent intensity. Therefore, the transition from **AggH** to **AggJ is** faster than the reverse rearrangement (Fig 5.14) process.

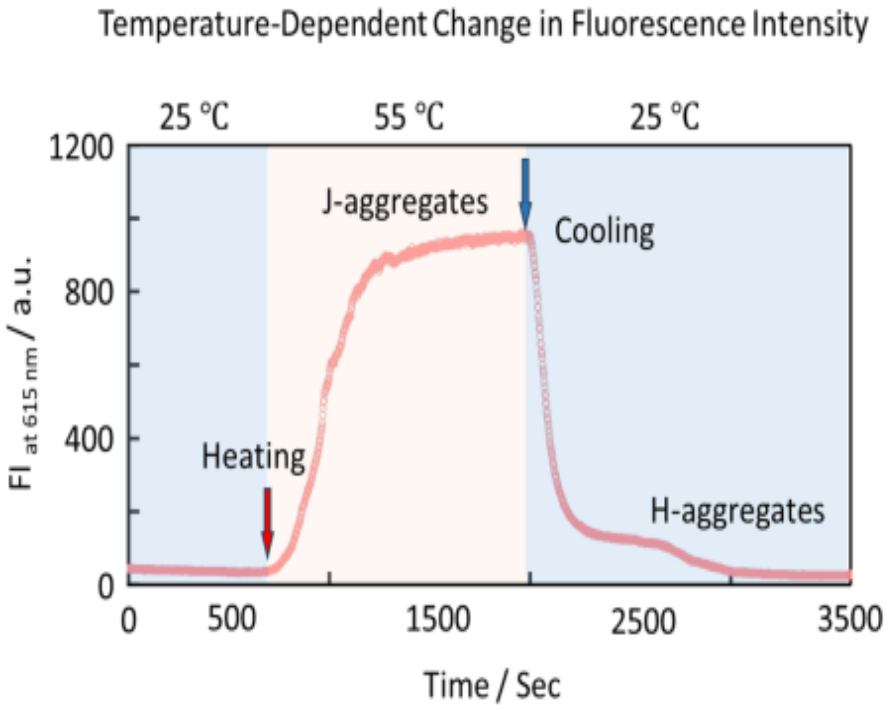

Fig 5.14 Variable temperature emission spectra of **6p** in 83% of water in THF as a function of time.

❖ 5.2.3 Morpholgical studies via microscopy

Further insight into the morphology of aggregates was obtained from microscopic measurements. For the **AggH**, a solution of **6p** in water-THF (83/17 v/v) was dried at 25 °C on a glass plate and the sample was used for study. AFM image (Fig 5.15) of the **AggH** showed the formation of nanofiber. Similar morphology was obtained when the sample was analysed using FESEM. Getting exact morphology for the **AggJ** was challenging because of the nature of sample preparation method. Drying a solution of the dye from 70% water in THF might lead to its transition to **AggH**. However, efforts have been given in a best possible

way. The solution was dried on a plate at 55℃, and the sample was analysed. Co-existence of spherical nanoparticles were observed along with the nanofiber of **AggH**.

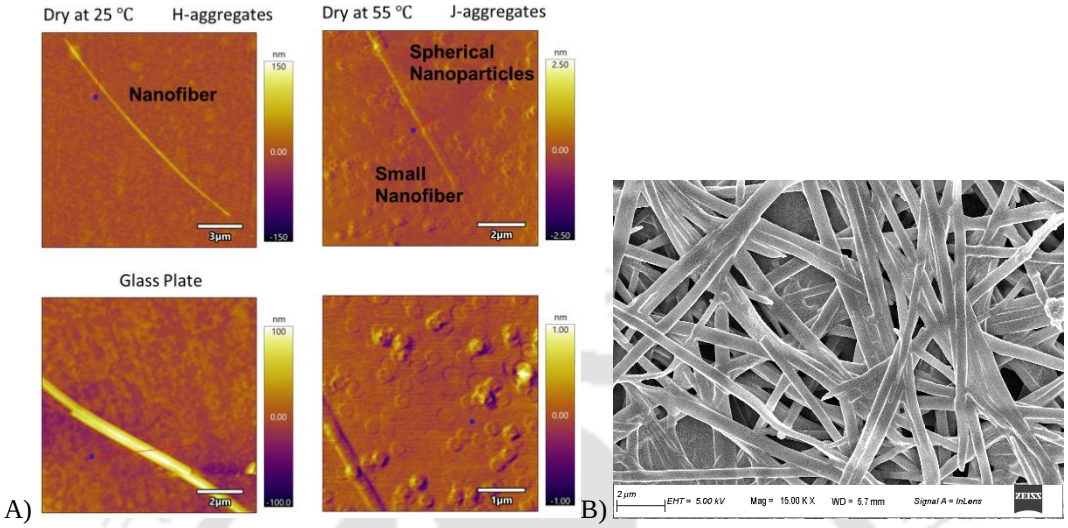

Fig 5.15 a) AFM images dried at 25 ℃ (left) and 55 ℃ (Right) b) FESEM images of **6p** in a 90/10 (v/v) mixture of water/THF(**AggH**).

❖ 5.3 Conclusion

In summary, self-assembly properties of PNTIs were investigated in details. The effect of the chain length in the alkylamino group was analysed by using dyes with variable substituents. Accordingly, two PNTIs, **6p** and **4p**, were chosen. Long dodecyl group was used in **6p**, while a shorter hexyl chain was attached in **4p**. Both the dyes existed as monomer in THF and exhibited same absorption maximum as the alkyl chain has no effect on the UV-vis properties. When different increments of water were added to the monomer in THF, both the dyes behaved in a similar way; till the percentage of water reached to 70. Formation of J-aggregates was noticed in both cases. However, **6p** behaved differently after increment of water percentage. At ≥ 83% of water in THF, **6p** produced H-aggregates. On the other, **4p** maintained J-aggregate even at 90% of water in THF. The differences in self-assembly propertied were originated from the different hydrophobicity of the alkyl chain. In case of

docedcyl chain, the hydrophobicity is very severe ≥ 83% of water in THF. To avoid the unfavourable interactions, the chain first folded and then underwent aggregation. The H-aggregate of **6p**, in a 83/17 (v/v) water/THF mixture, was converted into J-aggregate by heating the solution at 55 °C. The reverse switching was accomplished simply by cooling down the solution to 25 °C. Since the two types of aggregates have different emission behaviours, switching from H- to J-aggregates led to the fluorescence being turned on from off state upon heating. The dye has potential as use in fluorescence thermometer, and the concept has been demonstrated by measuring temperature dependent fluorescence of **6p**. While limited examples on unidirectional switching between J- and H-aggregates being reported, reversible switching between the aggregates has never been realised. The PNTI **6p** is the first example which demonstrated reversible switching between J- and H-aggregates simply by varying the temperature of the solution. The self-assembly of PNTIs not only cover a void area in supramolecular chemistry but give a new and unique moiety to the area.

❖ 5.4 References

[**1**] (a) Würthner, F.; Kaiser, T.E. and Saha-Möller, C.R., *Angew. Chem., Int. Ed.* **2011**, 50, 3376–3410; (b) Spano, F.C. and Silva, C., *Annu. Rev. Phys. Chem*. **2014**, 65, 477-500.

[2] (a) Hestand, N.J. and Spano, F.C.,*Chem. Rev.* **2018**, 118, 7069–7163; (b) Klymchenko, A.S.; *J. Nanosci. Lett.* **2013**, 3, 21

[3] Ma, S.; Du, S.; Pan, G.; Dai, S.; Xu, B.; Tian, W., *Aggregate* **2021**, 2, e96.

[4] Deng, Y.; Yuan, W.; Jia, Z. and Liu, G.; *J. Phys. Chem. B* **2014**, 118, 49, 14536–14545

[**5**] Zhao, Q.; Lai, H.; Chen, H.; Li, H. And He, F.; *J. Mater. Chem. A* **2021**, 9, 1119-1126

[6] Más-Montoya, M. and Janssen, R.A.; *Adv. Funct. Mater.* **2017**, 27, 1605779.

[7] Kim, S.-O.; An, T. K.; Chen, J.; Kang, I.; Kang, S. H.; Chung, D. S.; Park, C. E.; Kim, Y.-H.; Kwon, S.-K. H-.; *Adv. Funct. Mater.* **2011**, *21*, 1616– 1623

[8] Deing, K. C.; Mayerhöffer, U.; Würthner, F.; Meerholz, K.;. *Phys. Chem. Chem. Phys.* **2012**, 14, 8328– 8334

[9] Liang, W.; He, S. And Fang, J.; *Langmuir* **2014**, 30, 3, 805–811.

[10] (a) Eder, T.; Stangl, T.; Gmelch, M.; Remmerssen, K.; Laux, D.; Höger, S.; Lupton, J.M.; Vogelsang, J.; *Nat Commun* **2017**, 8, 1641 (b) Sarbu, A.; Biniek, L.; Guenet, J.-M.; Mésini, P.J.; Brinkmann, M..; *J. Mater. Chem. C* **2015**,3, 1235-1242 (c) Rhodes, S.; Liang, W.; Wang, X.; Reddy, N.R. and Fang, J.; *J. Phys. Chem. C* **2020**, 124, 21, 11722-11729. (d) Zhang, G. And Liu, M.; *J. Phys. Chem. B* **2008**, 112, 25, 7430–7437

[**11**] (a) Fennel, F.; Wolter, S.; Xie, Z.; Plötz, P.-A.; Kühn, O.; Würthner, F. and Lochbrunner, S.; *J. Am. Chem. Soc*. **2013**, 135, 18722–18725 (b)Wagner, W.; Wehner, M.; Stepanenko, V. Ogi, S. and Würthner, F.; *Angew. Chem., Int. Ed.* **2017**, 56, 16008–16012

[**12**] Fukui, T.; Kawai, S.; Fujinuma, S.; Matsushita, Y.; Yasuda, T.; Sakurai, T.; Seki, S.; Takeuchi, M. and Sugiyasu, K.; *Nat. Chem.* **2017**, 9, 493–499.

[13] (a) Yao, H.; Zhou, M.; Yu, X.; Bai, M., *Chem. Comm*. **2022**, 58, 4985-4988. (b) Tsuji, H.; Nakahata, M.; Hishida, M.; Seto, H.; Motokawa, R.; Inoue, T.; Egawa, Y.; *J. Phys. Chem. Lett.* **2023**, 14, 49, 11235–11241.

Chapter 6

Conclusion and future prospective

❖ 6.1 Conclusion

In summary, the accumulated research report described in this thesis involves the properties of two different *peri*-annulated dyes, namely the derivatization products of the novel dye PNI, and the completely novel PNTI. All of the previously discussed dyes possesses amphiphilic character and thus are significantly dependent on the polarity of the solvent for the display of unique properties. Synthesis of the dyes were accomplished with minimal difficulties and purification of the same was also achieved with little to no hurdles. Yields of most of the numerous molecules that form an important part of this thesis were quite decent, however any issue faced with some other molecules were not without reason and explained with proper justification.

An early stage of the thesis deals with the preparation of the boron difuoride complex of PNI, i.e. PNIBF_2 and an insight into its photophysical properties. The complexation instills forced planarity on the dye, causing lesser solubility, however with an increased emission yield, increased extinction, bathochromic shift and vibronic fine structure in absorption maxima with a lesser FWHM, and a decreased Stokes shift. All these properties are general trends of restricted rotation in a molecule, which is the case that is also generated for the dye PNI. The molecule PNIBF2 aggregates in non-polar solvents (99% MCH) in emissive and linear nanoaggregates **Agg1**. In a polar solvent (at an exact ratio of 76:24 of water:THF), the molecule displays supramolecular polymorphism between nano-ellipsoidal **Agg2** and nanospherical **Agg3**. **Agg2** and **Agg3** are classified as the kinetic and thermodyanmic aggregates respectively, an observation that can be justified by SA/V ratios of shapes and the corresponding stabilities. **Agg2** and **Agg3** are both non-emissive and are distinguished by unignorable differences in their absorbance spectra.

A butyl derivative of PNI was also prepared, where the butyl group is attached to the peri position of both the naphthalene rings, and its self assembly in non-polar solvents was studied. The group delivers better solubility to the dye, with a slight bathochromic shift in absorbance. According to previous studies, aggregation of PNI in non-polar solvents occured through three-dimensional stacking of the dye monomers and this installation of the butyl groups hinders the growth in one dimension, thus providing flexible chains in lieu of rigid cuboids for PNI. Acid coordination to the dye in non-polar solvents causes folding of the chains, the degree of which is affected by the non-polarity of the solvent. The dye also forms a charge transfer complex with fullerene C_{60}, and thus a system is designed to study the effect of fullerene and acid coordination on the morphology of the dye in non-polar solvents, in a process known as supramolecular rearrangement.

A novel kind of dye PNTI was also prepared, the naphthalene analogue of isatogen, but without any substitution at the C2 position, which is a first in the world of dye chemistry. The stability of such dyes was enforced via the installation of an amino group at the peri-position, thus making use of the strong donating capability of this group. The five dyes (five different alkyl chains) were synthesized using strongly acidic conditions via a new kind of mechanism termed 'aldrone' condensation. The dyes displayed good solubility, strong colour and moderate emission, which increases in polar solvents such as ethanol and DMSO. Presence of a dipole in the molecule also allowed for facile 1,3-dipolar cycloaddition of ethyl acrylate, resulting in the formation of an aza-phenalenone, which proceeds through intended iso-oxazolidine ring formation, however undergoes rupture at N-O bond to gain stability through planarity. Photophysical properties of the derivative **2p1′** too was studied, with similar strong colour and moderate emission, however bathochromically shifted in comparison to the dye **2p**.

Presence of ambipolar groups in this PNTI dye also presented the opportunity for the study of the self assembly of the dyes. Difference in chain length played a huge part in the aggregation of the dyes **6p** (dodecyl chain) and **4p** (hexyl chain) in polar solvents. The dye **4p** with a shorter chain length displays J-aggregation upto 90% water fractions, however **6p** with a dodecyl chain was significantly more apprehensive to the increased water fractions, and thus displays J-aggregation only upto 70% water after which at higher water fractions it switches to H-aggregates. Reversible interconversion between H and J-aggregates was also achieved at a precise water fraction via application of temperature as a control, with resulting changes in absorption bands and emission intensities.

❖ 6.2 Future scope

Based on the results accomplished in this thesis, it is clear that derivatization of a dye manifests in distinctive properties for the prepared derivative compared to the original dye. Unique substituents may have a significant role in the photophysical and supramolecular interaction behaviour of the derivatives. Considering that the peri-annulated dyes studied in this thesis are still in their prime, a lot more is to be achieved by a deeper dive into these fields.

Study of the redox behaviour of the boron complex of PNI is hindered by its low solubility, which can be overcome by the installation of solubilizing groups. Redox behaviour of boron difluoride complexes of dyes are an intriguing domain of research. These solubilizing groups in turn can also increase the prospect of the attainment of different aggregation pathways, due to the hindrance of the three dimensional growth of PNI mentioned above. The example of butyl PNI self assembly is indeed an encouragement that substituents can affect the supramolecular chemistry of the dye. As exemplified in this thesis, template or guest based aggregation of PNI and PNI-derived molecules are yet to be explored in exhaustive detail.

This encourages the creation of new and exciting molecules to fuel the study of the impact of the novel dye PNI on the world of dye and supramolecular chemistry; even the applicability of this dye and its derivatives in the field of organic electronics is completely open to exploration, inspired by the versatility of indigo and its derivatives in this specified field. Commenting on the future of the dye PNTI, the molecule is completely novel in the field of dye chemistry, and hence is an unexplored mine for unique and exciting molecules, with their own unique photophysics and aggregation tendencies, as demonstrated perfectly by previous experiments in this thesis. Derivatization of this PNTI dye is an undeniable possibility which can be accomplished through various synthetic pathways, one of the prominent ones of which is dipolar cycloaddition, and the C2 position in this molecule being unsubstituted opens up the avenue for multiple functionalization potential. Even late stage ring substitution is an undeniable possibility for PNTIs if the example of isatogens are to be followed. A simple investigation into the diverse reactions of isatogens are an encouragement for the potential of PNTIs. With sufficient investigation, PNTIs may find their way into the pharmacological field or may be the precursor for other bioactive molecules, inspired by the well-reported dominion of isatogens in this particular niche.

Chapter 7

Experimental Section

❖ 7. 1 General information and instrumentation

Silica gel for column chromatography (60-120 mesh) was obtained from Spectrochem. Analytical thin layer chromatography (TLC) plate (silica gel 60 F254) was purchased from Merck. Reactions were monitored by TLC and visualized under 254 nm and 365 nm UV-light. All chemicals were purchased from common vendors such as Spectrochem, Merck, Loba, Himedia, Avra and Sigma-Aldrich and used without further purification. Solvents and acids were mostly purchased from Merck and used without subsequent treatment unless specified. Reactions were carried out in open air unless specified otherwise.

❖ 7.1.2 IR-spectroscopy

Infra-red (IR) spectra were collected as a film on KBr pellets using Perkin-Elmer FT-IR spectrometer or via ATR in Perkin-Elmer Spectrum Two FT-IR spectrometer and frequencies are presented in reciprocal centimetre (cm^{-1}).

❖ 7.1.3 Mass-spectrometry

High resolution mass spectrometry (HRMS) measurements were done with Agilent QTOF 6520 mass spectrometer, Agilent QTOF ESI-MS HAB-273 or with a Waters Xevo XS QTOF mass spectrometer (ACQUITY UHPLC) using electrospray ionization (ESI) mode. Isotopic distributions of the mass were calculated using Agilent Mass Hunter Data analysis (version 8.0.8208.0) software.

❖ 7.1.4 NMR spectroscopy

^{1}H and ^{13}C NMR and ^{1}H-^{1}H COSY NMR spectra were recorded using either Bruker Ascened TM 400 MHz NMR spectrometer, NMR measurements were carried out on Bruker Avance 500 MHz NMR spectrometer, or Bruker Avance III 600 MHz NMR spectrometer using the deuterated solvent as the lock and residual solvent as the internal reference. The chemical shifts were reported in δ (ppm) relative to the residual protonated solvent peak of the deuterated solvent ($CDCl_3$: δ_H = 7.26 ppm, δ_C = 77.0 ppm). All of the reported NMR measurements were carried out at 293 K unless mentioned otherwise. The following abbreviations were utilized to describe peak patterns: s = singlet, d = doublet, t = triplet, q = quartet, dd = doublet of doublet, dt = doublet of triplet, ddd = doublet of doublet of doublet, m = multiplet, and br = broad. ^{19}F and ^{11}B NMR data were calibrated using BF_3•Et_2O as external standard. The numbering of the carbon atoms of the molecular formulas shown in the Experimental Section is only used for the assignments of the NMR signal and is not in accordance with the IUPAC nomenclature rules.

❖ 7.1.5 UV/Vis spectroscopy

The UV-Vis absorption spectra were recorded on Perkin-Elmer Lambda-25, Lambda-35, Cary 100 and Cary 3500 UV spectrophotometers at 293 K and higher temperatures. Depending upon concentrations, samples were loaded either in 1 mm or in 10 mm path length quartz UV-cuvettes. Cary 100 (equipped with Peltier accessory) and Cary 3500 UV spectrophotometers were specifically used for higher temperature measurements.

❖ 7.1.6 Photoluminescence spectroscopy

Photoluminescence (PL) spectra were recorded on a Horiba Fluoromax-4 spectrofluorometer. A 10 mm × 10 mm quartz cuvette was used for the solution spectra at 293 K. The spectra were corrected using the correction factor implemented in the software. Absolute quantum yields were measured using K-sphere on the same instrument. Temperature dependent fluoescence spectroscopy

❖ 7.1.7 Time resolved fluorescence spectroscopy

Fluorescence lifetimes are measured using an Edinburg instrument Lifespec II & FSP 920.

❖ 7.1.8 Microscopic imaging

Microscopic images were recorded either on FESEM Sigma 300 or FESEM Gemini 300 microscope. Samples were prepared by drop-cast method from the respective solvent system and followed by room temperature evaporation for 10-16 h.

❖ 7.1.9 Photoluminescence quantum yield

Relative quantum yield (QY) of PNTIs was measured in $CHCl_3$ against using the following equation.[3]

$$\Phi^{i} = \frac{F^{i} f_{s} n_{i}^{2}}{F^{s} f_{i} n_{s}^{2}} \Phi^{s}$$

where Φ^{i} and Φ^{s} are the photoluminescence QY of the sample and that of the standard, respectively; F^{i} and F^{s} are the integrated intensities (areas) of sample and standard spectra,

respectively ; *fx* is the absorption factor ($f_x = 1 - 10^{-Ax}$, where A = absorbance); the refractive indices of the sample and reference solution are n_i and n_s, respectively.

❖ 7.1.10 Mathematical modelling and curve fitting

Curve fitting for the denaturation model of **Agg1** was carried out by Stef A. Jansen and that for **Agg2** and **Agg3** were performed by Jonas Matern and Gustavo Fernandez.

❖ 7.2 Synthetic details of compounds described in the thesis

❖ 7.2.1 Synthesis of PNI-BF_2

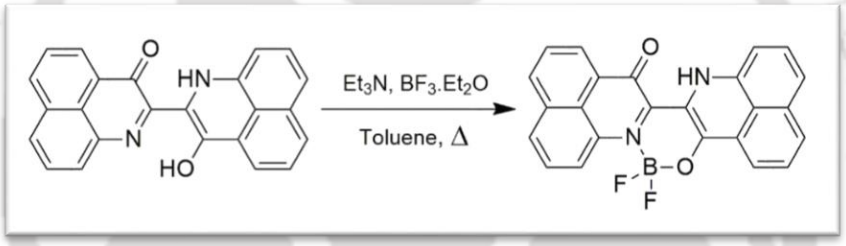

PNI (50.0 mg, 138 µmol) was loaded into a round-bottomed flask and dissolved in 10 mL of toluene. Triethylamine (95.0 µL, 689 µmol) was added to the solution and stirred at 90 ºC for a period of 10 minutes. To the hot solution BF_3•Et_2O (170 µL, 1.38 mmol) was added, and the mixture was refluxed for overnight. After cooling down the reaction mixture to room temperature, the organic solvent was evaporated to dryness under reduced pressure. The solid was then dissolved in a mixture of 1:1 (v/v) chloroform-THF and passed through a pad of basic alumina. After removal of the organic solvents under reduced pressure, the solid was washed with hexane (3 x 10 mL) and methanol (3 x 10 mL). The BF_2-coordinated compound was dried and used for investigation without doing further purification. Yield = 32.0 mg (57%); 1H-NMR (600 MHz, $CDCl_3$, 293 K) δ 8.78 (d, ^3J = 7.8 Hz, 1H), 8.67 (d, ^3J = 7.2 Hz,

1H), 8.33 (d, ^{3}J = 7.8 Hz, 1H), 8.30 (d, ^{3}J = 7.2 Hz, 1H), 8.17 (d, ^{3}J = 7.8 Hz, 1H), 7.92 (d, ^{3}J = 7.2 Hz, 1H), 7.81-7.86 (m, 4H), 7.68-7.74 (m, 2H), 7.49 (s, 1H) ppm; ^{19}F NMR (376 MHz, $CDCl_3$, 293 K) δ -130.7 (q, $^{1}J_{B\text{-}F}$ = 34.6 Hz, 2F) ppm; ^{11}B NMR (128 MHz, $CDCl_3$, 293 K) δ 3.17 (t, $^{1}J_{B\text{-}F}$ = 34.6 Hz, 1B) ppm; HRMS (ESI) m/z calcd for $[M\text{-}2F + Na]^+$ 395.0967, found: 395.1062; IR (KBr) 764, 775, 808, 826, 841, 903, 934, 990, 1021, 1072, 1112, 1178, 1195, 1225, 1264, 1295, 1345, 1372, 1392, 1423, 1467, 1503, 1524, 1550, 1595, 1658, 2851, 2921, 3061, 3432. cm^{-1} ; UV/vis (CHCl3) λ_{max}/nm ($\varepsilon/M^{-1}cm^{-1}$) 659 (43 255), 606 (29530).

- **7.2.2 Synthesis of butylPNI**
- **7.2.2.1 Synthesis of IIIB**

Synthesis of the reactant **IIIA** was already reported in a past thesis compiled by a past member of our team.

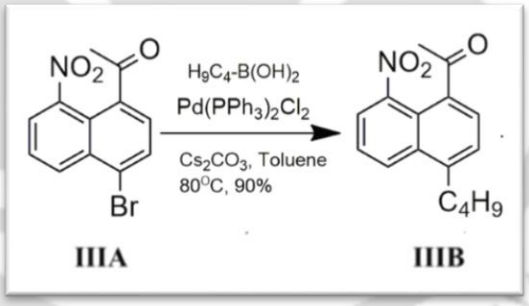

To a solution of **IIIA** (250 mg, 0.850 mmol) in toluene (10 mL), loaded in a Schlenk flask equipped with a stirring bar; butylboronic acid (104 mg, 1.020 mmol), $Pd(PPh_3)_2Cl_2$ (60 mg, 0.085 mmol) and Cs_2CO_3 (692 mg, 2.125 mmol) are added in quick succesion. The entire reaction system is sparged and saturated with argon to maintain an inert atmosphere. The reaction vessel is then dipped in a preheated oil bath at 80°C. The reaction is allowed to run for 7 hours at this temperature and in inert condition, after which the vial is unsealed and

toluene is removed under reduced pressure, and filtration with an organic solvent as eluent ensures removal of the catalyst and the base. Minor purifications of the fitrate using EtOAc/hexane (10/90 v/v) provides the pure product. Yield = 208 mg, 91%. ^{1}H NMR (400 MHz, $CDCl_3$) δ = 8.34 (d, ^{3}J= 8.4 Hz, 1H), 8.07 (d, ^{3}J =7.6 Hz, 1H), 7.82 (d, ^{3}J =7.2 Hz , 1H), 7.61 (t, ^{3}J = 8.4 Hz, ^{3}J = 7.6 Hz, 1H). 7.46 (d, ^{3}J= 7.2 Hz, 1H), 3.12 (t, ^{3}J = 8.0 Hz, 2H), 2.72 (s, acetyl-CH3, 3H). 1.76-1.68 (m, 2H), 1.51-1.42 (m, 2H), 0.98 (t, ^{3}J=7.2 Hz, 3H). ^{13}C NMR (150 MHz, $CDCl_3$) 200.9, 148.7, 143.5, 135.2, 133.8, 129.8, 128.4, 126.3, 125.1, 124.5, 121.9, 33.5, 33.0, 29.8, 28.5, 22.8, 14.0. HRMS (ESI) m/z: $[M + H]^+$ Calculated for $C_{16}H_{18}NO_3$: 272.1287. Found : 272.1290.

❖ 7.2.2.2 Synthesis of butylPNI

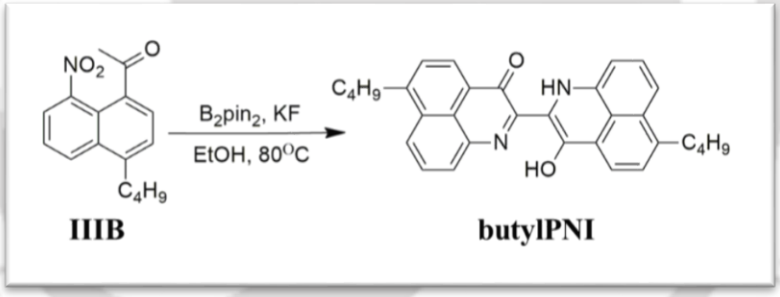

Into a 50 mL round-bottomed flask, 100 mg of **IIIB** (0.369 mmol) was loaded along with 10 mL of ethanol and the reaction vessel was suspended in an oil bath. The temperature was set at 80°C and allowed to gradually heat up, while the rest of reactants- 201 mg of bis-pinacolato-diborane (0.792 mmol) and 106 mg of potassium fluoride (1.840 mmol) were added in succession. The refluxing mixture was allowed to react for 16 h, after which the ethanol was evaporated under reduced pressure. The dry mixture was subsequently washed with water (3 x 20 mL), EtOH (3 x 10 mL) and Et_2O (3 x 5 mL). The crude mixture was then purified via column chromatography using DCM/hexane as eluent (v/v = 1 : 2 to 1 : 1). The

pure product was obtained as as blue-brown solid. Yield = 41 mg (47 %). ^{1}H NMR (400MHz, $CDCl_3$) δ = 12.48 (br,1H, -OH), 8.54 (d, ^{3}J = 7.60 Hz, 1H), 7.97 (d, ^{3}J = 8.40 Hz, 1H), 7.94 (d, ^{3}J = 7.20 Hz, 1H), 7.81 (d, ^{3}J = 7.60 Hz, 1H), 7.66 (d, ^{3}J = 8.00 Hz, 1H), 7.63 (d, ^{3}J = 7.60 Hz, 1H), 7.58 (d, ^{3}J = 8.40 Hz, 1H), 7.51-7.46 (m, 2H), 7.16 (s, 1H), 7.16 (d, ^{3}J = 7.20 Hz, 1H), 3.19 (t, ^{3}J = 7.60 Hz, 2H), 3.10 (t, ^{3}J = 7.60 Hz, 2H), 1.83-1.73 (m, 4H), 1.52-1.42 (m, 4H), 1.00 (t, ^{3}J = 7.20 Hz, 3H), 0.9 (t, ^{3}J = 7.20 Hz, 3H) ppm. ^{13}C NMR (150 MHz, $CDCl_3$) 179.6, 155.5, 153.8, 149.6, 144.9, 143.1, 139.0, 132.6, 131.6, 129.7, 129.6, 128.9, 128.6, 128.0, 127.6, 127.6, 127.3, 126.0, 124.5, 122.6, 121.5, 117.3, 108.4, 90.5, 34.1, 33.9, 33.8, 32.4, 23.0, 22.9, 14.1, 14.1 ppm. HRMS (ESI) m/z: $[M + H]^+$ Calculated for $C_{32}H_{31}N_2O_2^+$: 475.2386; Found: 475.2379. IR 2953, 2929, 2858, 1651, 1598, 1570, 1520, 1476, 1448, 1399, 1374, 1357, 1282, 1207, 1179, 1043, 911, 856, 805, 776, 741, 691, 632 cm^{-1}. UV-vis ($CHCl_3$) λ_{max}/nm (ε/M^{-1} cm^{-1}) 638 (30400). mp 190°C.

❖ 7.2.3 Synthesis of PNTIs and 2p1′

The synthetic procedure and the analytical and spectroscopic data of the reactants beginning from **2** till (**ni,nr**), final products (**np**), and the cycloaddition product **2p1'** are described here.

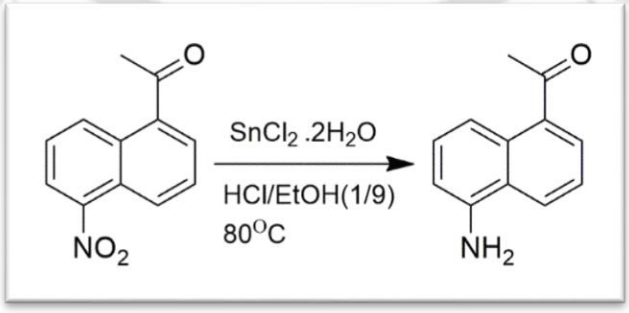

To a solution of 5-nitro-1-acetylnaphthalene (2.70 g, 12.6 mmol) in 80 mL of EtOH/HCl (95/5) mixture, was added 14.2 g (62.7 mmol) of $SnCl_2$•$2H_2O$. The mixture was refluxed for

5 h. After cooling down to room temperature, the mixture was diluted with 250 mL of ethyl acetate. The organic layer was then washed with brine solution (5 x 300 mL), separated and dried over Na_2SO_4. After filtration, the solvent evaporated under reduced pressure to obtained a brown solid. The desired compound **2** was received as yellowish-brown solid after purification through column chromatography using DCM/Hexane (4:1 v/v) as eluent. Yield = 1.29 g, 56 %. ^{1}H NMR (600 MHz, $CDCl_3$) δ 8.04 (d, ^3J = 8.4 Hz, 1H), 8.02 (d, ^3J = 8.4 Hz, 1H), 7.84 (d, ^3J = 7.2 Hz, 1H), 7.47 (dd, ^3J = 8.4 Hz, ^3J = 7.2 Hz, 1H), 7.39 (dd, ^3J = 8.4 Hz, ^3J = 7.2 Hz, 1H), 6.85 (d, ^3J = 7.2 Hz, 1H), 4.17, (s, 2H, N-H), 2.73, (s, 3H, acetyl-H) ppm; ^{13}C NMR (150 MHz, $CDCl_3$) δ 202.6, 142.3, 136.7, 130.9, 128.4, 127.8, 125.2, 124.3, 123.2, 116.7, 110.6, 30.4 ppm. HRMS (ESI) m/z: $[M + H]^+$ Calculated for $C_{12}H_{12}NO^+$: 186.0913; Found 186.0927.

General synnthetic methods are reported for the successful conclusions reported in the Chapter 3, mainly **2-4a**, **2-4r** and **2-6p**, along with **2p1′**. The butoxy and butyl analogues, for which succesful conclusion was not reached, are indicated by **7-7r** and **8-8r** respectively.

❖ **7.2.3.1 Synthesis of na (2a-6a)**

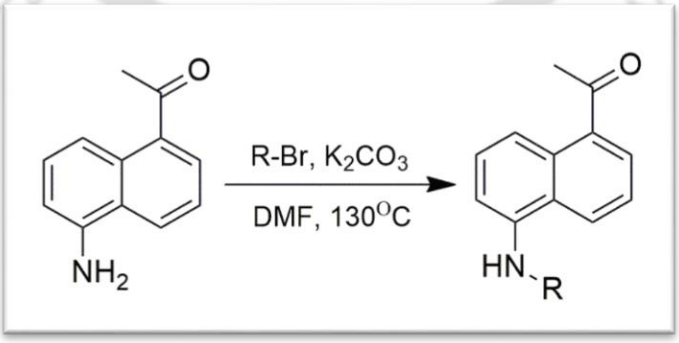

To a solution of **2** (1.00 mmol) in dry DMF (5 mL), was added alkyl bromide (4.00 mmol) and K_2CO_3 (5.00 mmol). This mixture was stirred at 65-70 °C for 24 h. The temperature was

subsequently raised to 130 ℃ with continuous stirring for additional 24 h. After cooling down to the room temperature, 50 mL of dichloromethane was added to the mixture. The carbonate residue was filtered off and washed with dichloromethane (3 x 10 mL). The combined organic layer was then washed with ice-cold water (3 x 50 mL), washed over anhydrous Na_2SO_4, and concentrated under reduced pressure to obtain the crude product. Purification was accomplished using column chromatography with EtOAc/Hexane (0/100 to 15/85 v/v) to provide the pure product.

Compound **2a** was obtained as light orange solid in 42% yield. ^{1}H NMR (600 MHz, $CDCl_3$) δ

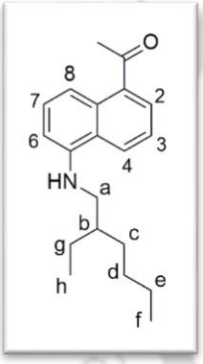

= 7.98 (d, ^3J = 8.4 Hz, 1H, 8-H), 7.89 (d, ^3J = 8.4 Hz, 1H, 2-H), 7.81 (d, ^3J = 7.2 Hz, 1H, 4-H), 7.46-7.43 (m, 2H, [3,7]-H), 6.66 (d, ^3J = 7.8 Hz, 1H, 6-H), 4.35 (s, 1H, N-H), 3.18 (d, ^3J = 6.0 Hz, 2H, a-H), 2.72 (s, 3H, acetyl-H), 1.75- 1.71 (m, 1H, b-H), 1.54-1.48 (m, 2H, g-H), 1.47-1.44 (m, 2H, c-H) 1.38-1.31 (m, 4H, [d,e]-H), 0.97 (t, ^3J = 7.2 Hz, 3H, h-H), 0.92 (t, ^3J = 6.6 Hz, 3H, f-H) ppm; ^{13}C NMR ($CDCl_3$, 150 MHz) 202.9, 144.1, 137.0, 130.8, 128.8, 127.4, 124.0, 124.0, 122.9, 114.3, 104.9, 47.3, 39.0, 31.6, 29.0, 24.8, 23.1, 14.1, 11.0 ppm; HRMS (ESI) m/z: $[M + H]^+$ Calculated for $C_{20}H_{28}NO^+$: 298.2165; Found: 298.2179

Compound **3a** was obtained as light orange solid in 30% yield. ^{1}H NMR (600 MHz, $CDCl_3$) δ

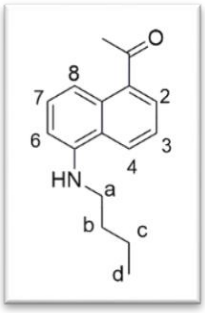

= 7.99 (d, ^3J = 9.0 Hz, 1H, 8-H), 7.90 (d, ^3J = 8.4 Hz, 1H, 2-H), 7.81 (d, ^3J = 7.2 Hz, 1H, 4-H), 7.46-7.42 (m, 2H, [3,7]-H), 6.67 (d, ^3J = 7.8 Hz, 1H, 6-H), 4.31 (s, 1H, N-H), 3.27 (t, ^3J = 7.2 Hz, 2H, a-H), 2.72 (s, 3H, acetyl-H), 1.79-1.74 (m, 2H, b-H), 1.55-1.51 (m, 2H, c-H), 1.01 (t, ^3J =

7.2 Hz, 3H, d-H) ppm; ^{13}C NMR ($CDCl_3$, 150 MHz) 202.8, 143.9, 136.9, 130.8, 128.7, 127.4, 124.1, 123.9, 122.9, 114.5, 105.1, 44.0, 31.5, 30.5, 20.5, 14.0 ppm; HRMS (ESI) m/z: $[M + H]^+$ Calculated for $C_{16}H_{20}NO^+$: 242.1539; Found: 242.1566.

Compound **4a** was obtained as light orange solid in 52% yield. ^{1}H NMR (600 MHz, $CDCl_3$) δ

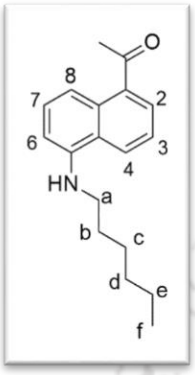

= 7.99 (d, ^3J = 8.4 Hz, 1H, 8-H), 7.90 (d, ^3J = 9.0 Hz, 1H, 2-H), 7.81 (d, ^3J = 7.2 Hz, 1H, 4-H), 7.46-7.42 (m, 2H, [3,7]-H), 6.67 (d, ^3J = 7.8 Hz, 1H, 6-H), 4.31 (s, 1H, N-H), 3.26 (t, ^3J = 6.6 Hz, 2H, a-H), 2.72 (s, 3H, acetyl-H), 1.80- 1.75 (m, 2H, b-H), 1.52-1.47 (m, 2H, c-H), 1.40-1.32 (m, 4H, [d,e]-H), 0.92 (t, ^3J = 6.6 Hz, 3H, f-H) ppm; ^{13}C NMR ($CDCl_3$, 150 MHz) 202.8, 143.9, 136.9, 130.8, 128.7, 127.4, 124.1, 123.9, 122.9, 114.5, 105.0, 44.3, 31.7, 30.5, 29.4, 27.0, 22.6, 14.0 ppm; HRMS (ESI) m/z: $[M + H]^+$ Calculated for $C_{18}H_{24}NO^+$: 270.1852; Found: 270.1855.

Compound **5a** was obtained as light orange solid in 64% yield. ^{1}H NMR (400 MHz, $CDCl_3$) δ

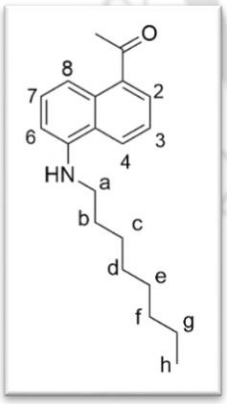

= 7.99 (d, ^3J = 8.4 Hz, 1H, 8-H), 7.90 (d, ^3J = 8.4 Hz, 1H, 2-H), 7.81 (d, ^3J = 7.2 Hz, 1H, 4-H), 7.47-7.41 (m, 2H, [3,7]-H), 6.67 (d, 3J = 8.0 Hz, 1H, 6H), 4.30 (s, 1H, N-H), 3.26 (t, ^3J = 6.8 Hz, 2H, a-H), 2.72 (s, 3H, acetyl-H), 1.80-1.74 (m, 2H, b-H), 1.53-1.45 (m, 2H, c-H), 1.40-1.24 (m, 8H, [d, e, f, g]-H), 0.89 (t, ^3J = 6.8 Hz, 3H, h-H) ppm; ^{13}C NMR ($CDCl_3$, 150 MHz) : 202.7, 143.9, 136.7, 130.8, 128.7, 127.4, 124.1, 123.9, 122.8, 114.3, 104.9, 44.2, 31.8, 30.4, 29.4, 29.3, 29.2, 27.3, 22.6, 14.0 ppm. HRMS (ESI) m/z: $[M + H]^+$ Calculated for $C_{20}H_{28}NO^+$: 298.2165; Found: 298.2169.

Compound **6a** was obtained as light orange solid in 48% yield. ^{1}H NMR (400 MHz, $CDCl_3$) δ

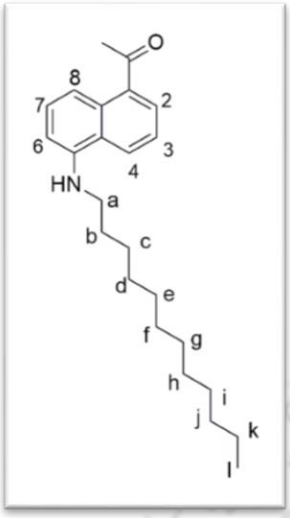

= 7.99 (d, ^{3}J = 8.8 Hz, 1H, 8-H), 7.90 (d, ^{3}J = 8.4 Hz, 1H, 2-H), 7.81 (d, 3*J* = 7.0 Hz, 1H, 4-H), 7.47-7.41 (m, 2H, [3,7]-H), 6.67 (d, ^{3}J = 7.6 Hz, 1H, 6H), 4.30 (s, 1H, N-H), 3.26 (t, ^{3}J = 7.0 Hz, 2H, a-H), 2.72 (s, 3H, acetyl-H), 1.81-1.74 (m, 2H, b-H), 1.53-1.45 (m, 2H, c-H), 1.41-1.21 (m, 16H, [d, e, f, g, h, i, j, k]-H), 0.88 (t, ^{3}J = 6.8 Hz, 3H, l-H) ppm. ^{13}C NMR ($CDCl_3$, 150 MHz): 202.9, 144.0, 136.9, 130.9, 128.8, 127.5, 124.2, 124.0, 122.9, 114.5, 105.1, 44.3, 31.9, 30.4, 29.6 (4C), 29.5, 29.3 (2C), 27.3, 22.6, 14.1 ppm. HRMS (ESI) m/z: $[M + H]^+$ Calculated for $C_{24}H_{36}NO^+$: 354.2791; Found: 354.2796.

❖ **7.2.3.2 Synthesis of nr (2r-6r)**

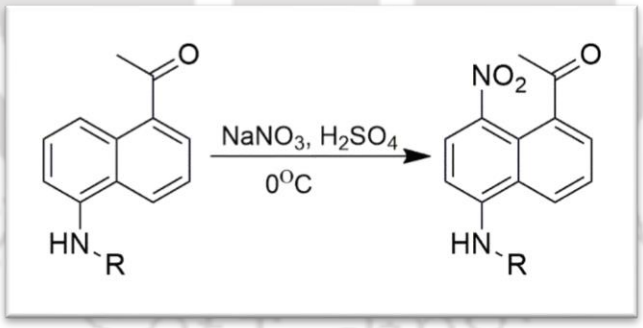

General method (**nr**): The respective 5-alkylamino-1-acetylnaphthalene (1.00 mmol) was dissolved in 5 mL of concentrated sulphuric acid and the solution was placed inside an ice bath. To the cold solution, was added $NaNO_3$ (1.00 mmol) in portion-wise. The course of the reaction was monitored using thin-layer chromatography (TLC). After 20 minutes, as evidenced from TLC, the reaction was quenched by addition of 50 mL of water. The crude

product was extracted by DCM (3×20 mL). The combined organic solvent was dried over Na_2SO_4, filtered, and evaporated to dryness under reduced pressure. The desired product nr was purified using column chromatography with EtOAc/Hexane (v/v) (5/95 to 25/75) as eluent.

Compound **2r** was obtained as brownish-yellow solid in 57 % yield. ^{1}H NMR (500 MHz, $CDCl_3$) δ = 8.22 (d, ^3J = 9.0 Hz, 1H, 7-H), 7.85 (d, ^3J = 8.0 Hz, 1H, 2-H), 7.81 (d, ^3J = 7.0 Hz, 1H, 4-H), 7.53 (dd, ^3J = 8.0 Hz, ^3J = 7.5 Hz, 1H, 3-H), 6.51 (d, ^3J = 9.0 Hz, 1H, 6-H), 5.21 (s, 1H, N H), 3.29–3.27 (m, 2H, a-H), 2.71 (s, 3H, acetyl-H), 1.78-1.74 (m, 1H, b-H), 1.53-1.47 (m, 2H, g-H), 1.46-1.41 (m, 2H, c-H), 1.38-1.32 (m, 4H, [d,e]-H), 0.97 (t, ^3J = 7.5 Hz, 3H, h-H), 0.92 (t, ^3J = 6.5 Hz, 3H, f-H) ppm; ^{13}C NMR ($CDCl_3$, 150 MHz) δ 200.9, 149.3, 138.3, 135.8, 129.4, 127.7, 124.7, 123.6, 122.9, 122.3, 101.6, 47.1, 38.7, 31.4, 28.9, 28.6, 24.6, 23.0, 14.0, 10.9 ppm; HRMS (ESI) m/z: $[M+H]^+$ Calculated for $C_{20}H_{27}N_2O_3^+$: 343.2016; Found: 343.2038; IR ν 3409, 2957, 2925, 2856, 1683, 1575, 1543, 1494, 1464, 1355, 1300, 1277, 1194, 1093, 1053, 990, 809, 756 cm^{-1}.

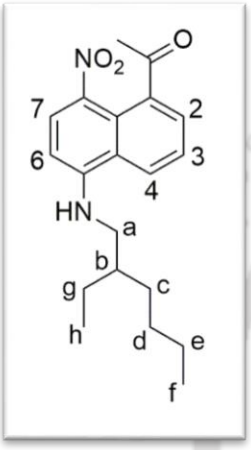

Compound **3r** was obtained as brownish-yellow solid in 54 % yield. ^{1}H NMR (600 MHz, $CDCl_3$) δ = 8.21 (d, ^3J = 8.4 Hz, 1H, 7-H), 7.85 (d, ^3J = 8.4 Hz, 1H, 2-H), 7.80 (d, ^3J = 7.2 Hz, 1H, 4-H), 7.51 (dd, ^3J = 8.4 Hz, ^3J = 7.2 Hz, 1H, 3-H), 6.51 (d, ^3J = 9.0 Hz, 1H, 6-H), 5.18 (s, 1H, N-H), 3.38–3.35 (m, 2H, a-H), 2.71 (s, 3 H, acetyl-H), 1.81-1.76 (m, 2H, b-H), 1.54–1.50 (m, 2H, c-H), 1.02 (t, ^3J = 7.2 Hz, 3H, d-H) ppm; ^{13}C NMR ($CDCl_3$, 150 MHz) δ 200.9, 149.1, 138.3, 136.0, 129.4, 127.7, 124.7, 123.5, 122.9, 122.4, 101.7, 43.7, 30.9, 28.6, 20.3, 13.8 ppm; HRMS (ESI) m/z: $[M+H]^+$ Calculated for

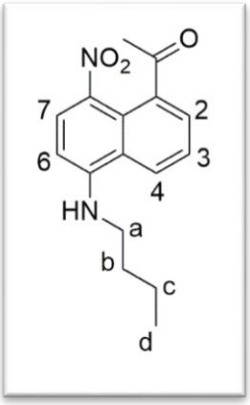

$C_{16}H_{19}N_2O_3^+$: 287.1390; Found: 287.1410; IR ν 3405, 2957, 2925, 2855, 1683, 1574, 1542, 1488, 1355, 1277, 1193, 1092, 1051, 975, 809, 755 cm^{-1}.

Compound **4r** was obtained as brownish-yellow solid in 54 % yield. ^1H NMR (600 MHz, $CDCl_3$) δ = 8.22 (d, ^3J = 8.8 Hz, 1H, 7-H), 7.87 (d, ^3J = 8.4 Hz, 1H, 2-H), 7.81 (d, ^3J = 7.2 Hz, 1H, 4-H), 7.53 (dd, ^3J = 8.4 Hz, ^3J = 7.2 Hz, 1H, 3-H), 6.52 (d, ^3J = 8.8 Hz, 1H, 6-H), 5.16 (s, 1H, N-H), 3.38–3.35 (m, 2H, a-H), 2.71 (s, 3 H, acetyl-H), 1.81–1.78 (m, 2H, b-H), 1.51–1.47 (m, 2H, c-H), 1.40–1.33 (m, 4H, [d,e]-H), 0.92 (t, ^3J = 7.2 Hz, 3H, f-H) ppm; ^{13}C NMR ($CDCl_3$, 150 MHz) δ 200.9, 149.1, 138.3, 136.0, 129.4, 127.7, 124.7, 123.5, 122.9, 122.4, 101.7, 44.0, 31.5, 28.8, 28.6, 26.8, 22.6, 14.0 ppm; HRMS (ESI) m/z: $[M+H]^+$ Calculated for $C_{18}H_{23}N_2O_3^+$: 315.1703; Found: 315.1705; IR ν 3405, 2953, 2925, 2855, 1682, 1575, 1542, 1489, 1355, 1277, 1193, 1093, 1058, 990, 809, 755 cm^{-1}.

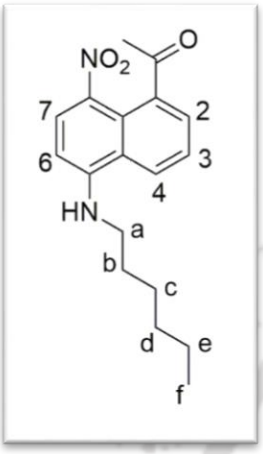

- Compound **5r** was obtained as brownish-yellow solid in 59 % yield. ^1H NMR (400 MHz, $CDCl_3$) δ = 8.21 (d, *J* = 8.8 Hz, 1H, 7-H), 7.85 (d, ^3J = 8.4 Hz, 1H, 2-H), 7.79 (d, ^3J = 7.2 Hz, 1H, 4-H), 7.50 (dd, ^3J = 7.2 Hz, ^3J = 8.4 Hz, 1H, 3-H), 6.50 (d, ^3J = 8.8 Hz, 1H, 6-H), 5.19 (s, 1H, N H), 3.37–3.32 (m, 2H, a-H), 2.71 (s, 3 H, acetyl-H), 1.83–1.76 (m, 2H, b-H), 1.52–1.45 (m, 2H, c-H),1.40–1.26 (m, 8H, [d, e, f, g]-H), 0.89 (t, ^3J = 6.8 Hz, 3H, h-H) ppm; ^{13}C NMR ($CDCl_3$, 150 MHz) δ 201.3, 149.3, 137.7, 135.2, 129.4, 127.5, 124.4, 123.3, 122.8, 122.7, 101.5, 43.9,

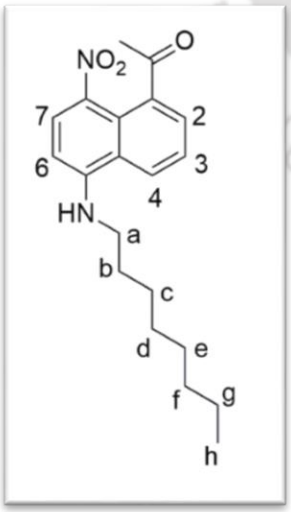

31.7, 29.2 (2 C), 28.6 (2 C), 27.1 22.6, 14.0 ppm; HRMS (ESI) m/z: $[M+H]^+$ Calculated for $C_{20}H_{27}N_2O_3^+$: 343.2016; Found: 343.2019; IR ν 3401, 2953, 2924, 2853, 1682, 1574, 1542, 1487, 1355, 1271, 1193, 1093, 1058, 989, 808, 755 cm^{-1}.

Compound **6r** was obtained as brownish-yellow solid in 44 % yield. ^1H NMR (400 MHz, CDCl) δ = 8.21 (d, ^3J = 8.8 Hz, 1H, 7-H), 7.86 (d, ^3J = 8.4 Hz, 1H, 2-H), 7.80 (d, ^3J = 7.2 Hz, 1H, 4-H), 7.52 (dd, ^3J = 7.2 Hz, ^3J = 8.4 Hz, 1H, 3-H), 6.51 (d, ^3J = 8.8 Hz, 1H, 6-H), 5.18 (s, 1H, N-H), 3.38–3.33 (m, 2H, a-H), 2.71 (s, 3 H, acetyl-H), 1.83–1.76 (m, 2H, b-H), 1.52-1.44 (m, 2H, c-H), 1.42–1.20 (m, 16H, [d, e, f, g, h, i, j, k]-H), 0.88 (t, ^3J = 6.6 Hz, 3H, l-H) ppm; ^{13}C NMR ($CDCl_3$, 150 MHz) δ 201.3, 149.5, 137.5, 134.8, 129.3, 127.4, 124.2, 123.2, 122.9, 122.6, 101.3, 43.9, 31.8, 29.6, 29.5 (3 C), 29.3 (2 C), 28.5 (2 C), 27.1, 22.6, 14.0 ppm. HRMS (ESI) m/z: $[M+H]^+$ Calculated for $C_{24}H_{35}N_2O_3^+$: 399.2642; Found: 399.2641; IR ν 3406, 2956, 2922, 2852, 1682, 1574, 1542, 1489, 1354, 1277, 1193, 1093, 1057, 989, 808, 755 cm^{-1}.

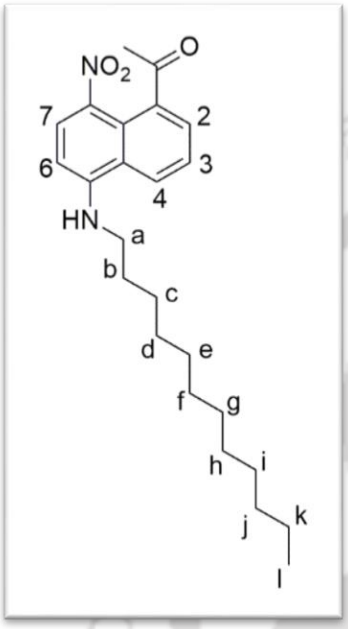

❖ 7.2.3.3 Synthesis of np (2p-6p)

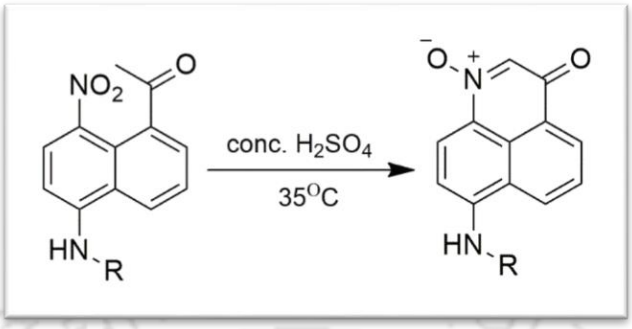

In a typical run, 25.0 mg of **nr** was taken in 1.5 mL of concentrated H_2SO_4 and stirred at 35 °C for 2.5 h. At the end of the stipulated time, the reaction was quenched using water (50 mL). The crude product was extracted using dichloromethane (3 x 15 mL). The combined organic layer was dried over anhydrous Na_2SO_4, filtered, and concentrated under reduced pressure to receive crude product. The aldonitrone **np** was purified using preparative TLC with EtOAc/DCM (3: 7 v/v) as eluent.

Compound **2p** was obtained as dark purple solid in 27% yield. ^{1}H NMR (600 MHz, $CDCl_3$)

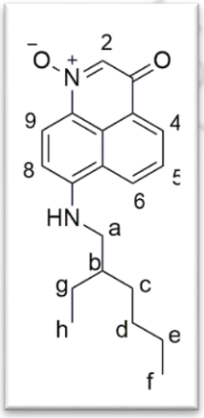

δ=8.60 (d, ^3J=7.2 Hz, 1H, 4-H), 8.53 (d, ^3J=9.0 Hz, 1H, 9-H), 8.16 (d, ^3J=8.0 Hz, 1H, 6-H), 7.83 (s, 1H, 2-H), 7.73 (dd, 3J=8.0 Hz, ^3J=7.2 Hz, 1H, 5-H), 6.68 (d, ^3J=9.0 Hz, 1H, 8-H), 5.51 (s, 1H, N H), 3.36–3.34 (m, 2H, a-H), 1.82–1.76 (m, 1H, b-H), 1.55–1.50 (m, 2H, g-H), 1.49–1.41 (m, 2H, c-H), 1.40–1.32 (m, 4H, [d,e]-H), 0.99 (t, ^3J=7.2 Hz, 3H, h-H), 0.93 (t, ^3J=7.2 Hz, 3H, f-H) ppm; ^{13}C NMR ($CDCl_3$, 150 MHz) δ 177.6, 150.2, 132.3, 130.1, 128.0, 127.2, 126.9, 126.8, 125.8, 124.4, 120.7, 104.0, 47.0, 38.9, 31.4, 28.9, 24.6, 23.0, 14.0, 10.9 ppm; HRMS (ESI) m/z: $[M+H]^+$ Calculated for $C_{20}H_{25}N_2O_2^+$: 325.1911; Found: 325.1893; IR ν 3312, 2957, 2925, 2857, 1704, 1630, 1567, 1543, 1453,

1399, 1357, 1277, 1202, 1138, 809, 763, 704 cm ^{1}; mp 145 °C; UV-vis ($CHCl_3$) λ_{max}/nm ($\varepsilon/M^{-1}cm^{-1}$) 551 (12500).

Compound **3p** was obtained as purple solid in 17 % yield. ^{1}H NMR (600 MHz, $CDCl_3$) δ

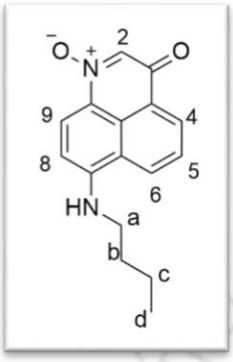

8.59 (d, ^{3}J = 7.2 Hz, 1H, 4-H), 8.53 (d, ^{3}J = 8.8 Hz, 1H, 9-H), 8.17 (d, ^{3}J = 8.0 Hz, 1H, 6-H), 7.83 (s, 1H, 2-H), 7.71 (dd, ^{3}J = 8.0 Hz, ^{3}J = 7.2 Hz, 1H, 5-H), 6.67 (d, ^{3}J = 8.8 Hz, 1H, 8-H), 5.49 (s, 1H, N-H), 3.46–3.43 (m, 2H, a-H), 1.84–1.80 (m, 2H, b-H), 1.55–1.52 (m, 2H, c-H), 1.04 (t, ^{3}J = 7.2 Hz, 3H, d-H) ppm; ^{13}C NMR (150 MHz, $CDCl_3$) δ 177.6, 150.1, 132.2, 130.1, 128.0, 127.1, 127.1, 126.8, 125.7, 124.3, 120.5, 104.0, 43.6, 30.9, 20.3, 13.8 ppm; HRMS (ESI) m/z: $[M+H]^+$ Calculated for $C_{16}H_{17}N_2O_2^+$: 269.1285; Found: 269.1291; IR ν 3313, 2956, 2927, 2870, 1738, 1629, 1565, 1542, 1455, 1398, 1357, 1278, 1203, 1134, 810, 758, 704 cm^{-1}; mp 160 °C; UV-vis ($CHCl_3$) λ_{max}/nm ($\varepsilon/M^{-1}cm^{-1}$) 549 (13200).

Compound **4p** was obtained as dark purple solid in 18 % yield. ^{1}H NMR (600 MHz, $CDCl_3$)

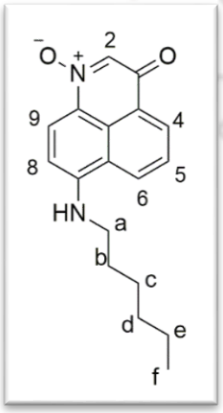

δ 8.59 (d, ^{3}J = 7.2 Hz, 1H, 4-H), 8.52 (d, ^{3}J = 9.0 Hz, 1H, 9-H), 8.18 (d, ^{3}J = 7.8 Hz, 1H, 6-H), 7.83 (s, 1H, 2-H), 7.71 (dd, ^{3}J = 7.8 Hz, ^{3}J = 7.2 Hz, 1H, 5-H), 6.67 (d, ^{3}J = 9.0 Hz, 1H, 8-H), 5.50 (s, 1H, N H), 3.45–3.42 (m, 2H, a-H), 1.85–1.81 (m, 2H, b-H), 1.53–1.49 (m, 2H, c-H), 1.42-1.35 (m, 4H, [d,e]-H), 0.93 (t, ^{3}J = 7.2 Hz, 3H, f-H) ppm; ^{13}C NMR (150 MHz, $CDCl_3$) δ 177.6, 150.1, 132.3, 130.1, 128.1, 127.1, 127.1, 126.8, 125.8, 124.3, 120.5, 104.0, 43.9, 31.5, 28.6, 26.8, 22.6, 14.0 ppm; HRMS (ESI) m/z: $[M+H]^+$ Calculated for $C_{18}H_{21}N_2O_2^+$: 297.1603; Found: 297.1604; IR ν 3316, 2954,

2922, 2853, 1736, 1630, 1568, 1543, 1456, 1358, 1278, 1208, 1135, 809, 762, 704 $cm^{—1}$; mp 150 °C; UV-vis ($CHCl_3$) λ_{max}/nm ($\varepsilon/M^{-1}cm^{-1}$) 549 (12300).

Compound **5p** was obtained as dark purple solid in 26 % yield. ^{1}H NMR (400 MHz, $CDCl_3$)

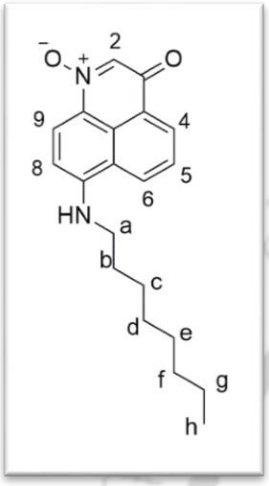

δ= 8.59 (d, ^3J = 7.8 Hz, 1H, 4-H), 8.52 (d, ^3J = 8.8 Hz, 1H, 9-H), 8.18 (d, ^3J = 8.2 Hz, 1H, 6-H), 7.82 (s, 1H, 2-H), 7.70 (dd, ^3J = 8.2 Hz, ^3J = 7.8 Hz, 1H, 5-H), 6.66 (d, ^3J = 8.8 Hz, 1H, 8-H), 5.51 (s, 1H, N—H), 3.46-3.41 (m, 2H, a-H), 1.86-1.79 (m, 2H, b-H), 1.54-1.47 (m, 2H, c-H), 1.43-1.24 (m, 8H, [d, e, f, g]-H), 0.89 (t, ^3J = 6.8 Hz, 3H, h-H), ppm; ^{13}C NMR ($CDCl_3$, 150 MHz) δ 177.6, 150.2, 132.2, 130.1, 128.1, 127.3, 127.1, 126.8, 125.7, 124.3, 120.6, 104.0, 44.0, 31.8, 29.3, 29.2, 28.9, 27.2, 22.6, 14.1 ppm. HRMS (ESI) m/z: $[M+H]^+$ Calculated for $C_{20}H_{25}N_2O_2^+$: 325.1911; Found: 325.1914; IR ν 3294, 2953, 2915, 2850, 1746, 1632, 1567, 1536, 1462, 1399, 1363, 1287, 1221, 1134, 801, 768, 707; mp 152 °C; °C; UV-vis ($CHCl_3$) λ_{max}/nm ($\varepsilon/ M^{-1}cm^{-1}$) 550 (13800).

❖ 7.2.3.4 Synthesis of 2p1′

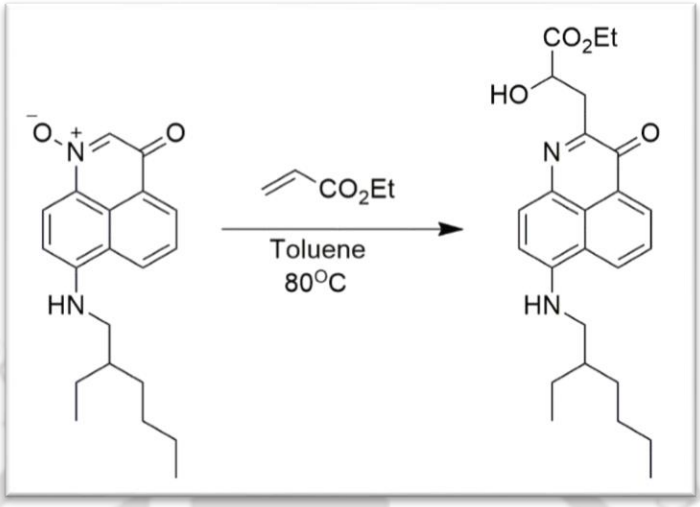

Aldonitrone **2p** (12.0 mg, 37.0 μmol) was loaded into a 10 mL round-bottomed flask. After addition of 4 mL of toluene and ethyl acrylate (47.0 μL, 443 μmol), the suspension was stirred at 80 °C for 3 h. The solvent was then evaporated and the crude residue was purified by column chromatography. After washing with hexane to remove the residual ethyl acrylate, the product was collected using EtOAc/DCM as eluent (1/3 v/v). Finally, the pure product was isolated through preparative TLC.

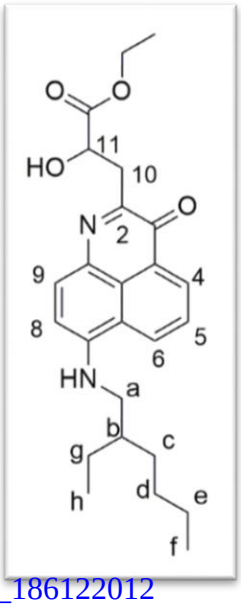

The product was obtained as a dark bluish-purple sticky solid. Yield 38 %; ^{1}H NMR (500 MHz, $CDCl_3$) δ 8.68 (d, ^{3}J= 7.5 Hz, 1H, 4-H), 8.23 (d, ^{3}J=8.0 Hz, 1H, 6-H), 7.85 (d, ^{3}J=8.5 Hz, 1H, 9-H), 7.75 (dd, ^{3}J=8.0 Hz, ^{3}J=7.5 Hz, 1H, 5 -H), 6.61 (d, ^{3}J=8.5 Hz, 1H, 8-H), 5.47 (s, 1H, N H), 4.76 (dd, ^{3}J=7.0 Hz, ^{3}J=4.0 Hz, 1H, 11- H), 4.22 (q, ^{3}J=7.0 Hz, 2H, l2-H), 3.45 (dd, ^{2}J=16.5 Hz, ^{3}J=4.0 Hz, 1H, 10-H), 3.37 (dd, ^{2}J=16.5 Hz, ^{3}J=7.0 Hz, 1H, 10-H), 3.34–3.32 (m, 2H, a-H), 1.81–1.76 (m, 1H, b-H), 1.55 -1.49 (m, 2H, g-H), 1.48–1.43 (m, 2H, c-H), 1.40–1.33 (m, 4H, [d,e]-H), 1.24 (t, ^{3}J=7.0

Hz, 3H, l3-H), 0.99 (t, ^{3}J=7.0 Hz, 3H, h-H), 0.92 (t, ^{3}J=7.0 Hz, 3H, f-H) ppm; ^{13}C NMR ($CDCl_3$, 150 MHz) 177.3, 174.0, 156.3, 149.0, 136.6, 131.3, 128.2, 127.7, 127.5, 126.0, 124.3, 122.3, 104.6, 69.6, 61.2, 47.0, 38.9, 35.9, 31.4, 28.9, 24.7, 23.0, 14.2, 14.0, 10.9 ppm; HRMS (ESI) m/z: $[M+H]^+$ Calculated for $C_{25}H_{33}N_2O_4^+$: 425.2435; Found: 425.2436; IR ν 3363, 2958, 2925, 2855, 1738, 1631, 1572, 1529, 1439, 1403, 1378, 1338, 1251, 1201, 1099, 770 cm^{-1}; UV-vis ($CHCl_3$) λ_{max}/nm ($\varepsilon/M^{-1}cm^{-1}$) 561 (11300).

❖ 7.2.3.5 Synthesis of 1p

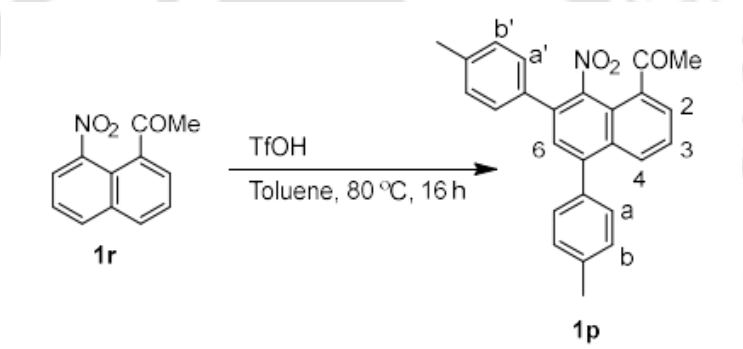

Compound **1r** (100 mg, 465 µmol) was loaded into a 10 mL round-bottomed flask with 0.5 mL of toluene, and the mixture was heated up to 80 °C. To the hot stirring mixture, triflic acid (20.0 µL) was added, and the resultant mixture was allowed to run at the same temperature for 16 h. The reaction mixture was then cooled down to room temperature, and 100 mL of DCM was added to the mixture. The organic layer was washed with water (75 mL x 3), separated, and suspended over anhydrous Na_2SO_4. After filtration, the combined organic layer was concentrated under reduced pressure to provide crude mixture. Finally, the product **1p** was purified through column chromatography with EtOAc/Hexane (25/75 v/v) as eluent. Compound **1p** was obtained as yellowish-brown solid. Yield = 17 %; 1H NMR (600 MHz, $CDCl_3$) δ 8.08 (d, ^{3}J = 7.8 Hz, 1H, 2-H), 7.98 (d, ^{3}J = 7.8 Hz, 2H), 7.94 (d, ^{3}J = 6.6 Hz, 1H,

4- H), 7.75 (s, 1H, 6-H), 7.64 (d, 3*J* = 7.8 Hz, 3*J* = 6.6 Hz, 1H, 3-H), 7.53 (d, 3*J* = 7.8 Hz, 2H), 7.37-7.33 (m, 4H), 2.85 (s, 3H, acetyl-H), 2.47 (s, 3H, methyl-H), 2.43 (s, 3H, methyl-H) ppm.

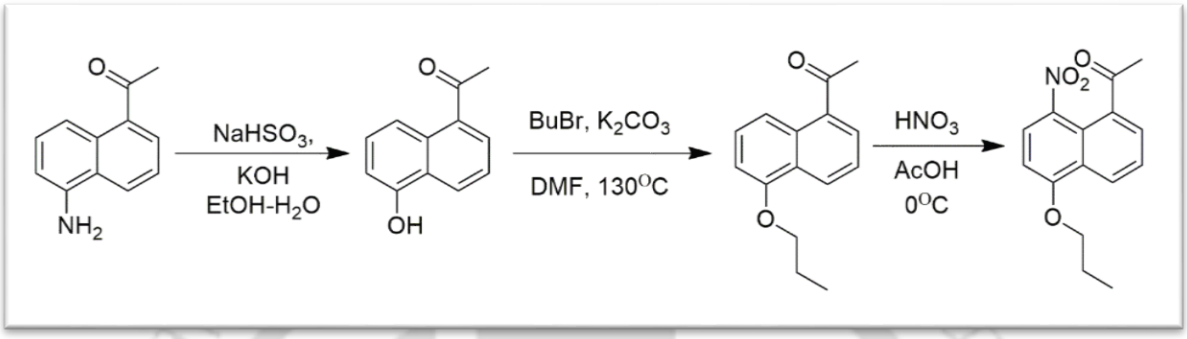

❖ **7.2.3.6 Synthesis of 7**

To a solution of **2** (300 mg, 1.62 mmol) in 3 mL of ethanol, water (6 mL) was added slowly

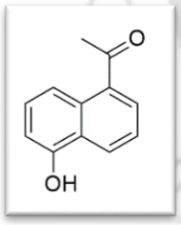

to produce a suspension. A saturated $NaHSO_3$ solution (15 mL) was added into the mixture. After refluxing for 24 h, a solution (8 mL) of 6 M KOH was added to the stirring mixture. The hot mixture was stirred for another 2 h. Concentrated HCl (9 mL) was added in a dropwise fashion until the effervescence was complete. The mixture was then cooled down to room temperature, and filtered. The greenish residue was washed three times with water and used for next step without doing further purification. Yield 30 %. ^{1}H NMR (500 MHz, CDCl3) δ 8.44 (d, ^3J = 8.0 Hz, 1H), 8.26 (d, ^3J = 8.0 Hz, 1H), 7.93 (d, ^3J = 7.0 Hz, 1H), 7.50 (dd, 3*J* = 7.0 Hz, ^3J = 7.0 Hz, 1H), 7.41 (dd, ^3J = 8.0 Hz, 3*J* = 8.0 Hz 1H), 6.88 (d, ^3J = 7.0 Hz, 1H), 5.56 (s, 1H, OH), 2.74 (s, 3H, COMe)

❖ 7.2.3.7 Synthesis of 7a

Compound **7** (50.0 mg, 206 µmol) was dissolved in 7 mL of DMF in a 25 mL round-

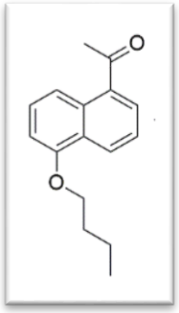

bottomed flask. To the solution, was added 190 mg (1.39 mmol) of K_2CO_3, and 120 µL (1.39 mmol) of *n*-bromobutane. The resulting mixture was then stirred at 130°C for overnight. The reaction was quenched by addition of 50 mL of water. The crude mixture was extracted with DCM (3 X 20 mL), dried Na_2SO_4, and concentrated under reduced pressure to provide a sticky residue which was purified through column chromatography (hexane to 1:9 EtOAc:hexane) to afford a sticky off-white semi-solid. Yield 76 %. ^{1}H NMR (500 MHz, $CDCl_3$) δ 8.52 (d, ^3J = 8.5 Hz, 1H), 8.23 (d, ^3J = 8.5 Hz, 1H), 7.92 (d, ^3J = 7.0 Hz, 1H), 7.45-7.46 (m, 2H), 6.87 (d, ^3J = 8.0 Hz, 1H), 4.15 (t, ^3J = 6.5 Hz, 2H, OCH_2), 2.73 (s, 3H, COMe), 1.95-1.89 (m, 2H,-CH_2-), 1.64-1.58 (m, 2H, -CH_2-), 1.03 (t, ^3J = 7.0 Hz, 3H, - CH_3).

❖ 7.2.3.8 Synthesis of 7r

To a stirred solution of compound **7a** (20.0 mg, 82.5 µmol) in 350 µL of glacial acetic

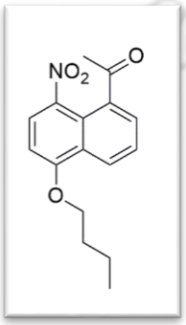

acid was added 29 µL of concentrated HNO_3 at 0-5°C. The resultant mixture was stirred for additional 30 minutes at same temperature, followed by stirring at room temperature for 5 h. The reaction mixture was quenched by ice-water (20 mL) and extracted with DCM (3 x 30 mL). The combined extracts were washed with saturated aqueous $NaHCO_3$ to reach neutralization. Purification was achieved using column chromatography (1:3 EtOAc:Hexane). **7r** was obtained as sticky solid in 33% yield.

^{1}H NMR (600 MHz, CDCl3) δ 8.48 (d, ^3J = 8.4 Hz, 1H), 8.14 (d, ^3J = 8.4 Hz, 1H),

7.88 (d, ^{3}J = 7.2 Hz, 1H), 7.60 (dd, ^{3}J = 8.4 Hz, ^{3}J = 7.2 Hz, 1H), 6.83 (d, ^{3}J = 8.4 Hz, 1H), 4.24 (t, ^{3}J = 6.0 Hz, 2H, OCH2), 2.73 (s, 3H, COMe), 1.96-1.93 (m, 2H, -CH2-), 1.63-1.59 (m, 2H, -CH_2), 1.04 (t, ^{3}J = 7.2 Hz, 3H, -CH_3).

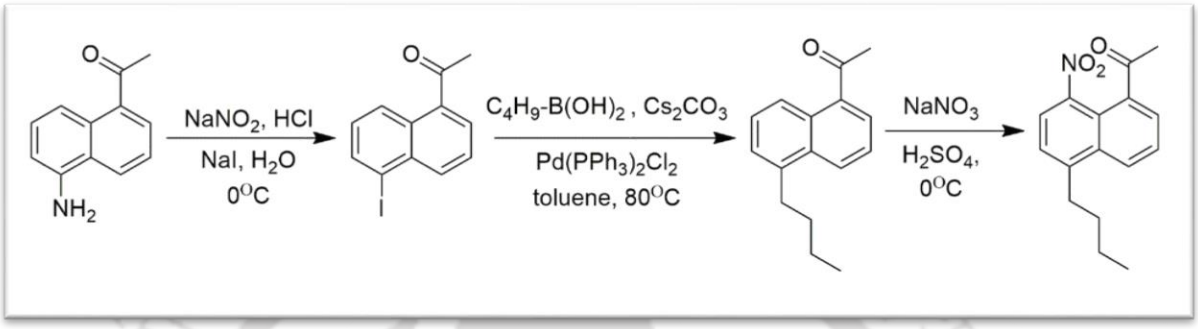

❖ **7.2.3.9 Synthesis of 8**

Concentrated HCl (10 mL) and **2 (**350 mg, 1.26 mmol) were loaded into a 50 mL round-

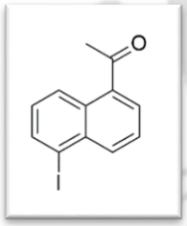

bottomed flask and the mixture was sonicated and sonicated for 15 min. After cooling down the solution in an ice-bath, 1 mL of aqueous $NaNO_2$ (131 mg, 1.89 mmol) solution was addedto the mixture under constant stirring. After 20 min, 2.5 mL of aqueous NaI (471 mg, 3.15 mmol) was added drop-wise. The reaction mixture was stirred for additional 30 min at same reaction condition. After quenching the mixture with deionised water (50 mL), the organic part was extracted with DCM (30 mL). The organic layer was washed with $Na_2S_2O_3$ solution (2 x 20 mL), dried over anhydrous Na_2SO_4, filtrated, and then concentrated under reduced pressure. The crude residue was purified using column chromatography (10% EtOAc/Hexane) to obtain compound **8** in 36 % yield. ^{1}H NMR (400 MHz, CDCl3) δ 8.68 (d, ^{3}J = 8.4 Hz, 1H), 8.33 (d, ^{3}J = 8.4 Hz, 1H), 8.15 (d, ^{3}J =

7.2 Hz, 1H), 7.94 (d, ^3J = 7.0 Hz, 1H), 7.58 (dd, ^3J = 8.4 Hz, ^3J = 7.2 1H), 7.27 (dd, ^3J = 8.4 Hz, ^3J = 7.0 1H), 2.75 (s, 3H) ppm. HRMS (ESI) m/z: $[M + H]^+$ Calculated for $[C_{12}H_9IO+H]^+$: 296.9771; found: 296.9772.

❖ 7.2.3.10 Synthesis of 8a

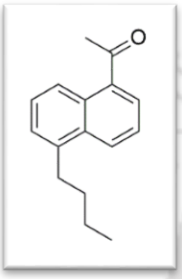

Under an inert-condition, 160 mg (540 µmol) of compound **8**, 22.0 mg of $Pd(dppf)Cl_2$ (5 mol %), 528 (1.62 mmol) mg of Cs_2CO_3 and 82.6 mg (810 µmol) butylboronic acid were loaded into a Schlenk flask. After addition of 5 mL of argon-purged toluene, the flask was tightly closed, and dipped into a preheated bath at 80°C. The mixture was stirred at the same condition for 5 h. After cooling down to room temperature, the reaction mixture was diluted with 10 mL of DCM and filtered. After evaporation of the solvents, the crude product was purified using column chromatography (10% EtOAc/Hexane). Yield 72%. ^{1}H NMR (400 MHz, CDCl3) δ 8.48 (d, ^3J = 8.6 Hz, 1H), 8.23 (d, ^3J = 8.6 Hz,1H), 7.87 (d, ^3J = 7.0 Hz, 1H) 7.54-7.48 (m, 2H), 7.38 (d, ^3J = 7.0 Hz, 1H), 3.08 (t, ^3J = 7.8 Hz, 2H), 2.74 (s, 3H), 1.76-1.68 (m, 2H), 1.50-1.40 (m, 2H), 0.97 (t, ^3J = 7.4 Hz, 3H) ppm. HRMS (ESI) m/z: $[M + H]^+$ Calculated for $[C_{16}H_{18}O+H]^+$: 227.143; found: 227.1431.

❖ **7.2.3.11 Synthesis of 8r**

In an ice-bath, compound 8a (65.0 mg, 290 µmol) and 2 mL of concentrated H_2SO_4 were

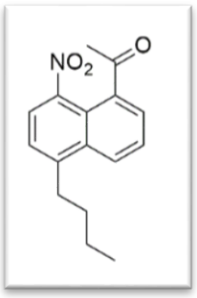

loaded together into a 25 mL round-bottomed flask and allowed to stir for complete mixing and subsequent cooling. To this cold stirring mixture, solid $NaNO_3$ (29.0 mg of 340 µmol) was added over 5 minutes. The reaction mixture was stirred at same condition and the progress was monitored using TLC. After quenching with cold deionised water (25 mL), the organic mixture was separtated through extraction with DCM (3 x 20 mL). The organic layer was dried over anhydrous Na_2SO_4, filtered and concentrated under reduced pressure. The crude residue was purified using column chromatography (25% EtOAc/Hexane) to obtain the desired product. Yield 32%. ^{1}H NMR (600 MHz, CDCl3) δ 8.67 (d, ^3J = 9.4 Hz, 1H), 8.36 (d, ^3J = 8.4 Hz, 1H), 8.05 (d, ^3J = 7.2 Hz, 1H), 7.83 (d, ^3J = 9.4 Hz, 1H), 7.70 (dd, ^3J = 7.2 Hz, ^3J = 8.4 Hz, 1H), 3.19 (t, ^3J = 8.2 Hz, 2H), 2.77 (s, 3H), 1.80-1.75 (m, 2H), 1.56-1.52 (m, 2H), 1.01 (t, ^3J = 7.4 Hz, 3H). HRMS (ESI) m/z: $[M + H]^+$ Calculated for $[C_{16}H_{17}NO_3 + H]^+$: 272.1281; found: 272.1278.

- **7.3 NMR spectra**
- **7.3.1 Chapter 1**

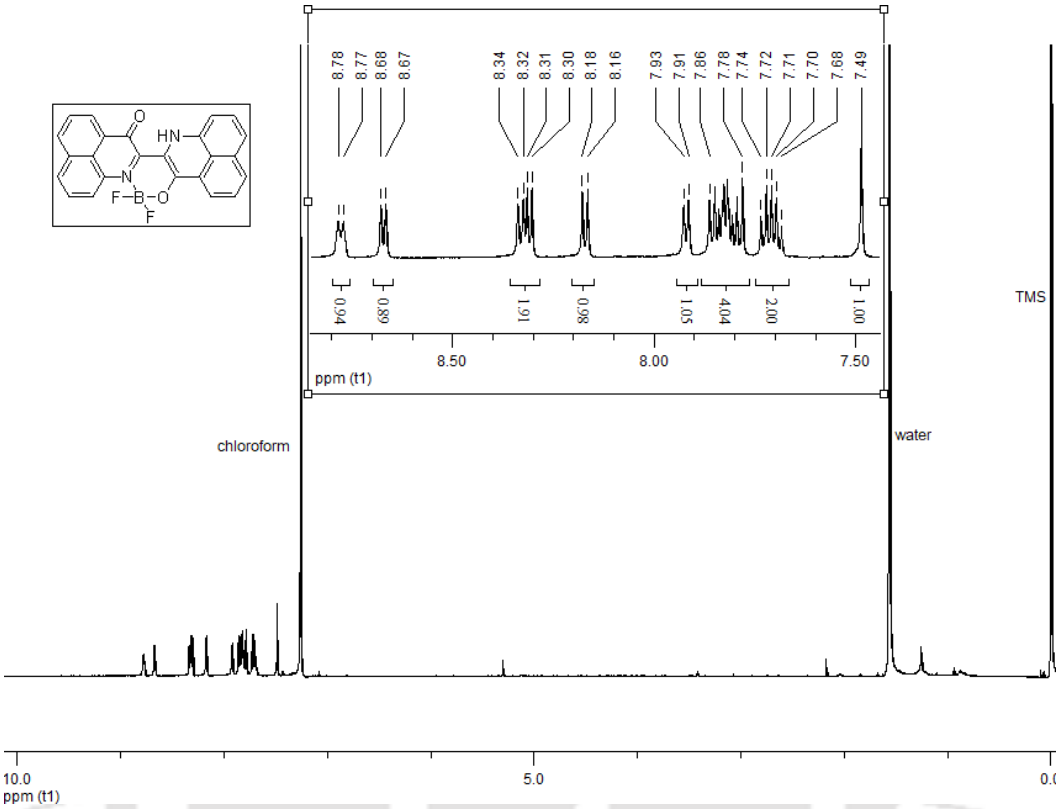

Fig 7. 1 ^{1}H NMR (600 MHz, $CDCl_3$) of **PNI-BF_2**.

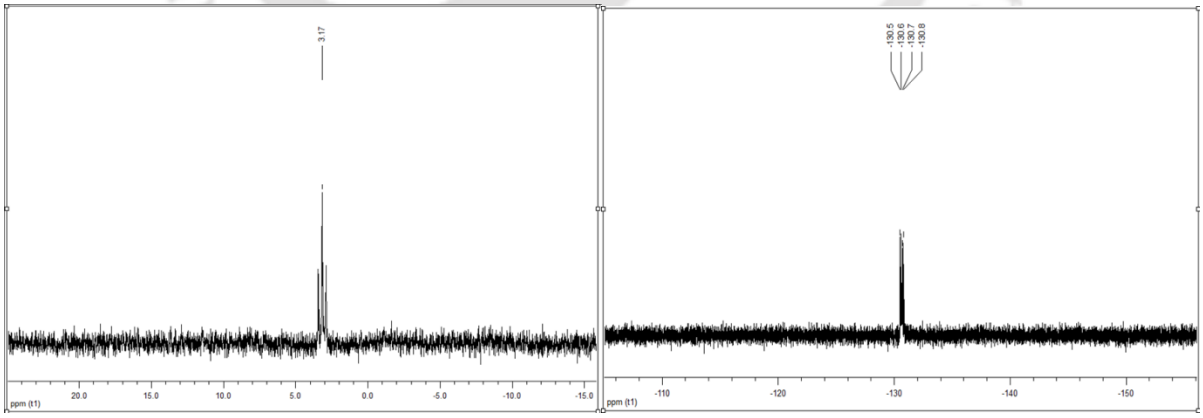

Fig 7. 2 ^{11}B (128 MHz) and ^{19}F NMR (376 MHz, $CDCl_3$) of **PNI-BF_2**.

❖ 6.3.2 Chapter 2

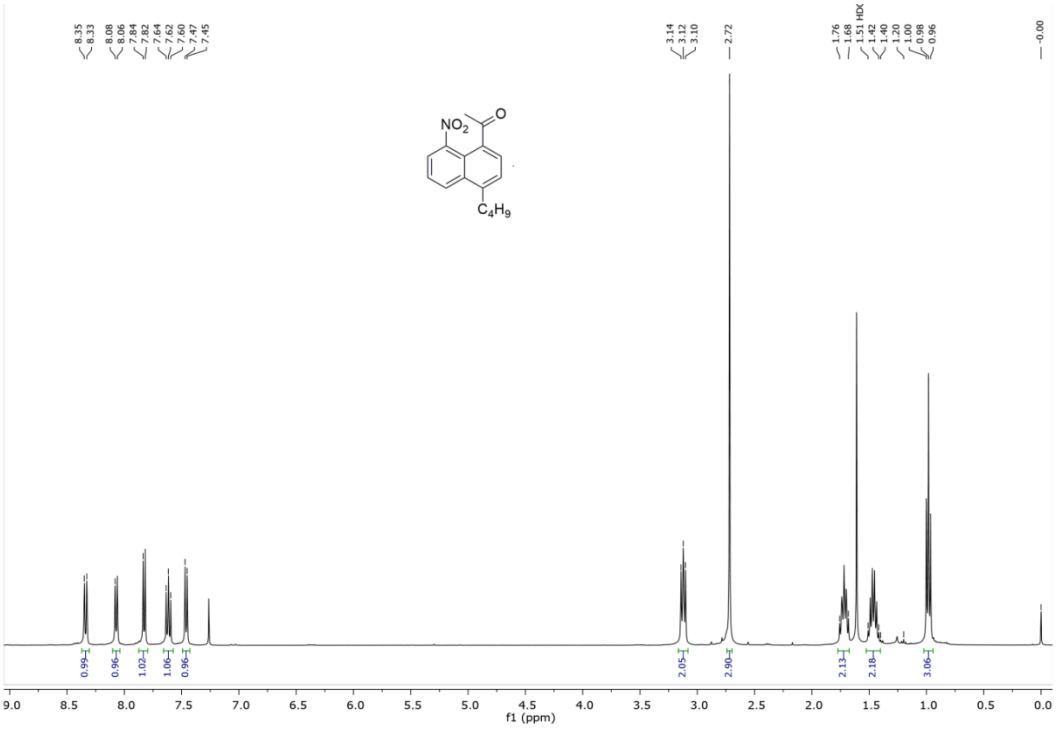

Fig 7. 3 ^{1}H (600 MHz, $CDCl_3$) NMR of **IIIB**

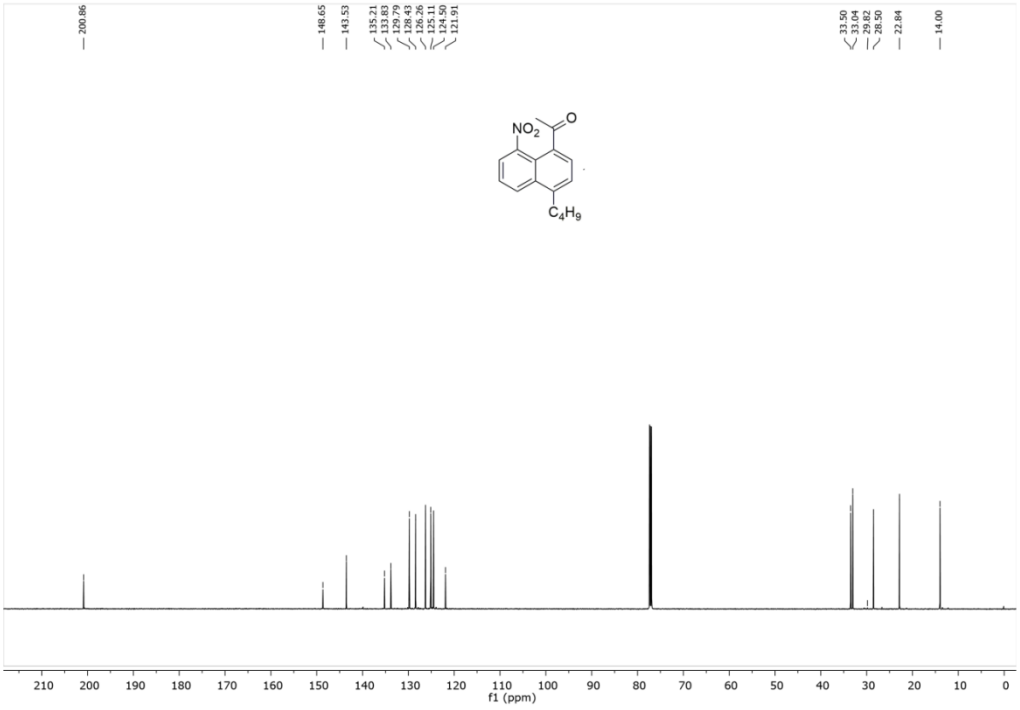

Fig 7. 4 ^{13}C (150 MHz, $CDCl_3$) NMR of **IIIB**

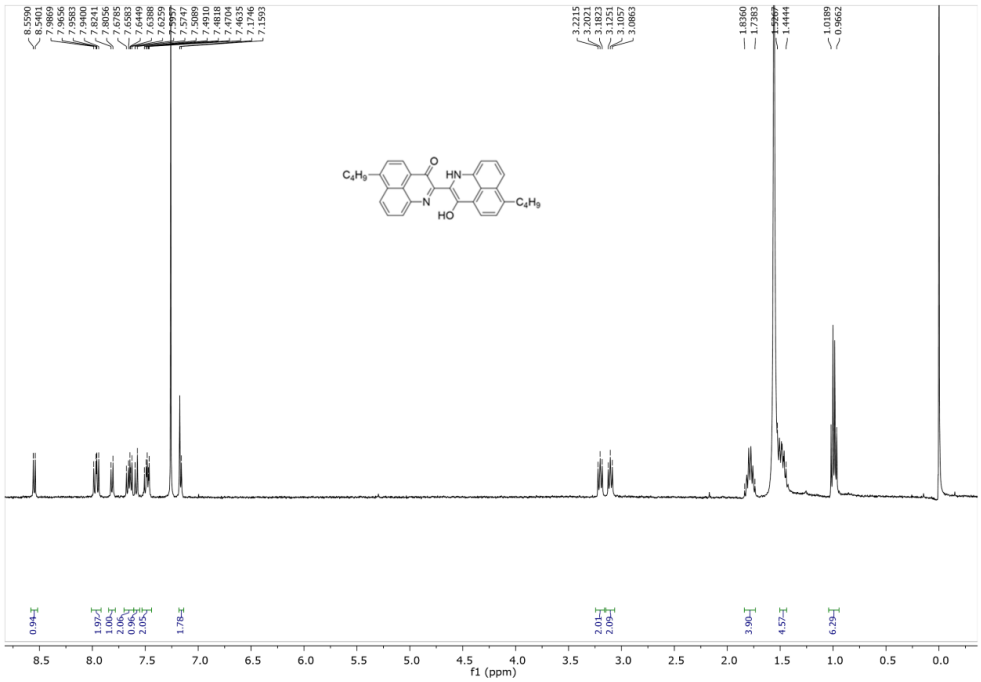

Fig 7. 5 ^{1}H NMR (400 MHz, $CDCl_3$) of butylPNI

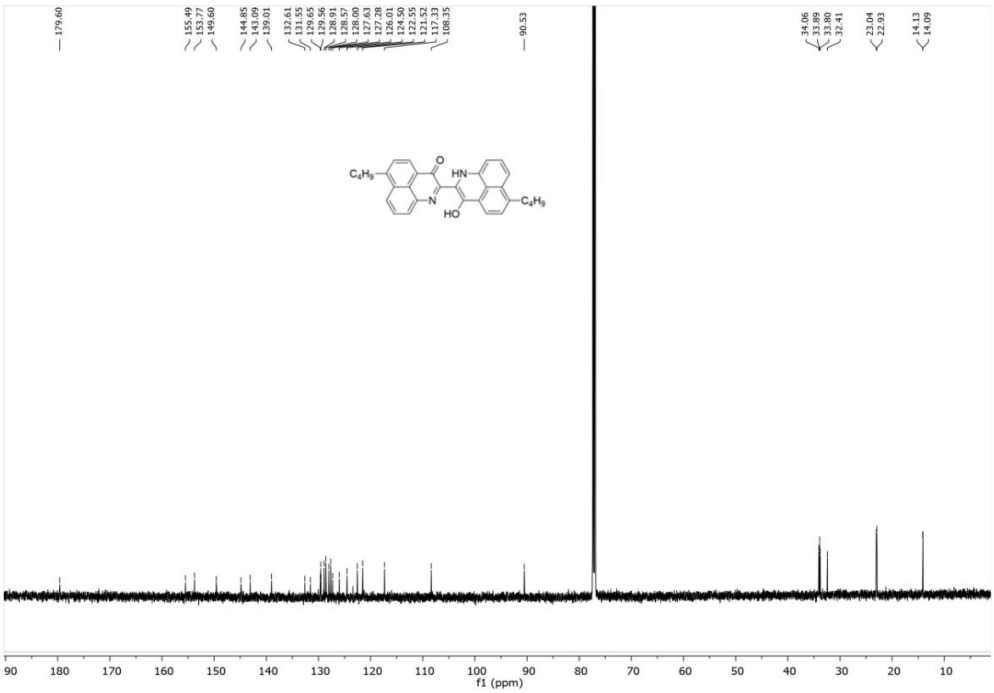

Fig 7. 6 ^{13}C (150 MHz, $CDCl_3$) NMR of butylPNI

❖ 6.3.3 Chapter 3

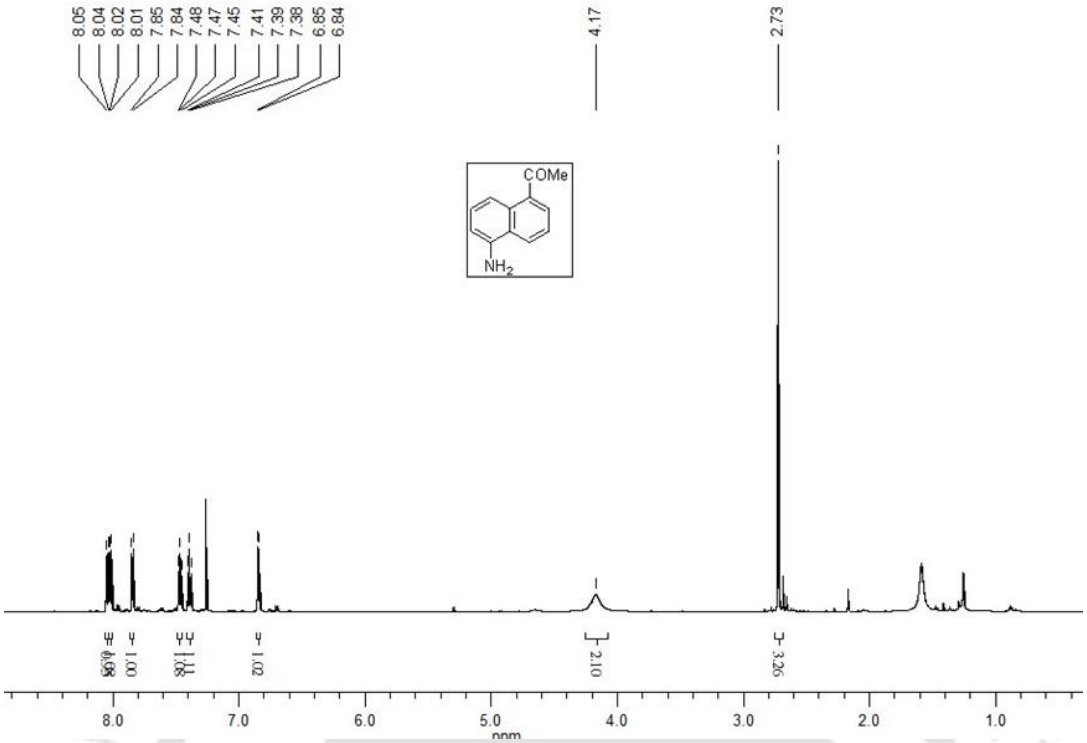

Fig 7. 7 ^{1}H (600 MHz, $CDCl_3$) NMR of **2**

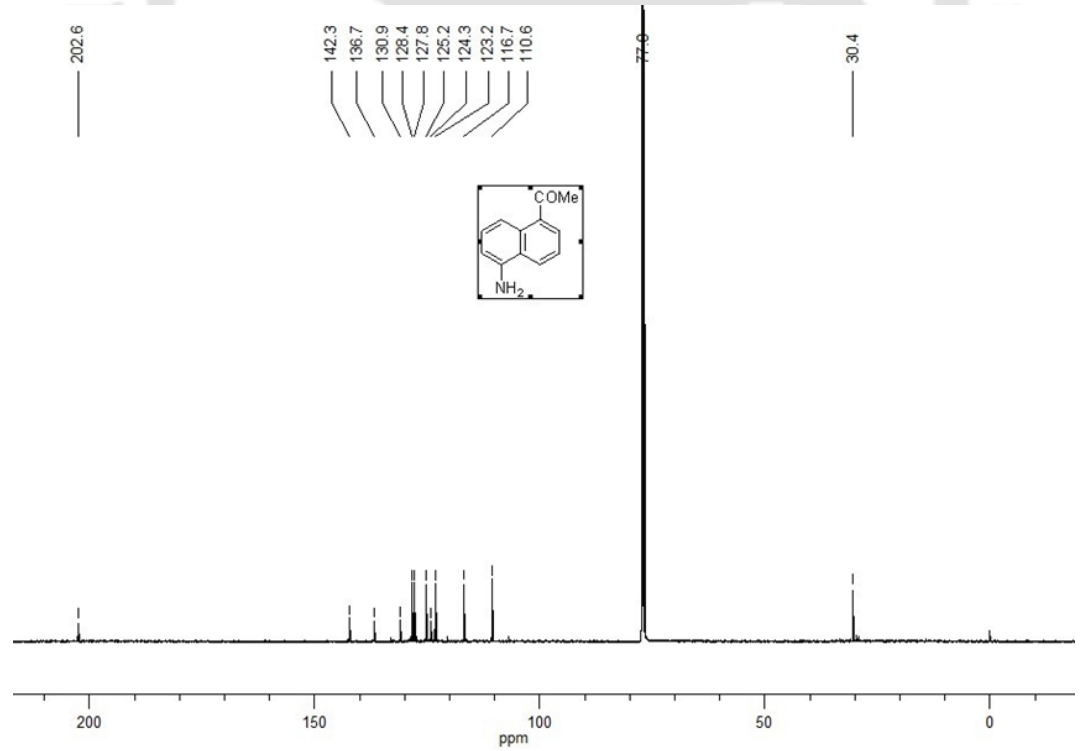

Fig 7. 8 ^{13}C (150 MHz, $CDCl_3$) NMR of **2**

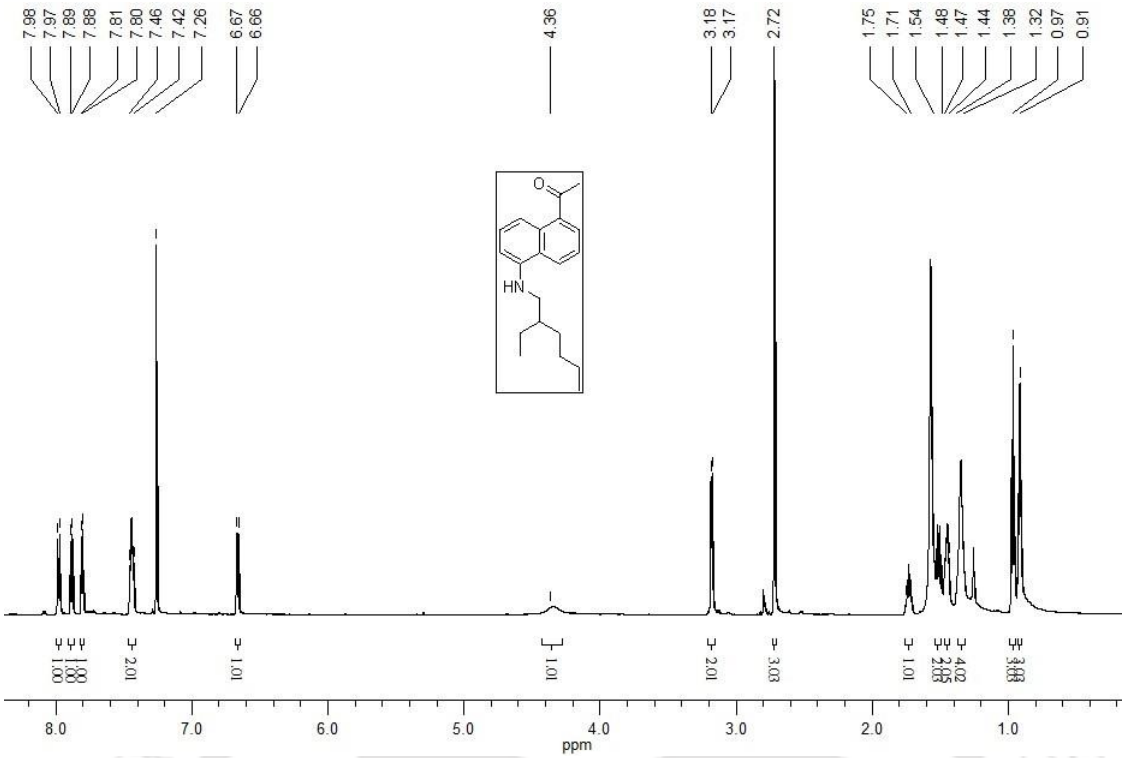

Fig 7. 9 ^{1}H (600 MHz, $CDCl_3$) NMR of **2a**

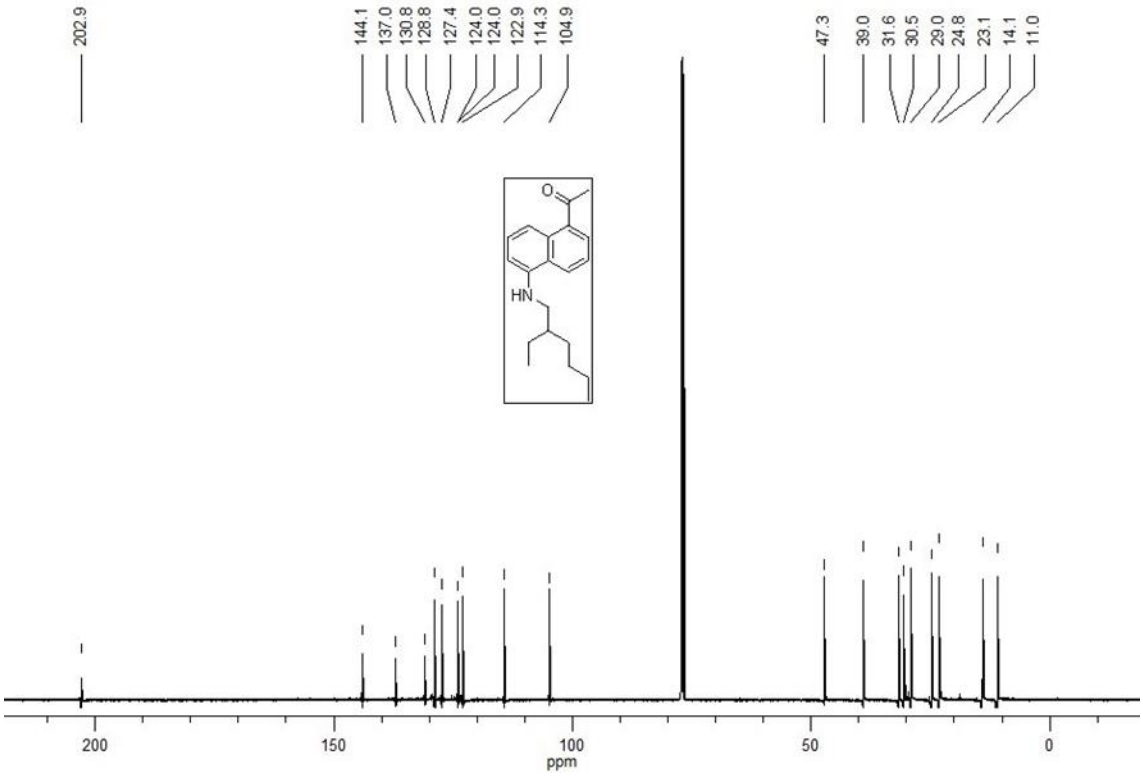

Fig 7. 10 ^{13}C (150 MHz, $CDCl_3$) NMR of **2a**

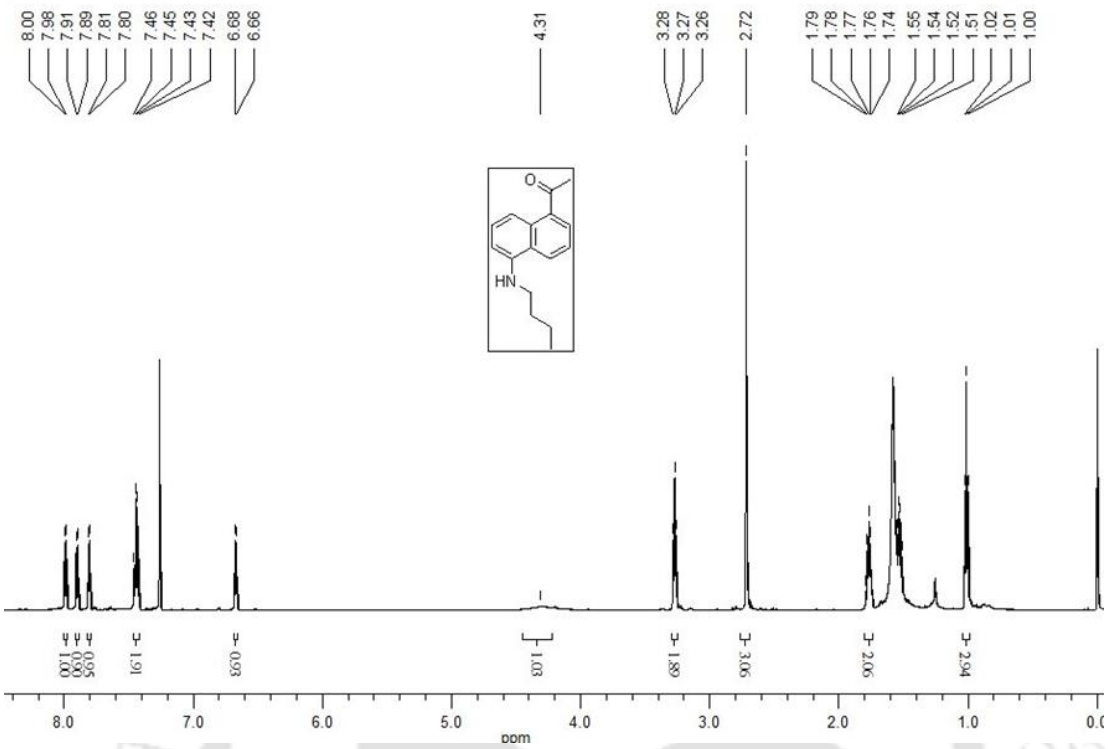

Fig 7. 11 ^{1}H (600 MHz, $CDCl_3$) NMR of **3a**

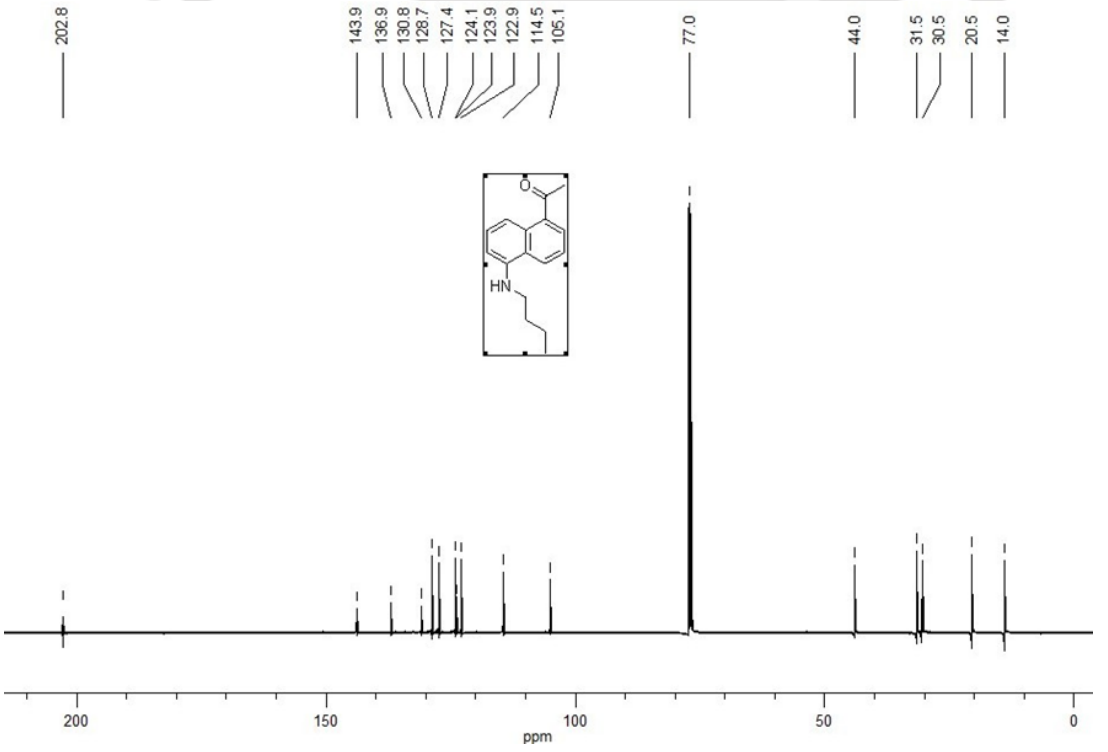

Fig 7. 12 ^{13}C (150 MHz, $CDCl_3$) NMR of **3a**

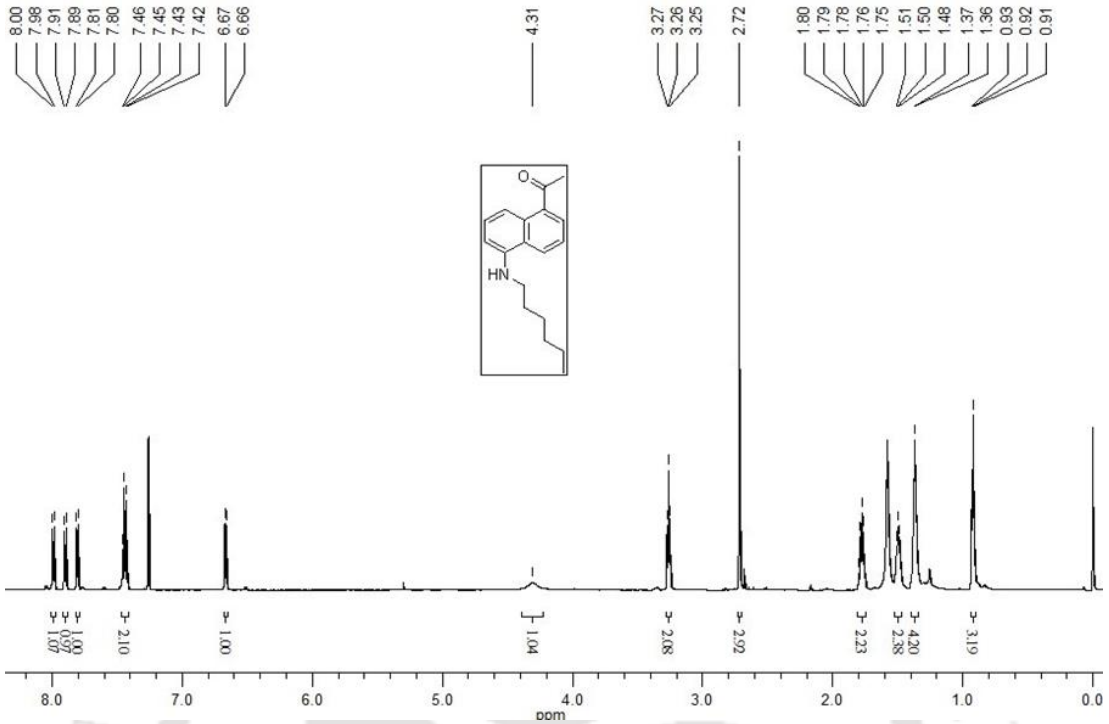

Fig 7. 13 ^{1}H (600 MHz, $CDCl_3$) NMR of **4a**

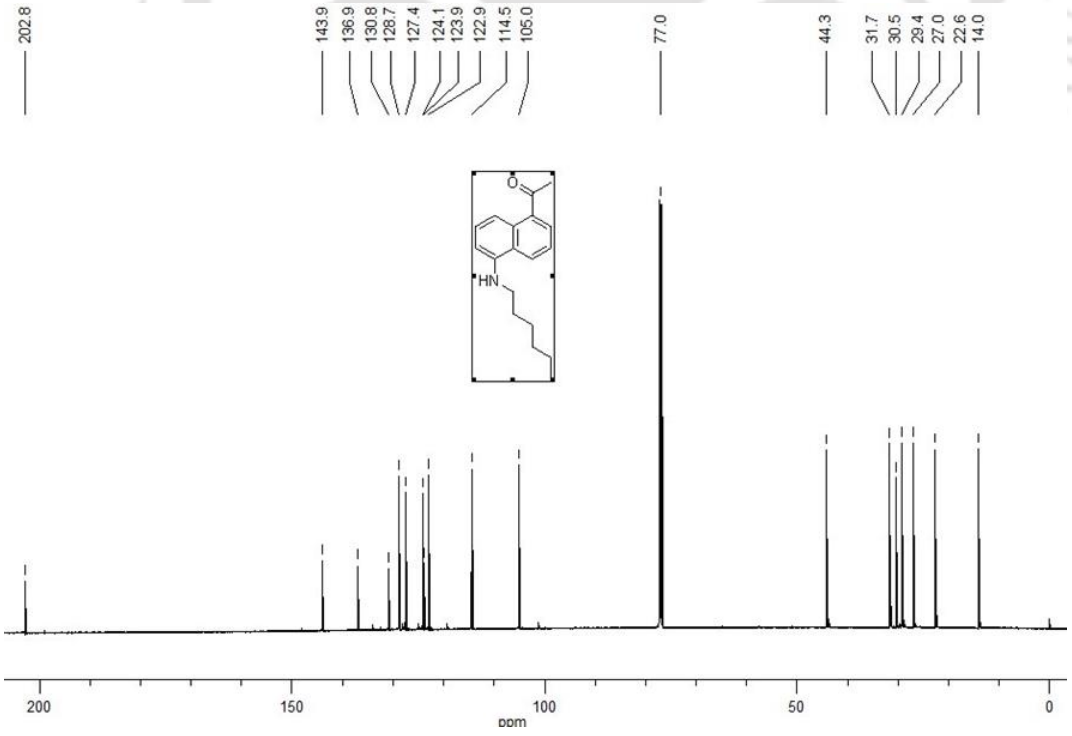

Fig 7. 14 ^{13}C (150 MHz, $CDCl_3$) NMR of **4a**

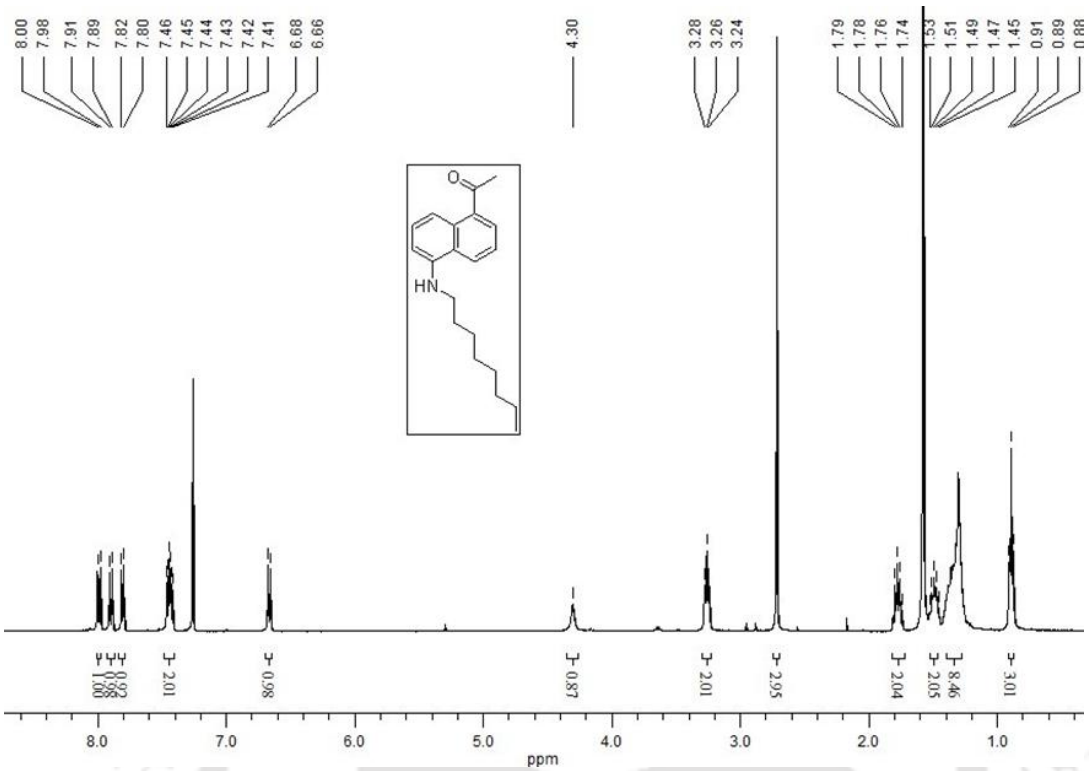

Fig 7. 15 ^{1}H (400 MHz, $CDCl_3$) NMR of **5a**

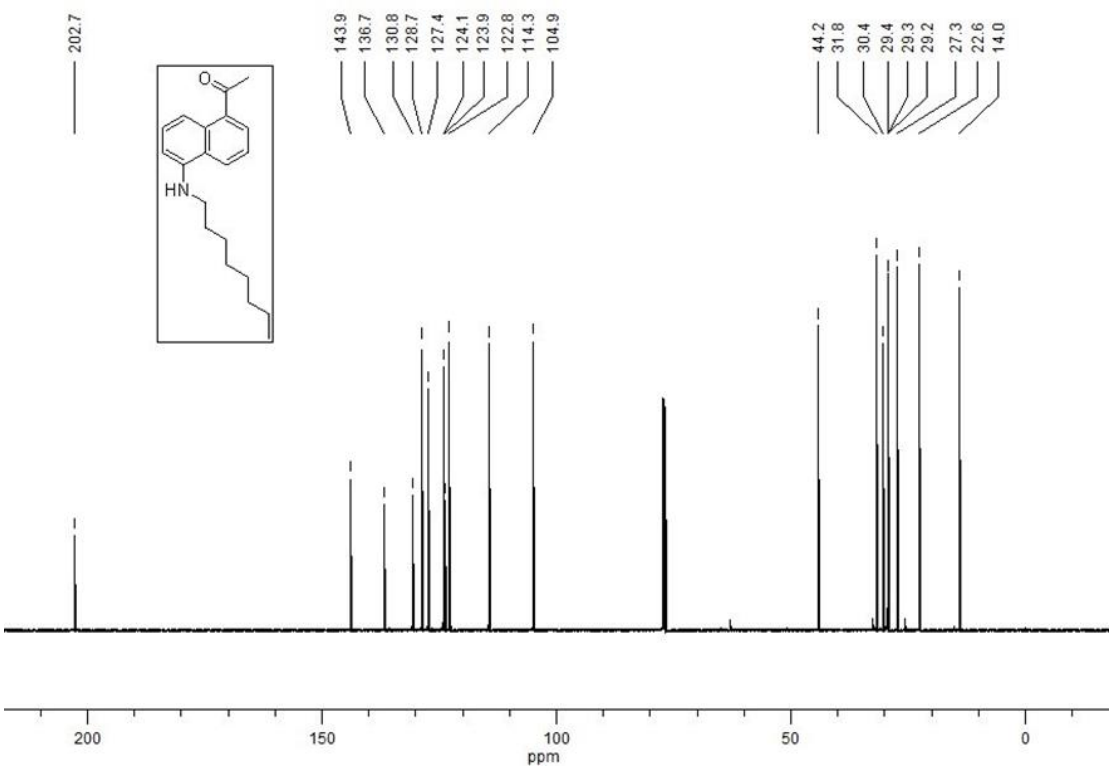

Fig 7. 16 ^{13}C (150 MHz, $CDCl_3$) NMR of **5a**

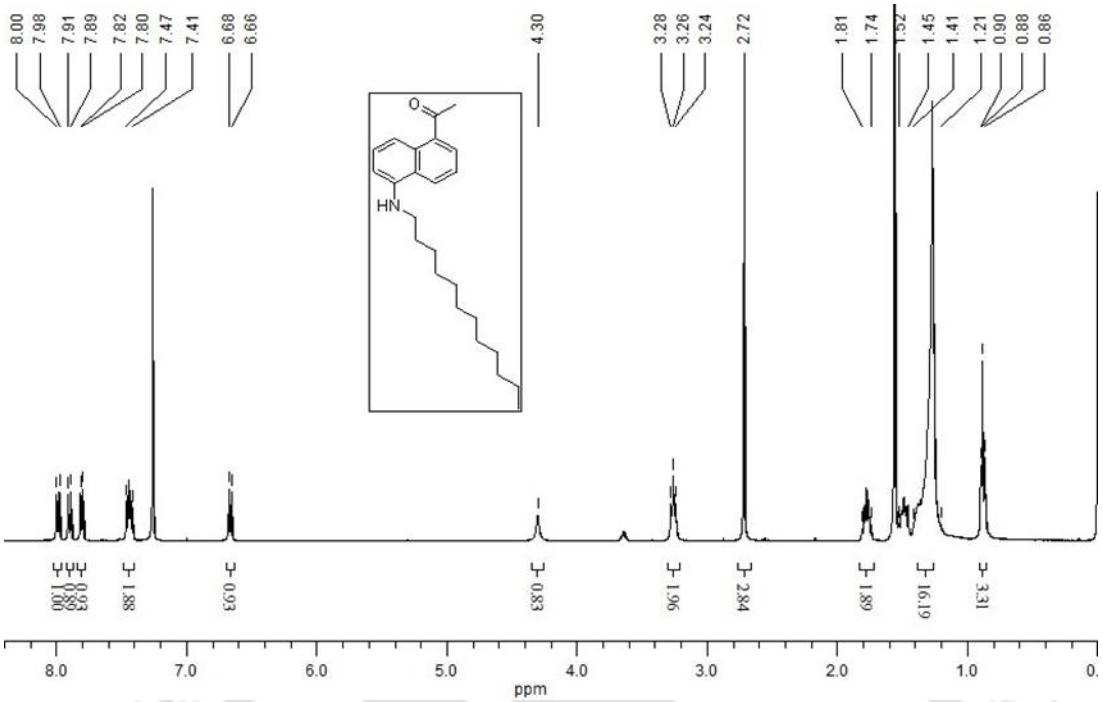

Fig 7. 17 ^{1}H (400 MHz, $CDCl_3$) NMR of **6a**

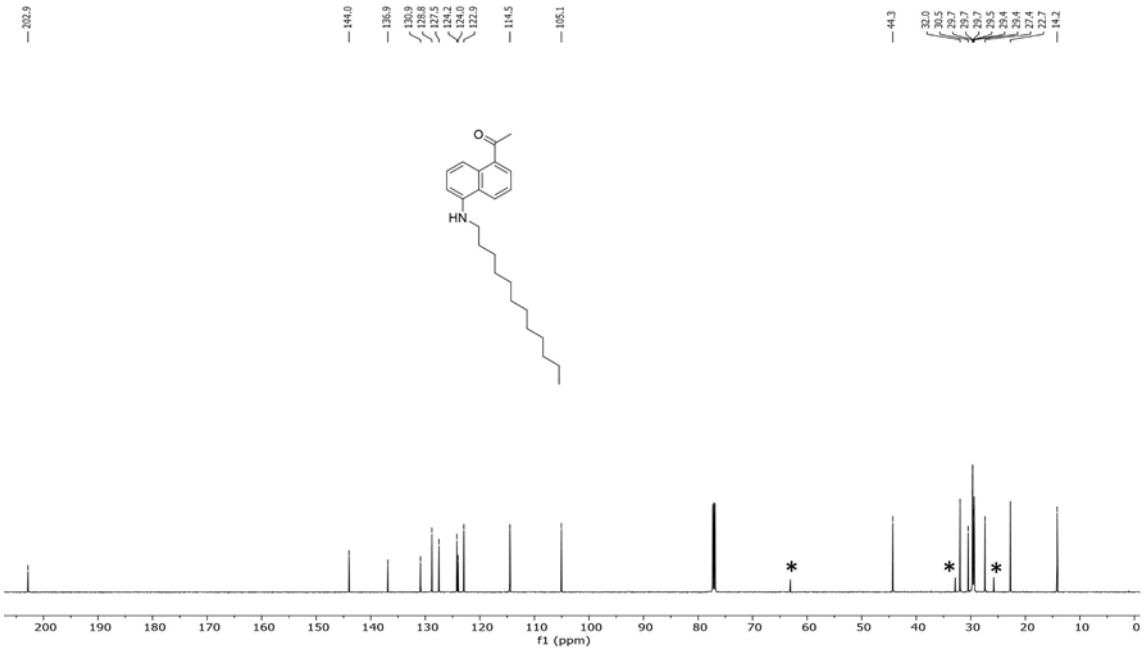

Fig 7. 18 ^{13}C (150 MHz, $CDCl_3$) NMR of **6a.** (*) Impurities.

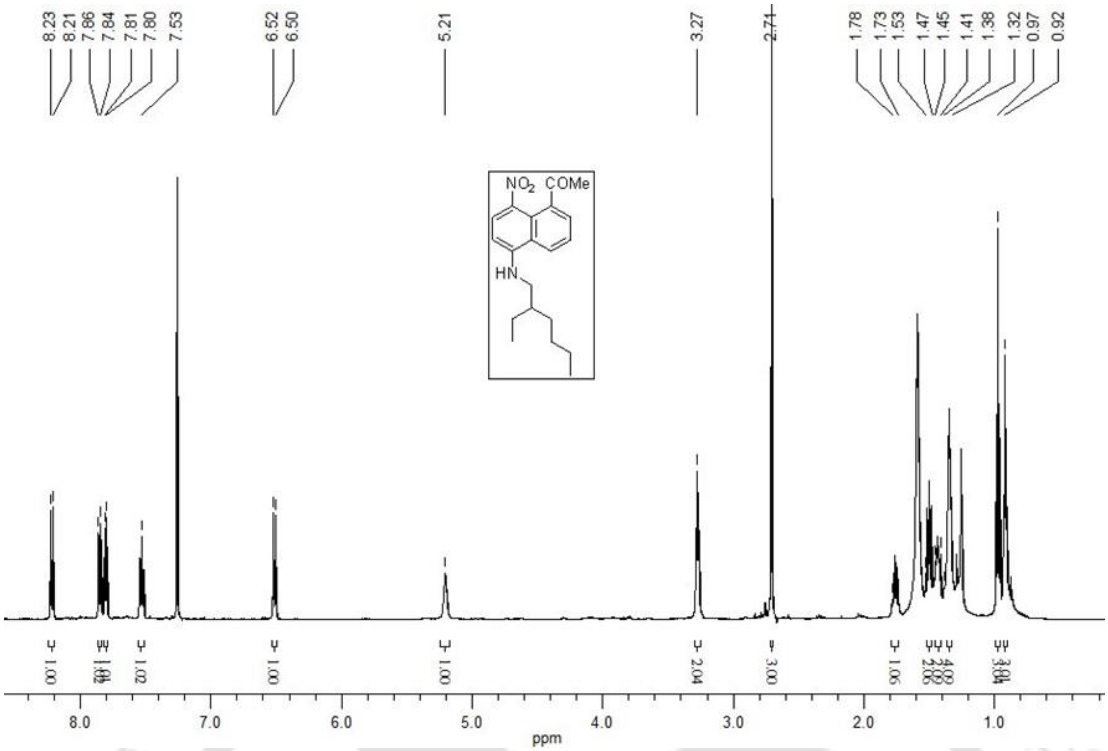

Fig 7. 19 ^{1}H (500 MHz, $CDCl_3$) NMR of **2r**

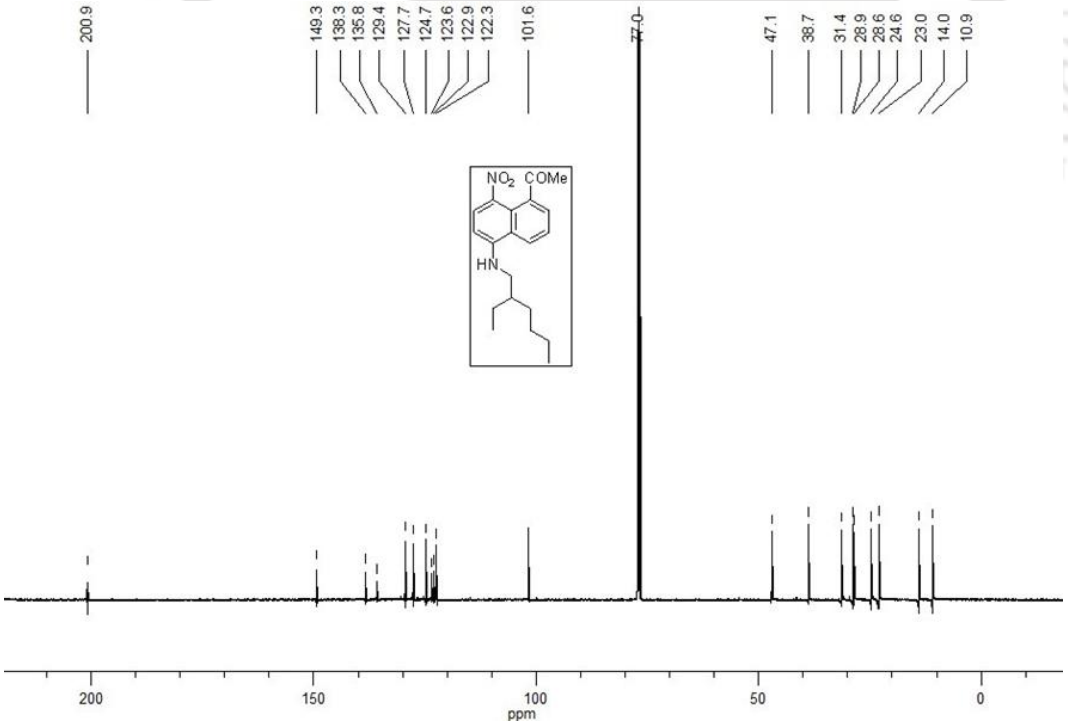

Fig 7. 20 ^{13}C (150 MHz, $CDCl_3$) NMR of **2r**

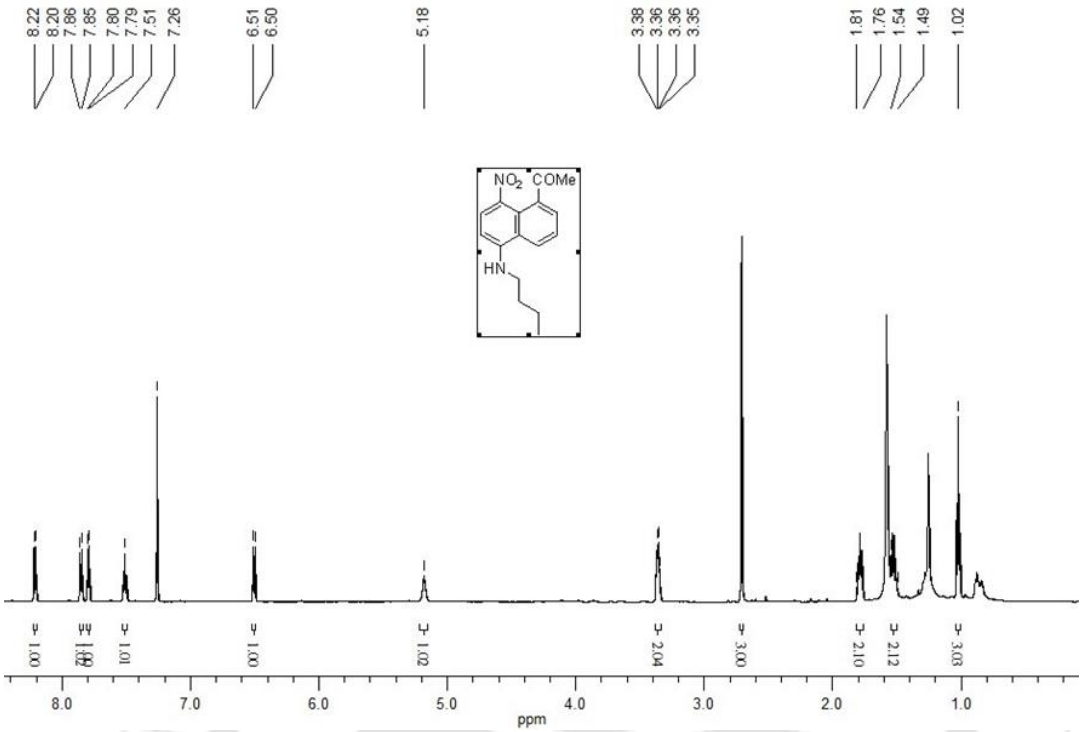

Fig 7. 21 ^{1}H (600 MHz, $CDCl_3$) NMR of **3r**

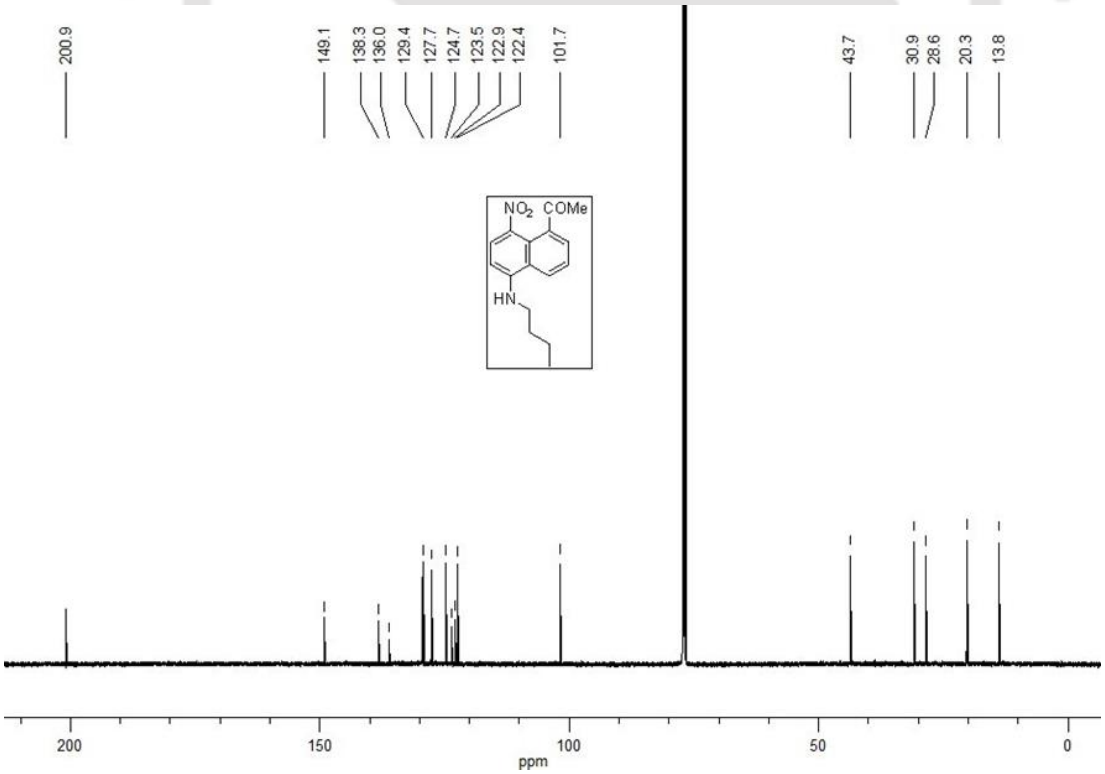

Fig 7. 22 ^{13}C (150 MHz, $CDCl_3$) NMR of **3r**

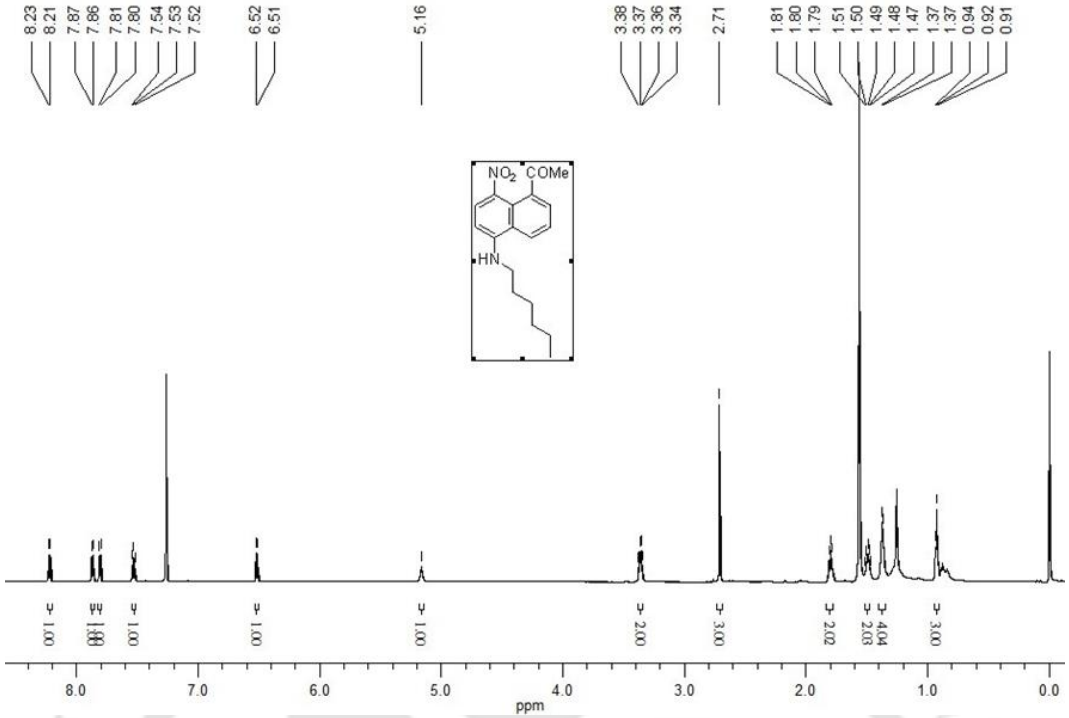

Fig 7. 23 ^{1}H (600 MHz, $CDCl_3$) NMR of **4r**

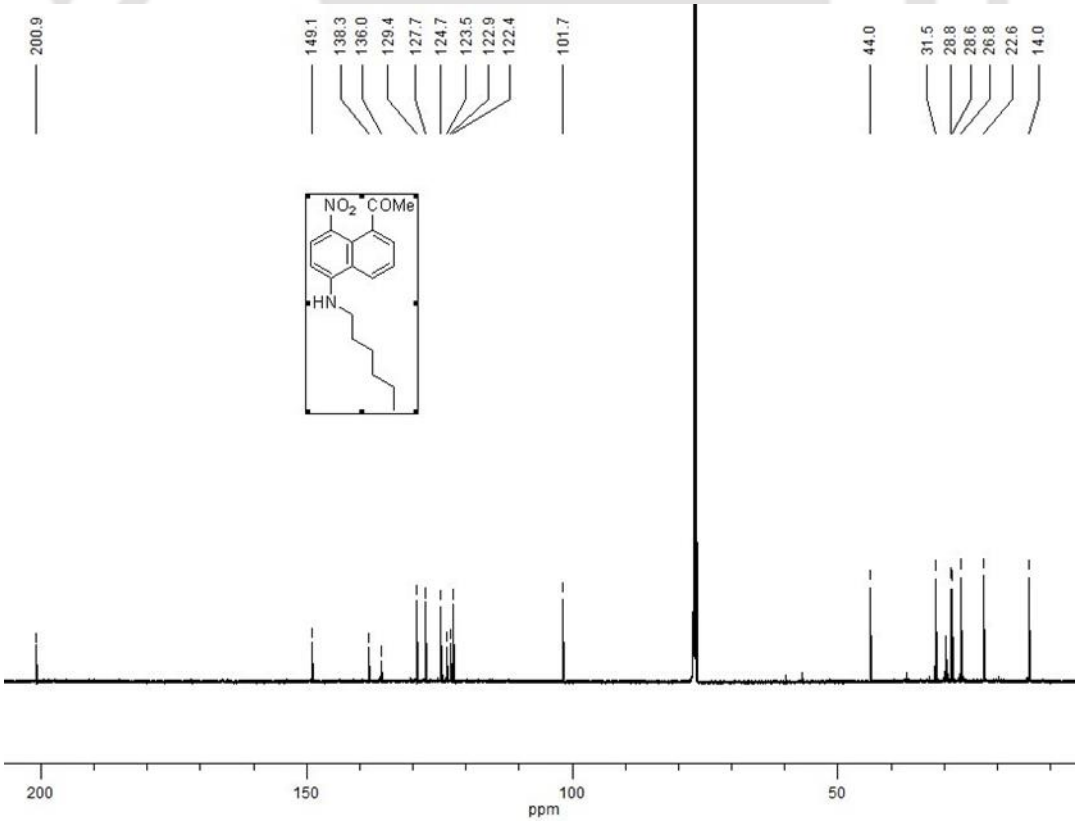

Fig 7. 24 ^{13}C (150 MHz, $CDCl_3$) NMR of **4r**

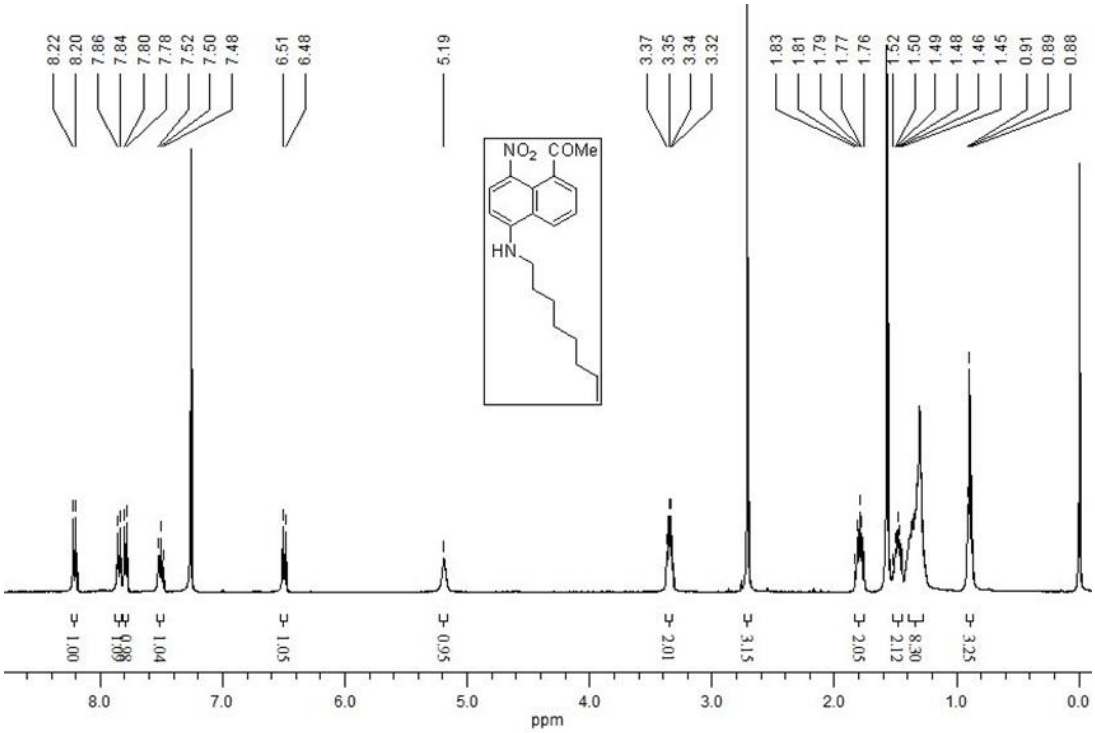

Fig 7. 25 ^{1}H (400 MHz, $CDCl_3$) NMR of **5r**

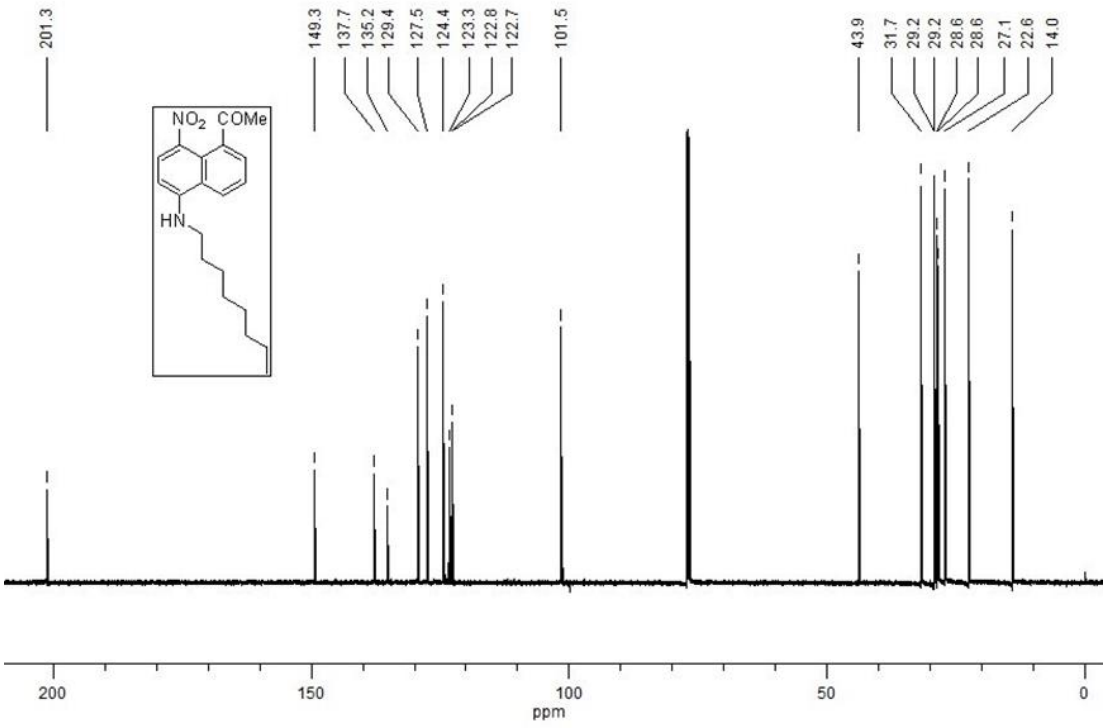

Fig 7. 26 ^{13}C (150 MHz, $CDCl_3$) NMR of **5r**

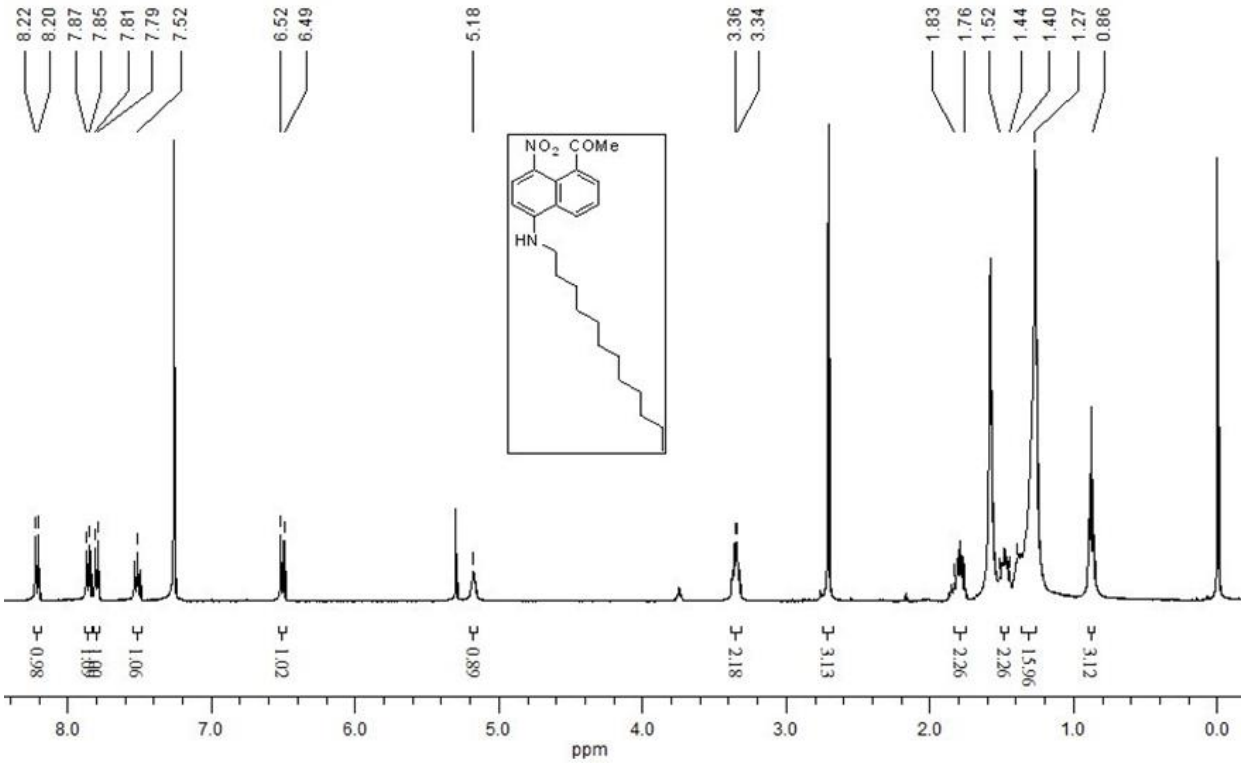

Fig 7. 27 ^{1}H (400 MHz, $CDCl_3$) NMR of **6r**

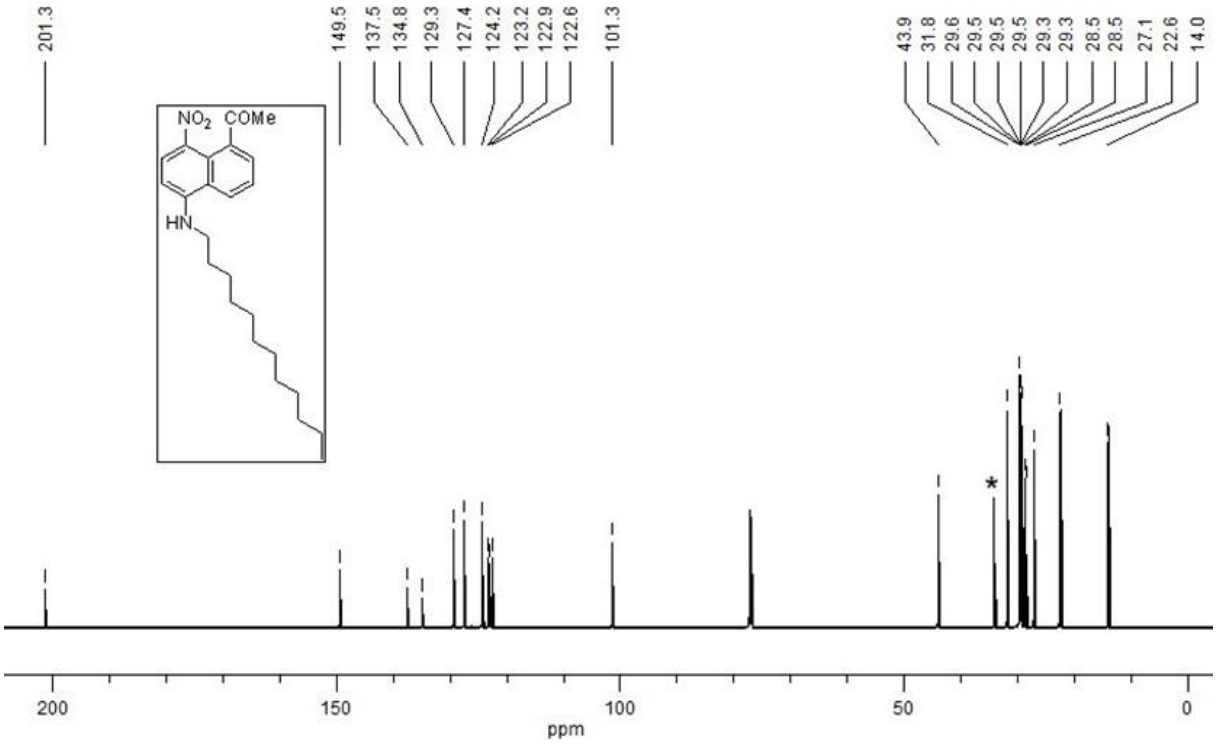

Fig 7. 28 ^{13}C (150 MHz, $CDCl_3$) NMR of 6r. (*) Residual peak from pentane.

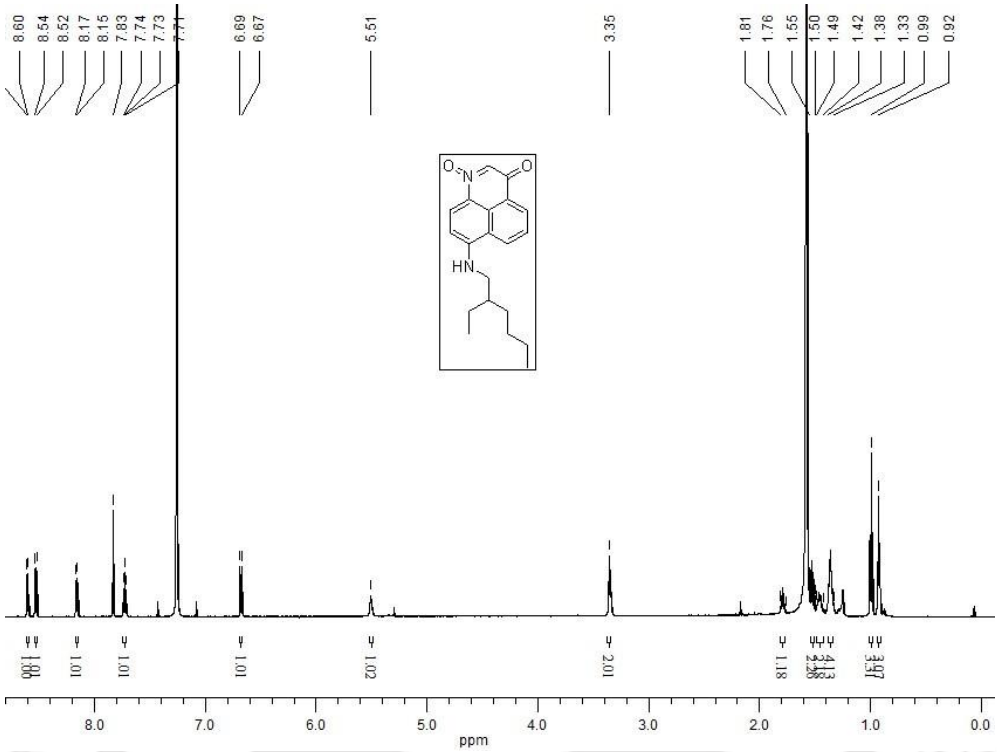

Fig 7. 29 ^{1}H (600 MHz, $CDCl_3$) NMR **of 2p**

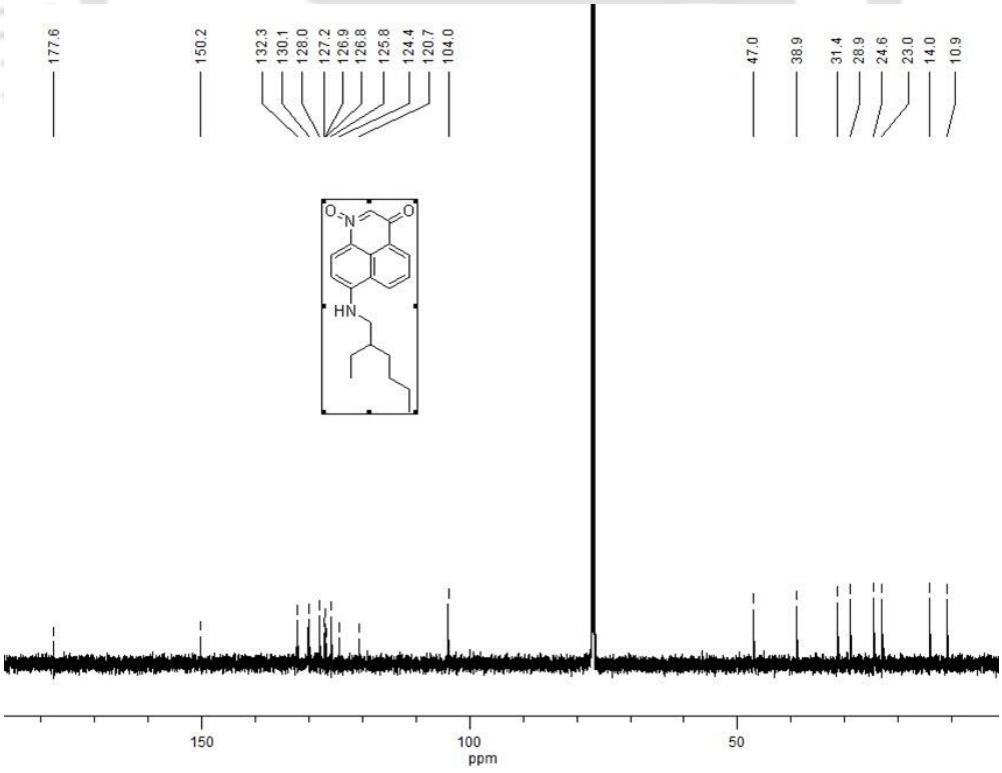

Fig 7. 30 ^{13}C (150 MHz, $CDCl_3$) NMR of **2p**

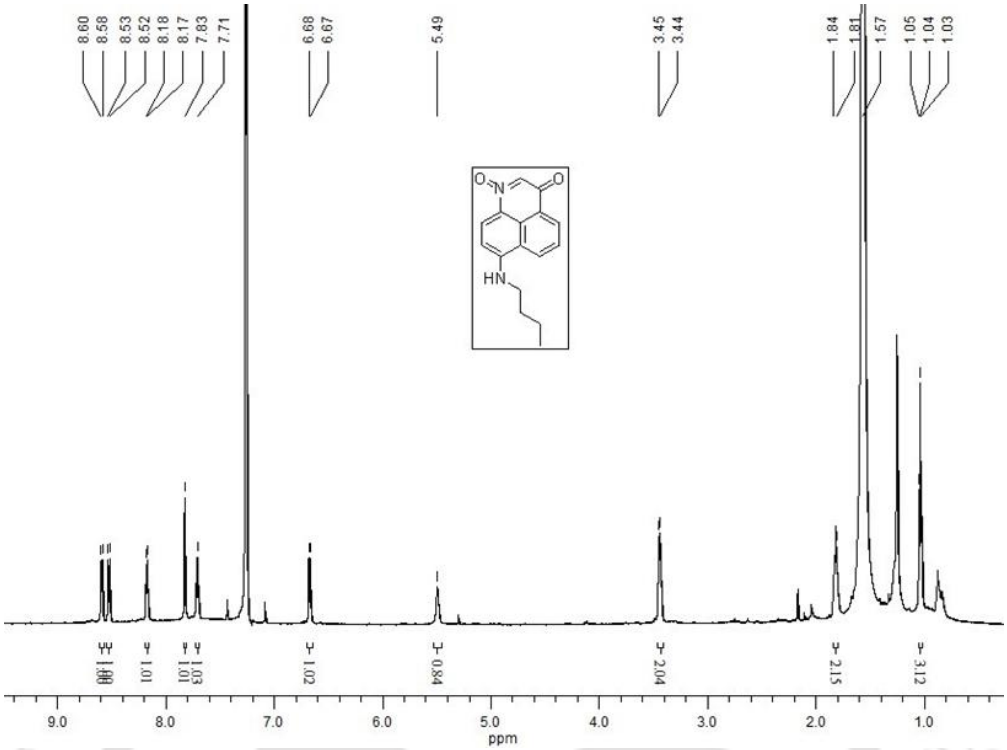

Fig 7. 31 ^{1}H (600 MHz, $CDCl_3$) NMR of **3p**

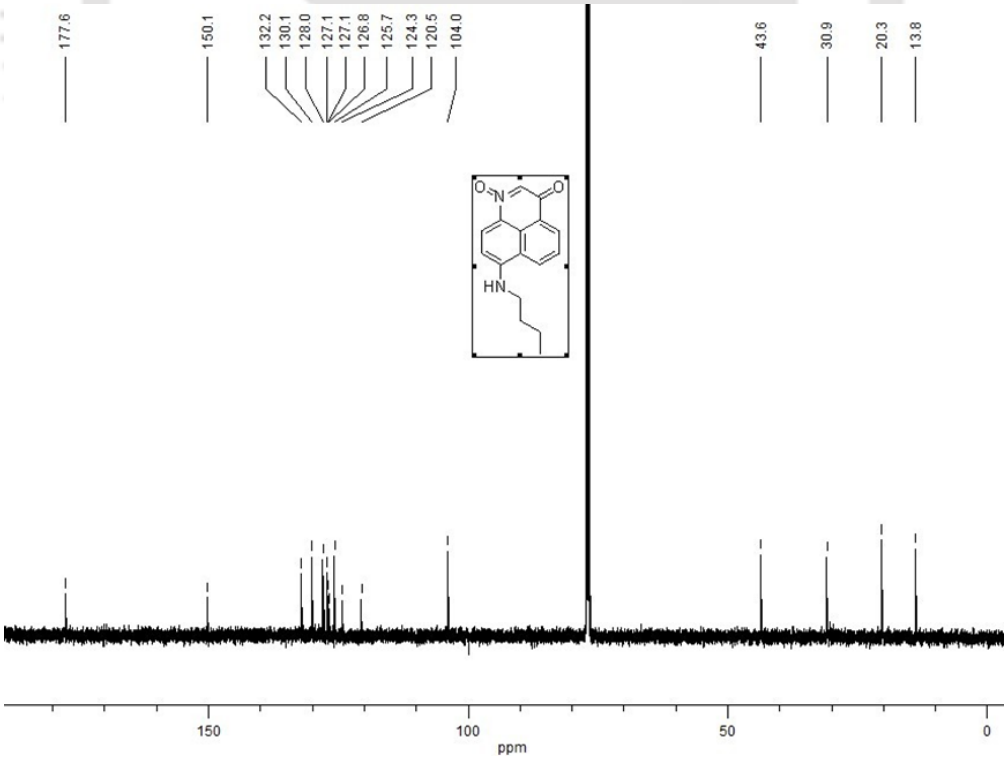

Fig 7. 32 ^{13}C (150 MHz, $CDCl_3$) NMR of **3p**

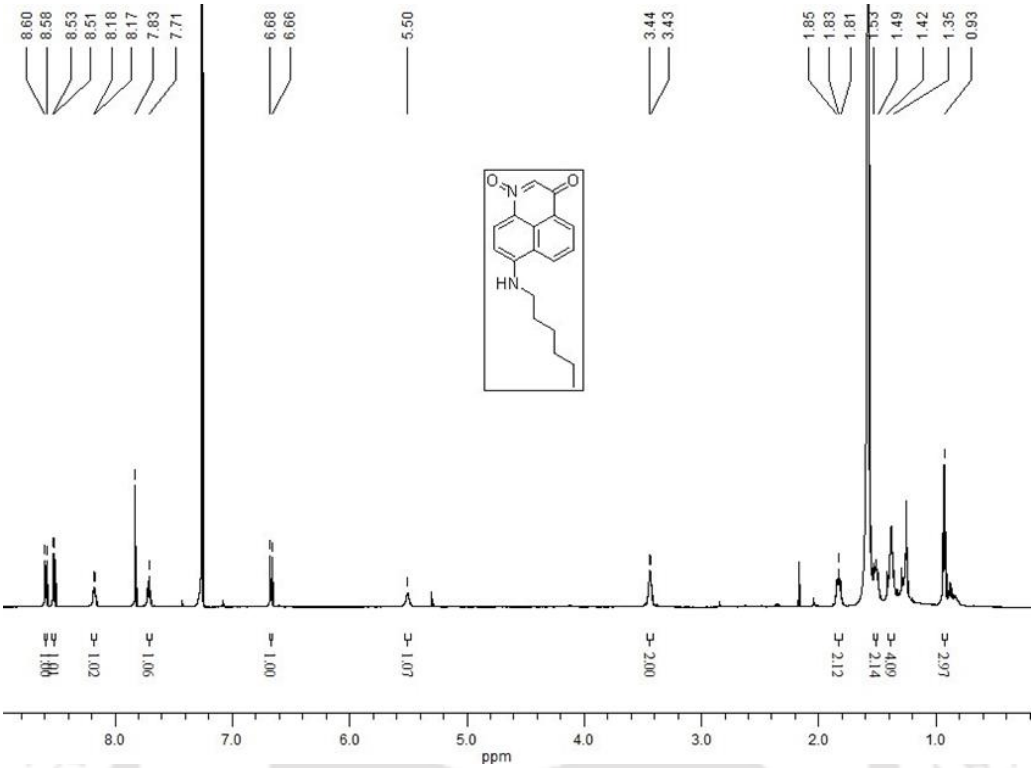

Fig 7. 33 ^{1}H (600 MHz, $CDCl_3$) NMR of **4p**

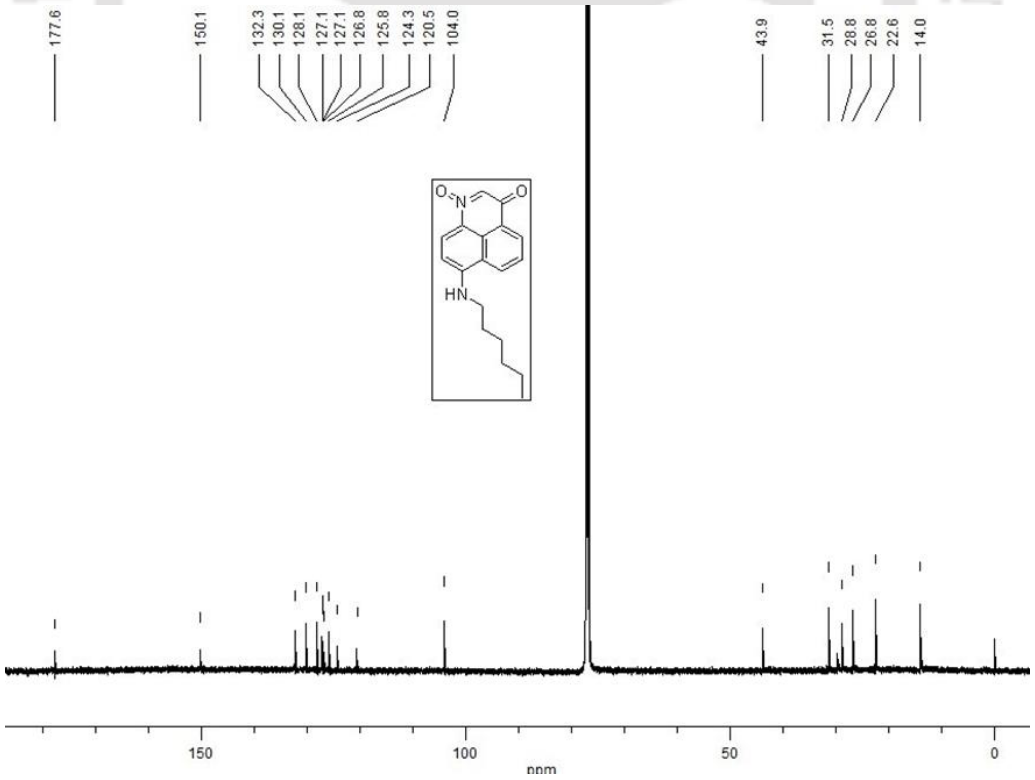

Fig 7. 34 ^{13}C (150 MHz, $CDCl_3$) NMR of **4p**

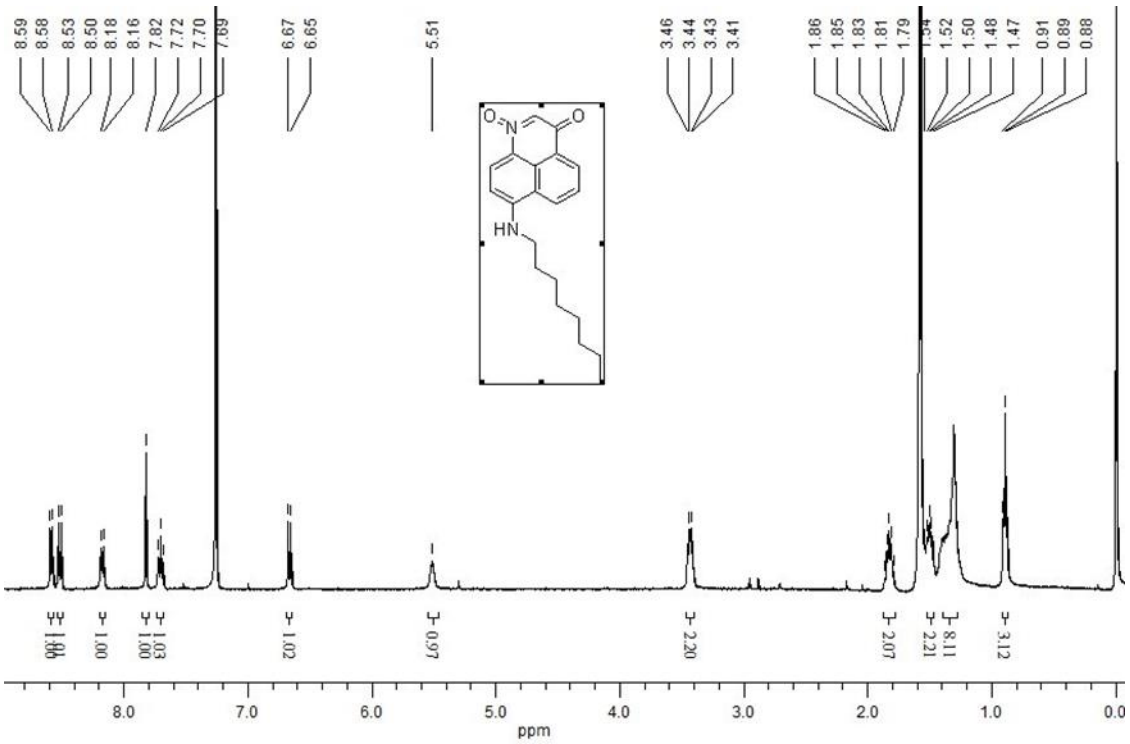

Fig 7. 35 ^{1}H (400 MHz, $CDCl_3$) NMR of **5p**

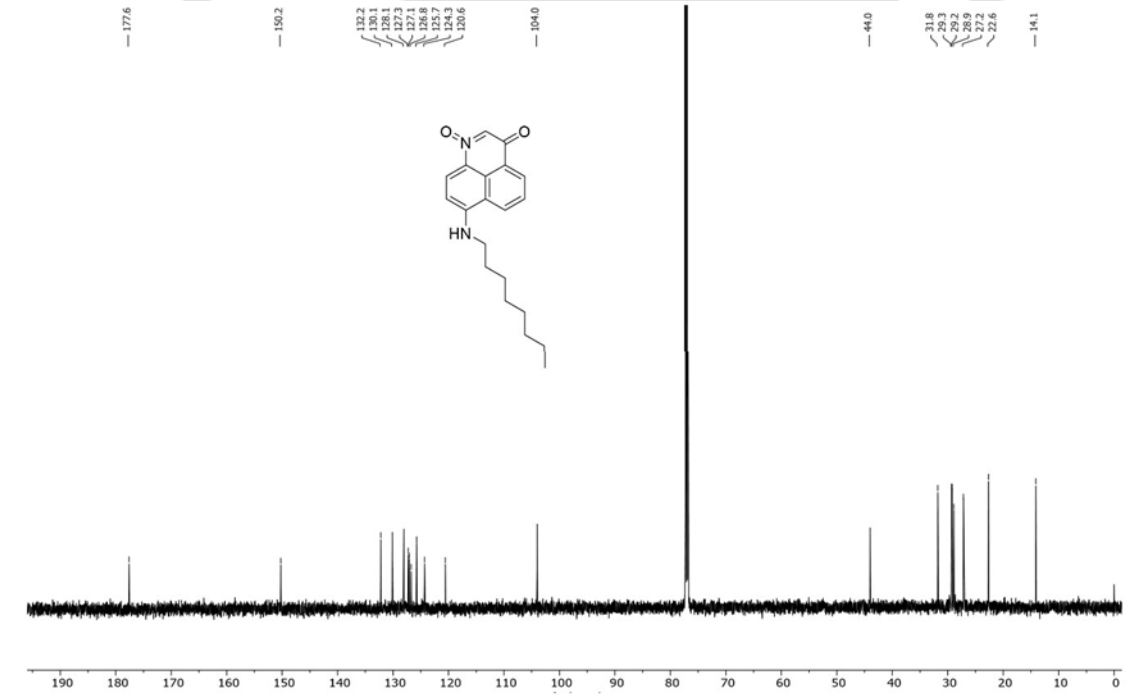

Fig 7. 36 ^{13}C (150 MHz, $CDCl_3$) NMR of **5p**

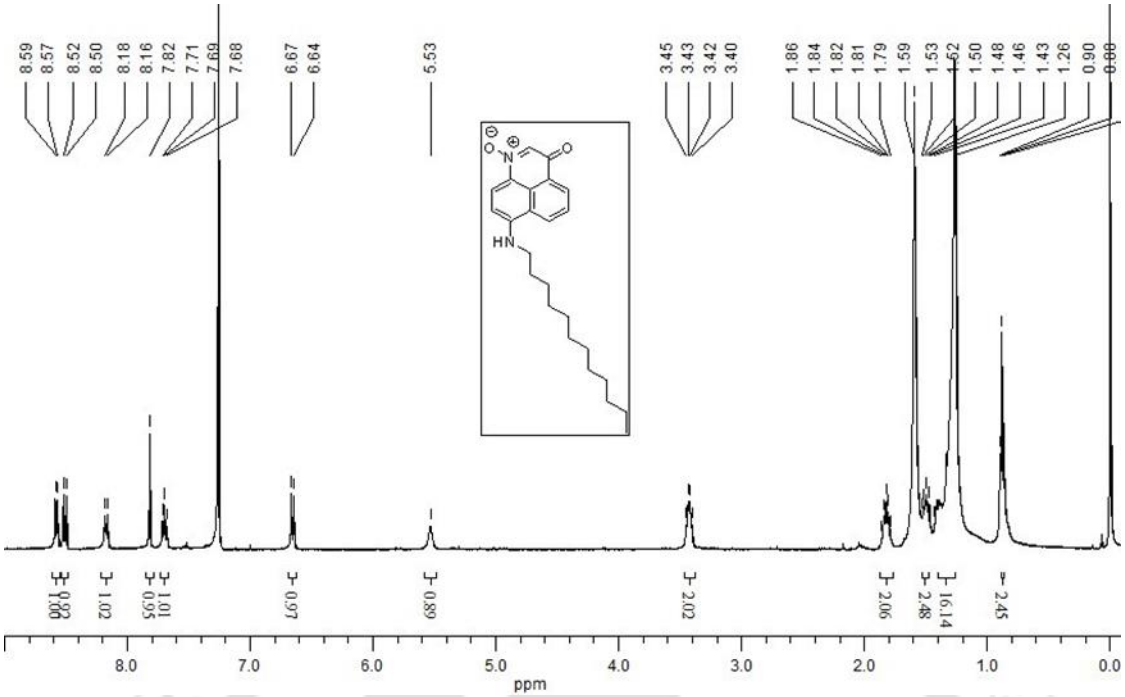

Fig 7. 37 ^{1}H (400 MHz, $CDCl_3$) NMR of **6p**

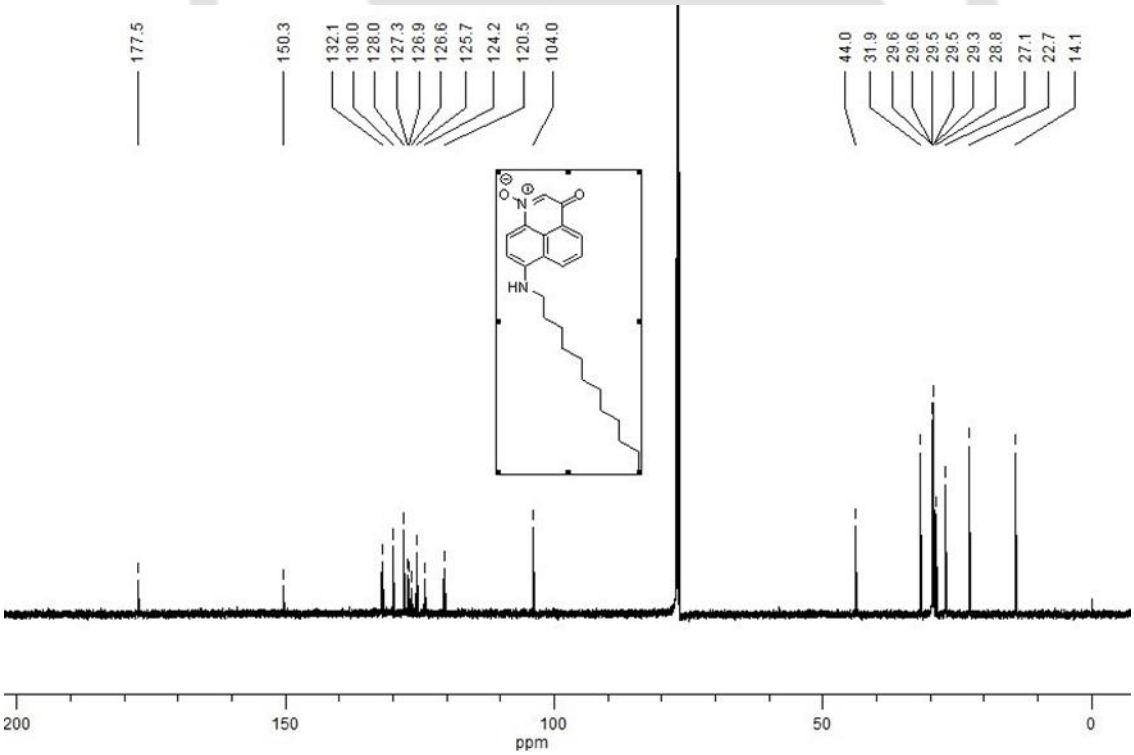

Fig 7. 38 ^{13}C (150 MHz, $CDCl_3$) NMR of **6p**

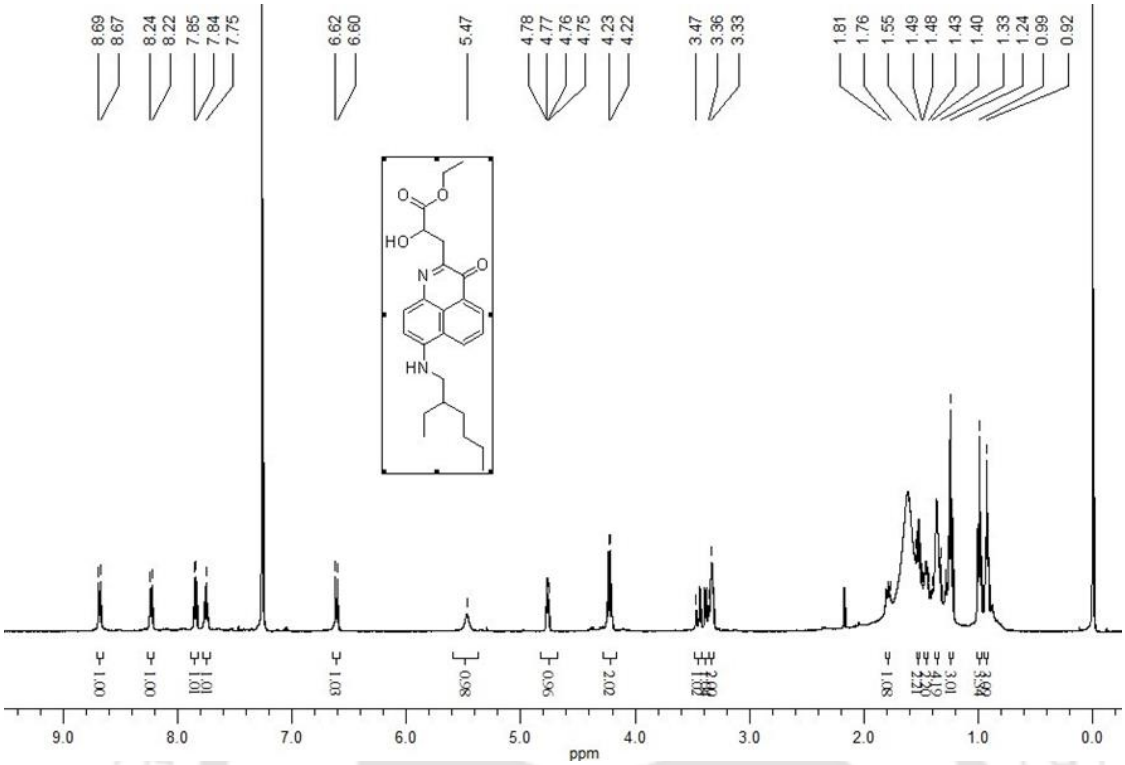

Fig 7. 39 ^{1}H (500 MHz, $CDCl_3$) NMR of **2p1′**

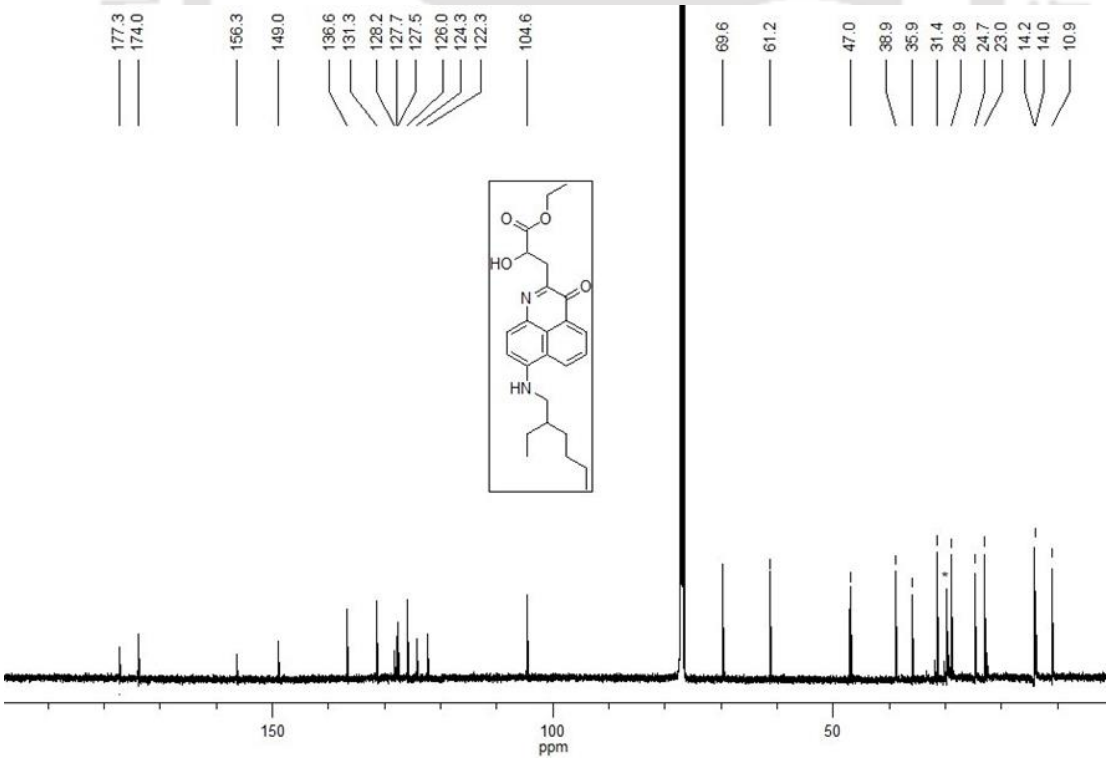

Fig 7. 40 ^{13}C (150 MHz, $CDCl_3$) NMR of **2p1′**. (*) Residual peak from grease.

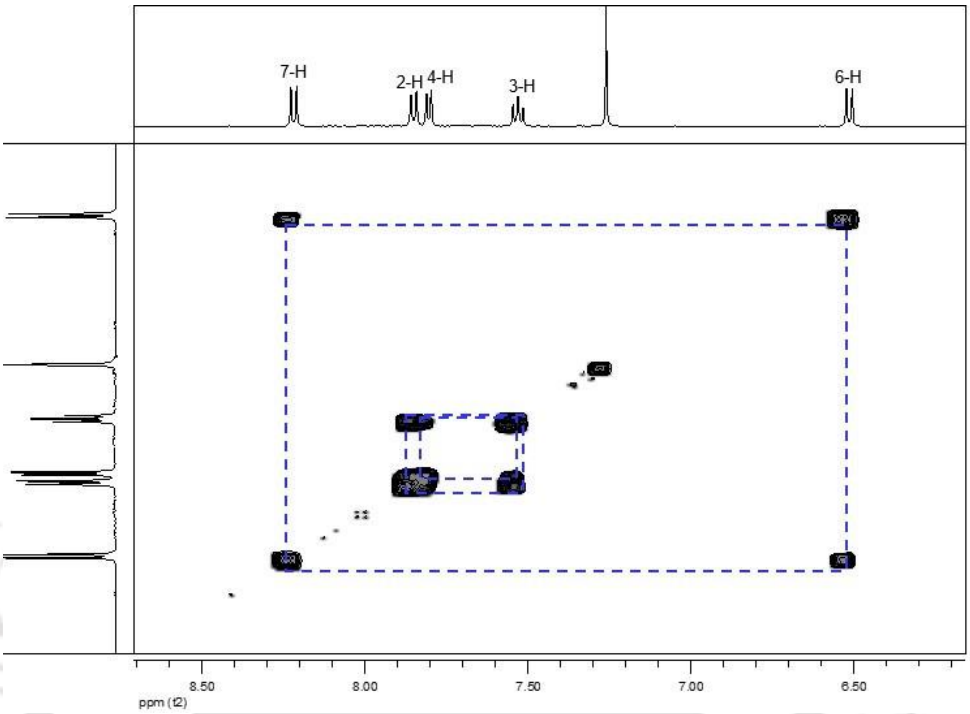

Fig 7. 41 Partial ^{1}H -^{1}H-COSY (aromatic region) NMR spectra of **2r** (500 MHz, $CDCl_3$, 293K).

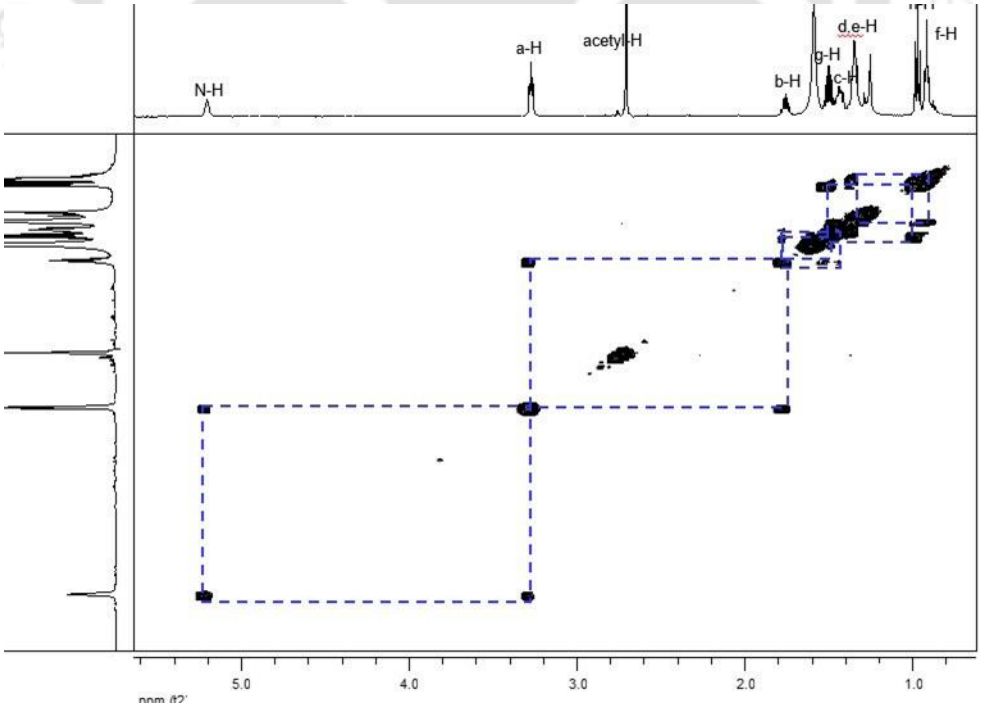

Fig 7. 42 Partial ^{1}H -^{1}H-COSY (aliphatic region) NMR spectra of **2r** (500 MHz, $CDCl_3$, 293K).

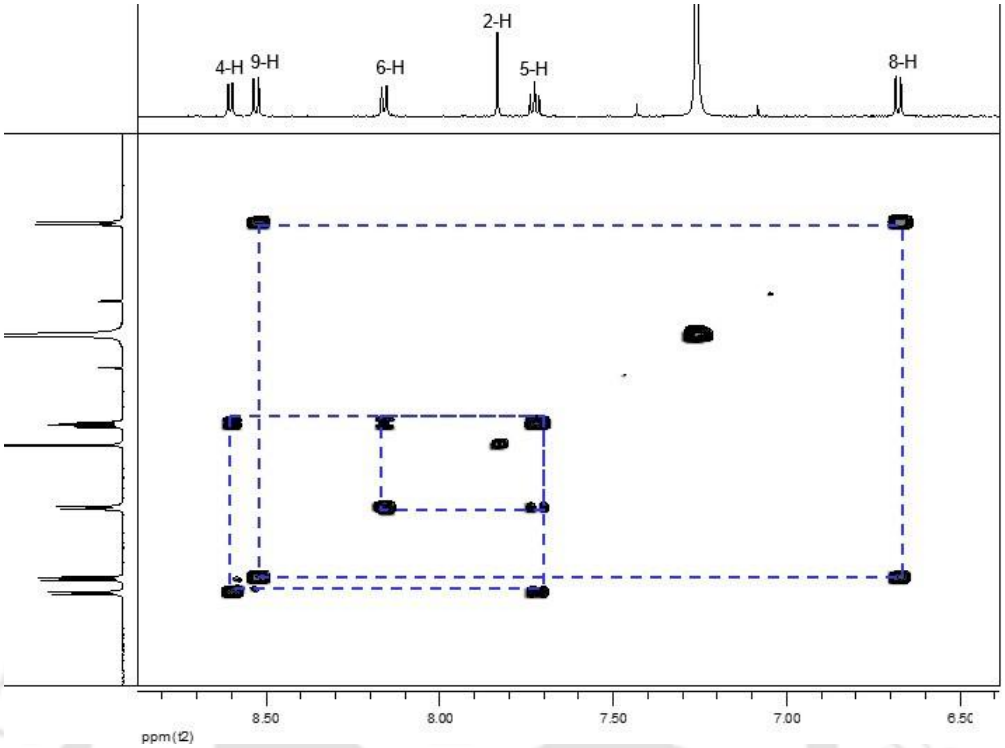

Fig 7. 43 Partial ^{1}H -^{1}H-COSY (aromatic region) NMR spectra of **2p** (500 MHz, $CDCl_3$, 293K).

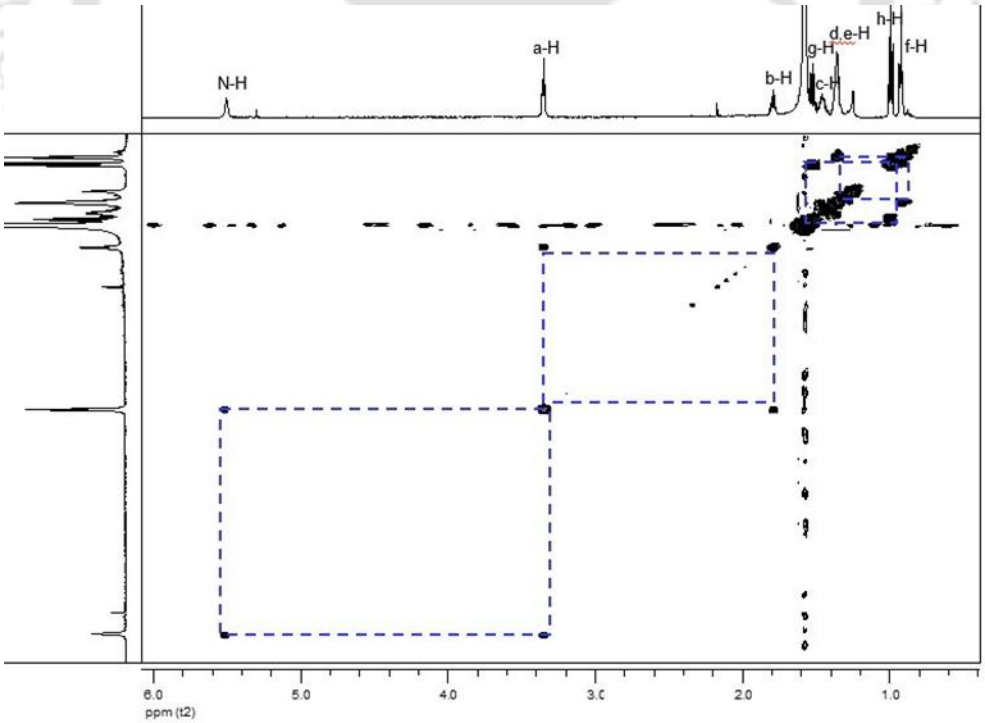

Fig 7. 44 Partial ^{1}H -^{1}H-COSY (aliphatic region) NMR spectra of **2p** (500 MHz, $CDCl_3$, 293K).

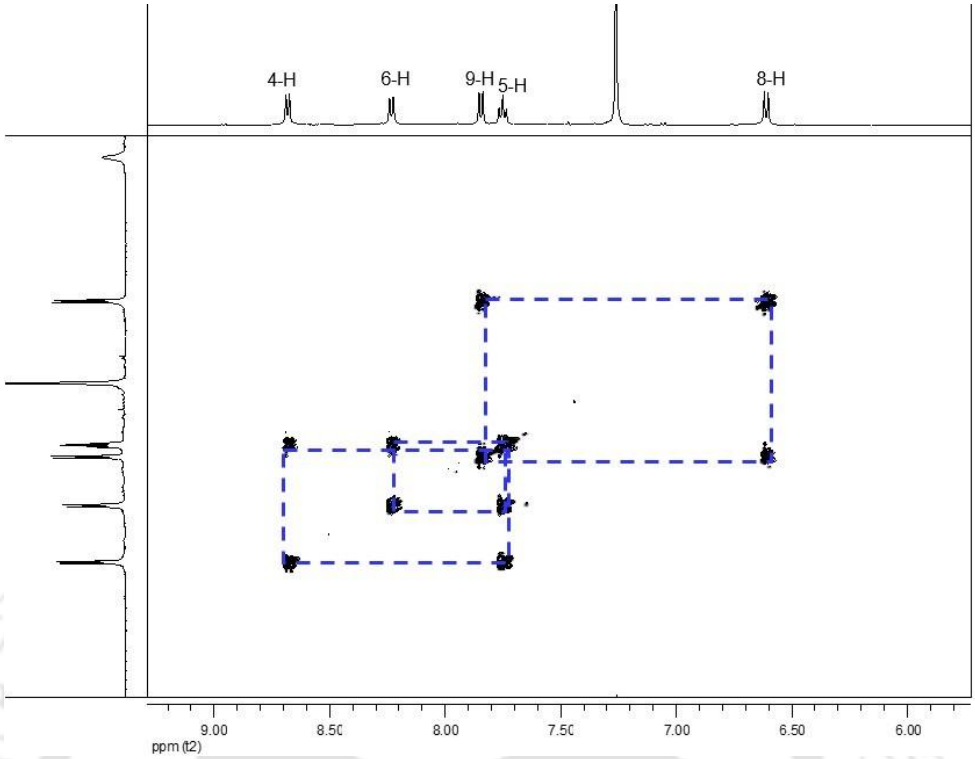

Fig 7. 45 Partial ^{1}H -^{1}H-COSY (aromatic region) NMR spectra of **2p1′** (500 MHz, $CDCl_3$, 293K).

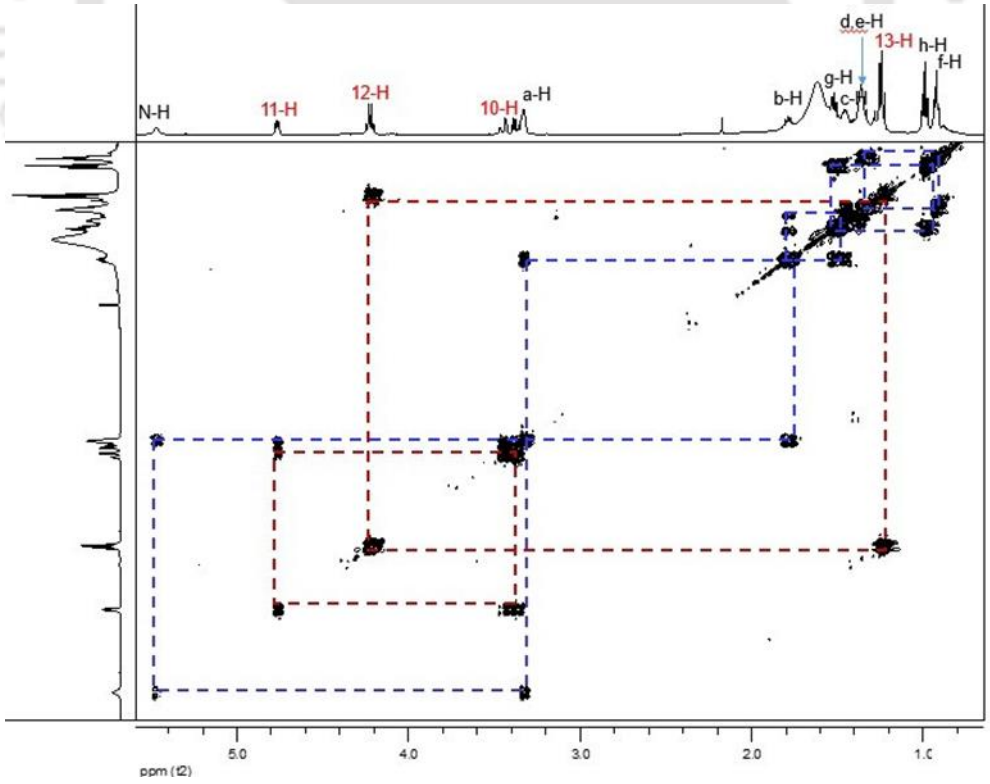

Fig 7. 46 Partial ^{1}H -^{1}H-COSY (aliphatic region) NMR spectra of **2p1′** (500 MHz, $CDCl_3$, 293K

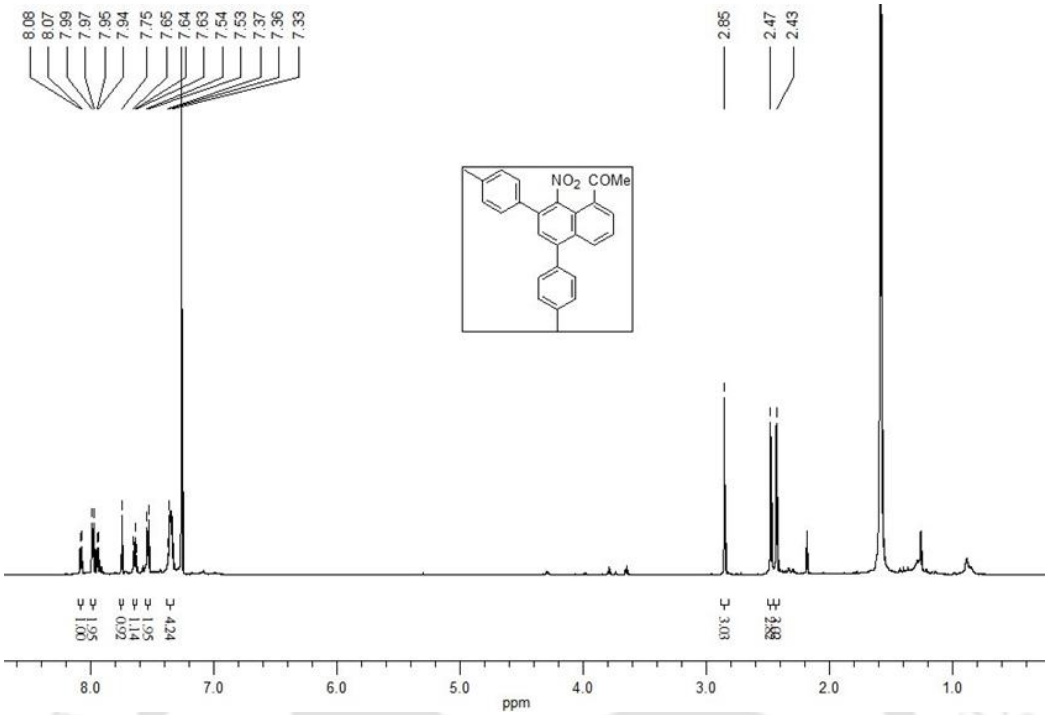

Fig 7. 47 ^{1}H (600 MHz, $CDCl_3$) NMR of **1p**

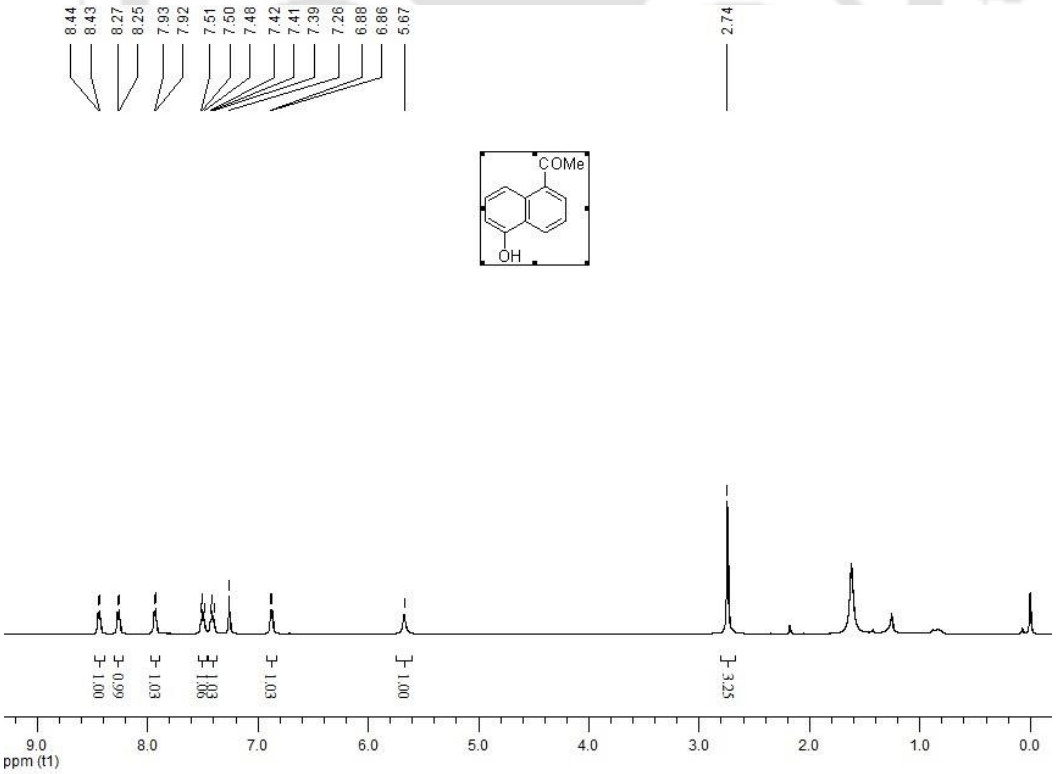

Fig 7. 48 ^{1}H (500 MHz, $CDCl_3$) NMR of **7**

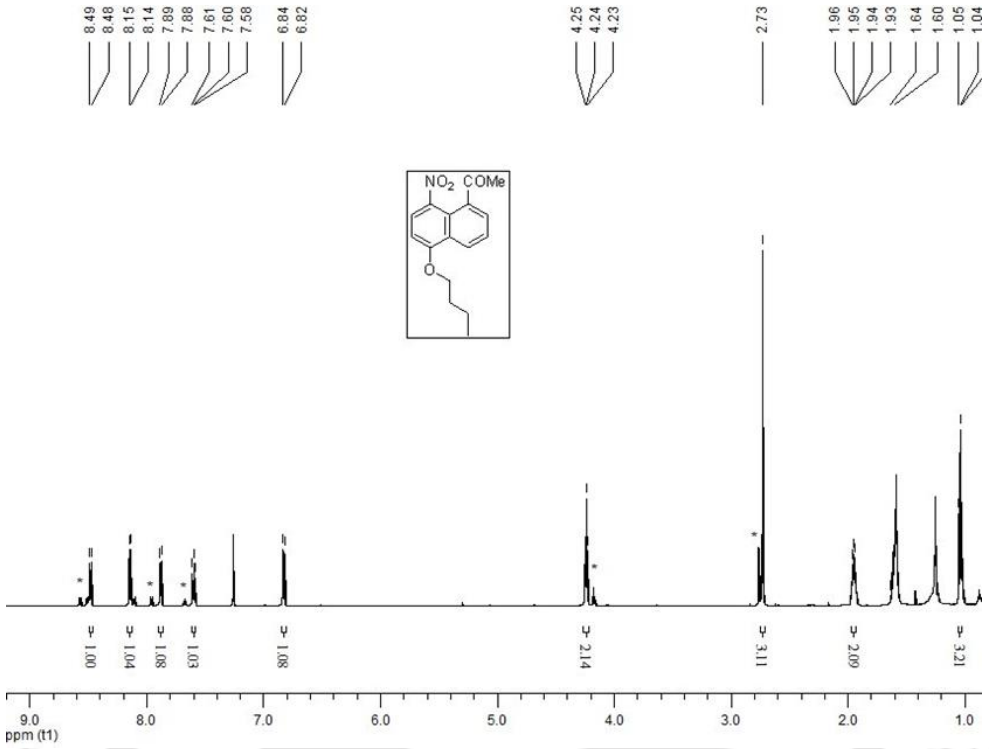

Fig 7. 49 ^{1}H NMR (500 MHz, $CDCl_3$) spectra of **7a**

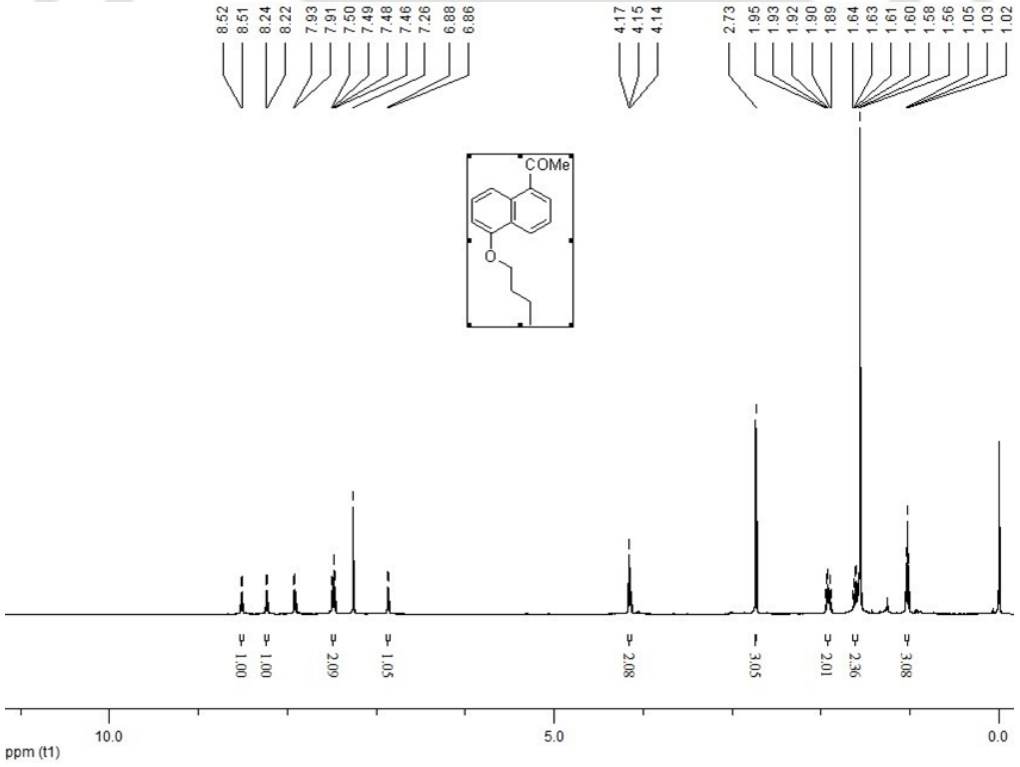

Fig 7. 50 ^{1}H (600 MHz, $CDCl_3$) NMR of **7r.** (*) Residual peak from other isomer.

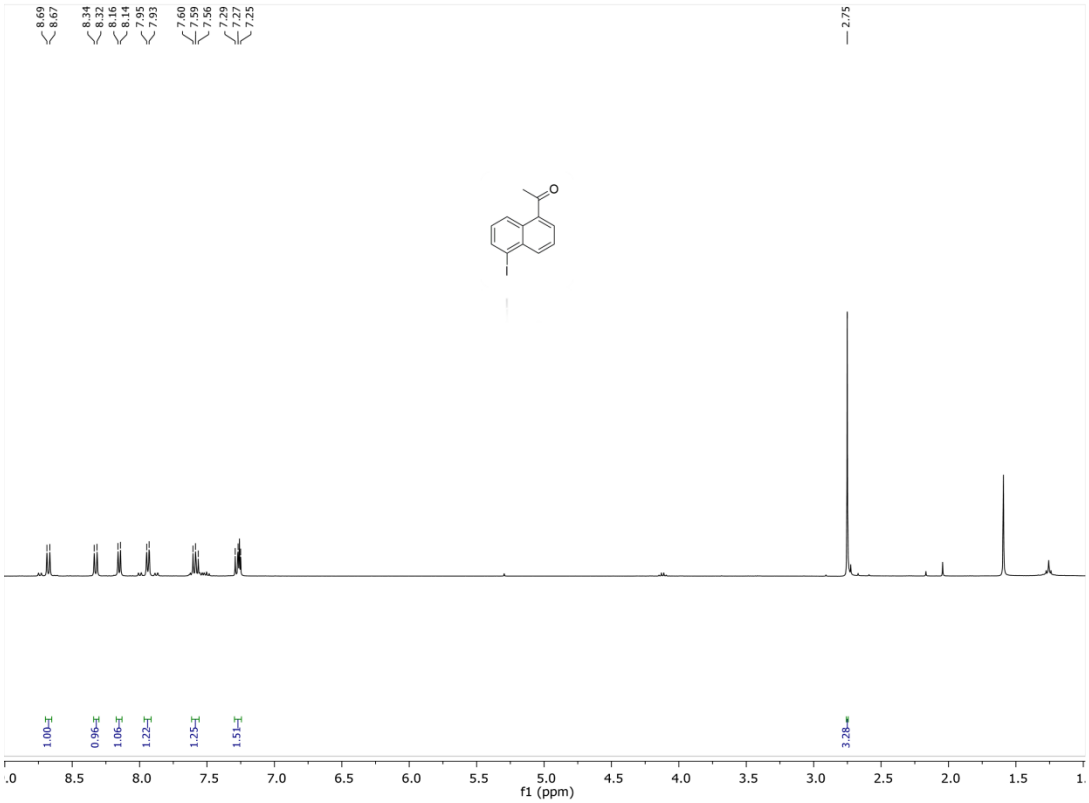

Fig 7. 51 ^{1}H (400 MHz, $CDCl_3$) NMR of **8**

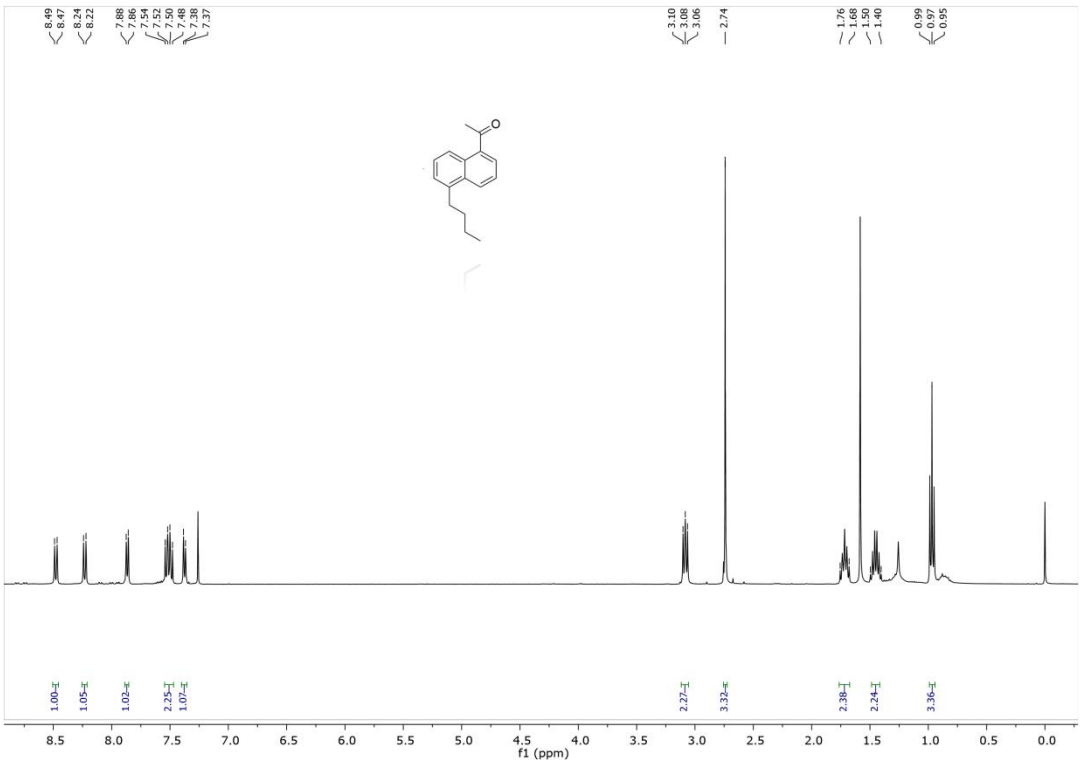

Fig 7. 52 ^{1}H (400 MHz, $CDCl_3$) NMR of **8a**

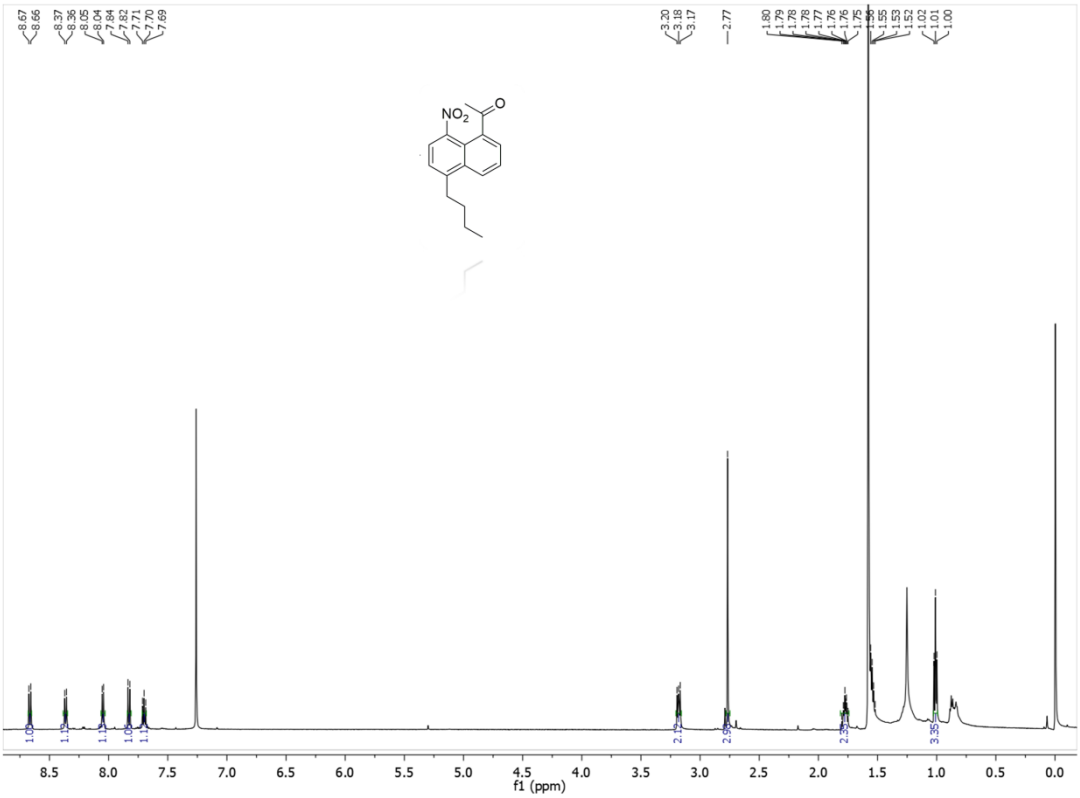

Fig 7. 53 ^{1}H (600 MHz, $CDCl_3$) NMR of **8r.**

❖ 7.4 HRMS spectra

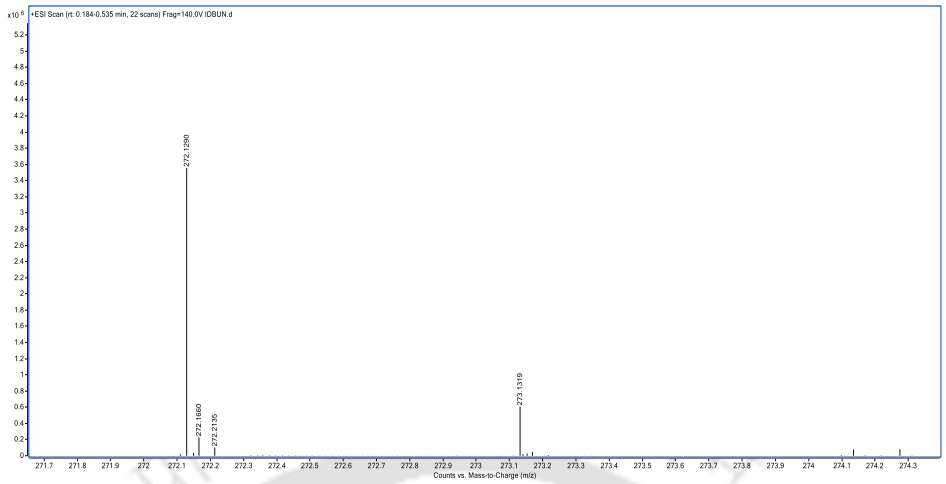

Fig 7. 54 HRMS (ESI) spectrum of [**IIIB** + H]$^+$

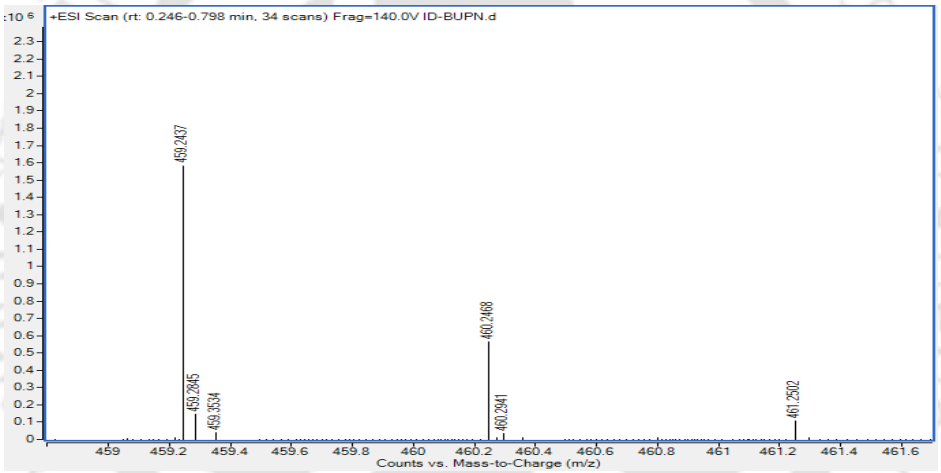

Fig 7. 55 HRMS (ESI) spectrum of [**butylPNI- OH** + H]$^+$

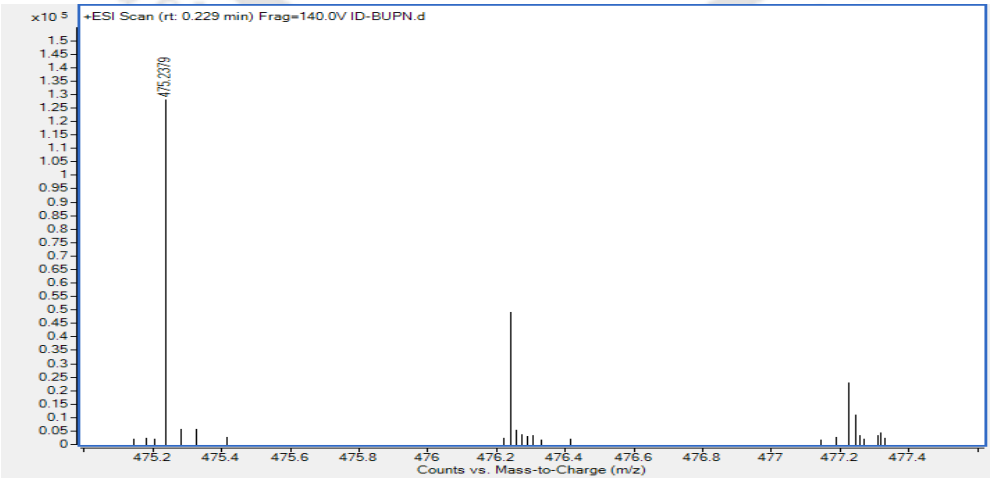

Fig 7. 56 HRMS (ESI) spectrum of [**butylPNI** + H]$^+$

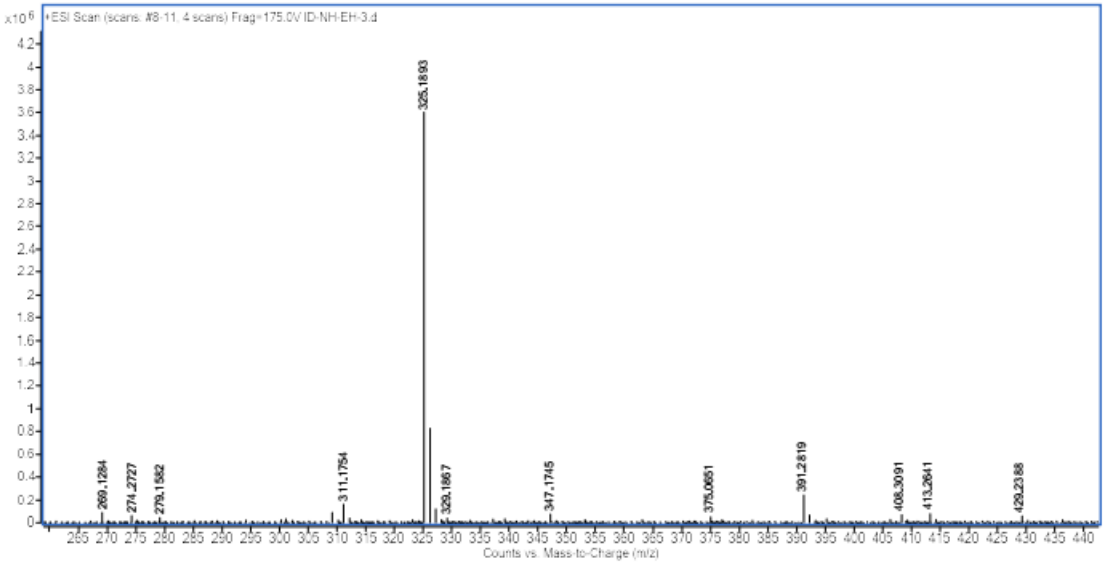

Fig 7. 57 HRMS (ESI) spectrum of [**2p** + H]$^+$

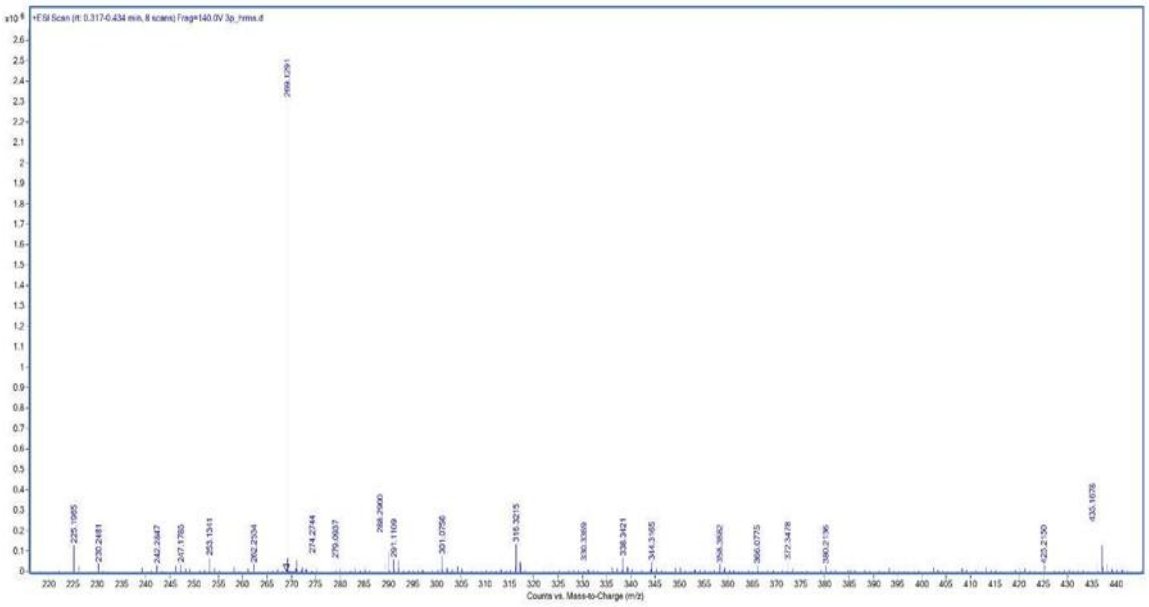

Fig 7. 58 HRMS (ESI) spectrum of [**3p** + H]$^+$

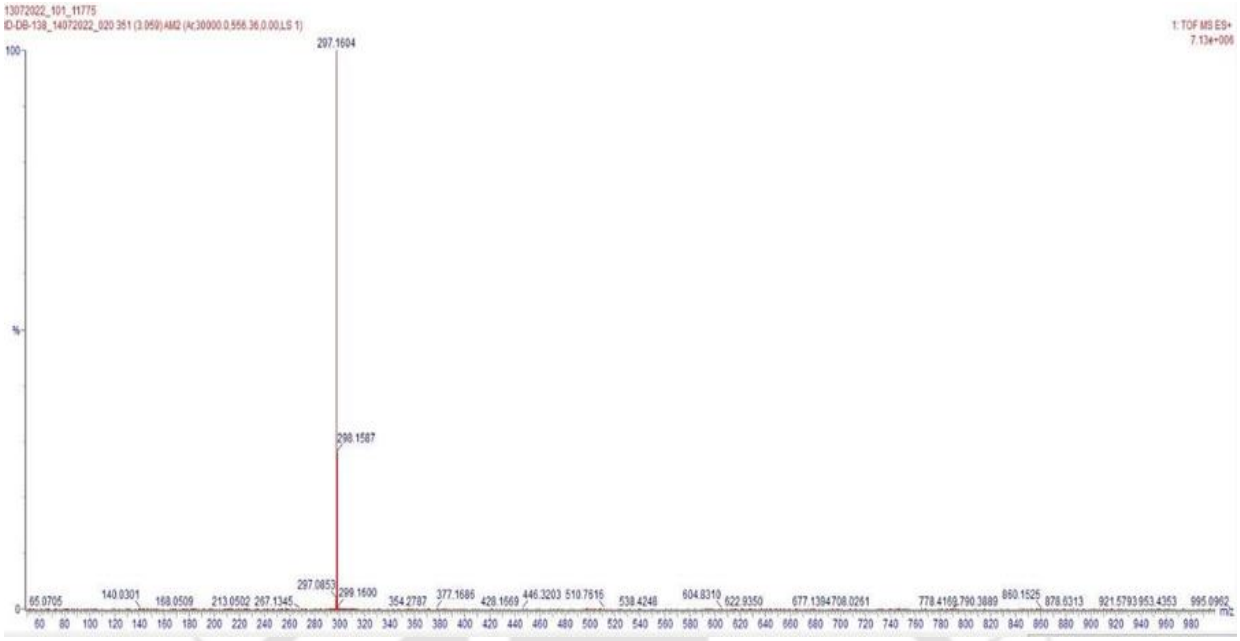

Fig 7. 59 HRMS (ESI) spectrum of [**4p** + H]$^+$

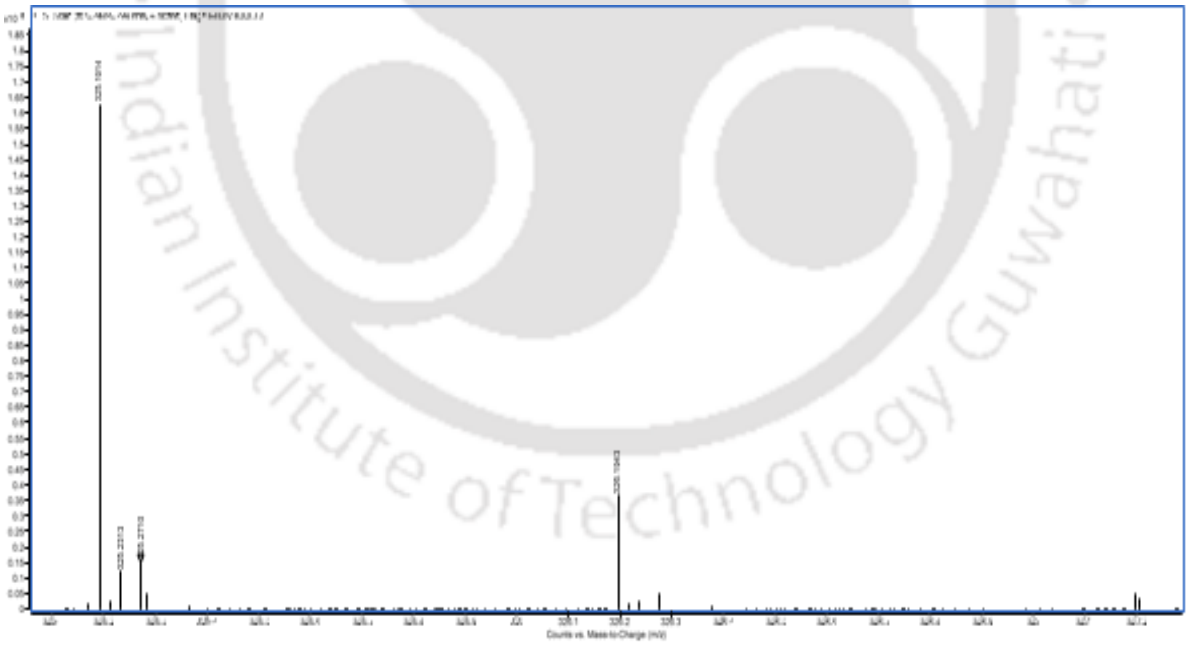

Fig 7. 60 HRMS (ESI) spectrum of [**5p** + H]$^+$

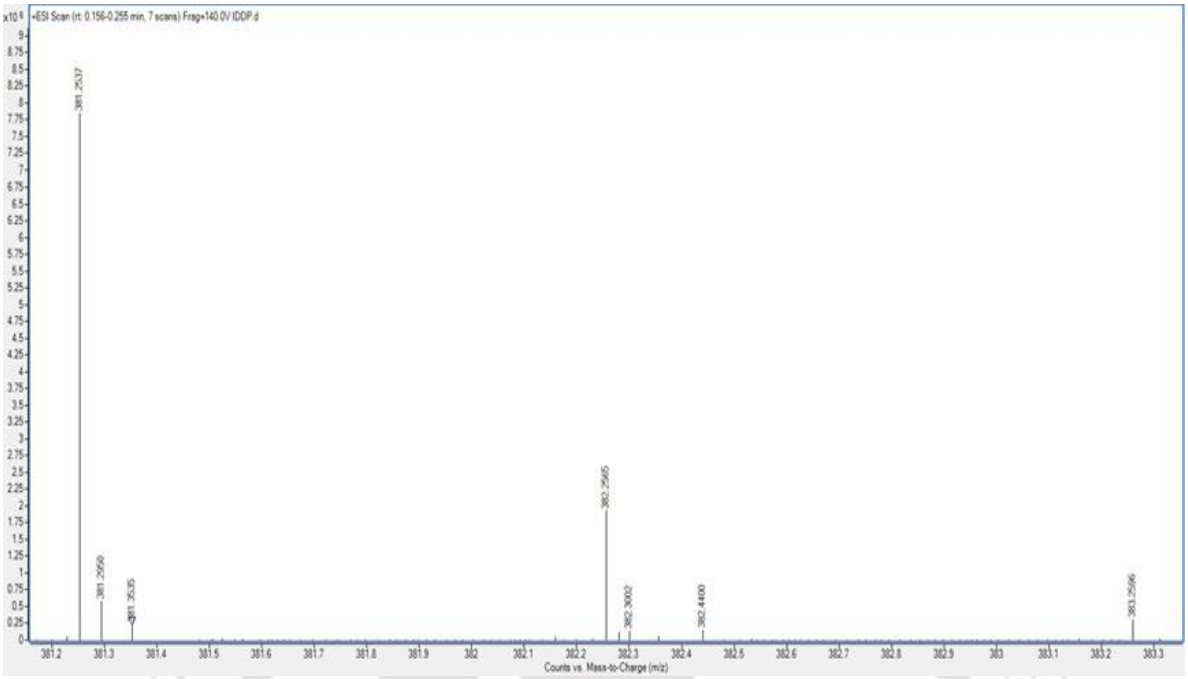

Fig 7. 61 HRMS (ESI) spectrum of [**6p** + H]$^+$

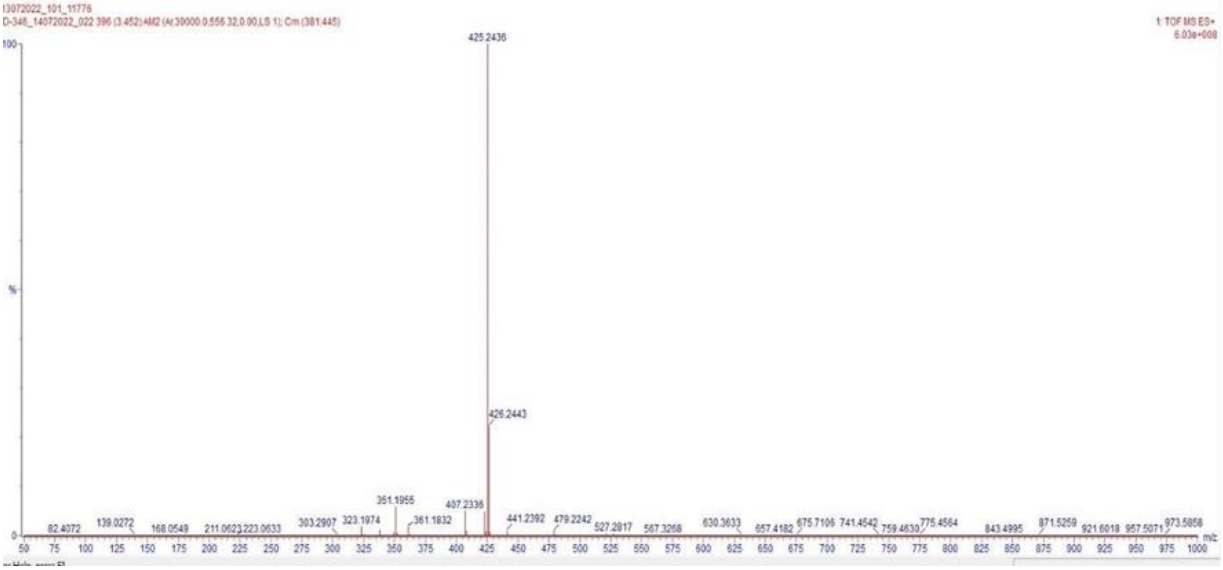

Fig 7. 62 HRMS (ESI) spectrum of [**2p1′** + H]$^+$

❖ 7.5 General photophysical properties of PNTIs and 2p1′

The general optical properties of the prepared PNTIs were independent of the alkyl chain substituent on the amino-alkyl group. As a figurative representation of their class, only the optical properties of **2p** have been reported.

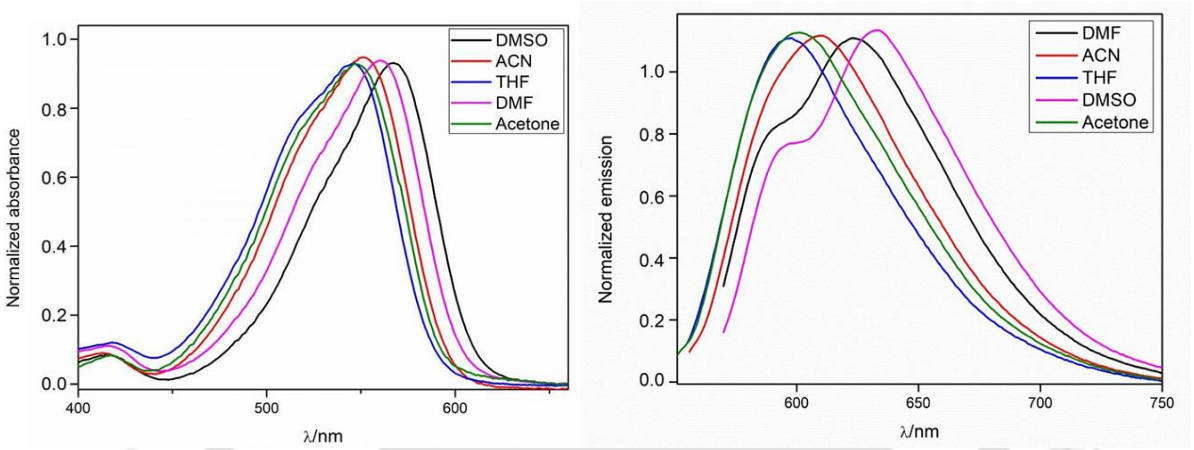

Fig 7. 63 Absorption and emission screening of **2p**

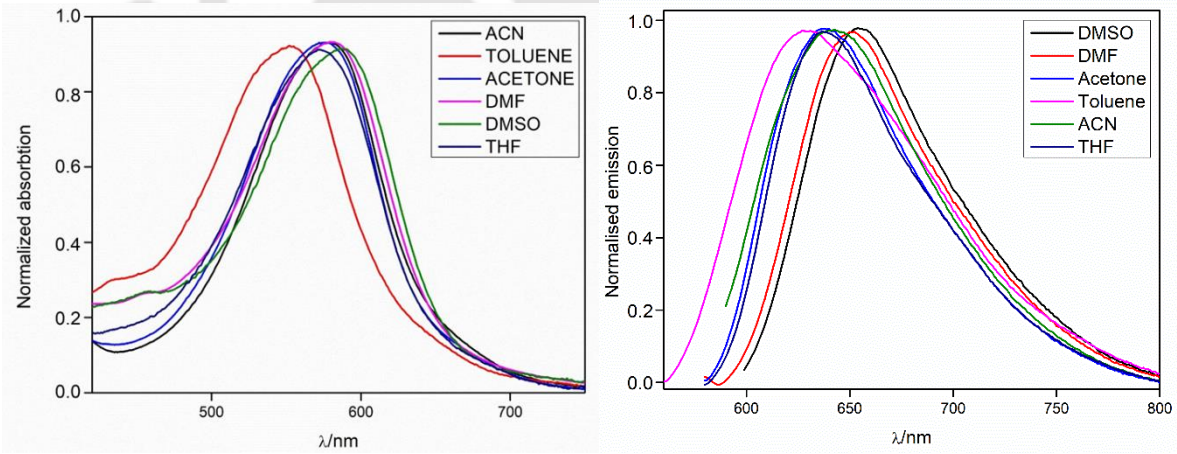

Fig 7. 64 Absorption and emission screening of **2p1′**

❖ **Table 7.1** optical properties of PNTIs and **2p1′**

Compounds	λ_{abs}/nm	ε/M^{-1} cm^{-1}	λ_{em}/nm	ϕ_{pl}
2p	551	12500	594	13.8
3p	549	13200	591	12.4
4p	549	12300	590	11.9
5p	550	13800	592	-----
6p	551	13300	591	-----
2p1′	561	11300	635	12.3

❖ **7.5.1 Measurement of emission quantum yield**

Relative quantum yield of **2p, 3p** and **4p** were found to be 13.8%, 12.4% and 11.9% respectively.

Compound	Excitation Wavelength (nm)	F_x	Absorbance	f_x	Solvent / n_x	Quantum Yield (%)
Rhodamine 6G	480 nm	4.537 x 10^8	0.0142	0.0323	Ethanol /1.3614	95
Rhodamine 6G	475 nm	3.342 x 10^8	0.0108	0.0246	Ethanol /1.3614	95
2p (1^{st} reading)	480 nm	1.055 x 10^8	0.0264	0.0589	Chloroform /1.4458	13.7
2p (2^{nd} reading)	475 nm	0.891 x 10^8	0.0225	0.0505	Chloroform /1.4458	13.9
3p (1^{st} reading)	480 nm	0.860 x 10^8	0.0237	0.0531	Chloroform /1.4458	12.4
3p (2^{nd} reading)	475 nm	0.720 x 10^8	0.0205	0.0461	Chloroform /1.4458	12.3

4p (1st reading)	480 nm	1.063 x 108	0.03065	0.0681	Chloroform /1.4458	11.9
4p (2nd reading)	475 nm	0.896 x 108	0.02645	0.0591	Chloroform /1.4458	11.9
Rhodamine 6G	480 nm	2.800 x 10^8	0.01477	0.0119	Ethanol /1.3614	95
Rhodamine 6G	475 nm	2.093 x 10^8	0.01051	0.0239	Ethanol /1.3614	95
Rhodamine 6G	460 nm	1.029 x 10^8	0.00519	0.0119	Ethanol /1.3614	95
2p1′ (1st reading)	480 nm	0.520 x 10^8	0.02199	0.0494	Chloroform /1.4458	13.5
2p1′ (2nd reading)	475 nm	0.446 x 10^8	0.01971	0.0444	Chloroform /1.4458	12.3
2p1′ (3rd reading)	460 nm	0.293 x 10^8	0.01353	0.0307	Chloroform /1.4458	11.8

List of Publications

Related to this thesis

1. **I. Debnath**, T. Roy**,** J. Matern, S. A. H. Jansen, G Fernández, K. Mahata, "Supramolecular polymorphism in aggregates of a boron-difluoride complex of peri-naphthoindigo via solvent- and pathway-dependent self-assembly" *Org. Chem. Front.,* 2021, 8, 5432.
2. **I. Debnath**, T. Roy**,** D. Borah, K. Mahata, "Stable peri-Naphthoisatogens without C2 Protection: Synthesis via Aldrone Condensation, Optical Properties and1,3-Dipolar Cycloaddition Reaction" *Chem Asian J.* 2023, 18, e202300827.
3. **I. Debnath**, T. Roy**,** K. Mahata, "Remote controlled supramolecular switching using a ring-substituted *peri*-naphthoindigo derivative" *Org. Chem. Front.,* 2024, Advance Article.

Other publications

1. T. Roy**, I. Debnath**, K. Mahata, "Synthesis, optical properties and cation mediated tuning of the reduction potentials of core-annulated naphthalene diimide derivatives", *Org. Chem. Front.,* 2022, 9, 3255.
2. T. Roy**, I. Debnath**, K. Mahata, "Tunable optical properties and self-assemblies of a water-soluble perimidinium imide dye" S*ynlett* 2024, 34, 125–129.

Conference and Symposium

1. **JNOST (Nov'20):** Attended a 3-day conference and presented a poster.
2. **Workshop on functional pi systems (July'21):** Attended workshop at JMU of Wurzburg.
3. **NERC (April'22**): Presented a **poster** in 3-day Research conclave.
4. **FICS (Dec'22**): Presented a **poster** in 3-day Research conclave.
5. **ETCS (Mar'23):** Presented a **poster** in 3-day conference.